TRIARYLBORON COMPOUNDS AND THEIR PLATINUM(II) COMPLEXES: PHOTOPHYSICAL PROPERTIES AND APPLICATIONS IN OPTOELECTRONICS

by

Zachary M. Hudson

A thesis submitted to the Department of Chemistry

In conformity with the requirements for

the degree of Doctor of Philosophy

Queen's University

Kingston, Ontario, Canada

August, 2012

Dedicated to my Mom, Dad and brother Cam.

Abstract

This work concerns the development of π-conjugated materials for optoelectronic applications, with emphasis on organoboron- and organoplatinum-containing compounds. The preparation of a nonconjugated two-chromophore emissive material is described, containing both organoplatinum and organoboron units. This material exhibits simultaneous fluorescent and phosphorescent emission at ambient temperature. Both emission colours are switchable in the presence of fluoride, giving a dual-emissive compound with multiple observable luminescent colours.

The preparation of a nonconjugated donor-acceptor triarylborane containing both Lewis acidic and basic receptor sites is also described. This highly fluorescent compound is reversibly switchable between three emissive states upon addition of acid or fluoride. Furthermore, platinum(II)-acetylacetonates with nonconjugated antenna chromophores were prepared, and their luminescent properties were investigated.

A series of directly conjugated platinum(II)-acetylacetonates have been synthesized incorporating a triarylboron group. The presence of boron was found to enhance the electron-transporting capabilities, film-forming properties, and phosphorescent quantum yields of these complexes. Highly efficient OLEDs were prepared incorporating these materials as dopants, including the first example of a Pt(II)-based OLED with an external quantum efficiency >20%. Triarylboron-containing Pt(II) complexes of *N*-heterocyclic carbenes were also prepared. Using this design, blue to blue-green phosphorescence was achieved with high quantum yield, and their use in OLEDs was demonstrated.

A new high-yield synthetic route has been developed to cyclometalated Pt(II)-*β*-diketonates, requiring stoichiometric reagents and short reaction times at ambient temperature. This methodology has broad substrate scope across a variety of *N^C*-chelate ligands, as well as *P^C*-chelate phosphines and *C^C*-chelate carbenes as well.

The preparation of *N*-heterocyclic carbazole-based host materials for OLEDs is also described. These materials exhibit improved electron-transporting capabilities relative to the more commonly used host 4,4'-*N*,*N*'-dicarbazolylbiphenyl (CBP), and were used to fabricate the first single-layer electrophosphorescent devices with efficiencies competitive with conventional multilayer structures.

Finally, the discovery of a triarylboron-based vapochromic material is described. This Pt(II)-alkyne complex was shown to change luminescent colour in response to a variety of volatile organic compounds, with distinct responses dependent on the nature of the analyte. The mechanism of vapochromism was investigated in detail by optical and multinuclear solid-state NMR spectroscopy, and differs in origin from all previously reported examples.

Acknowledgements

First I would like to thank my supervisor, Prof. Suning Wang, for her hard work, guidance and support during my time at Queen's. Her keen mind, bright personality and dedication to the success of her students are what make Dr. Wang an exceptional scientist and advisor, and it has been a pleasure to be a part of her group. Furthermore, the opportunities I have been given to seek out new collaborations and conduct research at other universities in Canada and abroad have enriched my graduate experience beyond measure. Finally, I wish to thank my advisor for giving me the freedom to follow my own interests over the course of my research, an experience that has been invaluable in helping me grow as an independent scientist.

I am also thankful to the many distinguished researchers I have been fortunate to work with during my years at Queen's. I am sincerely grateful to Prof. Robert Lemieux for giving me my first opportunity to work in a chemical laboratory, for inspiring me to pursue a career in chemistry, and for his support and guidance in the years since. I am also grateful to Prof. Peter Loock for a thoroughly enjoyable term in his group as a summer student, and to Mark Moran, Jeff Roberts, Scott Hopkins, Jeff Crouse, Shu-Bin Zhao, Philipp Wucher and Julian Morey for making my undergraduate research experiences fun and memorable.

My time in the Wang group would not have been the same without the many talented chemists I have had the privilege to work with. I have benefited tremendously from the experience of exceptional postdoctoral fellows and visiting professors, and would like to thank Drs. Yi Sun, Chul Baik, Xiang-Yang Liu, Barry Blight, Young-Jin Kang and Soo-Byung Ko for their guidance. I am also grateful to many of my fellow students, including Theresa McCormick, Sanela Martić, Wade White, Hazem Amarne, Ying-Li Rao, Peng Jia, Vladimir Zlojutro, Nan Wang, Maria Varlan, Jiasheng Lu, Yufei Li, Xiang Wang and Ming Zhu for their friendship and assistance during my time in the group. Finally, I would like to give special thanks to

Christina Sun for her many contributions to this work, as well as her encouragement, companionship and unwavering support.

I am also grateful for the many contributions from the faculty and staff in the department of chemistry at Queen's. In particular, I would like to thank my committee members Prof. Nick Mosey and Prof. Ralph Whitney for their assistance throughout this work. Furthermore, I am grateful to Dr. Rui-Yao Wang for his help with X-ray crystallographic analyses and Dr. Françoise Sauriol for her expertise in NMR spectroscopy.

This work would not be what it is without the critical contributions of many talented collaborators. I would like to thank Prof. Zheng-Hong Lu at the University of Toronto for the opportunity to conduct research in his laboratory, and to Michael Helander, Zhibin Wang and Yi-Lu Chang for their hard work and unmatched ingenuity throughout our collaborative research. I am also grateful to Prof. Robert Schurko, Dr. Kris Harris and Brian Lucier at the University of Windsor for their exceptional work in solid-state NMR spectroscopy.

I have been very fortunate to have had opportunities to study abroad during my doctoral work, both of which were incredible cultural and research experiences. I would like to thank Prof. Yue Wang and his group at Jilin University in the city of Changchun, China for hosting me as an exchange student, and for valuable training in the fabrication of organic electronic devices. I am also grateful to Hai Bi, Yu Yang and Chuandong Dou for their kindness and assistance with my work during my stay in China. I would like to thank Profs. Shigehiro Yamaguchi, Aiko Fukazawa, and Shohei Saito for hosting me in their laboratory at Nagoya University in Nagoya, Japan, and will always remember the hospitality and work ethic of my labmates there. In particular, I would like to thank Azusa Iida, Tomokatsu Kushida, Christoph Glotzbach and Julien Roger for helping to make my time in Japan both memorable and productive.

I am grateful to many people and organizations for financial support of this work, whose contributions to our group and my research have made our discoveries possible. I would first like to thank Queen's University and its many benefactors for the scholarships and prizes I have been fortunate to receive during my time here. I also gratefully acknowledge the Natural Sciences and Engineering Council of Canada (NSERC), the Japan Society for the Promotion of Science (JSPS), the International Center for Diffraction Data (ICDD), Sun Microsystems and the High-Performance Computing Virtual Laboratory (HPCVL), the Business Development Bank of Canada (BDC), the Canadian Society for Chemistry (CSC), Fisher Scientific, and the Miller Thompson Foundation for generous research funding and scholarship support.

I would also like to thank some of the many friends and colleagues outside the lab who have helped make my time at Queen's the amazing experience it was. Craig Johnston, Mike Delorme, Ryan Marble, Marc Carvalho and Jesse Schwartz helped maintain my sanity and made my undergraduate years at Queen's great. I am also grateful for many lifelong friends, and in particular would like to thank Ben Jokuty, Mitch Hansen, Steve Lee and Ben Kane for all the good times over the years. Finally, I would like to thank my teachers John Holden and Margaret Houlihan for their help in making my time at Queen's possible.

Last but not least, I would like to thank my family. I could not have asked for more caring and supportive parents, and it is their kindness and encouragement that got me where I am today. I am grateful to them for always believing in me, and for giving me every opportunity to achieve my dreams. Finally, I would like to thank my brother for his friendship, support, and inspiring in me a fascination with the natural world that lasts to this day. This work is dedicated to them.

Statement of Originality

I hereby certify that all of the work described within this thesis is the original work of the author under the supervision of Prof. Suning Wang, with the following exceptions:

Chapter 2: The synthesis of compound **2.6** was performed by Shu-Bin Zhao, who also obtained single crystals of **2.1** and **2.6** for X-ray diffraction analyses.

Chapter 3: NMR titration experiments were performed by Dr. Xiang-Yang Liu, who also obtained single crystals of **3.1** for X-ray diffraction analyses.

Chapter 4: Bdfp and its Pt(II) complex were synthesized by Christina Sun. Electroluminescent devices were fabricated and tested by Michael Helander at the University of Toronto in the laboratory of Prof. Zheng-Hong Lu.

Chapter 6: The syntheses of compounds **6.2b**, **6.2c**, **6.5**, **6.6** and **6.7** were performed by Dr. Barry Blight.

Chapters 7 and 8: Electroluminescent devices were fabricated and tested by Zhibin Wang, Michael Helander, and Yi-Lu Chang in the laboratory of Prof. Zheng-Hong Lu.

Chapter 9: The work described herein was carried out by both myself and Christina Sun. Solid-state NMR experiments were performed by Dr. Kristopher Harris and Brian Lucier in the laboratory of Prof. Robert Schurko at the University of Windsor.

Any published (or unpublished) ideas and/or techniques from the work of others are fully acknowledged in accordance with standard referencing practices.

Table of Contents

List of Symbols and Abbreviations

°	degrees
°C	degrees Celsius
^{1}MLCT	singlet MLCT state
^{3}MLCT	triplet MLCT state
α	light outcoupling factor
γ_{EL}	electroexcitation efficiency
δ	chemical shift
Δ	change/difference
ε	molar extinction coefficient
η_{ext}	external quantum efficiency
η_{int}	internal quantum efficiency
η_L	current efficiency
η_P	luminous power efficiency
η_r	singlet-triplet branching ratio
θ	angle
κ	skew
λ	wavelength
λ_{max}	absorption/emission maximum
λ_{em}	emission wavelength
λ_{ex}	excitation wavelength
μ	bridging ligand; absorption coefficient
μm	micron
μs	microsecond
Σ	sum
τ	decay lifetime
Φ	quantum efficiency
Ω	ohms; span
Å	angstrom
A	amp; absorbance
A	device active area
Ac	acetyl
acac	acetylacetonate

Alq_3	tris(8-hydroxyquinolate)aluminum(III)
Anal. calcd.	elemental analysis calculated
Ar	aromatic
Ar^F	pentafluorophenyl
a.u.	arbitrary units
B2bpy	5,5'-$BMes_2$-2,2'-bipyridine
Bbtp	5'-(dimesitylboryl)-(2-(2'-pyridyl)benzothiophene)
Bbzf	5'-(dimesitylboryl)-(2-(2'-pyridyl)benzofuran)
BC1	[1-(3-dimesitylboryl)phenyl-3-methylimidazol-2-ylidene-C_2,$C_{2'}$]platinum(II) acetylacetonate
BC2	[1-(4-dimesitylboryl)phenyl-3-methylimidazol-2-ylidene-C_2,$C_{2'}$]platinum(II) acetylacetonate
Bdfp	5-(dimesitylboryl)-2',3'-difluoro-(2-phenylpyridine)
Bmeop	5-(dimesitylboryl)-3'-methoxy-(2-phenylpyridine)
BNPB2	5-(dimesitylboryl)-4'-(*N*-(1-naphthyl)-*N*-phenylamino)-(2-phenylpyridine)
BNppy	5-(dimesitylboryl)-4'-(*N*,*N*-diphenylamino)-(2-phenylpyridine)
BNPB	4-dimesitylboryl-4'-(*N*-(*1*-naphthyl)phenylamino)biphenyl
bpy	bipyridine
br	broad
Brbtp	5'-bromo-(2-(2'-pyridyl)benzothiophene)
Brbzf	5'-bromo-(2-(2'-pyridyl)benzofuran)
Brdfp	5-bromo-2',3'-difluoro-(2-phenylpyridine)
Brmeop	5-bromo-3'-methoxy-(2-phenylpyridine)
BrNppy	5-bromo-4'-(*N*,*N*-diphenylamino)-(2-phenylpyridine)
Bu	butyl
CBP	4,4'-*N,N'*-dicarbazolebiphenyl
cd	candelas
CE	current efficiency
CIE	Commision Internationale de l'Éclairage
cm	centimetres
Cp	cyclopentadienyl
CP	cross-polarization
CPHP	4,5'-*N*,*N*'-dicarbazolyl-(2-phenylpyrimidine)

CPMG	Carr-Purcell Meiboom-Gill
CPPY	4,5'-*N*,*N*'-dicarbazolyl-(2-phenylpyridine)
CS	chemical shift
CT	charge-transfer
CV	cyclic voltammetry
Cy	cyclohexyl
Cz	carbazole
d	doublet
dbbpy	4,4'-di-*tert*-butyl-2,2'-bipyridine
D_{calc}	calculated density
dd	doublet of doublets
DFT	density functional theory
DMF	dimethylformamide
DMSO	dimethylsulfoxide
DOI	digital object identifier
dppp	1,3-diphenylphosphinopropane
e^-	electron
$E_{1/2}^{ox}$	half-cell oxidation potential
$E_{1/2}^{red}$	half-cell reduction potential
E_F	Fermi level
EL	electroluminescent
EML	emissive layer
E_P	average photon energy
ESR	electron spin resonance
EQE	external quantum efficiency
equiv.	equivalents
Et	ethyl
ETL	electron transport layer
eV	electronvolts
F	fluorescence; structure factor
$FeCp_2^{0/+}$	ferrocene/ferrocenium redox couple
FW	formula weight
g	grams
I	intensity

I	current
IC	internal conversion
Im	imidazole
^{i}Pr	isopropyl
IQE	internal quantum efficiency
ISC	intersystem crossing
J	coupling constant
L	luminance
h	hours
h^{+}	hole
hν	light
HOMO	highest occupied molecular orbital
HRMS	high-resolution mass spectrometry
HTL	hole transport layer
Hz	hertz
ITO	indium tin oxide
J	coupling constant
K	Kelvin
K	binding constant
kHz	kilohertz
kJ	kilojoules
k_{nr}	rate of nonradiative decay
k_{r}	rate of radiative decay
kV	kilovolts
LC	ligand-centered; liquid crystal
lm	lumens
LMCT	ligand-to-metal charge transfer
LUMO	lowest unoccupied molecular orbital
m	metres
M	molar; mass
mA	milliamps
MAS	magic-angle spinning
mCP	*N*,*N*′-dicarbazolyl-3,5-benzene
Me	methyl

MeCN	acetonitrile
Mes	mesityl
mg	milligrams
MHz	megahertz
min	minutes
mL	millilitre
MLCT	metal-to-ligand charge-transfer
MO	molecular orbital
mol	mole
MOF	metal-organic framework
m.p.	melting point
mV	millivolts
MV	megavolts
n	refractive index
NHC	*N*-heterocyclic carbene
nm	nanometres
NMR	nuclear magnetic resonance
NMS	nuclear magnetic shielding
NLO	nonlinear optic(al)
NPA	*N*-(2'-pyridyl)-7-azaindole
NPB	*N,N'*-di-[(1-naphthyl)-*N,N'*-diphenyl]-(1,1'-biphenyl)-4,4'-diamine
OLED	organic light-emitting diode
P	phosphorescence
PE	power efficiency
Ph	phenyl
1,10-phen	1,10-phenanthroline
PHOLED	phosphorescent organic light-emitting diode
PL	photoluminescent
PMMA	poly(methyl methacrylate)
ppm	parts per million
ppy	2-phenylpyridine
Pt-Bbtp	Pt(*N^C*-Bbtp)(*O^O*-acac)
Pt-Bbzf	Pt(*N^C*-Bbzf)(*O^O*-acac)
Pt-Bdfp	Pt(*N^C*-Bdfp)(*O^O*-acac)

Pt-Bmeop	Pt(*N^C*-Bmeop)(*O^O*-acac)
Pt-BNPB2	Pt(*N^C*-BNPB2)(*O^O*-acac)
Pt-BNppy	Pt(*N^C*-BNppy)(*O^O*-acac)
Pt-BppyA	Pt(*N^C*-BppyA)(*O^O*-acac)
Pt-BppyB	Pt(*N^C*-BppyB)(*O^O*-acac)
PXRD	powder X-ray diffraction
py	pyridyl
pyr	pyrimidine
quant.	quantitative
QY	quantum yield
Reflns	reflections
RT	room temperature
s	second; singlet
S_0	singlet ground state
S_n, (n > 0)	n^{th} singlet excited state
S(λ)	photopic response of the human eye as a function of wavelength
SPhos	2-Dicyclohexylphosphino-2',6'-dimethoxybiphenyl
SSNMR	solid-state NMR
t	triplet; time
T	temperature; tesla
T_n (n > 0)	n^{th} triplet excited state
TBAF	tetrabutylammonium fluoride
TBAP	tetrabutylammonium hexafluorophosphate
TD-DFT	time-dependent density functional theory
TEACN	tetraethylammonium cyanide
Tf	triflyl
TFA	trifluoroacetic acid
THF	tetrahydrofuran
TPBI	1,3,5-tris(*N*-phenylbenzimidazole-2-yl)benzene
TPPM	two-pulse phase-modulated
Ts	tosyl
UPS	ultraviolet photoelectron spectroscopy
UV	ultraviolet
V	volt; volume

V	applied voltage
VACP	variable-amplitude cross polarisation
VOC	volatile organic compound
Vis	visible
W	watt
WURST	wideband uniform rate smooth truncation

List of Figures

Chapter 1

Chapter 2

Chapter 3

Chapter 8

Chapter 9

List of Tables

Chapter 7

Chapter 8

Chapter 9

Chapter 1

Introduction

Triarylboron compounds have recently emerged as an important class of optoelectronic materials due to the empty p_π orbital on the boron center. Isoelectronic with carbocations, these functional groups are capable of acting as powerful electron acceptors and Lewis acids, and can promote bright charge-transfer luminescence when combined with electron donors in π-conjugated materials.[1] (Figure 1.1) The electrophilicity of the boron center also leads to exciting new reactivities, making these compounds ideal for applications in catalysis[2] and small-molecule activation.[3] For use in optoelectronic materials and devices, however, the boron center must be rendered stable to nucleophilic attack and hydrolysis. This can be readily achieved by functionalization of the boron center with bulky aryl substituents, such as 2,4,6-trimethylphenyl, or mesityl (Mes). With this design, triarylboron compounds have been successfully developed as robust materials for nonlinear optics[4] and anion sensing,[5] and used as emissive and electron-transport materials for organic light-emitting diodes (OLEDs).[6,7]

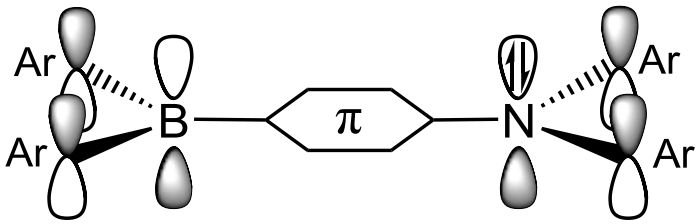

Figure 1.1: A typical donor-acceptor triarylborane.

The development of phosphorescent transition-metal complexes for optoelectronic applications has concurrently become a highly active field of research. Characterized by long-lived emission from triplet excited states, these compounds are ideal for a variety of uses. For example, phosphorescent materials are

capable of harvesting both singlet and triplet excitons in OLEDs, such that maximum internal quantum efficiencies approaching 100% can be achieved in devices incorporating a phosphorescent emitter.[8] Furthermore, the use of long-lived phosphorescent materials as luminescent sensors can greatly reduce interference from background fluorescence or scattering by time-gated detection, which is important for luminescent sensing and imaging in biological systems.[9] Phosphorescent materials have also gained attention as sensitizers in photodynamic therapy for cancer treatments[10a] and as probes for molecular oxygen, which has led to their use as biological imaging agents for hypoxic tissue.[10b]

With these applications in mind, recent investigations on triarylboron-containing metal complexes have produced many new optoelectronic materials, as well as provided opportunities for rich photophysical studies. The work described in this thesis details our efforts to better understand the photophysical properties of both organic and metal-containing triarylboranes, with emphasis on triarylboron-functionalized complexes of Pt(II). Studies on nonconjugated two-chromophore boron compounds will be described, with emphasis on their luminescent properties and use as anion sensors. Furthermore, the development of triarylboron-containing Pt(II) complexes as sensors for volatile organic compounds and as efficient emitters for OLEDs will be discussed. This thesis will also describe our efforts to address problems in related fields, including the development of host materials for highly efficient single-layer OLEDs and the development of improved synthetic methods for the preparation of Pt(II) β-diketonate phosphors.

The motivation and research background for this work will be described in the following sections of this chapter. Due to the breadth of this work, this chapter will focus on recent research on the photophysical properties and applications of triarylboron-containing materials, with a brief discussion of the principles of luminescence and OLED technology. Subsequent chapters will also provide an introductory discussion more specific to each topic.

1.1 Principles of Luminescence

Luminescence is the emission of light from a substance that does not result from heating, and comes in many forms. This release of energy, resulting in emission of a photon, can be the result of excitation of a material with light (photoluminescence), an applied voltage (electroluminescence), a chemical reaction (chemiluminescence) or mechanical force (triboluminescence) to name a few. The luminescence of a material may be further classified as either fluorescence or phosphorescence, two emission pathways with distinct characteristics. Fluorescence involves radiative relaxation of a material from a singlet excited state, a state in which its ground and excited state electrons have antiparallel spins with a magnetic quantum number m_l of zero. This process, represented as $S_1 \rightarrow S_0$ in Figure 1.2, is typically very fast, with excited state lifetimes on the order of picoseconds (10^{-12}s) to nanoseconds (10^{-9}s). In contrast, phosphorescence involves radiative relaxation from a triplet excited state, or one in which the ground and excited state electrons are unpaired with a magnetic quantum number m_l of one. As direct relaxation of such an excited state would violate the Pauli exclusion principle, relaxation of a triplet excited state also requires the inversion of spin of one of the participating electrons. As this $T_1 \rightarrow S_0$ process violates quantum mechanical rules of spin conservation it is typically much slower, with excited state lifetimes ranging from microseconds (10^{-6}s) to seconds or even hours.

These processes are outlined schematically in Figure 1.2, along with several other processes that play a role in determining a material's luminescent properties.[9] As described above, the electronic excitation of a material may occur in a number of ways, but need not always generate a species in its lowest energy singlet excited state (S_1) immediately. Depending on the magnitude of the energy absorbed, this excitation may occur as an $S_0 \rightarrow S_1$ transition or between the ground state and higher energy excited states (S_2, S_3, etc). However, nonradiative relaxation of higher-energy excited states to the S_1 state is typically very rapid, occurring by a process known as internal conversion (IC) by dissipation of the excess energy as

heat. For this reason, the emission spectra of most materials exhibit only a single band, despite the presence of multiple bands in their UV-visible absorption spectra.

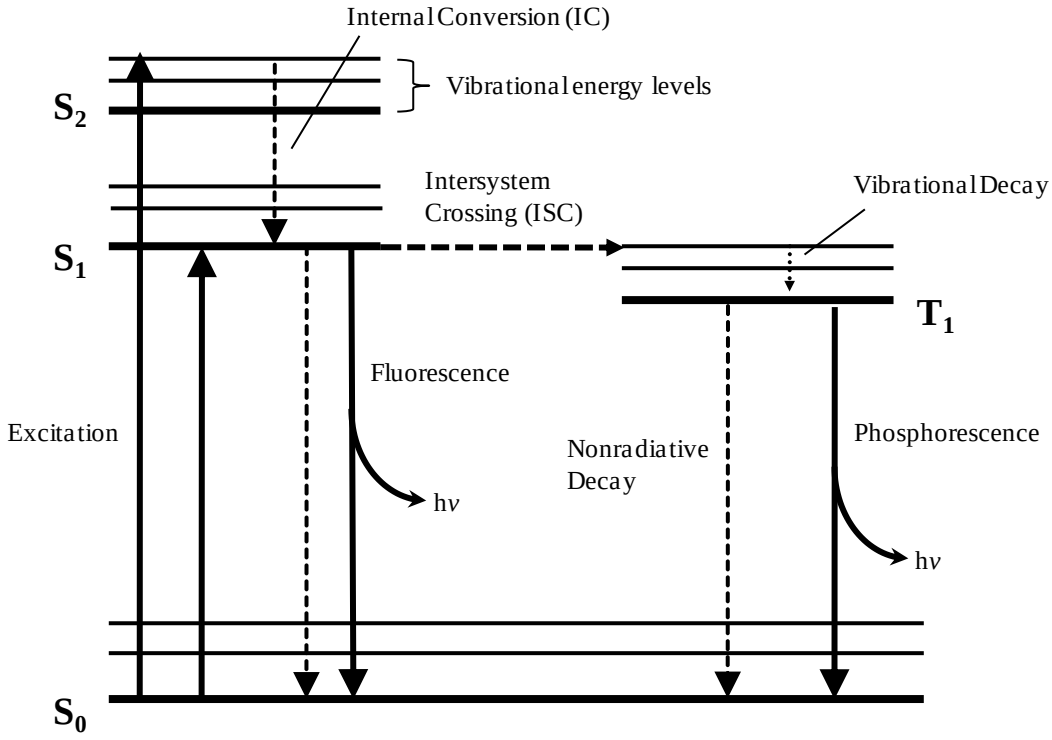

Figure 1.2: Jablonski diagram illustrating the processes involved in luminescence.

Once excited, a process known as intersystem crossing (ISC) may convert the material to a triplet excited state. This spin-forbidden $S_1 \rightarrow T_1$ process is genrally not favoured in pure organic molecules, as the lack of any spin-orbit coupling to perturb the relevant excited states results in only a low probability of generation of the lower energy T_1 state. As materials in the triplet excited state must undergo a second spin-forbidden process to release this energy as light, organic materials typically display only fluorescent emission. However, cooling organic materials to very low temperatures (for example, in liquid nitrogen at 77 K) can suppress thermal decay pathways sufficiently to allow organic phosphorescence to be visible, with decay lifetimes often on the order of seconds. The presence of a heavy atom, however, readily facilitates these spin-forbidden processes by spin-orbit coupling, mixing singlet states and the T_1 state

sufficiently to allow rapid intersystem crossing to occur. As such, many transition metal complexes are phosphorescent at ambient temperature, with decay lifetimes on the order of microseconds.

Both excited state singlet and triplet materials may also relax to their ground states by competing nonradiative thermal decay pathways, which reduce the efficiency of luminescence. By examining the rates of radiative and nonradiative decay for a material, we define its *quantum efficiency* as:

$$\Phi = \frac{k_r}{k_r + \Sigma k_{nr}}$$

Where k_r is the rate of radiative decay and Σk_{nr} is the sum of the rates of all competing nonradiative decay processes. Maximizing Φ can thus be achieved either by designing a material with a rapid rate of radiative decay, or by minimizing competing nonradiative processes.

The nature of luminescence in a material can vary substantially depending on the orbitals involved in the emissive transition. Charge-transfer (CT) transitions involve significant redistribution of electron density from the ground state of a material to the excited state, and result in broad, featureless emission bands. In solution-based systems, the large transition dipole moment of CT transitions makes this class of emission highly sensitive to the polarity of the environment. For example, a CT transition with a large excited-state dipole will give lower-energy emission in polar solvent, as the stabilization of the excited state in polar media will reduce the S_0-S_1 gap. In contrast, π- π* transitions (that is, electronic transitions from a filled π orbital to an empty π antibonding orbital) involve little redistribution of electron density and typically give structured emission bands that are relatively insensitive to solvent polarity, with the transitions from the S_1 state to the different vibrational levels of the S_0 state well-resolved.[9]

In metal complexes, the nature of these transitions depends greatly on the relative positions of the *d* orbital energy levels relative to the frontier orbitals of the ligands. If the highest occupied molecular orbital (HOMO) and lowest unoccupied molecular orbital (LUMO) are both ligand-based, a material will likely exhibit ligand-centered (LC) emission, which may take the form of a CT transition, π- π^* transition, etc. If the HOMO and LUMO are both *d* orbitals, the lowest energy transition will involve *d-d* excited states, which are typically non-emissive due to significant perturbations in the bonding geometry around the metal centre upon reorganization of the metal *d* electrons. Complexes with a ligand-based HOMO and a metal-based LUMO show ligand-to-metal charge-transfer (LMCT) transitions, and generally require a highly electron-deficient metal centre. While typically non-emissive as well, LMCT transitions give high-oxidation state metal complexes such as MnO_4^- and $Cr_2O_7^{2-}$ their characteristic deep absorption colours. Finally, complexes with a metal-based HOMO and a ligand-based LUMO exhibit metal-to-ligand charge-transfer (MLCT) transitions, a process common to phosphorescent complexes of Pt(II) and Ir(III) and the basis for much of the research described in this thesis.

1.2 Organic Light-Emitting Diodes

Organic light-emitting diodes (OLEDs) have attracted enormous research interest in the past 20 years, since the discovery of the efficient electroluminescence of tris(hydroxyquinolate)aluminum(III) (Alq_3) by Tang and VanSlyke in 1987.[12] This scientific motivation has been matched by considerable market demand, with commercially viable OLED technologies now entering use in flat-panel displays, music players, and cellular phones.

This interest in OLEDs is driven by a number of advantages that they offer over conventional display technologies. For example, while many OLEDs are still manufactured by vacuum vapour deposition, many of the materials used in device fabrication are amenable to solution processing, making low-cost fabrication by spin-coating or inkjet printing possible. Also, OLEDs require significantly less power than

conventional liquid crystal (LC) displays, as the pixels themselves are emissive and so do not require a backlight. This also allows for the fabrication of extremely thin OLED displays, which in turn can be printed onto flexible substrates. Finally, the image quality in an LC display is limited by its contrast ratio and viewing angle, neither of which are problematic for OLED displays.

An OLED itself is a luminescent electronic device with nonlinear current-voltage characteristics; a resistor that does not obey Ohm's Law. A layer of luminescent organic material is placed between two electrodes, most often an indium tin oxide (ITO) anode and a cathode composed of a low work function metal such as aluminum. When a voltage is applied across the electrodes, electrons are injected into the organic material from the cathode, while positive charges, or holes, are injected in the opposite direction from the anode. In the emissive layer these charges form electron-hole pairs, or excitons, which can then recombine in the emissive material to produce light. In order to increase the efficiency of the device, additional organic layers designed to effectively transport charge are often placed between the emissive material and the electrodes, known as the hole- and electron-transport layer (HTL and ETL). Each layer of organic material is usually between 10-100 nm thick, meaning that the thickness of the OLED is limited largely by the thickness of the substrate. This type of traditional multilayer OLED design is depicted in Figure 1.3, and the basic operating mechanism of an OLED is shown in Figure 1.4.

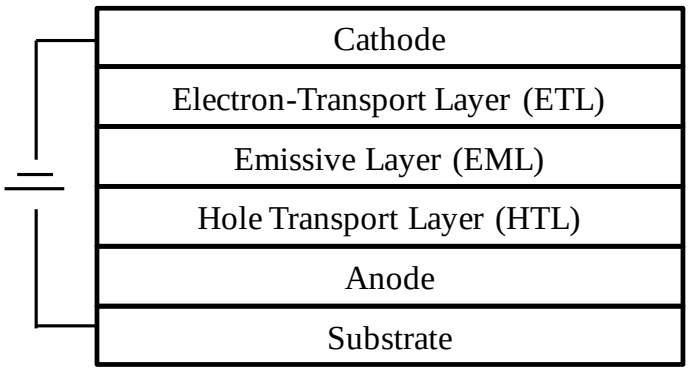

Figure 1.3: Structure of a typical three-layer OLED.

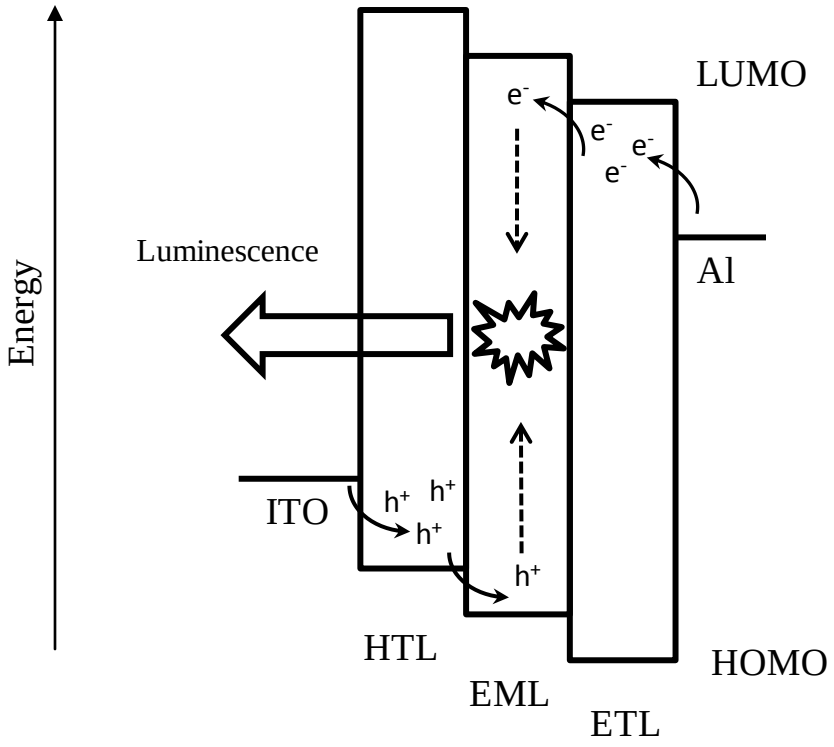

Figure 1.4: A diagram depicting the operating mechanism of an OLED. Electrons (e^-) and holes (h^+) are injected at opposite electrodes, and recombine in the emissive layer to produce light, which is emitted through the transparent electrode.

The efficiencies of OLEDs may be described in a number of ways.[12] The *internal quantum efficiency* (IQE, η_{int}) for an OLED is defined as the ratio of the total number of photons generated within the device to the number of electrons injected. This measure of device efficiency most closely resembles the quantum yield of the emissive material, and may be defined as:

$$\eta_{int} = \gamma_{EL}\eta_r\Phi$$

In this equation, γ_{EL} represents the *electroexcitation efficiency*, or the probability that an electron-hole pair travelling through the device will form an exciton. η_r is known as the *singlet-triplet branching ratio*, and refers to the fraction of excitons that can recombine on a particular material due to spin statistics. Since electrons and holes are produced at opposite electrodes in an OLED with uncorrelated spins, charge injection will generate singlet and triplet excitons with 25% and 75% probability, respectively. Since only

singlet excitons can recombine on a fluorescent material, η_r for fluorescent materials is 0.25. Since phosphorescent materials can harvest triplet excitons directly, and may convert singlet excitons to triplet excitons by intersystem crossing, η_r for phosphorescent materials is 1. The practical consequence of this equation is that the maximum theoretical internal quantum efficiency is 25% for fluorescent OLEDs and 100% for phosphorescent OLEDs, contributing to the shift on the whole of OLED research to the use of phosphorescent emitters in recent years.

More commonly measured, however, is the *external quantum efficiency* (EQE, η_{ext}) of the device, defined as the ratio of the number of photons emitted from the device in the viewing direction to the number of electrons injected. The inclusion of the viewing direction in this term is of particular importance to display applications, as a significant fraction of the emitted light may be waveguided by the substrate and organic layers or backscattered from the cathode, and thus will not contribute to the brightness perceived by an observer. The EQE may be defined simply as:

$$\eta_{ext} = \alpha\eta_{int}$$

Where α is the light outcoupling factor that gives the fraction of light emitted from the device in the viewing direction. α may be approximated as $1/2n^2$, where n is the refractive index of the emitting organic material, though this approximation is often poor due to the presence of multiple organic materials in the device through which light must pass, and due to enhancements in outcoupling efficiency resulting from constructive interference of the emitted light.

Two other measures are also commonly used to quantify the efficiency of OLED devices that more clearly relate device performance with its electrical characteristics. The luminous power efficiency η_P of a device defines the ratio of output light power to input electrical power in lumens per watt (lm W^{-1}), as:

$$\eta_P = \frac{\eta_{ext} E_P S(\lambda)}{V}$$

Where E_P is the average energy of the photons being emitted, V is the applied voltage, and $S(\lambda)$ is a curve quantifying the photopic response of the human eye, which varies in sensitivity according to wavelength, being more sensitive to green and less sensitive to red or blue. The current efficiency η_L of a device defines the luminance produced per unit current in candelas per ampere (cd A^{-1}) as simply:

$$\eta_L = \frac{AL}{I}$$

Where A is the device active area, L is the luminance of the OLED (cd m^{-2}), and I is the OLED current. These terms will be used where necessary to describe the performance of the OLEDs fabricated as part of the present work.

1.3 The Role of Boron in Optoelectronic Materials

1.3.1 The Triarylboron Group

The triarylboron group is a powerful π-electron acceptor due to the empty p_π orbital on boron, which typically makes a large contribution to the LUMO of materials including this functional group. However, due to the electropositive nature of the boron atom, this substituent also acts as an inductive σ donor. Furthermore, the mesityl or tripyl (2,4,6-triisopropylphenyl) groups used to protect the boron center are also fairly electron-rich, and give rise to a characteristic absorption at approximately 350-370 nm due to π (Mes) → p (B) charge transfer in the UV-Vis spectrum of such triarylboranes. The empty p_π orbital also renders these compounds redox-active, allowing triarylboranes to undergo reversible reduction to form a stable radical anion.

Triarylboranes are also highly Lewis acidic, though bulky mesityl groups provide steric protection from most nucleophiles. However, small anions such as fluoride and cyanide are capable of binding to the boron center with remarkable selectivity despite these bulky groups, blocking the p_π orbital on boron. As this orbital is often a key contributor to the LUMO of the material, this binding event can be monitored by colorimetric, luminescent or electrochemical changes, and in this way triarylboranes have been successfully developed as highly sensitive chemical sensors for fluoride and cyanide.[5]

These same bulky mesityl groups also promote the formation of amorphous films with high glass transition temperatures, which can greatly improve the performance and long term stability of optoelectronic devices such as OLEDs by removing grain boundaries and promoting the formation of homogeneous films.[6] Finally, when paired with strong electron donors such as triarylamines in π-conjugated materials, triarylboranes show intense charge-transfer luminescence with quantum efficiencies often approaching unity.[7c] This donor-acceptor charge transfer results in a highly polarized excited state, giving materials that display strong solvatochromism and a large transition dipole moment, and making them useful nonlinear optical materials.

1.3.2 Photophysical Properties of Metal-Containing Triarylboranes

1.3.2.1 Enhancing Metal-to-Ligand Charge Transfer

Due to its role as a strong electron acceptor, the triarylboron group has been found to greatly facilitate metal-to-ligand charge transfer (MLCT) transitions in a variety of metal complexes. This has important implications for triarylboron-containing phosphorescent materials, as many of these emit either from a triplet MLCT state or one of mixed ligand centered (LC) and MLCT character. Functionalization with triarylboron in many cases thus results in 1) more intense MLCT absorption, 2) red-shifted absorption and emission bands due to lower-lying MLCT excited states, and 3) phosphorescence with greater MLCT

character, namely, greater sensitivity to solvent polarity, shorter decay lifetimes, and non-structured emission bands.[13] In some cases, the increased MLCT contribution to the emissive state facilitated by triarylboron has also resulted in enhanced phosphorescent quantum yields.

The observation that an arylboron functionality could enhance metal-to-ligand charge transfer was first made in 2001 by Chujo and Dixneuf, for a polymeric system prepared by hydroboration of a Ru(II) diacetylide with mesitylborane.[14] (Figure 1.5) The ruthenium monomer exhibited an intense absorption band at 373 nm in $CHCl_3$, which underwent a dramatic bathochromic shift to 514 nm when the boron center was introduced. This was ascribed to d_π-p_π conjugation between ruthenium and boron along the polymer backbone, and represented significant stabilization of the MLCT excited state by the boron centre. The same year, Chujo and coworkers reported similar polymers of Pt and Pd, and though the interaction between boron and the metal centers was less clear, both were found to exhibit green luminescence at room temperature.[15]

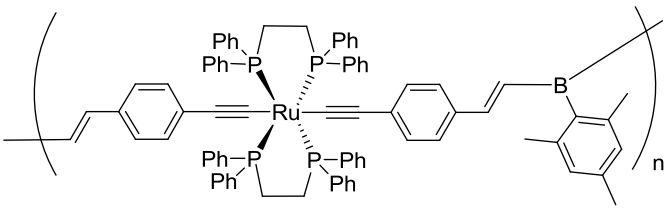

Figure 1.5: A ruthenium- and boron-containing polymer reported by Chujo and Dixneuf.

Further reports on this phenomenon began to appear in 2006, when Kitamura and coworkers noted that addition of a triarylboron group could enhance MLCT in the case of two Pt-terpyridine complexes linked with a boron center by either a phenyl or duryl bridge[16] (Figure 1.6). Incorporation of the boryl unit in **1.1** had a dramatic effect on the absorption spectrum of the molecule, resulting in nearly tenfold enhancement of the intensity of the MLCT absorption band over the simpler **1.3**. Furthermore, similar enhancement was not observed for **1.2**, which was found to have a larger dihedral angle between the duryl and

terpyridyl groups (84°) by X-ray crystallography, than that of **1.1** (26°), suggesting that effective conjugation with the boron center was necessary to achieve enhanced MLCT. Significantly, of the three complexes, only **1.1** was observably phosphorescent with a quantum yield of 0.011.

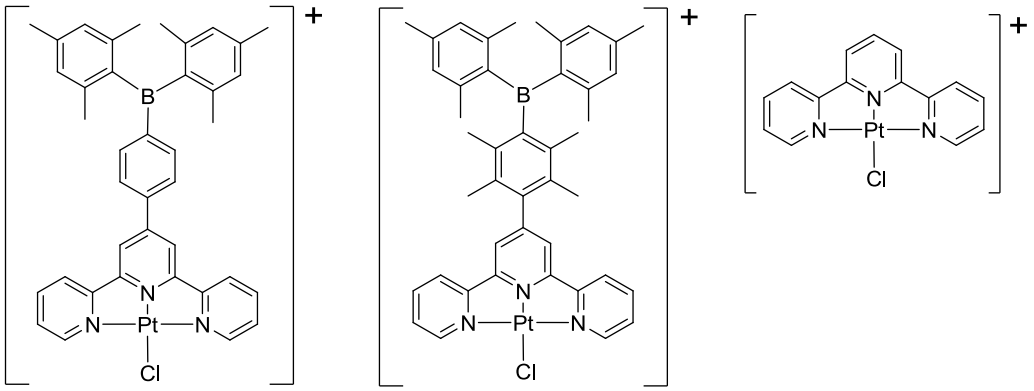

1.1 **1.2** **1.3**

Figure 1.6: Pt(II)-terpyridine complexes reported by Kitamura.

In the following year, our group reported Pt(II) and Cu(I) complexes of an *N^N* chelating 1-(2-pyridyl)-7-azaindolyl ligand (NPA), with remarkable properties.[17] The non-borylated ligand NPA forms an essentially non-emissive complex when coordinated to $PtPh_2$, with only very weak room-temperature phosphorescence. However, $PtPh_2$ or $[Cu(PPh_3)_2]^+$ complexes **1.4** and **1.5** of the corresponding 5-pyridyl-$BMes_2$ derivative are both brightly emissive in solution and the solid state at room temperature, exhibiting broad and featureless emission bands characteristic of MLCT phosphorescence (Figure 1.7). In fact, the Cu(I) complex of this ligand was found to exhibit the highest solid-state quantum yield of any Cu(I) complex reported to date (Φ = 0.88), demonstrating the potential of the triarylboron group for the preparation of bright phosphorescent materials. Shortly thereafter, Marder and Wong reported complex **1.6**, an arylboron-functionalized derivative of the well-known phosphor $Ir(ppy)_2(acac)$.[18] It was noted that the $BMes_2$ group stabilizes the MLCT state of **1.6**, shifting the emission maximum from 516 nm in the parent molecule to give bright red phosphorescence at 605 nm (Φ= 0.18).

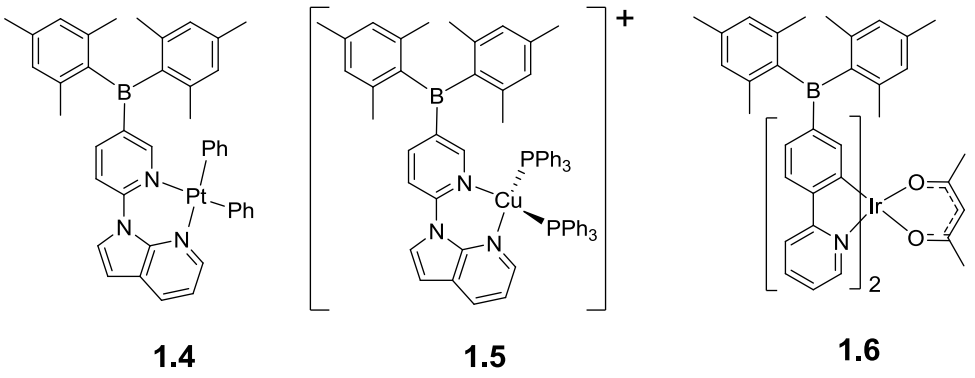

Figure 1.7: Pt(II) and Ir(III) complexes with boron-functionalized NPA and phenylpyridine ligands.

The impact of $BMes_2$ substitution on MLCT transitions was also observed in the *N^N*-chelate compounds based on 5,5'-$BMes_2$-2,2'-bipydine (5,5'-B2bpy) shown in Figure 1.8.[19] For example, the parent molecule of **1.7a**, Pt(bpy)Ph_2, has a yellow color with a MLCT band at ~440 nm in CH_2Cl_2 while **1.7a** has a deep red color with a broad and well resolved MLCT band at 525 nm.

1.3.2.2 Enhancing Electron-Accepting Ability by Metal Chelation

Highly Lewis acidic triarylboranes remain sought-after materials due to their potential for use as electron-transport materials in OLEDs and as sensors for anions. The preparation of sterically protected triarylboranes, however, presents a challenge, as the alkylated aryl groups typically employed to protect the boron center are themselves electron-rich. A number of strategies have been taken to address this, including functionalization of triarylboranes with cationic groups,[20] internal hydrogen-bond donors,[21] and the incorporation of multiple boron centers.[22] Alternatively, the boron centre may be attached to an electronegative aromatic heterocycle to enhance the electron-accepting ability of the molecule *via* inductive and π-conjugation effects.[7,19] With the appropriate choice of the heterocyclic group, it is possible to attach a metal ion to the triarylboron molecule *via* chelation or cyclometalation, which has been found to further improve the electron-accepting ability of triarylboranes by Coulombic and inductive effects.

This was demonstrated most impressively using 5,5'-B2bpy (Figure 1.8).[19] This ligand displays two fully reversible and similar reduction peaks at -1.69 and -2.07 V vs. $FeCp_2/FeCp_2^+$, indicative of sequential one-electron addition to each of the conjugated boron centers with much higher electron affinity compared to the biphenyl analogue.[22a] When coordinated to Pt(II) or Cu(I), the complexes display two similar and highly reversible reduction peaks. However, the first reduction potentials were observed to shift more than 300 mV to -1.34 V for $PtPh_2$ (5,5'-B2bpy) (**1.7a**) and -1.36 V for the $[Cu(PPh_3)_2$(5,5'-B2bpy)$]^+$ (**1.8**) complex. The replacement of $PtPh_2$ by $PtCl_2$ further shifts the reduction potential by ~170 mV to -1.17 V due to the much weaker σ donation by the chloride ion, thus demonstrating the high tunability of the electron affinity of the boryl group by ancillary ligands. This enhancement in electron-accepting ability can be attributed to extended conjugation with metal *d*-orbitals, resulting in a lower LUMO, as well as coordination of the ligand to a formally cationic metal center. A similar enhancement of electron accepting ability was also observed for the *N^N*-chelate compounds **1.4** and **1.5**, but was less pronounced than the 5,5'-B2bpy compounds. Furthermore, this enhancement in electron accepting ability has been found to greatly enhance the binding strength of the metal complexes with anions such as fluoride.

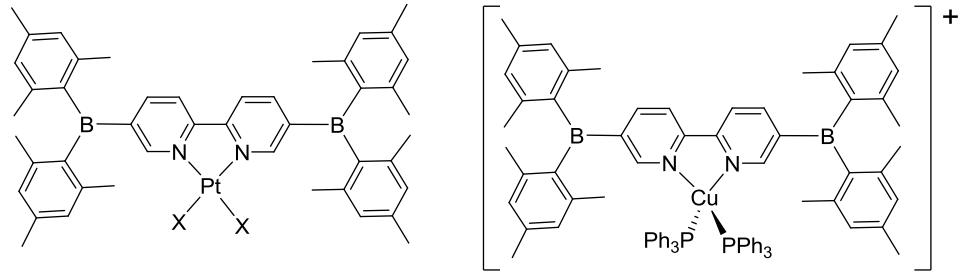

x = Ph, **1.7a**; Me, **1.7b**; Cl, **1.7c** **1.8**

Figure 1.8: Pt(II) and Cu(I) complexes of B2bpy.

1.3.2.3 The Impact of Ligand Structure

While the triarylboron group is capable of enhancing the electron-accepting ability and phosphorescent quantum yield of many metal complexes, the type of the ligand to which the boryl group is attached has a profound impact on the properties of these complexes as well. The most commonly used ligands for triarylboron functionalized metal complexes are *N^N*- and *N^C*-chelating, although one example of a '*C^C* chelate' $BMes_2$-functionalized Rh(III) "rhodacyclopentadiene" has recently been reported, which surprisingly exhibits intense fluorescence with high quantum yield (0.69).[23] 2,2'-bipyridine and 2-phenylpyridine are representative examples of *N^N*- and *N^C*-chelate ligands, and give remarkably different properties when coordinated to metal centres.

N^N'-chelate ligands: To date, a number of arylboron-functionalized bipyridine complexes have been prepared, though many of these compounds suffer from low emission efficiency due to the comparatively weak ligand field strength of the *N^N* chelate. The $BMes_2$-functionalized ligand in **1.7a** is a very weak emitter in solution and the solid state (Φ = 0.01 in CH_2Cl_2). Its Pt(II) complexes **1.7a-c** display weak phosphorescence only at 77 K, despite the presence of strong MLCT bands in their absorption spectra. To achieve highly phosphorescent *N^N* chelate complexes, it is possible to take advantage of the bright emission observed in donor-acceptor triarylboron molecules,[1] giving complexes with distinct ligand-centered charge-transfer luminescence. In contrast to the free ligand in **1.7a**, the ligand in complex **1.9a** (Figure 1.9) is brightly fluorescent with a quantum yield of 0.95.[19c] Its Pt(II) exhibits red room-temperature phosphorescence in solution, while complex **1.7a** is non-emissive. To examine the effect of extended conjugation and ligand geometry on the luminescent properties of these complexes, compounds **1.10**-**1.12** were prepared in our group.[19c] The acceptor-only complexes **1.10** and **1.11** do not have any ambient temperature phosphorescence in solution, while the donor-acceptor complex **1.12** is phosphorescent with λ_{max} at 577 nm, attributable to a donor-acceptor ^{3}LC transition. These examples

illustrate that incorporation of an internal donor group can facilitate phosphorescence in *N^N*-chelate triarylboron complexes, if the ligand field splitting energy at the metal centre is too low.

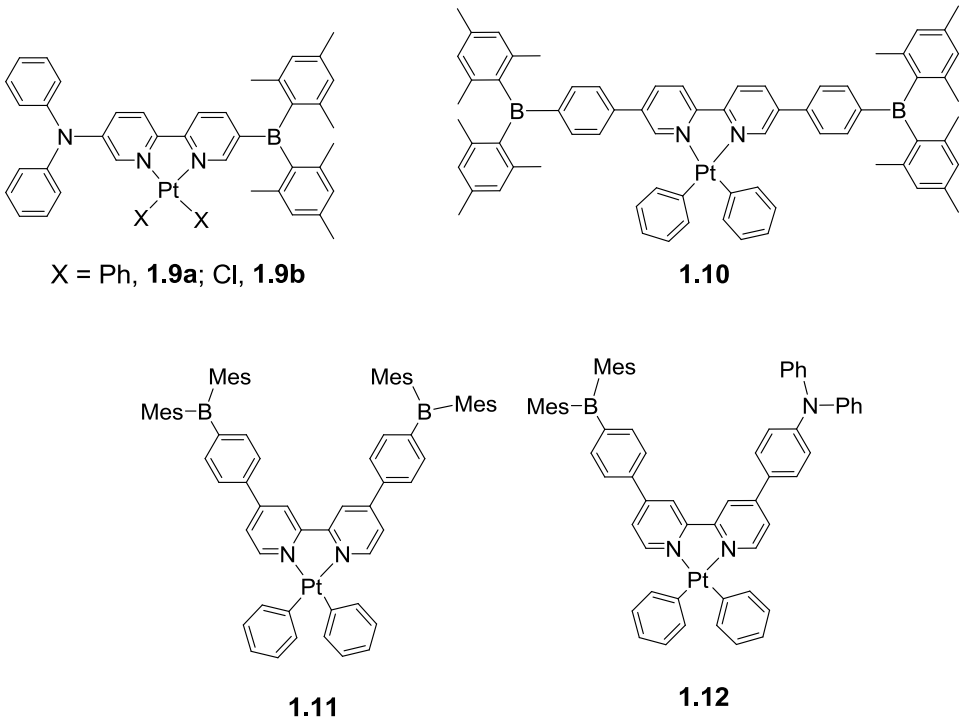

Figure 1.9: Acceptor-only and donor-acceptor Pt(II) complexes.

N^C-chelate ligands: N^C-chelate ligands such as 2-phenylpyridine (ppy) have been demonstrated by Thompson and others to be highly effective in preparing Pt(II) and Ir(III) complexes with bright phosphorescence at ambient temperature.[24] These ligands are excellent candidates for achieving highly phosphorescent metal complexes, as the phenyl anion is a strong σ-donor and the pyridyl group a strong π-acceptor, thereby providing a strong ligand field for the metal center on coordination. This helps to ensure that the non-emissive *d-d* excited states of the metal center are sufficiently higher in energy than the emissive states (^{3}LC and MLCT), minimizing non-radiative quenching and providing higher phosphorescent quantum yields.[12,13] The *d-d* states of *N^C* chelate complexes are typically higher in energy than those of comparable *N^N* chelate complexes, contributing to the higher luminescent quantum yields generally observed for the former.[12]

Due to the asymmetric nature of *N^C*-chelate ligands, the location of the arylboron group on the ligand can have a distinct impact on the properties of the molecule. Several studies have demonstrated that attachment of the boron moiety to an electronegative pyridyl group gives substantially lower reduction potentials compared to its attachment to a phenyl site.[25,26] In addition, the synergistic action of the triarylborane and pyridyl acceptors has been shown to promote metal-to-ligand charge-transfer, giving higher phosphorescent quantum yields than phenyl-substituted analogs in some cases. For example, examination of constitutional isomers **1.13** and **1.14** showed the reduction potential of **1.14** to be 140 to 200 mV more positive than that of **1.13**. This same phenomenon was later noted for the corresponding Pt(acac) complexes of boron-substituted phenylpyridines, which showed not only a greater electron affinity but also a much increased phosphorescent quantum yield for the pyridyl-functionalized isomer.[26]

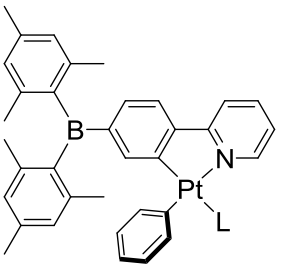

L = DMSO, **1.13a**; py, **1.13b**

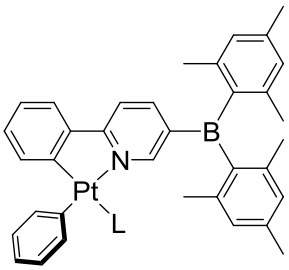

L = DMSO, **1.14a**; py, **1.14b**

1.4 Triarylboranes in OLEDs

Much of the research to date on both organic and metal-containing triarylboron compounds has concerned their use in OLEDs, due to their ability to function both as efficient electron-transport layers and emissive materials. This was first demonstrated by Shirota and coworkers in 1998, who successfully incorporated triarylboranes supported by a bi- or terthiophene backbone into OLEDs with Alq_3 as the emitting layer.[6a] These devices gave 10-20% higher luminous efficiencies and 60-80% higher maximum luminance relative to a reference device employing Alq_3 as both the emitter and ETL. (Figure 1.10)

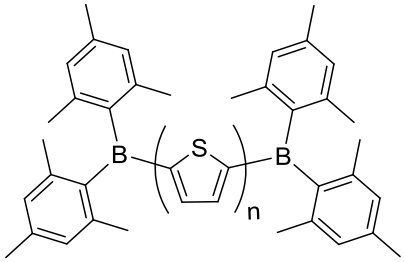

BMB-nT; n = 2,3

Figure 1.10: Electron-transport materials developed by Shirota.

It was later discovered that these compounds themselves showed bright blue emission.[6b] At the time, materials for the production of efficient red and green OLEDs were well-known, but blue emitters with high colour purity and long device lifetimes presented a problem, and still remain an active area of research today. Shirota thus demonstrated that these thiophene-boranes could be used as effective bifunctional emissive/electron-transport materials in OLEDs, exhibiting blue emission bands at λ_{max} = 446 and 472 nm with a maximum brightness of 1100 cd/m^2, luminous efficiency of 0.05 lm/W, and external quantum efficiencies reaching 0.17%. While poor by today's standards, these devices were at the time among the most efficient blue OLEDs reported in the literature,[27] and provided substantial motivation for further research on triarylboranes.

Shirota later recognized that since holes and electrons must recombine in the emissive layer, it can be advantageous to design emissive materials with bipolar character, such that they can support both reversible oxidation and reduction. With this in mind, he designed a series of π-conjugated amine-boranes that showed good hole and electron-transport properties.[6d] (Figure 1.11) These were successfully incorporated into efficient devices, with tunable emission colour from blue-green to yellow based on the extent of conjugation of the π-skeleton.

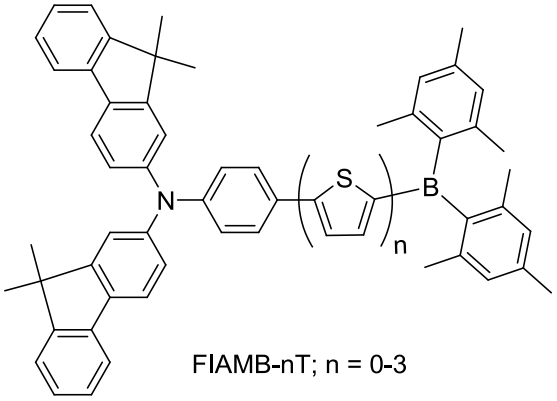

Figure 1.11: Bipolar fluorescent emitters designed by Shirota.

The body of work presented by Shirota then led to further research in our group on donor-acceptor triarylboranes as blue emitters for OLEDs. Preliminary investigations using either 2,2'-dipyridylamine or 7-azaindole as donors gave bright blue emitters, in some cases with quantum efficiencies approaching 100% in solution.[7a] When representative examples of these compounds were incorporated into OLEDs, it was demonstrated that they could function as both electron-transport and emissive materials. Though the device structures were not optimized, devices were successfully fabricated with moderate brightness and efficiency.

Following these studies, a bipolar molecule BNPB was designed as a trifunctional OLED material.[7c] This compound contains the well-known (1-naphthyl)phenylamino hole-transport functionality, as well as a triarylboron centre, to facilitate both hole and electron transport. (Figure 1.12) In addition, this compound in itself showed bright blue emission (Φ = 95% in THF solution, 31% in the solid state). This strategy allowed for the preparation of single-layer OLEDs, which would be both cheaper and simpler to fabricate than their triple-layer counterparts. It was demonstrated that this compound could indeed act as a monofunctional, bifunctional, or trifunctional material in electroluminescent devices, and while the most efficient devices studied remained those with a dedicated HTL and ETL, the proof of concept remained

significant nonetheless. Since this initial report, the device structure of BNPB-based OLEDs has been optimized considerably, giving devices that exhibit much higher brightness and maximum efficiencies.[7d]

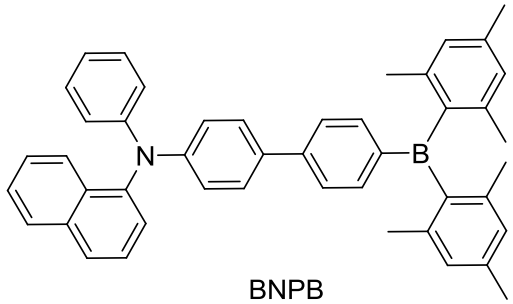

BNPB

Figure 1.12: BNPB, a trifunctional fluorescent OLED material.

Another important class of triarylboranes that have recently been examined for applications in OLEDs are those with a "starburst" topology, which typically show high glass transition temperatures and thus tend to cleanly form amorphous films during vacuum vapour deposition. Yamaguchi and coworkers have reported a series of starburst triarylboranes, and while they were not incorporated into organic devices, good colour tunability was achieved by substituting the π-skeleton of the material with either electron-donating or electron-withdrawing groups.[28] (Figure 1.13a) Shirota has successfully employed starburst triarylboranes as hole-blocking layers in OLEDs, which can be inserted between the ETL and EML to prevent holes from escaping the emissive layer.[29] Furthermore, a series of donor-acceptor tridurylboranes have been reported by our group,[7b] although the bulky duryl groups prevented effective conjugation of the donor and acceptor moieties, reducing emission efficiency and making these materials unsuitable for use in an ETL or EML. (Figure 1.13b) Nonetheless, these materials did show some promise as hole-transport materials, due to the presence of the peripheral triarylamine moieties. Finally, a starburst triarylborane recently reported by Kido (Figure 1.13c) has been used as an electron-transport layer in blue OLEDs with exceptional efficiencies, with reported EQEs as high as 21%.[30]

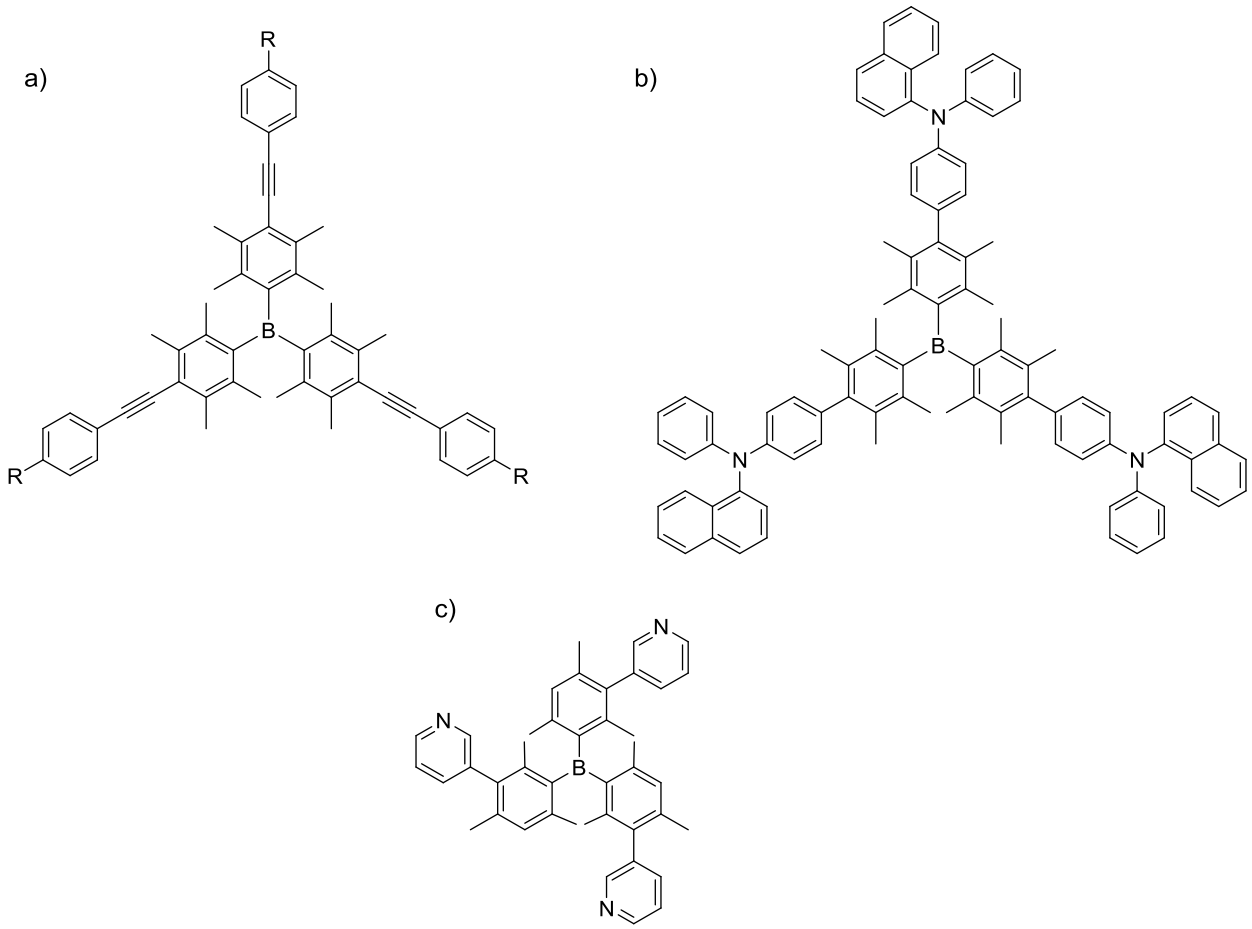

Figure 1.13: a) Starburst organoboranes prepared by Yamaguchi and coworkers (R = electron donating or withdrawing group). b) A donor-acceptor starburst compound prepared in our group. c) Electron-transporting triarylborane prepared by Kido and coworkers.

While the majority of the device-oriented research on triarylboranes thus far has focused on the development of fluorescent OLEDs, in recent years emphasis in OLED research on the whole has shifted to devices based on phosphorescent emitters, or PHOLEDs. Phosphorescent materials containing heavy atoms such as Ir and Pt are capable of harvesting both singlet and triplet excitons due to spin-orbit coupling, giving a maximum theoretical EQE of 100%. At the outset of this thesis work, however, only one example of a triarylboron-based red PHOLED has been reported in the literature based on iridium complex **1.6** (Figure 1.7).[18] This device displayed excellent performance, with a maximum luminance of 16148 cd/m^2, current efficiency of 10.3 cd/A and peak EQE of 9.4%. These results merited further

research, and have served as motivation for the work on phosphorescent boron-containing phosphors described herein.

1.5 Triarylboranes as Anion Sensors

To date the most significant driving force behind research into luminescent triarylboranes has been their development as chemical sensors for small anions such as fluoride and cyanide. Though low doses of fluoride can be found in drinking water, toothpaste, and drugs for osteoporosis, high doses of fluoride are toxic and can lead to skeletal fluorosis.[31] In addition, fluoride concentrations can serve as an indicator of uranium enrichment (*via* hydrolysis of UF_6) or the presence of sarin gas, which releases F^- on hydrolysis.[5d] However, the detection of fluoride in aqueous media remains a challenge due to the high hydration enthalpy of this anion (-504 kJ/mol).

Sterically hindered triarylboranes have emerged as a promising class of selective fluoride sensors, which readily form fluoroborates in organic solvents. These compounds are attractive sensors because the LUMO typically contains substantial boron *p* character, and is populated on fluoride binding. This produces responses that can be observed colorimetrically, electrochemically, or as changes in the emission spectrum of the sample. Though their use in water remained problematic for years, recent research has improved their utility in aqueous media substantially.

The use of organoboranes as fluoride sensors was first demonstrated by Tamao and coworkers in 2001, using a 10 μM solution of tris(9-anthryl)borane in THF.[32] This solution is orange in colour, and readily becomes colourless on addition of fluoride with a binding constant of 10^5-10^6 M^{-1}. (Figure 1.14) More remarkably, this compound exhibits a binding constant of only 10^3 M^{-1} with AcO^- and OH^-, and shows no response to Cl^-, Br^-, or I^- due to the steric crowding around the boron centre. Tamao later demonstrated that this binding event could be observed in emission mode, using a two-chromophore system including a

triarylboron centre and a porphyrin ring.[33] On fluoride addition, distinct changes in the absorption bands of both chromophores could be observed, with a switch in the fluorescent emission of the sample from red to pale blue. However, in both systems, the fluoride anion dissociates readily in the presence of water.

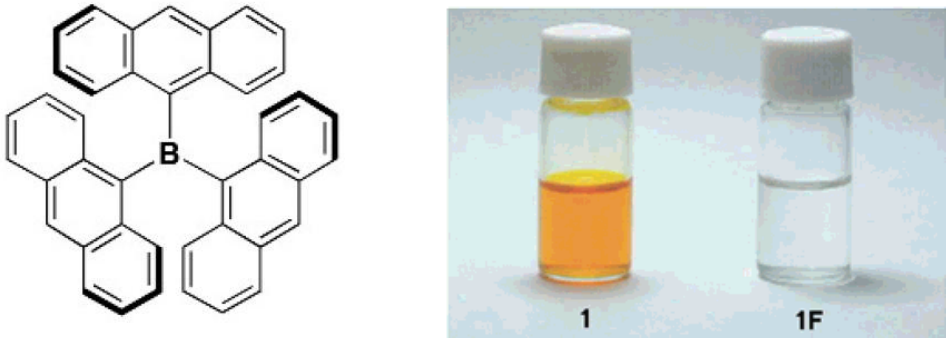

Figure 1.14: Left: the first triarylborane-based sensor for fluoride ions. Right: A solution of this compound before and after addition of F^- in THF.[21]

In recent years, extensive work by Gabbaï and coworkers has sought to overcome this limitation by increasing the binding constant between the organoborane sensor and the fluoride anion. One early approach by this group was to synthesize chelating diboranes, with B-B separation distances on the order of 3.2-3.4 Å.[34] These compounds were found to bind fluoride with a binding constant of 5×10^9 M^{-1} in THF, approximately 1000 times that of the simple borane $BMes_3$, but were unstable to the addition of water.

At present, the most useful strategy for increasing the boron-fluoride binding constant has proven to be the synthesis of cationic boranes. Functionalization of triarylboranes with ammonium[21] or phosphonium[20a,b] groups has not only been shown to improve the solubility of the sensors in aqueous media, but has also given molecules that can detect fluoride in biphasic ($H_2O/CHCl_3$) or mixed organic solutions with high water content (60:40 H_2O/DMSO v/v). In a recent study, Gabbaï reported a cationic phosphonium-borane capable of detecting fluoride in pure water down to the maximum contaminant level set by the US Environmental Protection Agency (4 ppm), as detected by complete quenching of the

lowest energy absorption band in the UV-visible spectrum of the sensor.[20c,d] The most effective detection was achieved when the pH of the sample was buffered to 4.9, since HF formation becomes significant as the pH is lowered, and hydroxide binding to the boron centre becomes competitive as the pH is raised. This study represents the most successful report to date of the detection of fluoride using triarylboranes in aqueous media. (Figure 1.15)

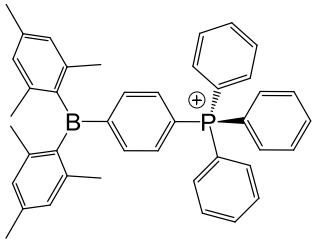

Figure 1.15: Structure of a phosphonium-borane capable of fluoride detection below 4 ppm in aqueous media.

The sensors discussed so far, however, typically only respond with quenching of either the absorbance or the emission of the sample. For practical reasons, it is desirable to design systems with an activated, or "turn-on" response to the analyte of interest. Our group has demonstrated that this can be achieved using nonconjugated chromophores separated by either rigid naphthyl or nonrigid silane linkers.[35] (Figure 1.16) In the absence of fluoride, the emission of the sample on UV excitation occurs due to through-space charge transfer, as confirmed by DFT calculations and the synthesis of control compounds containing only one of the two types of chromophore. When fluoride is added, the boron centre is blocked, and emission simply occurs from the chromophore that does not contain the fluoride binding site.

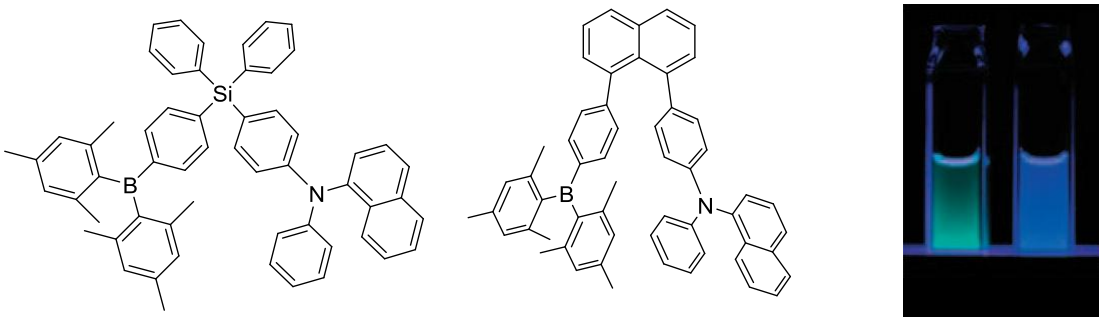

Figure 1.16: "Switch-on" sensors for fluoride synthesized by Wang and coworkers. The silane shown exhibits green fluorescence in solution, which readily switches to blue on fluoride addition.

Transition metal-containing triarylboranes offer the advantage of long lived phosphorescence that minimizes interference from background fluorescence or scattering in sensing applications. In addition, transition metal compounds offer new possibilities for redox-active sensors, in which the analyte binding event triggers a redox event observable electrochemically or by visible color change. Nonetheless, the high sensitivity of phosphorescence toward oxygen certainly hinders the use of many metal complexes in practical sensing applications in emission mode.

Phosphorescent chemosensors for fluoride were first reported by Melaïmi and Gabbaï, who prepared a heteronuclear bidentate Lewis acid containing a "B/Hg chelate" site for F^- (**1.15**),[36] shown in Figure 1.17. As the fluorophilicity of mercury had been recently demonstrated, the synergistic action of the boron and mercury Lewis acidic sites was proven capable of binding fluoride with a binding constant *K* of 2.3 (± 0.2) x 10^3 M^{-1} in 9:1 THF:H_2O. This binding constant was impressive given that the binding constant for $BMes_3$ was observed to be only 1.0 ± 0.3 in the same solvent, given the high hydrogen bond enthalphy for fluoride. Furthermore, while **1.15** showed red phosphorescence at 77K in the solid state, the phosphorescence of the fluoride adduct of this species was green due to the disruption of π conjugation at boron.

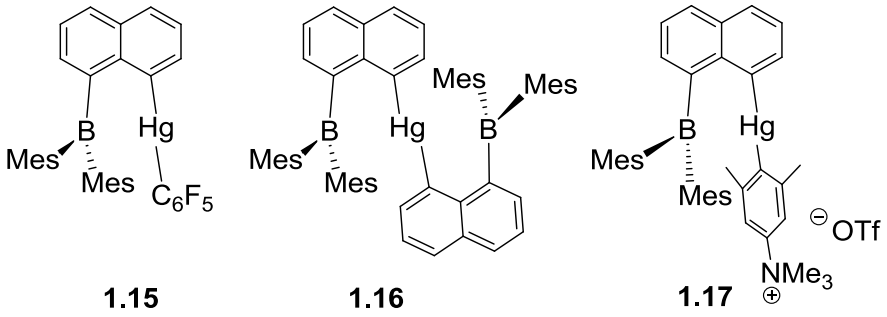

Figure 1.17: Heteronuclear B-Hg chelates developed by Gabbaï.

It was later demonstrated[37] that still higher binding constants could be achieved by addition of multiple boron centers to the sensor molecule (**1.16**), or by combining this chelate effect with favorable Coulombic interactions (**1.17**).[38] (Figure 1.17) The cationic -NMe_3^+ group in **1.17** increased the stability constant with fluoride by a factor of nearly 500 over the -NMe_2 derivative, with a binding constant of 6.2 x 10^4 M^{-1} vs 1.3 x 10^2 M^{-1} for the neutral species in 9:1 THF/H_2O.

Further colorimetric sensors were then demonstrated from complexes of Re(I), Pt(II), and Ir(III). Yam and coworkers reported fluoride sensing recently based on to date the only triarylboron-containing complexes of rhenium(I).[39] (**1.18**, Figure 1.18) While this compound displayed some phosphorescence in degassed solution, the complex proved to be most effective as a colorimetric sensor for F^-, with a color change from light yellow to dark red on addition of fluoride. This was attributed to the improved donor strength of the alkynyl ligand on fluoride binding, which raises the Re(I) *d* orbital energy and reduces the optical band gap.

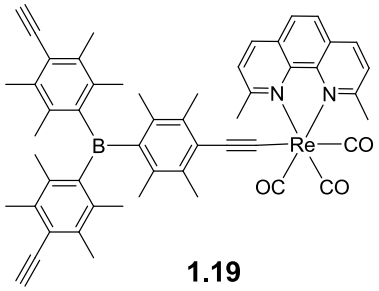

1.19

Figure 1.18: A Re(I)-triarylborane reported by Yam.

Several achievements in chemical sensing have also been made using a triarylboron-containing complex by taking advantage of the high Φ_P typical of many cyclometalated phosphorescent Ir(III) complexes. In 2008 You and Park reported a bis-cyclometalated Ir(III) complex **1.20**[40] (Figure 1.19) similar to that reported for use in OLEDs by Marder and Wong[18] (**1.6**, Figure 1.7). This compound had a high quantum yield of 0.57 in solution and 0.17 in solid PMMA film, exhibiting bright blue-green phosphorescence. Titration with fluoride resulted in a switch in emission colour to orange, as well as a red shift in the

absorption spectrum. Importantly, using the long-lived phosphorescence decay lifetime of the complex, the authors were able to separate the emission of the sensor from that of intentional fluorescent impurities by time-gated detection. Also, the authors noted that while detection of F^- in water using sensors such as these is difficult, this problem may be circumvented by evaporating a droplet of analyte solution on a PMMA film doped with **1.20**, producing a photoluminescent response in the solid state.

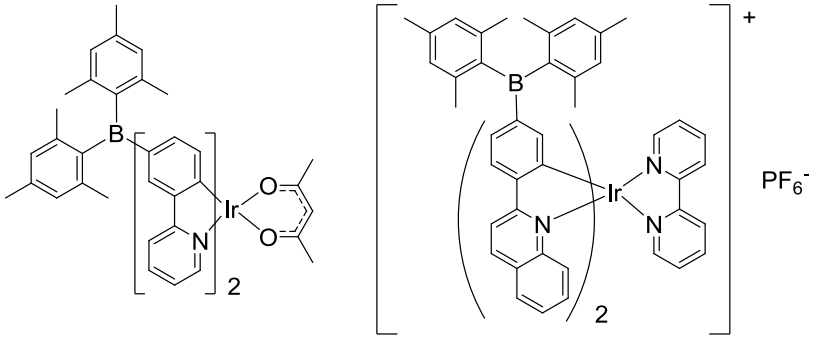

Figure 1.19: Ir(III)-triarylboranes used for fluoride sensing.

In the same year, a cationic iridium complex **1.21** functionalized by triarylboron was reported by Li and coworkers, containing a boron-functionalized phenylquinoline cyclometalating ligand.[41] This complex was found to exhibit red phosphorescence, with a quantum yield of 0.49 in degassed organic solution or 0.17 when aerated. This emission could readily be quenched on addition of fluoride. This compound was further capable of acting as a colorimetric sensor, by colour change from yellow to orange on fluoride addition.

Two recent reports have also shown that Coulombic and inductive effects can act together to increase the fluoro- or cyanophilicity of a boron centre in cationic complexes of Ru(II). The cyclometalated Ru(II) complex **1.22** (Figure 1.20) is capable of detecting both fluoride and cyanide in absorption mode, as addition of either anion causes a red shift in the MLCT band typical of Ru(II) bipyridines.[42] In this case

the LUMO was found to reside primarily on the bipyridine ligands, while the Ru *d* orbitals and the phenylpyridine chelate made the largest contributions to the HOMO. Binding of F^- or CN^- thus made the HOMO of this molecule more electron-rich, reducing the optical band gap. Our group has recently reported a series of diboryl Ru(II) complexes with linear and bent 2,2'-bpy ligands (Figure 1.20), capable of detecting F^- and CN^- in phosphorescent as well as absorption mode (**1.23**, **1.24**).[43] In this case, the boron-containing *N^N* chelate ligand was found to introduce a low energy MLCT state to the complex, giving these compounds distinct red phosphorescence. On addition of fluoride or cyanide, however, the LUMO switched from being localized on the boryl-functionalized bpy chelate to the nonborylated bpy ligands, producing orange phosphorescence typical of $[Ru(bpy)_3]^{2+}$ from an MLCT state at higher energy. Interestingly, while most triarylboranes exhibit higher binding constants with fluoride over cyanide, the Ru(II)-based sensors exhibited higher sensitivity to CN^- in both reports.

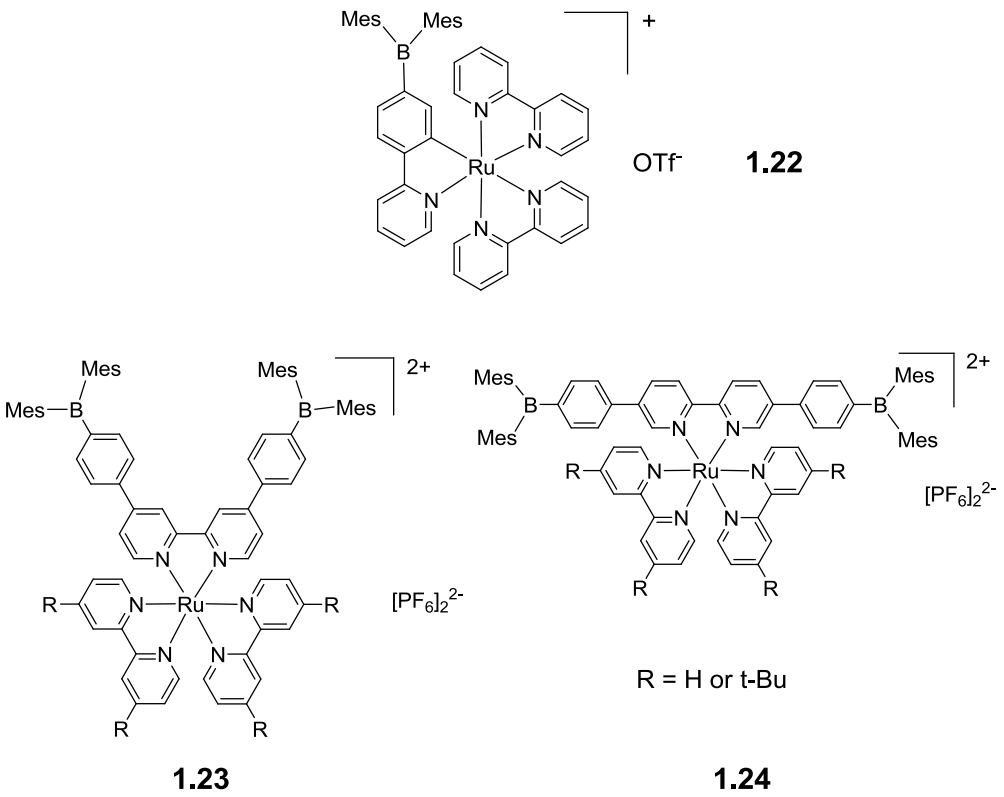

Figure 1.20: Boron-functionalized Ru(II) complexes used for detection of fluoride.

Selective anion sensing that relies on the change of electrochemical properties of a boron-functionalized metal compound is another highly effective but much less explored approach. An ideal system for such studies should have a redox active metal center that is stable under ambient conditions and strongly coupled to the triarylborane receptor electronically. Strong π-conjugation and pronounced electronic communication between a triarylboron center on a cyclopentadienyl (Cp) ring and an iron(II) center in ferrocenyl (**1.25**) or poly(ferrocenylene) compounds (**1.26**, Figure 1.21) was reported by Jäkle, Holthausen, Wagner and coworkers in 2006.[44a] The attachment of the boryl group to the ferrocene was found to positively shift the first oxidation potential by 0.196 V (**1.25a**) and 0.045 V (**1.25b**), due to the π-electron withdrawing nature of the $BMes_2$ group. This observation is important because of the implication that any event such as anion binding that leads to the disruption of the π-conjugation with the boryl group can cause a negative shift of the ferrocene oxidation potential.

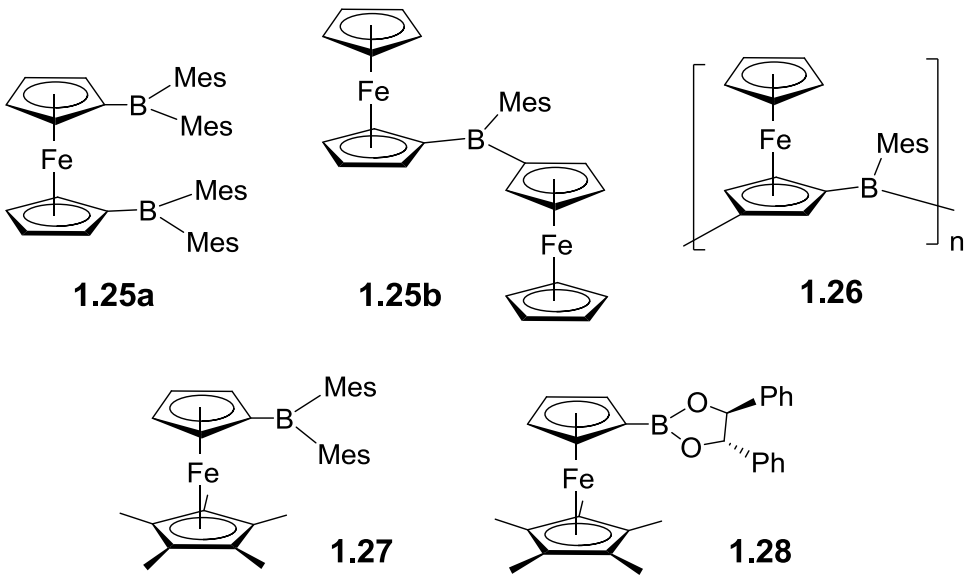

Figure 1.21: Boron-functionalized ferrocenes.

Anion sensing using this method has since been demonstrated by Aldridge and coworkers. They have shown that the presence of fluoride or cyanide can be differentiated using ferrocenyl-boranes such as **1.27**

and **1.28** (Figure 1.21) as redox-active sensors.[44b] Compound **1.27** can be oxidized at a potential of -176 mV relative to the ferrocene/ferrocenium couple. When bound to fluoride or cyanide, however, this oxidation occurs more readily, at a potential of ca. -700 mV. By adding a redox-active dye (in this case, tetrazolium violet) capable of oxidizing the bound species but not the free receptor, a colorimetric change can be observed on binding to fluoride or cyanide. This group also designed a weaker receptor **1.28** that binds only to fluoride, such that cyanide will not trigger a response from the dye. Using both sensors in tandem, they were thus able to detect and differentiate the presence of fluoride or cyanide using AND/NOT logic.

1.6 Other Optoelectronic Applications of Triarylboranes

1.6.1 Photochromic Boron Compounds

Four-coordinate mesitylboranes were first reported by Yamaguchi, who used thienylthiazole as a scaffold for intermolecular N→B coordination.[45] These compounds showed moderate fluorescence quantum yields and good electron-transport capability, but their stabilities were not discussed. Shortly thereafter, our group prepared similar materials based on a 2-phenylpyridine scaffold, which display bright fluorescence in solution.[46] (Figure 1.22) More remarkably, however, the emission of the solution gradually decreases on prolonged UV irradiation, eventually producing a colourless, non-emissive sample. When the sample is degassed and kept under an inert atmosphere, however, the sample turns nearly black.

It was later elucidated by extensive 2D NMR studies that a unique rearrangement reaction occurs on photoexcitation, causing these materials to react cleanly to give the bicycloboranes shown in Figure 1.22. The mechanism of this reaction is still unknown, though the sample is ESR silent at 298 and 77K, ruling out the existence of a radical product. This reaction is accompanied by the appearance of broad absorption bands covering the entire visible spectrum, giving bluish-black or greenish-black solutions. Furthermore,

this reaction is fully thermally reversible under N_2, giving the dimesitylboryl-phenylpyridine on heating or extended standing at room temperature.

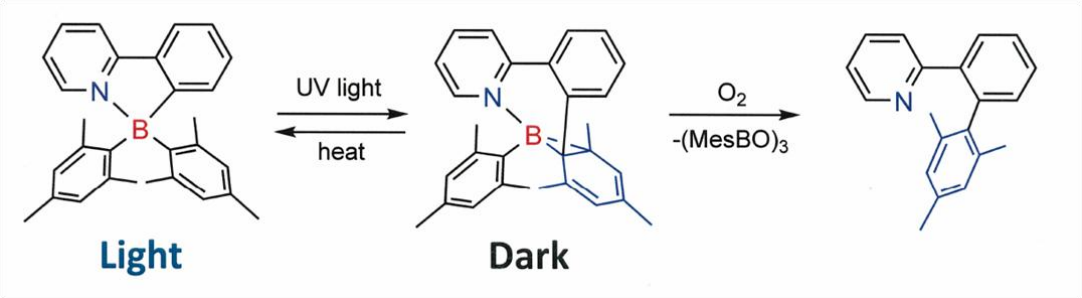

Figure 1.22: The photoisomerization of four-coordinate arylboranes.

This transformation is truly remarkable, and is currently an active area of research in our group. Further studies have obtained crystallographic evidence for this transformation,[47] and have provided insights as to how this photoisomerization reaction may be modified and kinetically controlled.[48] As this work is outside the scope of this thesis, the interested reader is directed to several recent reviews detailing progress in this area.[49]

1.6.2 Boron-Containing Metal-Organic Frameworks (MOFs)

Metal-organic frameworks have attracted considerable interest as extended functional networks, with applications in diverse fields such as gas storage, chemical sensing, and catalysis.[50] In 2008, the first examples of triarylboron-containing MOFs were reported, using the C_3-symmetric ligand **1.29** (Figure 1.23) as a rigid, π-conjugated linker.[51] It is known that octupolar chromophores may be prepared from molecules with trigonal symmetry, and such compounds are promising for applications in nonlinear optics (NLO).[52] Furthermore, ligand **1.29** exhibits axial chirality based on the hindered rotation of the bulky aromatic groups about the B centre. MOFs from **1.29** could be readily prepared by coordination to Cd(II), Cu(II) or Co(II), with each metal atom coordinated to three pyridine groups and each ligand to three metal centers. Interestingly, partial enantiomeric resolution of racemic **1.29** was found to occur on

formation of single crystals of these MOFs, inducing greater asymmetry and octupolarity in the extended network. Also, the NLO activity of the frameworks could readily be tuned by crystallization with various counter anions. Most importantly, these MOFs showed a significant second-harmonic generation NLO response up to 35 times that of α-quartz, highlighting the potential of incorporating triarylboron compounds into coordination networks as multidentate ligands.

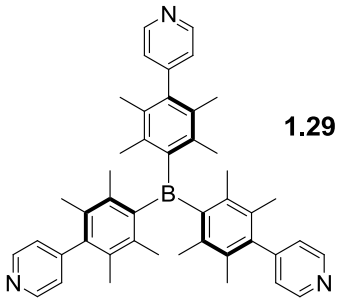

1.29

Figure 1.23: A trigonal linker used for the preparation of boron-containing MOFs.

1.6.3 Triarylboron Compounds as Sensors for Zn(II)

Sensitive and selective chemical sensors for Zn(II) are highly sought after due to the many biological roles this ion plays. Furthermore, many diseases such as epilepsy, Parkinson's, and Alzheimers are characterized by abnormal Zn(II) metabolism, further motivating research in this field.[53] Polypyridine ligands have emerged as an important class of luminescent sensors for Zn(II),[54] and due to the highly emissive nature of many triarylborane-functionalized polypyridine ligands, they may be useful in sensing Zn(II) ions. Our group recently investigated the spectral response of several triarylboron-functionalized compounds to this ion.[19c] Of the three ligands investigated, all form 2:1 tetrahedral complexes with Zn(II) when titrated with $Zn(ClO_4)_2$ in THF solution (**1.30** – **1.32**, Figure 1.24). Furthermore, the observed spectral changes were found to vary considerably depending on the nature of the ligand substituents as well as molecular geometry. All three ligands give colorless THF solutions, which give bright blue luminescence under a handheld UV lamp. This emission is quenched on addition of Zn(II) to form complexes **1.31** and **1.32**. However, the formation of complex **1.30** induces a 40 nm red shift in the

emission spectrum, causing the fluorescence of the sample to switch from deep blue to sky blue when Zn(II) is added. The overall binding constants with Zn(II) ions for all three ligands are on the order of 10^{11} M^{-2}, similar to those of other recently reported bipyridine derivatives.[54] Though the mechanism of this color change is not yet fully understood, the enhancement or disruption of donor-acceptor charge transfer luminescence by metal ion binding is a promising avenue for further research in chemical sensing.

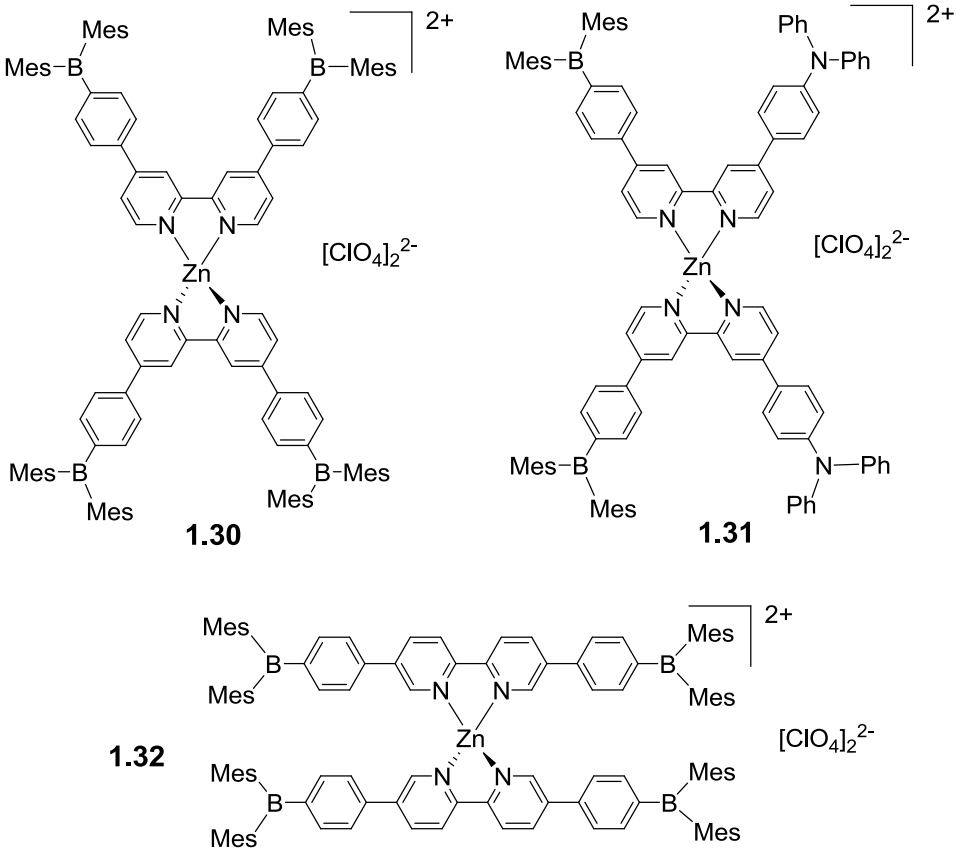

Figure 1.24: Triarylboron-functionalized Zn(II) complexes.

1.7 Scope of this Thesis

The work described in this thesis focuses on the development of luminescent triarylboron-containing compounds for optoelectronic applications, with emphasis on triarylboron-functionalized complexes of Pt(II). The work described herein will also address problems of interest in closely related fields, including the efficient synthesis of cyclometalated Pt(II) complexes and the development of efficient and simplified OLED structures.

Chapter 2 describes the preparation of a boron-functionalized Pt(II) complex capable of singlet-triplet dual emission at ambient temperature. Both emission colours in this molecule were found to be switchable on addition of fluoride, giving a single material capable of several emission modes. Chapter 3 describes the synthesis and ion-binding properties of a nonconjugated two-chromophore triarylborane, switchable between three emissive states by addition of fluoride ions or protic acid. Chapter 4 describes in detail our efforts to prepare boron-functionalized Pt(II) complexes with improved quantum yield, electron-transporting properties, and film-forming ability for the fabrication of highly efficient platinum-based OLEDs. Chapter 5 describes our investigations into the photophysical properties of Pt(II) complexes containing a nonconjugated triarylboron-containing second chromophore. Chapter 6 describes the development of an efficient one-pot synthesis of cyclometalated Pt(II) β-diketonates, using only stoichiometric reagents at ambient temperature. Chapter 7 describes the preparation of triarylboron-functionalized *C^C* chelate Pt(II) complexes and their use in OLEDs. Chapter 8 details the synthesis of *N*-heterocyclic carbazole-based host materials, which were used in the fabrication of highly efficient and simplified single-layer OLEDs. Finally, Chapter 9 reports the discovery of a vapochromic triarylboron-containing Pt(II) complex, which has been examined in detail by optical and multinuclear solid-state NMR spectroscopy.

1.8 Notes and References

The work described in this chapter includes contributions from the following publications:

- Z. M. Hudson, S. Wang, *Acc. Chem. Res.*, **2009**, *42*, 1584.
- Z. M. Hudson, S. Wang, *Dalton Trans.*, **2011**, *40*, 7805-7816.

References:

(1) a) J. C. Doty, B. Babb, P. J. Grisdale, M. E. Glogowski, J. L. R. Williams, *J. Organomet. Chem.* **1972**, *38*, 229. b) M. E. Long, J. Lumin. **1978**, *9*, 177. c) M. E. Glogowski, J. L. R. Williams, *J. Organomet. Chem.* **1981**, *216*, 1. d) W. Kaim, A. Shultz, *Angew. Chem. Int. Ed. Engl.* **1984**, *23*, 615. e) A. Shultz, W. Kaim, *Chem. Ber.* **1989**, *122*, 1863. e) C. D. Entwistle, T. B. Marder, *Angew. Chem., Int. Ed.* **2002**, *41*, 2927. f) C. D. Entwistle, T. B. Marder, *Chem. Mater.* **2004**, *16*, 4574. g) S. Yamaguchi, A. Wakamiya, *Pure Appl. Chem.*, **2006**, *78*, 1413. h) R. Stahl, C. Lambert, C. Kaiser, R. Wortman, R. Jakober, *Chem. Eur. J.* **2006**, *12*, 2358. i) Z. M. Hudson, S. Wang, *Acc. Chem. Res.*, **2009**, *42*, 1584. j) F. Jäkle, *Chem. Rev.* **2010**, *110*, 3985.

(2) For example, see: a) D. W. Stephan, *Dalton Trans.* **2009**, 3129. b) D.W. Stephan G. Erker, *Angew. Chem. Int. Ed.* **2010**, *49*, 46.

(3) a) C. Fan, L. G. Mercier, W. E. Piers, M. Parvez, *J. Am. Chem. Soc.* **2010**, *132*, 9604. b) K. Huynh, J. Vignolle, T. D. Tilley, *Angew. Chem. Int. Ed.* **2009**, *48*, 2835. c) C. Fan, W. E. Piers, M. Parvez, *Angew. Chem. Int. Ed.*, **2009**, *48*, 2835.

(4) a) Z. Yuan, N. J. Taylor, T. B. Marder, I. D. Williams, S. K. Kurtz, L.-T. Cheng. *J. Chem. Soc., Chem. Commun.* **1990**, 1489. b) M. Lequan, R. M. Lequan, K. Chane-Ching, J. Mater. Chem. **1991**, *1*, 997. c) Z. Yuan, N.J. Taylor, R. Ramachandran, T.B. Marder. *Appl. Organomet. Chem.*, **1996**, *10*, 305. d) M. Charlot, L. Porrès, C.D. Entwistle, A. Beeby, T.B. Marder, M. Blanchard-Desce, *Phys. Chem. Chem. Phys.*, **2005**, ***7***, 600. e) Z. Yuan, J. C. Collings, N. J. Taylor, T. B. Marder, C. Jardin, J.-F. Halet, J. *Solid State Chem.* **2000**, *154*, 5. f) Z. Yuan, C. D. Entwistle, J. C. Collings, D. Albesa-Jové, A. S. Batsanov, J. A. K. Howard, H. M. Kaiser, D. E. Kaufmann, S.-Y. Poon, W.-Y. Wong, C. Jardin, S. Fathallah, A. Boucekkine, J.-F. Halet, N. J. Taylor, T. B. Marder, *Chem. Eur. J.*, **2006**, *12*,

2758. g) J. C. Collings, S.-Y. Poon, C. Le Droumaguet, M. Charlot, C. Katan, L. O. Palsson, A. Beeby, J. A. Mosely, H. M. Kaiser, D. Kaufmann, W.-Y. Wong, M. Blanchard-Desce, T. B. Marder, *Chem. Eur. J.*, **2009**, *15*, 198.

(5) a) S. Yamaguchi, T. Shirasaka, S. Akiyama, K. Tamao, *J. Am. Chem. Soc*., **2002**, *124*, 8816. b) Y. Kubo, M. Yamamoto, M. Ikeda, M. Takeuchi, S. Shinkai, S. Yamaguchi, K. Tamao, *Angew. Chem. Int. Ed.* **2003**, *42*, 2036. c) C. R. Wade, A. E. J. Broomsgrove, S. Aldridge, F. P. Gabbaï *Chem. Rev.* **2010**, *110*, 3958, references therein. d) T. W. Hudnall, C. W. Chiu, F. P. Gabbaï, *Acc. Chem. Res.* **2009**, *42*, 388.

(6) a) T. Noda, Y. Shirota, *J. Am. Chem. Soc.*, **1998**, *120*, 9714. b) T. Noda, H. Ogawa, Y. Shirota, *Adv. Mater.*, **1999**, *11*, 283. c) Y. Shirota, M. Kinoshita, T. Noda, K. Okumoto, T. Ohara, *J. Am. Chem. Soc*., **2000**, *122*, 11021. d) H. Doi, M. Kinoshita, K. Okumoto, Y. Shirota, *Chem. Mater*., **2003**, *15*, 1080. e) Y. Shirota, *J. Mater. Chem.*, **2005**, *15*, 75.

(7) a) W. L. Jia, D. R. Bai, T. McCormick, Q. D. Liu, M. Motala, R. Wang, C. Seward, Y. Tao, S. Wang, *Chem. Eur. J.*, **2004**, *10*, 994. b) W. L. Jia, M. J. Moran, Y. Y. Yuan, Z. H. Lu, S. Wang, *J. Mater. Chem.*, **2005**, *15*, 3326. c) W. L. Jia, X. D. Feng, D. R. Bai, Z. H. Lu, S. Wang, G. Vamvounis, *Chem. Mater.*, **2005**, *17*, 164. d) F. H. Li, W. L. Jia, S. Wang, Y. Q. Zhao, Z. H. Lu, *J. Appl. Phys.* **2008**, *103*, 034509/1.

(8) a) M. E. Thompson, *MRS Bulletin*, **2007**, *32*, 694, references therein. b) K. Chen, C. H. Yang, Y. Chi, C. S. Liu, C. H. Chang, C. C. Chen, C. C. Wu, M. W. Chung, Y. M. Cheng, G. H. Lee, P. T. Chou, *Chem. Eur. J.* **2010**, *16*, 4315. c) Y. Chi, P. T. Chou, *Chem. Soc. Rev*., **2010**, *39*, 638.

(9) J. R. Lakowicz, *Principles of Fluorescence Spectroscopy*, 2nd ed., chapter 20, p. 573, Kluwer Academic, New York, 1999.

(10) a) D. E. J. G. J. Dolmans, D. Fukumura, R. K. Jain. *Nature Review*, **2003**, *3*, 380. b) A. Pfister, G. Zhang, J. Zareno, A. F. Horwitz , C. L. Fraser, *ACS Nano*, **2008**, *2*, 1252.

(11) C. W. Tang, S. A. VanSlyke, *Appl. Phys. Lett.*, **1987**, *51*, 913.

(12) a) S. R. Forrest, D. D. C. Bradley, M. E. Thompson, *Adv. Mater*. **2003**, *15*, 1043. b) J. A. G Williams, S. Develay, D. L. Rochester, L. Murphy, *Coord. Chem. Rev.*, **2008**, *252*, 2596.

(13) Y. You, S. Y. Park, *Dalton Trans.* **2009**, 1267.

(14) N. Matsumi, Y. Chujo, O. Lavastre, P. H. Dixneuf, *Organometallics*, **2001**, *20*, 2425.

(15) F. Matsumoto, N. Matsumi, Y. Chujo, *Polym. Bull.* **2001**, *46*, 257.

(16) E. Sakuda, A. Funahashi, N. Kitamura, *Inorg. Chem.*, **2006**, *45*, 10670.

(17) S. B. Zhao, T. McCormick, S. Wang, *Inorg. Chem.*, **2007**, *46*, 10965.

(18) G. J. Zhou, C. L. Ho, W. Y. Wong, Q. Wang, D. G. Ma, L. X. Wang, Z. Y. Lin, T. B. Marder, A. Beeby, *Adv. Funct. Mater.*, **2008**, *18*, 499.

(19) a) Y. Sun, N. Ross, S.-B. Zhao, K. Huszarik, W.-L. Jia, R.-Y. Wang, D. Macartney, S. Wang, *J. Am. Chem. Soc*., **2007**, *129*, 7510. b) Y. Sun, S. Wang, *Inorg. Chem.*, **2009**, *48*, 3755. c) Y. Sun, S. Wang. *Inorg. Chem.*, **2010**, *49*, 4395.

(20) a) C.-W. Chiu, F. P. Gabbaï, *J. Am. Chem. Soc.*, **2006**, *128*, 14248. b) T. W. Hudnall, F. P. Gabbaï, *J. Am. Chem. Soc.*, **2007**, *129*, 11978. c) M. H. Lee, T. Agou, J. Kobayashi, T. Kawashima, F. P. Gabbaï, *Chem. Commun.*, **2007**, 1133. d) T. W. Hudnall, Y.-M. Kim, M. W. P. Bebbington, D. Bourissou, F. P. Gabbaï, *J. Am. Chem. Soc.*, **2008**, *130*, 10890.

(21) T. W. Hudnall, M. Melaïmi, F. P. Gabbaï, *Org. Lett.* **2006**, *8*, 2747.

(22) a) A. Schulz, W. Kaim, W. *Chem. Ber.* **1989**, *122*, 1863. b) S. Yamaguchi, S. Akiyama, K. Tamao, *J. Am. Chem. Soc.*, **2000**, *122*, 6335. c) S.-B. Zhao, P. Wucher, Z. M. Hudson, T. M. McCormick, X.-Y. Liu, S. Wang, X.-D. Feng, Z.-H. Lu, *Organometallics*, **2008**, *27*, 6446.

(23) A. Steffen, M. G. Tay, A. S. Batsanov, J. A. K. Howard, A. Beeby, K. Q. Vuong, X.-Z. Sun, M. W. George, T. B. Marder, *Angew. Chem. Int. Ed.*, **2010**, *49*, 2349.

(24) S. Lamansky, P. Djurovich, D. Murphy, F. Abdel-Razzaq, H.-E. Lee, C. Adachi, P. E. Burrows, S. R. Forrest, M. E. Thompson, *J. Am. Chem. Soc.*, **2001**, *123*, 4304.

(25) Y.-L. Rao, S. Wang. *Inorg. Chem.*, **2009**, *48*, 7698.

(26) Z. M. Hudson, C. Sun, M. G. Helander, H. Amarne, Z.-H. Lu, S. Wang, *Adv. Funct. Mater.*, **2010**, *20*, 3426.

(27) a) Y. Hamada, C. Adachi, T. Tsutsui, S. Saito, *Jpn. J. Appl. Phys.* **1992**, *31*, 1812. b) J. Kido, M. Kimura, K. Nagai, Chem. Lett. **1996**, 47.

(28) S. Yamaguchi, T. Shirasaka, K. Tamao, *Org. Lett.* **2000**, *2*, 4129.

(29) M. Kinoshita, H. Kita, Y. Shirota, *Adv. Funct. Mater.* **2002**, *12*, 780.

(30) a) D. Tanaka, Y. Agata, T. Takeda, S. Watanabe, J. Kido, *Jpn. J. Appl. Phys.* **2007**, *46*, L117. b) D. Tanaka, T. Takeda, T. Chiba, S. Watanabe, J. Kido, *Chem. Lett.* **2007**, *36*, 262.

(31) a) M. A. Holland, L. M. Kozlowski, *Clin. Pharm.* **1986**, *5*, 737. b) R. J. Carton, *Fluoride* **2006**, *39*, 163.

(32) S. Yamaguchi, S. Akiyama, K. Tamao, *J. Am. Chem. Soc.* **2001,** *123*, 11372.

(33) Y. Kubo, M. Yamamoto, M. Ikeda, M. Takeuchi, S. Shinkai, S. Yamaguchi, K. Tamao, *Angew. Chem. Int. Ed.* **2003**, *42*, 2036.

(34) a) S. Solé, F. P. Gabbaï, *Chem. Commun.* **2004**, 1284. b) M. Melaïmi, S. Solé, C.-W. Chiu, H. Wang, F. P. Gabbaï, *Inorg. Chem.* **2006**, *45*, 8136.

(35) a) D.-R. Bai, X.-Y. Liu, S. Wang, *Chem. Eur. J.* **2007**, *13*, 5713. b) X.-Y. Liu, D.-R. Bai, S. Wang, *Angew. Chem. Int. Ed.*, **2006**, *45*, 5475.

(36) M. Melaïmi, F. P. Gabbaï, *J. Am. Chem. Soc.* **2005**, *127*, 9680.

(37) C. L. Dorsey, P. Jewula, T. W. Hudnall, J. D. Hoefelmeyer, T. J. Taylor, N. R. Honesty, C.-W. Chiu, M. Schulte, F. P. Gabbaï, *Dalton Trans*. **2008**, 4442.

(38) M. H. Lee, F. P. Gabbaï, *Inorg. Chem.* **2007**, *46*, 8132.

(39) S. T. Lam, N. Zhu, V. W. W. Yam, *Inorg. Chem.*, **2009**, *48*, 9664.

(40) Y. M. You, S. Park, *Adv. Mater.*, **2008**, *20*, 3820.

(41) Q. Zhao, F. Li, S. Liu, M. Yu, Z. Liu, T. Yi, C. Huang. *Inorg. Chem.* **2008**, *47*, 9256.

(42) C. R. Wade, F. P. Gabbaï, *Inorg. Chem.* **2010**, *49*, 714.

(43) Y. Sun, Z. M. Hudson, Y.-L. Rao, S. Wang. *Inorg. Chem*., **2011**, *50*, 3373.

(44) a) J. B. Heilmann, M. Scheibitz, Y. Qin, A. Sundararaman, F. Jakle, T. Kretz, M. Bolte, H. W. Lerner, M. C. Holthausen, M. Wagner, *Angew. Chem. Int. Ed.* **2006**, *45*, 920. b) A. E. J. Broomsgrove, D. A. Addy, C. Bresner, I. A. Fallis, A. L. Thompson, S. Aldridge, *Chem. Eur. J.* **2008**, *14*, 7525.

(45) A. Wakamiya, T. Taniguchi, S. Yamaguchi, *Angew. Chem. Int. Ed.* **2006**, *45*, 3170.

(46) Y.-L. Rao, H. Amarne, S.-B. Zhao, T. M. McCormick, S. Martić, Y. Sun, R.-Y. Wang, S. Wang, *J. Am. Chem. Soc.* **2008**, *130*, 12898.

(47) H. Amarne, C. Baik, R.-Y. Wang, S. Wang. *Organometallics*, **2011**, *30*, 665.

(48) a) H. Amarne, C. Baik, S. K. Murphy, S. Wang. *Chem. Eur. J.*, **2010**, *16*, 4750. b) C. Baik, Z. M. Hudson, H. Amarne, S. Wang. *J. Am. Chem. Soc.*, **2009**, *131*, 14549. c) C. Baik, S. K. Murphy, S. Wang. *Angew. Chem. Int. Ed.* **2010**, *49*, 8224.

(49) Y.-L. Rao, H. Amarne, S. Wang. *Coord. Chem. Rev.* **2012**, *256*, 759. b) Y.-L. Rao, S. Wang. *Inorg. Chem.*, **2011**, *50*, 12263.

(50) For example, see a) D. J. Tranchemontagne, J. L. Mendoza-Cortés, M. O'Keeffe, O. M. Yaghi, *Chem. Soc. Rev.*, **2009**, *38*, 1257. b) J.-Y. Lee, O. K. Farha, J. Roberts, K. A. Scheidt, S.-B. T. Nguyen, J. T. Hupp, *Chem. Soc. Rev.*, **2009**, *38*, 1450. c) S. S. Han, J. L. Mendoza-Cortés, W. A. Goddard III, *Chem. Soc. Rev.*, **2009**, *38*, 1460. d) J.-R. Li, R. J. Kuppler, H.-C. Zhou, *Chem. Soc. Rev.*, **2009**, *38*, 1477, references therein.

(51) Y. Liu, X. Xu, F. Zheng, Y. Cui, *Angew. Chem. Int. Ed.*, **2008**, *47*, 4538.

(52) J. Zyss, I. Ledoux, *Chem. Rev.*, **1994**, *94*, 77.

(53) M.P. Cuajungco, G.J. Lees, *Neurobiol. Dis.* **1997**, *4*, 137.

(54) For example, see: a) L. Hang, C. S. Murphy, G. C. Kuang, K. L. Hazelwood, M. H. Constantino, M. W. Davidson, L. Zhu, *Chem. Commun.* **2009**, 7408. b) L. Hang, R. J. Clark, L. Zhu, *Chem. Eur. J.*

2008, *14*, 2894. c) P. Jiang, Z. Guo, *Coord. Chem. Rev.*, **2004**, *248*, 205, references therein. d) J. Jaworski, S. C. Burdette, M. Sheng, S. J. Lippard, *Chem.& Biol.*, **2004**, *11*, 203.

Chapter 2

Switchable Singlet-Triplet Dual Emission in Nonconjugated Triarylboron-Pt(II) Complexes

2.1 Introduction

As described in Chapter 1, when triarylboron compounds contain an electron-donor group, donor–acceptor charge-transfer luminescence is commonly observed. Our group has shown recently that when the donor and acceptor groups are spatially separated, the binding of fluoride ions to the boron centre interrupts this charge transfer, activating alternative emission pathways such as π-π* transitions and enabling the use of these compounds as switch-on sensors for fluoride.[1] In this way, it is possible to achieve dual fluorescent emission in organoboron compounds by control of the donor–acceptor geometry, incorporating two fluorophores that are not linked by π-conjugation into a single molecule with a sufficient separation distance between them. Such dual emissive materials are highly sought after, due to their potential as highly sensitive ratiometric sensors and as broad-band or white light emitters in OLEDs.[2] Despite their importance and potential, dual emissive small molecules remain rare, in part because the molecular design requirements of such molecules are not well understood.[1a] We thus hypothesized that singlet–triplet or triplet–triplet dual emission could be achieved in a nonconjugated, two-chromophore organoboron compound, if one of these chromophores was instead a chelate ligand which could coordinate to a metal centre.

Based on this principle, we designed and synthesized a new two-chromophore compound **2.1**, which contains both $BMes_2$ and *N*-(2'-pyridyl)-7-azaindolyl (NPA) fluorophores linked together by a tetraphenylsilane unit. (Figure 2.2, page 53) The choice of NPA as the chelate site was motivated by recent research in our group on Pt(II) complexes of this ligand, which had been shown to undergo a

remarkable thermodynamically controlled "rollover" cyclometalation reaction giving an *N,N*- to *N,C*-chelate mode switch with new resulting reactivity.[3] (Figure 2.1) Furthermore, the NPA ligand functionalized with triarylboron (**2.4**, Figure 2.3) had been recently studied, and it was found that the presence of the boron centre greatly enhanced the phosphorescent emission of complexes of this ligand with Pt(II) and Cu(I).[4] Ligand **2.1** thus provides an opportunity to examine 1) if singlet-triplet or triplet-triplet emission could be achieved by incorporating a metal centre into a nonconjugated molecule containing two chromophores, 2) the impact of molecular geometry on the enhancement of MLCT phosphorescence by the triarylboron group, and 3) the impact of switching chelate mode on the phosphorescence of Pt(II) complexes of NPA.

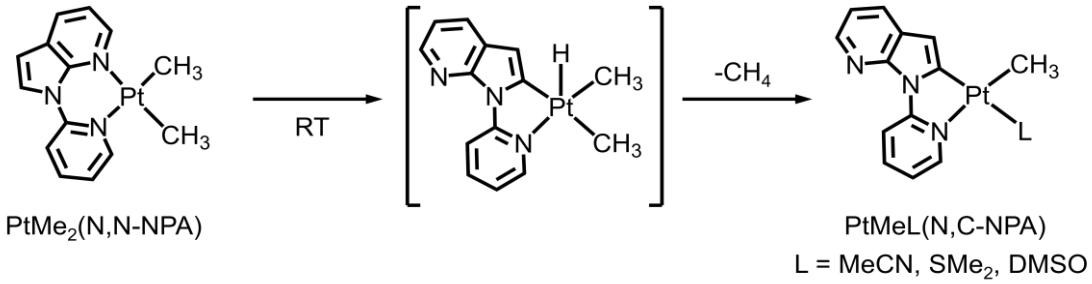

Figure 2.1: Reactivity of Pt(II) complexes of NPA

Our studies revealed that ligand **2.1** readily forms Pt(II) complexes with switchable *N,N*- and *N,C*-chelate modes (**2.2** and **2.3**) much like the NPA ligand itself, as does the directly conjugated ligand **2.4**. More importantly, **2.1** and its Pt(II) complexes do indeed display singlet–triplet dual emission at either 77 K or ambient temperature due to fluorescent emission from the boron chromophore and phosphorescent emission from the metal chelate site. Furthermore, both emissive colours are responsive to fluoride anions, giving single molecules capable of switchable singlet-triplet dual emission.

2.2 Experimental

2.2.1 General Procedures

All reagents were purchased from Aldrich chemical company and used without further purification unless otherwise noted. DMF, THF, Et_2O, and hexanes were purified by using an Innovation Technology Co. solvent purification system. CH_2Cl_2 was freshly distilled over P_2O_5 prior to use. Reactions were carried out under an inert atmosphere of dry N_2 unless otherwise stated. Thin-layer and flash chromatography were performed on silica gel. ^1H and ^{13}C NMR spectra were recorded on Bruker Avance 400, 500 or 600 MHz spectrometers. Deuterated solvents were purchased from Cambridge Isotopes and used without further drying. Excitation and emission spectra were recorded using a Photon Technologies International Quanta-Master Model 2 spectrometer. Phosphorescence spectra and phosphorescent decay lifetimes were measured on a Photon Technologies International Phosphorimeter (Time-Master C-631F). UV/Visible spectra were recorded on an Ocean Optics CHEMUSB4 absorbance spectrophotometer. Cyclic voltammetry experiments were performed with a BAS CV-50W analyzer with a scan rate of 0.2–1.0 Vs^{-1} using ~5 mg of sample in dry DMF (3 mL). The electrochemical cell was a standard three-compartment cell composed of a Pt working electrode, a Pt auxiliary electrode, and an Ag/AgCl reference electrode. CV measurements were carried out at room temperature with 0.1M tetrabutylammonium hexafluorophosphate (TBAP) as the supporting electrolyte, with ferrocene/ferrocenium as internal standard ($E° = 0.55$ V). High-resolution mass spectra were obtained with internal calibrants on an Applied Biosystems/MDS-Sciex QSTAR XL mass spectrometer in electrospray mode. Crystal structures were obtained at 180 K using a Bruker AXS Apex II X-ray diffractometer (50 kV, 30 mA, MoKα radiation). Data were processed on a PC with the aid of the Bruker SHELXTL software package (rev. 5.10 or newer) and were corrected for absorption effects. All structures were solved by direct methods with non-hydrogen atoms refined anisotropically. The positions of hydrogen atoms were calculated, and their contributions in structural factor calculations were included. Photoluminescent quantum yields were

measured using the optically dilute method (A ≈ 0.1) at room temperature. Fluorescent quantum yields were measured in CH_2Cl_2 relative to anthracene (Φ_r = 0.36),[5] while phosphorescent quantum yields were measured in degassed CH_2Cl_2 relative to *fac*-Ir(ppy)$_3$ (Φ_r = 0.97).[6] Molecular orbital and molecular geometry calculations were performed using the Gaussian 03 program suite[7] by using crystal structures as the starting point for geometry optimizations where possible. Calculations were performed at the B3LYP level of theory using 6–31+G* as the basis set for all atoms except Pt, for which LANL2DZ was used. Elemental analyses were performed by Canadian Microanalytical Service Ltd., Delta, British Columbia, or by the Laboratoire d'Analyse Élémentaire de l'Université de Montréal, Montreal, Quebec. (*N*-2'-(5'-bromopyridyl)-7-azaindole),[4] (*p*-dimesitylboronylphenyl)(p-bromophenyl)diphenylsilane,[1a] 5'-dimesitylboryl-NPA[4] (**2.4**) and Pt(*N*,*N*-(5'-dimesitylboryl-NPA)Ph$_2$[4], were synthesized by previously reported procedures. [{PtPh$_2$(SMe$_2$)}$_n$] (*n* = 2 or 3) was prepared by methods described in the literature.[8]

2.2.2 Synthesis of (*p*-(5'-NPA)phenyl)(*p*-dimesitylborylphenyl)diphenylsilane (2.1)

A solution of *n*-BuLi in hexanes (1.6 M, 2.6 mL) was added dropwise with stirring at -78°C to a solution of (*p*-dimesitylboronylphenyl)(*p*-bromophenyl)diphenylsilane (2.5 g, 3.8 mmol) in dry THF (40 mL) under N_2. After stirring at this temperature for 1h, B(O^{i}Pr)$_3$ (2.3 mL, 10.0 mmol) was added dropwise. The reaction mixture was then allowed to warm gradually to room temperature and stirred overnight before sat. $NH_4Cl_{(aq)}$ (30 mL) was added. The mixture was then extracted with CH_2Cl_2 (3 x 30 mL), and the combined organic layers were dried over $MgSO_4$ and filtered. Solvents were evaporated under reduced pressure, and the residue was subjected to column chromatography on silica gel (1:1 THF/hexanes as eluent) to give the corresponding boronic acid as a white solid (1.50 g, 63% yield). A mixture of 5'-bromo-NPA (491 mg, 1.80 mmol), Pd(OAc)$_2$ (16.2 mg, 0.072 mmol), SPhos (59.1 mg, 0.144 mmol), K_3PO_4 (1.15 g, 5.4 mmol) and the above boronic acid (1.36 g, 2.16 mmol) were added to a 100 mL Schlenk flask with stir bar. A mixture of 15 mL toluene, 5 mL EtOH and 5 mL H_2O was degassed and added to the flask. The reaction mixture was heated to 90°C and stirred overnight, then

allowed to cool to room temperature. The mixture was then partitioned between CH_2Cl_2 (30 mL) and H_2O (30 mL), and the layers separated. The aqueous layer was further extracted with CH_2Cl_2 (3 x 25 mL) and the combined organic layers were filtered through Celite. The solvent was then evaporated and the residue subjected to column chromatography (2:1 CH_2Cl_2/hexanes as eluent) to afford **2.1** as a white solid. (815 mg, 58% yield); m.p. 230-231°C; ^{1}H NMR ($CDCl_3$, 25°C): δ = 8.94 (d, J = 8.0 Hz, 1H), 8.77 (d, J = 2.2 Hz, 1H), 8.47 (d, J = 4.9 Hz, 1H), 8.40 (d, J = 3.9 Hz, 1H), 8.10 (dd, J = 8.5 Hz, J = 2.4 Hz 1H), 8.00 (d, J = 7.8 Hz, 1H), 7.68 (d, J = 7.9 Hz, 2H), 7.64 (d, J = 8.1 Hz), 7.54-7.62 (m, 6H), 7.51 (d, J = 7.7 Hz, 2H), 7.44 (d, J = 7.2 Hz, 2H), 7.39 (t, J = 7.5 Hz, 4H), 7.18 (dd, J = 7.8 Hz, J = 4.8 Hz 1H), 6.81 (s, 4H), 6.69 (d, J = 3.9 Hz, 1H), 2.29 (s, 6H), 2.02 (s, 12H); ^{13}C {^{1}H} NMR ($CDCl_3$, 25°C): δ = 149.83, 147.21, 146.87, 146.52, 142.78, 141.73, 140.76, 138.72, 138.43, 138.20, 137.15, 136.87, 136.37, 135.83, 135.06, 133.88, 133.78, 133.20, 129.76, 129.03, 128.16, 127.97, 126.45, 126.25, 123.61, 117.28, 115.27, 103.08, 23.42, 21.19; MS (EI) m/z 778 ($M+H^+$, 90), 658 (47), 452 (100), 374 (22), 256 (18), 202 (26), 189 (25), 181 (19), 165 (18); HRMS (ESI) calcd. for $C_{54}H_{49}BN_3Si$: 778.3788, found 778.3766. Anal. calcd. for $C_{54}H_{48}BN_3Si$: C 83.38, H 6.22, N 5.40, found C 83.52, H 6.23, N 5.26.

2.2.3 Synthesis of Pt(2.1)Ph_2 (2.2):

To a 50 mL round-bottom flask with stir bar was added **2.1** (25.0 mg, 0.032 mmol) and $[PtPh_2SMe_2]_n$ (13.6 mg, 0.033 mmol). THF (20 mL) was then added, affording a homogeneous solution. The mixture was cooled to -10°C and stirred for 8h under air. Keeping the mixture at -10°C, the solvent volume was slowly reduced ~80% under vacuum, at which point hexanes (10 mL) was added, forming a white precipitate. The mother liquor was decanted and the precipitate then dried under vacuum to afford **2.2** as a white solid (35 mg, 97% yield). ^{1}H NMR (500 MHz, C_6D_6): δ 8.44 (d, 1H, J = 6.5Hz), 8.06 (d, 4H, J = 7.7 Hz), 7.76 (d, 2H, J = 8.1 Hz), 7.71-7.65 (m; 6H) 7.61 (d, 2H, J = 7.7 Hz), 7.29 (dd; 1H, J = 8.8 Hz, J = 2.3 Hz), 7.25-7.11 (m, 7H) 7.06 (t, 1H, J = 7.2 Hz), 6.93 (t, 1H, J = 7.3 Hz) 6.83 (s, 4H), 6.68 (d, 1H, J = 3.9 Hz), 2.21 (s, 6H), 2.16 (s, 12H) ppm; ^{13}C {^{1}H} NMR (500 MHz, C_6D_6): δ 151.5, 147.0, 146.4, 144.2,

143.3, 142.3, 140.1, 139.4, 139.2, 139.0, 138.8, 137.6, 136.8, 136.4, 136.0, 135.7, 135.4, 134.0, 132.9, 130.1, 129.8, 128.8, 128.4, 128.3, 128.1, 127.9, 127.7, 127.6, 126.2, 125.8, 123.8, 122.3, 122.2, 119.2, 114.2, 106.5, 23.7, 21.3 ppm; Anal. calcd. for $C_{66}H_{58}BN_3PtSi$: C 70.33, H 5.19, N 3.73; found C 70.31, H 5.10, N 3.80.

2.2.4 Synthesis of Pt(N,C-2.1)Ph(SMe_2) (2.3):

To a 50 mL round-bottom flask with reflux condenser and stir bar was added **2.1** (49.4 mg, 0.064 mmol) and $[PtPh_2SMe_2]_n$ (27.5 mg, 0.033 mmol). Benzene (5 mL) was then added, affording a homogeneous solution. The mixture was then heated to 45°C and allowed to stir for 15h. The solution was cooled to room temperature and the solvent concentrated to 1 mL under a stream of air. Hexanes (10 mL) was added to precipitate the product, then after removal of the solvent, the product was washed with 1 mL hexanes. The product was dried in vacuo to afford **2b** as a light yellow solid (64 mg, 86% yield). ^{1}H NMR (600 MHz, C_6D_6): δ 9.60 (d, 1H, J = 8.8 Hz), 8.92 (d, 1H, J = 2.1 Hz), 8.30 (dd, 1H, J = 4.7 Hz, J = 1.0 Hz), 8.01 (d, satellites, 2H, J = 7.1 Hz), 7.86-7.78 (m, 9H), 7.72 (dd, 1H, J = 8.6 Hz, J = 2.2 Hz), 7.71 (d, 2H, J = 7.6 Hz), 7.45-7.40 (m, 5H), 7.34-7.28 (m, 6H), 6.88 (s, 4H), 6.83 (dd, 1H, J = 7.6 Hz, J = 4.8 Hz), 6.33 (s, satellites, 1H), 2.28 (s, 6H), 2.22 (s, 12H), 1.72 (s, 6H); ^{13}C {^{1}H} NMR (600 MHz, C_6D_6): δ 154.3, 151.0, 150.7, 143.6, 143.0, 142.04, 140.8, 140.1, 138.8, 138.7, 138.2, 137.5, 137.4, 136.6, 136.2, 135.5, 134.2, 134.0, 130.8, 129.9, 128.6, 128.2, 128.1, 127.8, 127.6, 127.4, 126.3, 126.1, 122.6, 117.4, 113.6, 110.8, 23.5, 21.0, 19.7 ppm; $C_{62}H_{58}BN_3PtSSi$: C 67.02, H 5.26, N 3.78; found C 66.27, H 5.30, N 3.62.

2.2.5 Synthesis of Pt(N,C-2.4)Ph(SMe_2) (2.6):

To a 20 mL screw-cap vial with stir bar was added **2.4**, 0.022g, 0.05 mmol), $[PtPh_2(\mu\text{-}SMe_2)]_n$ (n = 2 or 3) (0.021 g) and benzene (10 mL). The mixture was stirred for 3 days at ambient temperature, resulting in a bright yellow solution. After evaporation of the solvent, the residue was washed with Et_2O/hexanes (1:1)

(2 x 2 mL) to afford **2.6** as a yellow solid in 63% yield. ^{1}H NMR (500 MHz, CD_2Cl_2): δ 9.28 (d, 1H, J = 8.5 Hz), 8.63 (s, 1H), 8.14 (dd, 1H, J = 4.9 Hz, J = 1.6 Hz), 8.09 (dd, 1H, J = 8.5 Hz, J = 1.8 Hz), 7.59 (dd, 1H, J = 7.6 Hz, J = 1.6 Hz), 7.50 (dd, satellites, 2H, J = 8.0 Hz, J = 1.4 Hz, J_{Pt-H} = 62 Hz), 7.07 (t, 2H, J = 7.3 Hz), 7.02 (dd, 1H, J = 7.7 Hz, 4.9 Hz), 6.97 (tt, J = 7.3 Hz, J = 1.4 Hz), 6.93 (s, 4H), 5.70 (s, satellites, J_{Pt-H} = 62 Hz), 2.36 (s, 6H), 2.13 (s, 12H), 2.09 (s, satellites, J_{Pt-H} = 28 Hz) ppm. ^{13}C {^{1}H} NMR (500 MHz, CD_2Cl_2): δ 156.63, 155.27, 150.92, 147.99, 143.54, 141.33, 140.84, 139.95, 138.20, 138.05, 128.98, 128.04, 127.88, 127.67, 126.87, 122.74, 118.24, 113.06, 110.75, 23.92, 21.53, 20.96 ppm. Anal. calcd. for $C_{38}H_{40}BN_3SPt$: C 58.76, H 5.19, N 5.41, found C 59.01, H 5.39, N 5.44.

2.2.6 X-Ray Diffraction Analyses

Single crystals of **2.1**, **2.2** and **2.6** were grown by slow evaporation from solutions of hexanes and CH_2Cl_2. Crystal data for these compounds are listed in Table 2.1. These crystal structures have been deposited to the Cambridge Crystallographic Data Centre as CCDC 717963 (**2.1**), 747964 (**2.2**), and 717965 (**2.6**), and may be obtained free of charge via www.ccdc.cam.ac.uk/data_request/cif.

Table 2.1: Crystallographic data for compounds 2.1, 2.2 and 2.4

Compound	**2.1**	**2.2**	**2.6**
Formula	$C_{54}H_{48}BN_3Si$	$C_{66}H_{58}BN_3PtSi$	$C_{38}H_{40}BN_3PtS$
FW	777.85	1127.14	776.69
Space Group	P-1	P-1	P-1
a, Å	7.9606(6)	9.016(4)	11.6494(11)
b, Å	21.5444(16)	13.134(6)	11.7691(11)
c, Å	25.4876(19)	28.426(13)	13.7449(13)
α, °	86.1990(10)	95.603(6)	72.5360(10)
β, °	85.7780(10)	95.598(6)	78.6770(10)
γ, °	85.3190(10)	91.907(6)	69.1830(10)
V, $Å^3$	4336.9(6)	3331(3)	1671.7(3)
Z	4	2	2
D_{calc}, g cm^{-1}	1.191	1.124	1.543
T, K	180(2)	180(2)	180(2)
μ, mm^{-1}	0.095	2.160	4.290
$2\theta_{max}$, °	52.00	54.20	54.08
Reflns measured	45885	35454	18613
Reflns used (R_{int})	16982 (0.0668)	14341 (0.1184)	7217 (0.0369)
Parameters	1426	652	397
Final R Values [I > 2σ(I)]:			
R_1[a]	0.0626	0.0593	0.0325
wR_2[b]	0.1333	0.1099	0.0747
R values (all data):			
R_1[a]	0.1573	0.1123	0.0440
wR_2[b]	0.1749	0.1232	0.0792
Goodness-of-fit on F^2	0.997	0.891	1.056

[a] $R_1 = \Sigma[(|F_0| - |F_c|) / \Sigma |F_0|$

[b] $wR2 = [\Sigma w[(F_0^2-F_c^2)^2] / \Sigma[w(F_0^2)^2]]^{1/2}$

$w = 1 / [\sigma^2(F_0^2) + (0.075P)^2]$, where $P = [Max (F_0^2, 0) + 2F_c^2] / 3$

Table 2.2: Selected bond lengths (Å) and angles (°) for compounds 2.1, 2.2 and 2.6.

		Compound 2.1	
Si(1)-C(37B)	1.630(9)	Si(2)-C(55)	1.863(3)
Si(1)-C(7)	1.863(3)	Si(2)-C(61)	1.869(3)
Si(1)-C(1A)	1.867(7)	Si(2)-C(91)	1.871(3)
Si(1)-C(13)	1.872(3)	Si(2)-C(67)	1.874(3)
Si(1)-C(1B)	1.947(9)	B(1)-C(16)	1.569(4)
Si(1)-C(37A)	2.116(6)	B(1)-C(28)	1.573(4)
Si(1)-C(37B)	1.630(9)	B(1)-C(19)	1.575(4)
C(37B)-Si(1)-C(7)	103.8(4)	C(55)-Si(2)-C(91)	110.89(14)
C(7)-Si(1)-C(1A)	121.4(2)	C(61)-Si(2)-C(91)	109.21(13)
C(37B)-Si(1)-C(13)	114.6(4)	C(55)-Si(2)-C(67)	106.44(12)
C(7)-Si(1)-C(1B)	99.2(3)	N(1A)-C(44A)-C(43A)	125.5(8)
C(16)-B(1)-C(28)	118.7(2)	C(46A)-N(1A)-C(44A)	117.8(6)
C(16)-B(1)-C(19)	116.8(2)	C(45A)-C(46A)-N(1A)	120.0(12)
C(28)-B(1)-C(19)	124.4(2)	N(1A)-C(46A)-N(2A)	115.4(9)
		Compound 2.2	
Si(1)-C(31)	1.860(8)	Pt(1)-N(3)	2.154(5)
Si(1)-C(61)	1.861(7)	N(1)-C(19)	1.345(7)
Si(1)-C(28)	1.866(6)	N(1)-C(18)	1.357(7)
Si(1)-C(55)	1.879(8)	N(2)-C(19)	1.382(7)
Pt(1)-C(1)	1.973(7)	N(2)-C(20)	1.400(7)
Pt(1)-C(7)	1.994(6)	N(2)-C(13)	1.402(7)
Pt(1)-N(1)	2.113(5)	N(3)-C(24)	1.350(7)
C(34)-B(1A)	1.588(17)	C(34)-B(1)	1.606(16)
C(31)-Si(1)-C(61)	109.5(3)	C(7)-Pt(1)-N(1)	175.8(2)
C(31)-Si(1)-C(28)	113.3(3)	C(1)-Pt(1)-N(3)	179.1(3)
C(61)-Si(1)-C(28)	107.1(3)	C(7)-Pt(1)-N(3)	95.2(2)
C(31)-Si(1)-C(55)	107.0(4)	N(1)-Pt(1)-N(3)	88.84(19)
C(1)-Pt(1)-C(7)	84.4(3)	C(46A)-B(1A)-C(34)	131(2)
C(1)-Pt(1)-N(1)	91.5(2)	C(37A)-B(1A)-C(46A)	123(2)
		C(37A)-B(1A)-C(34)	105.2(17)

Compound 2.6

Pt(1)-C(9)	1.976(4)	N(2)-C(20)	1.373(5)
Pt(1)-C(3)	2.007(5)	N(2)-C(15)	1.398(5)
Pt(1)-N(1)	2.119(3)	N(2)-C(9)	1.433(5)
Pt(1)-S(1)	2.3517(13)	N(3)-C(15)	1.323(5)
S(1)-C(1)	1.770(6)	N(3)-C(14)	1.338(6)
S(1)-C(2)	1.786(6)	B(1)-C(17)	1.566(7)
N(1)-C(16)	1.346(5)	B(1)-C(30)	1.568(7)
N(1)-C(20)	1.359(5)	B(1)-C(21)	1.575(7)
C(9)-Pt(1)-C(3)	89.87(18)	C(1)-S(1)-C(2)	100.2(3)
C(9)-Pt(1)-N(1)	80.21(15)	C(1)-S(1)-Pt(1)	113.6(2)
C(3)-Pt(1)-N(1)	169.78(15)	C(2)-S(1)-Pt(1)	103.8(2)
C(9)-Pt(1)-S(1)	173.03(12)	C(16)-N(1)-C(20)	117.3(4)
C(3)-Pt(1)-S(1)	96.56(13)	C(16)-N(1)-Pt(1)	129.2(3)
N(1)-Pt(1)-S(1)	93.24(10)	C(20)-N(1)-Pt(1)	113.5(3)
C(20)-N(2)-C(15)	130.4(4)	C(17)-B(1)-C(30)	118.7(4)
C(20)-N(2)-C(9)	120.2(3)	C(17)-B(1)-C(21)	118.3(4)
C(15)-N(2)-C(9)	109.0(3)	C(30)-B(1)-C(21)	122.9(4)

2.3 Results and Discussion

2.3.1 Synthesis and Reactivity of 2.1 and 2.4

Compound **2.1** was synthesised using $SiPh_2(p\text{-}C_6H_4\text{-}Br)_2$ as starting material, by metal-halogen exchange and subsequent Suzuki-Miyaura cross coupling as shown in Figure 2.2, while **2.4** was synthesised according to a procedure reported recently by our group.[4] **2.1** reacts readily with the di- or trinuclear platinum complex $[\{PtPh_2(SMe_2)\}_n]$ (n = 2,3) to produce [Pt(*N*,*N*-**2.1**)Ph_2] (**2.2**), which can then be converted quantitatively to the "roll-over" C-H activation product [Pt(*N*,*C*-**2.1**)$Ph(SMe_2)$] (**2.3**) upon heating in the presence of a donor ligand such as SMe_2. Complex **2.3** can also be obtained directly from the reaction of **2.1** with $[\{PtPh_2(SMe_2)\}_n]$ at extended reaction times at ambient temperature. ^{1}H NMR experiments confirm that the facile and quantitative conversion of the *N*,*N*-chelate complex **2.2** to the *N*,*C*-chelate complex **2.3** follows the same intramolecular "roll-over" C-H activation mechanism established for the conversion of the NPA complex in Figure 2.1.[3] The directly conjugated compound **2.4** displays a similar reactivity toward Pt(II) as **2.1** and NPA, and as a result, complexes [Pt-(*N*,*N*-**2.4**)Ph_2] (**2.5**)[4] and [Pt(*N*,*C*-**2.4**)$Ph(SMe_2)$] (**2.6**) were obtained in the same manner as **2.2** and **2.3**. (Figure 2.3)

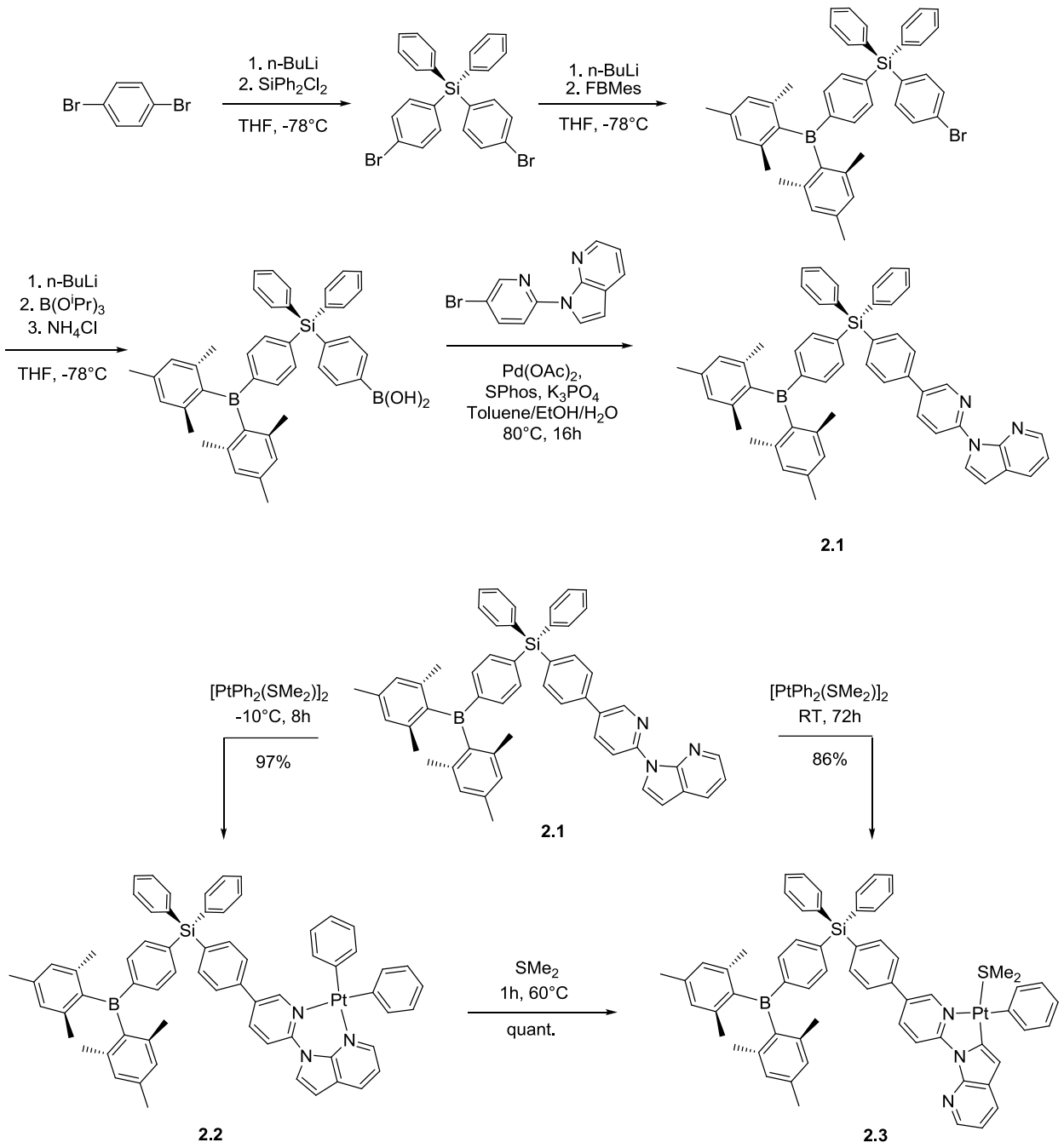

Figure 2.2: Synthesis of **2.1** and its Pt(II) complexes

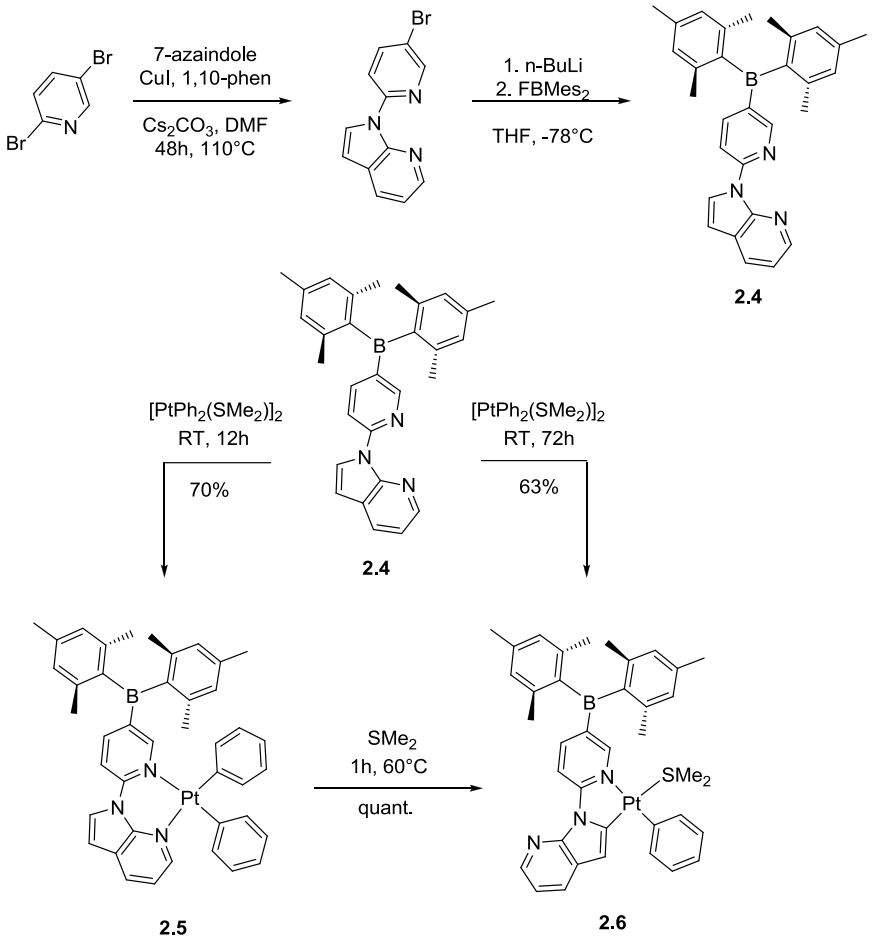

Figure 2.3: Synthesis of **2.4** and its Pt(II) complexes

The crystal structures of **2.1**, **2.2** and **2.6** have been determined by single-crystal X-ray diffraction analysis with **2.2** and **2.6** shown in Figure 2.4; efforts to obtain single crystals of **2.3** were not successful. It can be seen from the structure of **2.6** that the {Pt-(*N*,*C*-NPA)} chelate moiety is planar, while the structures of **2.2** and **2.5** show the {Pt(*N*,*N*-NPA)} chelate to be highly strained, with torsion angles of 25.01° and 19.56° respectively between the pyridyl and 7-azaindolyl moieties. The poor stability of the six-membered non-planar *N*,*N*-chelate ring thus provides a driving force for the facile transformation of **2.2** and **2.5** to the more stable five-membered *N*,*C*-chelate complexes **2.3** and **2.6**, respectively. This structural difference was also found to have a significant impact on the photophysical properties of the complexes. The separation distance between the B atom and the Pt atom in **2.2** was found to be 14.8 Å.

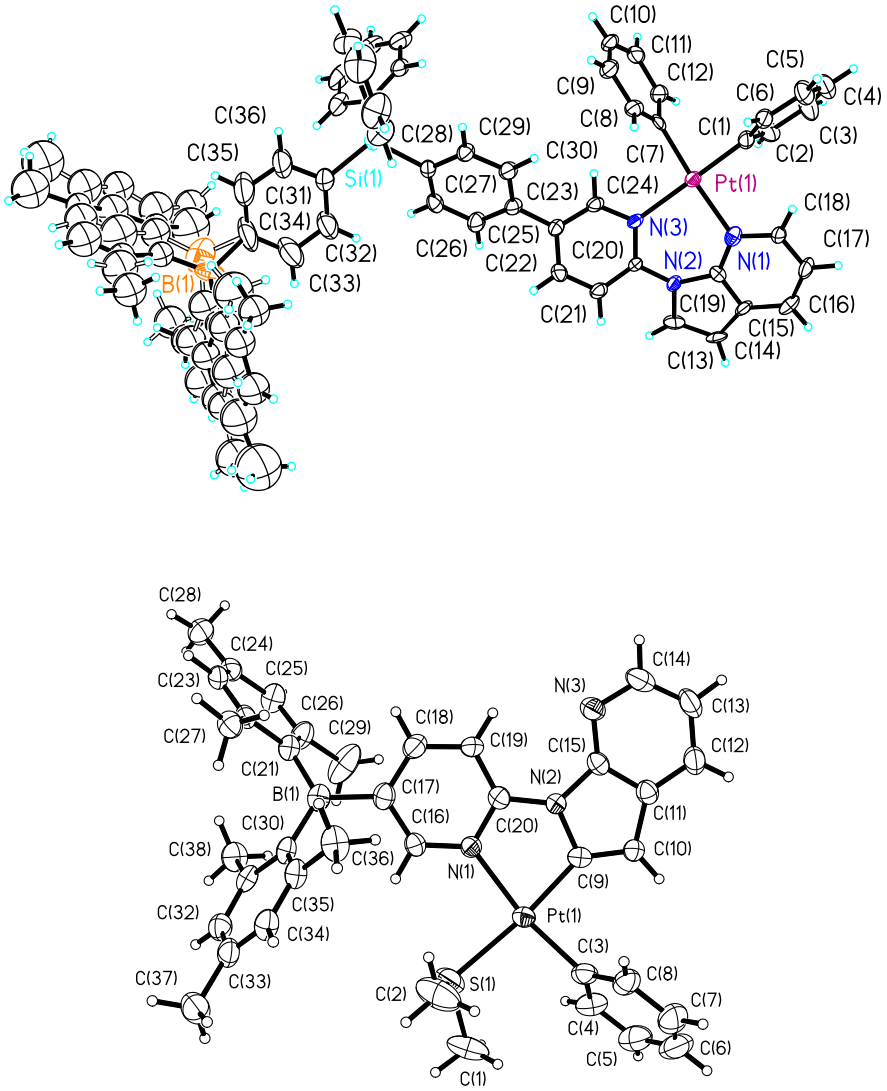

Figure 2.4: Crystal structures of **2.2** (top) and **2.6** (bottom) with 50% thermal ellipsoids

2.3.2 Luminescent Properties of Ligands 2.1 and 2.4

Both **2.1** and **2.4** are fluorescent with λ_{max} = 405 nm (Φ = 0.12) and 392 nm (Φ = 0.25) respectively in THF at ambient temperature. The emission of **2.4** was assigned to an NPA→B charge-transfer transition, based on its quenching response upon the addition of fluoride (by titration with NBu_4F, TBAF).[4] To establish the origin of the emission of **2.1**, we also conducted fluoride titration experiments in both

absorption and emission modes. The 405 nm emission peak of **2.1** was quenched by F^- with the appearance of a new emission peak at 362 nm, as shown in Figure 2.5. This "turn-on" response has some resemblance to that of $SiPh_2$(*p*-C_6H_4-$BMes_2$)(*p*-(1-naphthylphenylamino)biphenyl) reported previously by our group, in which F^- ions quench a very weak N→B charge transfer shoulder band and enhance a π–π* transition band on the arylamine donor group.[1a] Hence, it is tempting to assign the fluorescent emission of **2.1** to NPA→B charge transfer. However, careful comparison of the spectra of **2.1** with that of $SiPh_2$(*p*-C_6H_4-$BMes_2$)$_2$, (**2.7**)[9] which lacks a donor group, suggests that the emission of **2.1** most likely originates from Mes→B charge transfer localised on the boryl chromophore alone. This assignment can be made given that the emission of **2.1** and **2.7** are identical in shape and energy. To establish the origin of the singlet emission of the fluoride adduct, we examined the emission spectrum of $SiPh_3$(*p*-C_6H_4-(5'-NPA)), which can be obtained cleanly as a side product of the Suzuki coupling to form **2.1** and lacks a $BMes_2$ acceptor group. The emission spectrum of this molecule matches perfectly with that of the fluoride adduct of **2.1**, confirming that the emission of the fluoride adduct can be assigned to an NPA-based π–π* transition. The "switch-on" response of **2.1** toward fluoride can thus be explained by the presence of distinct emission pathways on the NPA donor and boron acceptor chromophores. Emission from the acceptor is turned off by F^-, activating the singlet emission from the NPA group as the next lowest energy transition in the molecule.

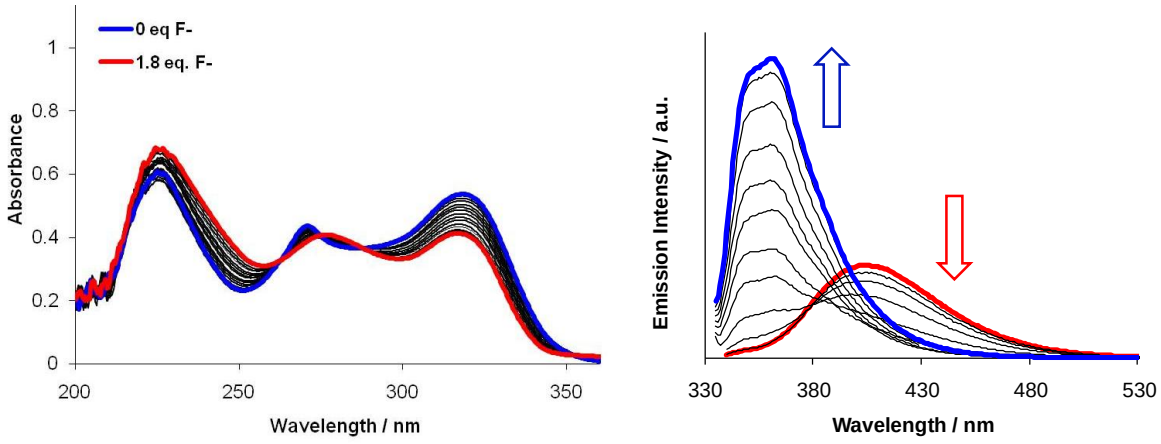

Figure 2.5: Absorption (left) and emission (right) titrations of **2.1** with 0-1.8 equivalents of TBAF, at 1.0 x 10^{-5} M in CH_2Cl_2 at 298 K (λ_{ex} = 300 nm).

These assignments are further supported by TDDFT calculations at the B3LYP/6-31+G* level of theory (see Appendix, section 2.6). Also significant was the observation of well-separated singlet and triplet emission peaks from **2.1** in solution at 77 K, as shown in Figure 2.6 ($\lambda_{F,em}$ = 363 nm, $\lambda_{P,em}$ = 463 nm, τ_P = 2.2 s in THF). Also, the shape and energy of the triplet peak are similar to the phosphorescent peak of free NPA at 77 K.[3] Thus, the singlet and triplet peaks of **2.1** may be assigned to the $BMes_2$ and NPA groups, respectively. The excitation profiles for both singlet and triplet emission peaks at 77 K are essentially identical, supporting that the dual emission is indeed from the same molecule. Because of this dual emission with long-lived green phosphorescence, compound **2.1** emits white light at 77 K under UV irradiation in solution and the solid state, which switches to long-lived green emission when the excitation source is removed as shown in Figure 2.6.

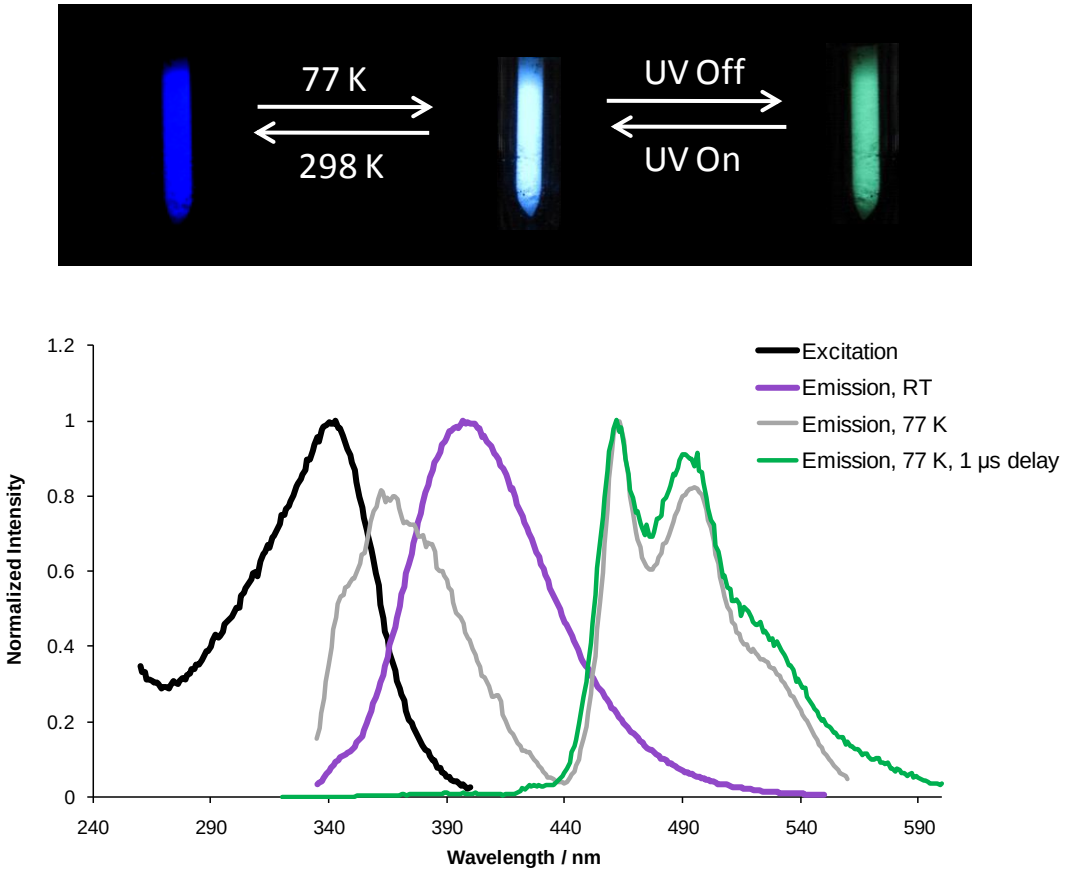

Figure 2.6: Top: Room temperature and 77 K emission of **2.1**. Bottom: Excitation (298 K) and emission spectra of **2.1** at 298 and 77 K. λ_{em} = 400 nm for the excitation spectrum shown.

2.3.3 Luminescent Properties of Pt(II) Complexes 2.2 and 2.3

As shown in Figure 2.7, both *N,N*- and *N,C*-chelate complexes **2.2** and **2.3** display dual emission at ambient temperature in solution, with room-temperature phosphorescence facilitated by the Pt(II) centre. The dual emission of **2.2** is dominated by the singlet peak ($\lambda_{F,em}$ = 399 nm with a shoulder at 362 nm) with a very weak triplet emission peak ($\lambda_{P,em}$ = 494 nm, τ = 12.2(1) μs at 298 K, 65(2) μs at 77 K), while the more stable, planar *N,C*-chelate **2.3** shows a similar singlet peak at $\lambda_{F,max}$ = 392 nm with a shoulder at ~348 nm and green phosphorescence at $\lambda_{P,em}$ = 495 nm (τ = 12.1(1) μs at 298 K, 43(2) μs at 77 K). The phosphorescent quantum yield of **2.3** (Φ_P = 0.06) is much greater than that of **2.2** (0.02). As observed in **2.1**, there is significant overlap in the excitation profiles for both singlet and triplet emission peaks of **2.2** and **2.3**. The dual emission peak profiles of both species do not change noticeably with excitation energy (300–350 nm) and remain consistent using several independently synthesized samples of **2.2** and **2.3**. Thus, we are confident that the dual emission arises from a single species in each case rather than from contamination of the phosphorescent sample by fluorescent free ligand.

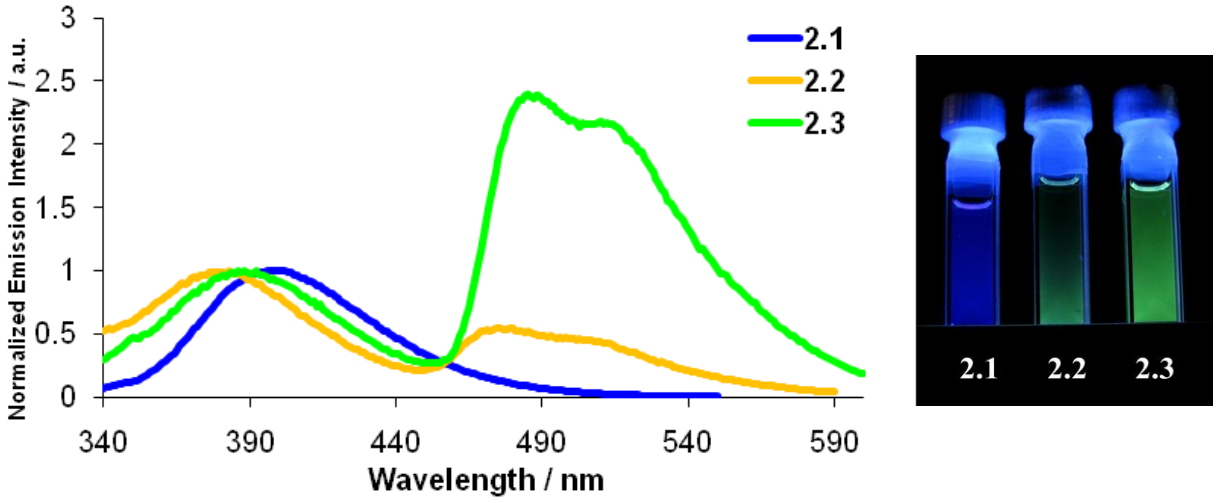

Figure 2.7: Left: Emission spectra of **2.1-2.3** in degassed THF at 1.0 x 10^{-5} M at 298 K (λ_{ex} = 330 nm). Right: Emission of these solutions under irradiation at 365 nm by a handheld UV lamp.

To confirm the origin of the dual emission peaks in **2.2** and **2.3**, we conducted fluoride titration experiments in both absorption and emission modes. The absorption spectral changes with F^- for both complexes are similar to those of **2.1**, and the saturation point is reached after ~1.5 equivalents of F^- is added. Because of the extremely high sensitivity of the triplet emission peak toward oxygen for both complexes, it is very difficult to obtain quantitatively meaningful titration data in emission mode. Nonetheless, addition of fluoride to either **2.2** or **2.3** quenches the singlet peak while enhancing the higher-energy shoulder band in the same manner as the free ligand **2.1,** and thus the singlet emission of these complexes can be assigned to mesityl→B charge transfer for the complexes and NPA-based $^1\pi\rightarrow\pi^*$ transitions for their fluoride adducts. At 77 K, the phosphorescent bands of both complexes have well-resolved vibrational features resembling those of NPA, and thus can be assigned to an NPA-centred $^3\pi\rightarrow\pi^*$ transition. Interestingly, while the phosphorescent band of **2.2** does not have a significant response to fluoride at ambient temperature, that of **2.3** experiences a considerable gain in intensity with the addition of ~2 equivalents of F^-, changing the emission colour from pale green to bright yellow-green (Figure 2.8).

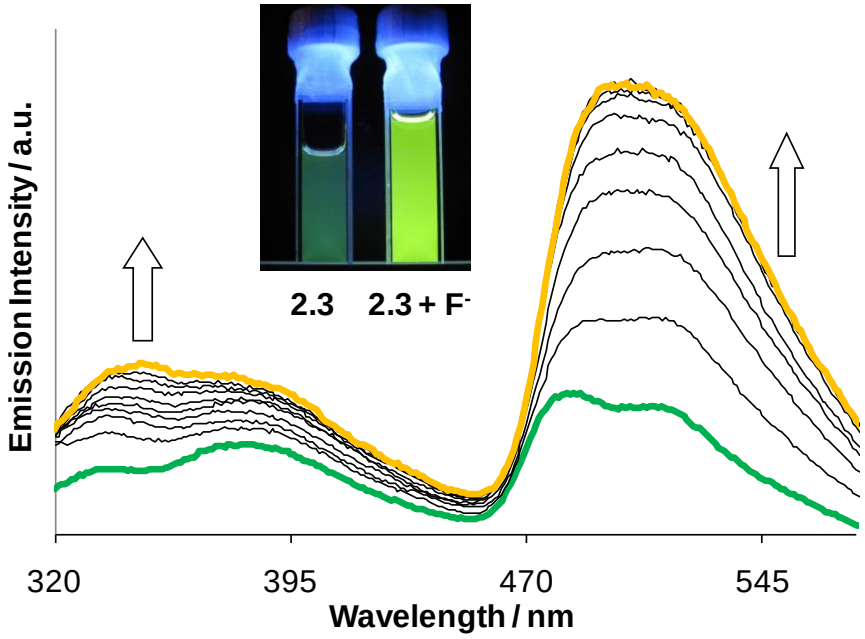

Figure 2.8: Emission mode titration of **2.3** with 0-1.8 equivalents of TBAF at 1.0 x 10^{-5} M in THF under N_2. λ_{ex} = 330 nm.

This may be understood as follows: first, fluoride switches the lowest energy singlet transition from a $BMes_2$-centered charge transfer to the $^1\pi\rightarrow\pi^*$ transition of the NPA group. Since the triplet emission is NPA-centred $^3\pi\rightarrow\pi^*$ emission, the enhanced population of the NPA $^1\pi\rightarrow\pi^*$ excited state increases the population of the NPA $^3\pi\rightarrow\pi^*$ excited state due to the presence of the Pt(II) centre, thus enhancing the overall emission intensity of the triplet peak. This same phenomenon was not observed in **2.2**, perhaps owing to the very weak initial phosphorescence of this material. The chelate mode thus has a significant impact on the relative ratio of the singlet and triplet emission peaks, due not only to the reduced strain of the five-membered chelate ring in **2.3**, but also to the stronger ligand field splitting of the *N,C*-chelate bonding mode.

Though assigning the photophysical properties of these molecules is somewhat complex, an elegant practical conclusion may be drawn from these experiments. In the absence of fluoride and oxygen, compound **2.3** emits both purple and green light, and when fluoride is added, these bands instead emit ultraviolet and yellow. Furthermore, the presence of oxygen completely quenches the observable phosphorescence of **2.3**, leaving the emission in the absence or presence of fluoride as simply purple or ultraviolet. Finally, the decay lifetimes of the triplet excited states in this molecule are several orders of magnitude larger than those of the singlet excited states, and thus all fluorescent emission is easily filtered out by the simple application of a ~1 μs detector delay – leaving the detected emission as solely green or yellow. Thus, using a combination of stimuli – fluoride, oxygen, and delay time – the emission of **2.3** may be detected in any of *six* states: ultraviolet, purple, green, yellow, purple and green, or ultraviolet and yellow. The potential to observe a pure sample of a single species emitting any of six colours is a truly remarkable feature of this system.

2.3.4 Luminescent Properties of Pt(II) Complexes 2.5 and 2.6

The contrasting photophysical properties of the linearly conjugated complexes **2.5** and **2.6** further illustrate the importance of electronically separating the donor and acceptor chromophores to achieve dual emission in a single molecule. The emission of these two complexes at 298 K consists of a single phosphorescent band at λ_{max} = 543 nm, τ = 25.0(1) μs for **2.5** and λ_{max} = 535 nm, τ = 11.9(1) μs for **2.6**. Consistent with complexes of **2.1**, the *N*,*C*-chelate complex **2.6** has a much greater quantum efficiency (0.08) than the *N*,*N*-chelate **2.5** (0.01). However, unlike **2.2** and **2.3**, in which the triplet emission originates from the NPA chelate, the lack of any vibrational features in the emission band of **2.5** and **2.6** indicates that phosphorescence in these complexes is ^{3}MLCT (metal-to-ligand charge transfer) in nature. Thus, direct conjugation of the electron-accepting $BMes_2$ group with the NPA moiety greatly facilitates charge-transfer from the metal centre. Furthermore, addition of fluorides to either **2.5** or **2.6** quenches this emission pathway with the appearance of a new phosphorescent band at a shorter wavelength (λ_{max} = 487 nm, **2.5**, λ_{max} = 480 nm, **2.6**) that resembles the corresponding phosphorescent bands of **2.2** and **2.3**. These can thus be assigned to *N*,*N*-NPA and *N*,*C*-NPA $^3\pi\rightarrow\pi^*$ transitions, respectively (see Figure 2.9). This phosphorescent switching changes the emission colour of solutions of **2.5** and **2.6** from yellow to green.

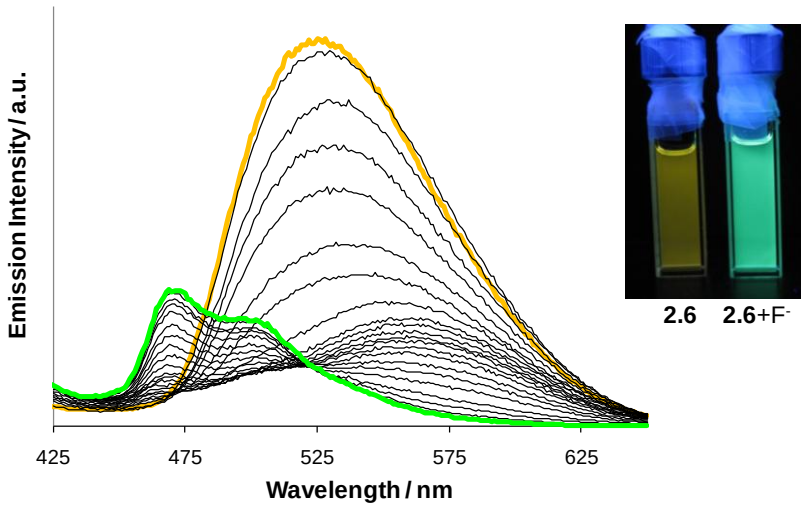

Figure 2.9: Emission mode titration of **2.6** with 0-9.0 equivalents of TBAF at 1.0 x 10^{-5} M in THF under N_2. λ_{ex} = 330 nm.

2.4 Conclusions

Herein we have described the syntheses of the first examples of metal-containing non-conjugated triarylboron compounds. Furthermore, we have demonstrated that persistent singlet–triplet dual emission in organoboron compounds can be achieved in solution at ambient temperature. This is possible through the use of both spatially separated chromophores that share a common excitation energy and metal chelation to facilitate phosphorescence. In addition, we have established that *N,N*- to *N,C*- chelate mode switching can further increase the phosphorescent efficiency of these complexes by the relief of ring strain, providing a means by which the ratio of singlet-to-triplet emission may be controlled. Lastly, we have shown that the singlet–triplet dual emission in the non-conjugated system can be perturbed selectively by fluoride ions through binding to the boron receptor site, thus providing a new strategy for the development of sensing systems based on singlet–triplet switching.

2.5 Notes and References

The work described in this chapter has been published as:

- Z. M. Hudson, S. B. Zhao, S. Wang, *Chem. Eur. J.* **2009**, *15*, 6081.

References

(1) a) X. Y. Liu, D. R. Bai, S. Wang, *Angew. Chem. Int. Ed.* **2006**, *45*, 5475. b) D. R. Bai, X. Y. Liu, S. Wang, *Chem. Eur. J.* **2007**, *13*, 5713.

(2) a) Y. M. Cheng, Y. S. Yeh, M. L. Ho, P. T. Chou, P. S. Chen, Y. Chi, *Inorg. Chem.* **2005**, *44*, 4594. b) K. K. W. Lo, K. Y. Zhang, S. K. Leung, M. C. Tang, *Angew. Chem. Int. Ed.* **2008**, *47*, 2213. c) R. L. Blakley, M. K. DeArmond, *J. Am. Chem. Soc.* **1987**, *109*, 4895. d) T. Suzuki, T. Kuchiyama, S. Kishi, S. Kaizaki, H. D. Takagi, M. Kato, *Inorg. Chem.* **2003**, *42*, 785 e) Z. Zhao, Y. Xing, Z. Wang, P. Lu, *Org. Lett.* **2007**, *9*, 547. f) S. Tao, Y. Zhou, C. S. Lee, S. T. Lee, D. Huang, X. Zhang, *J. Mater. Chem.* **2008**, *18*, 3981. g) Y. Liu, M. Nishiura, Y. Wang, Z. Hou, *J. Am. Chem. Soc.* **2006**, *128*, 5592. h) S. Park, J. E. Kwon, S. H. Kim, J. Seo, K. Chung, S.-Y. Park, D.-J. Jang, B. M. Medina, J. Gierschner, S. Y. Park, *J. Am. Chem. Soc.* **2009**, *131*, 14043.

(3) S. B. Zhao, R. Y. Wang, S. Wang, *J. Am. Chem. Soc.* **2007**, *129*, 3092.

(4) S. B. Zhao, T. McCormick, S. Wang, *Inorg. Chem.* **2007**, *46*, 10965.

(5) B. M. Krasovitskii, B. M. Bolotin, Organic Luminescent Materials, VCH, Weinheim, Germany **1988**.

(6) T. Sajoto, P. I. Djurovich, A. B. Tamayo, J. Oxgaard, W. A. Goddard III, M. E. Thompson, *J. Am. Chem. Soc.* **2009**, *131*, 9813.

(7) Gaussian 03, Revision C.02, M. J. Frisch, G. W. Trucks, H. B. Schlegel, G. E. Scuseria, M. A. Robb, J. R. Cheeseman, J. A. Montgomery Jr., T. Vreven, K. N. Kudin, J. C. Burant, J. M. Millam, S. S. Iyengar, J. Tomasi, V. Barone, B. Mennucci, M. Cossi, G. Scalmani, N. Rega, G. A. Petersson, H. Nakatsuji, M. Hada, M. Ehara, K. Toyota, R. Fukuda, J. Hasegawa, M. Ishida, T. Nakajima, Y. Honda, O. Kitao, H. Nakai, M. Klene, X. Li, J. E. Knox, H. P. Hratchian, J. B. Cross, V. Bakken, C.

Adamo, J. Jaramillo, R. Gomperts, R. E. Stratmann, O. Yazyev, A. J. Austin, R. Cammi, C. Pomelli, J. W. Ochterski, P. Y. Ayala, K. Morokuma, G. A. Voth, P. Salvador, J. J. Dannenberg, V. G. Zakrzewski, S. Dapprich, A. D. Daniels, M. C. Strain, O. Farkas, D. K. Malick, A. D. Rabuck, K. Raghavachari, J. B. Foresman, J. V. Ortiz, Q. Cui, A. G. Baboul, S. Clifford, J. Cioslowski, B. B. Stefanov, G. Liu, A. Liashenko, P. Piskorz, I. Komaromi, R. L. Martin, D. J. Fox, T. Keith, M. A. Al-Laham, C. Y. Peng, A. Nanayakkara, M. Challacombe, P. M. W. Gill, B. Johnson, W. Chen, M. W. Wong, C. Gonzalez, J. A. Pople, Gaussian, Inc., Wallingford CT, **2004**.

(8) D. Song, S. Wang, *J. Organomet. Chem.* **2002**, *648*, 302.

(9) S. B. Zhao, P. Wucher, Z. M. Hudson, T. M. McCormick, X. Y. Liu, S. Wang, X.-D. Feng, Z.-H. Lu, *Organometallics*, **2008**, *27*, 6446.

2.6 Appendix: TD-DFT Calculations

Frontier molecular orbital surfaces and calculated energy levels for compounds **2.1-2.3** and **2.6** are shown below. Isocontour = 0.03 au.

2.1:

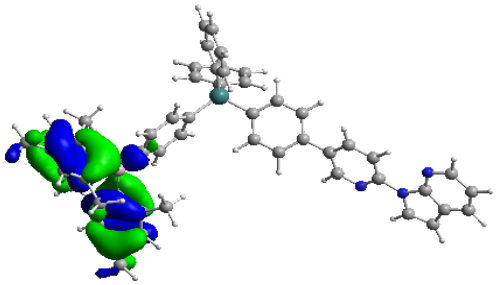

HOMO-1: -6.23 eV

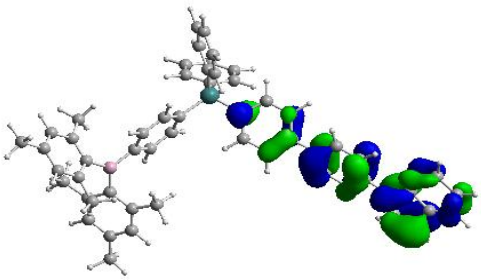

HOMO: -5.97 eV

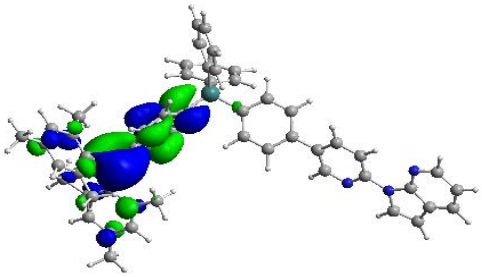

LUMO: -1.97 eV

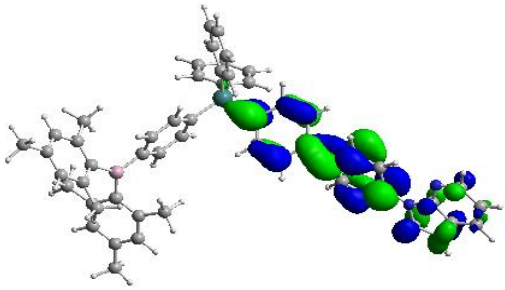

LUMO+1: -1.51 eV

2.2:

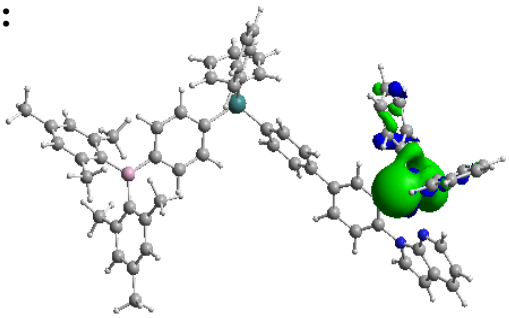

HOMO –1: -5.12 eV

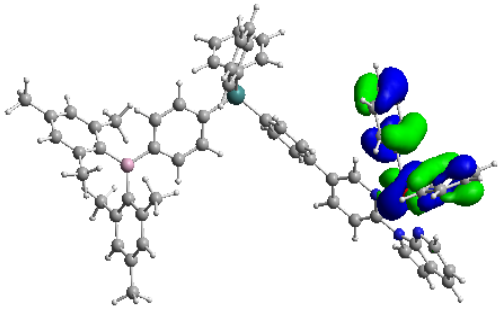

HOMO: -5.06 eV

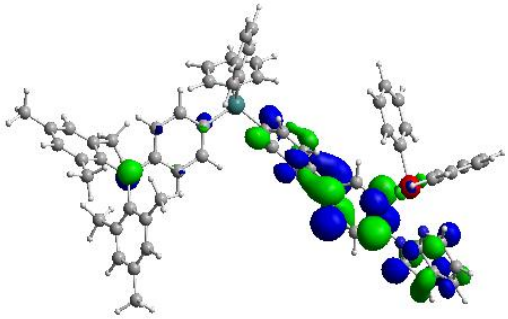

LUMO: -1.82 eV

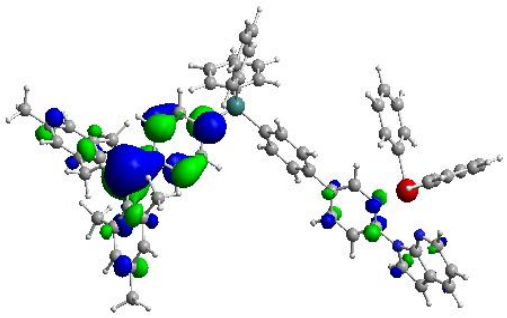

LUMO +1: -1.74 eV

2.3:

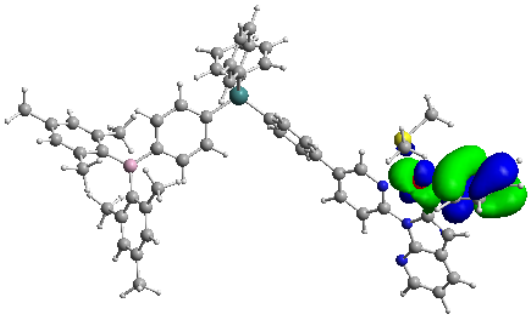

HOMO –1: -5.63 eV

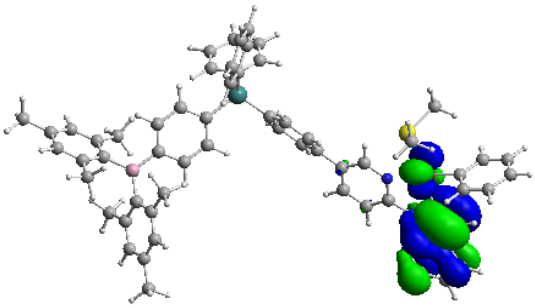

HOMO: -5.16 eV

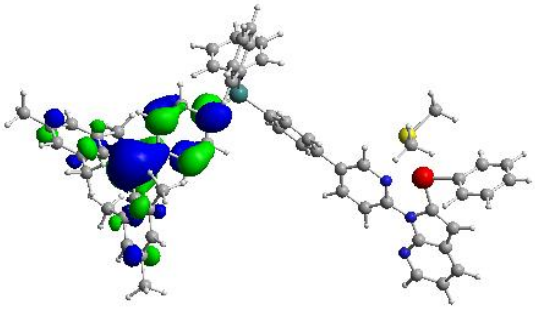

LUMO: -1.74 eV

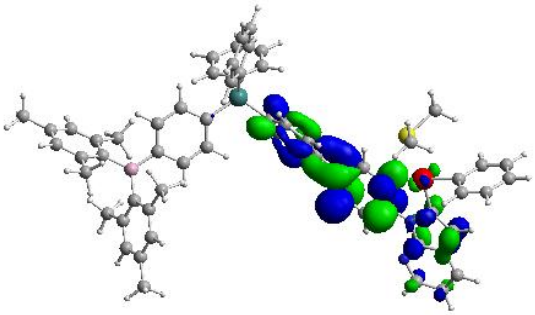

LUMO +1: -1.40 eV

2.6:

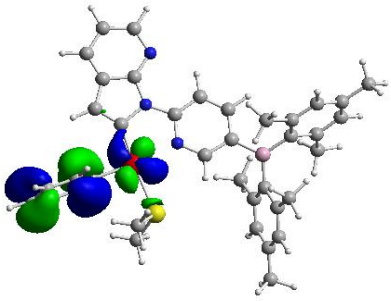

HOMO –1: -5.62 eV

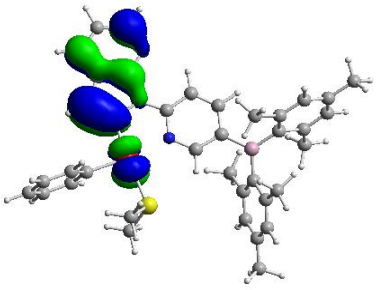

HOMO: -5.21 eV

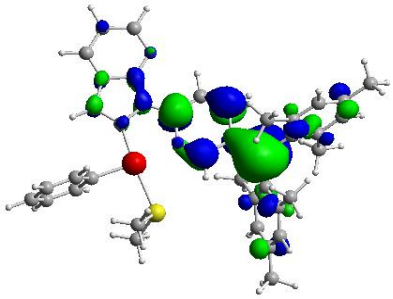

LUMO: -1.92 eV

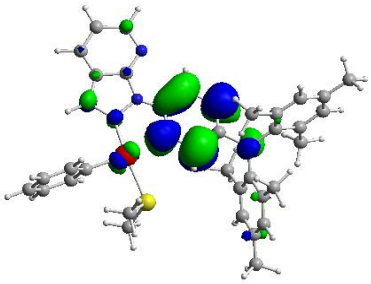

LUMO +1: -1.09 eV

Chapter 3

Switchable Three-State Fluorescence of a Nonconjugated Donor-Acceptor Triarylborane

3.1 Introduction

Triarylboranes have been the subject of considerable recent research as selective sensors for fluoride ions, due to the high selectivity for F^- binding over other anions such as Cl^- and Br^-. The electron-accepting boron atom readily promotes intramolecular charge-transfer (CT) luminescence, thereby facilitating rapid visual detection of F^- by visible or fluorescent colour change.[1] Furthermore, since fluoride ions can bind selectively to the boron centre and block the empty p_π orbital, fluoride addition can thus act as a simple probe to determine the impact of the boron moiety on the frontier orbitals of a π-conjugated organoborane.

The luminescent and anion-binding properties of triarylboranes based on a 1,8-naphthyl core have been the subject of several recent reports. Using this linker, bidentate Lewis acids may be prepared with binding constants much larger than comparable species with a single boron center.[2] Also, when donor and acceptor chromophores are connected by this bridge, the rigidity of the linker forces the π-systems of the chromophores out of coplanarity with that of the linker, promoting charge-transfer through-space rather than through a directly conjugated π-system.[3] The fluorescence of these materials is switchable between dual emission pathways, as the charge-transfer fluorescence exhibited by the pure compound can readily be deactivated if fluoride is added. This switches the emission color of the sample, leading to higher-energy π-π* fluorescence from the remaining donor chromophore.

We have herein extended this concept to a fluorescent material switchable between three emission pathways, incorporating donor and acceptor fluorophores both capable of acting as receptor sites (compound **3.1,** Figure 3.1). Using a more basic dimethylarylamine unit, this compound can be readily protonated to block the filled p orbital of the donor group. In this way, blocking of either the donor group with acid or the acceptor group with fluoride or cyanide disrupts through-space charge-transfer fluorescence, causing the material to emit with the colour of an alternate chromophore. In this way, these simple stimuli allow for facile and reversible switching between three emissive excited states.

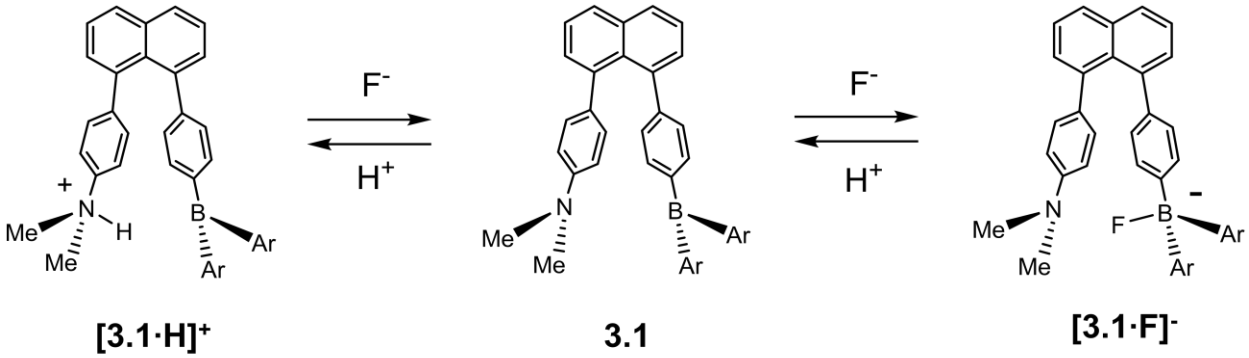

Figure 3.1: Dual switching modes in compound **3.1**

3.2 Experimental

3.2.1 General Procedures

Experimental techniques and instruments used follow those described in section 2.2. UV-visible and fluorescent titrations were carried out in 3 mL screw-cap quartz cuvettes using stock solutions of 3.0 x 10^{-3} M TBAF or HBF_4 in CH_2Cl_2. Binding constants were determined by fitting the absorption titration data to 1:1 binding isotherms.[4] 1-iodo-8-(*p*-dimesitylborylphenyl)naphthalene (intermediate **3.1a**) was synthesized according to literature procedures.[3a]

3.2.2 Synthesis of 1-(*p*-dimethylaminophenyl)-8-(*p*-dimesitylborylphenyl)naphthalene (3.1)

To a 50 mL Schlenk flask with stir bar was added *N,N*-dimethyl-4-bromoaniline (186 mg, 0.93 mmol) and 20 mL dry, degassed THF. The solution was cooled to -78°C for 15 min, then n-BuLi (0.64 mL, 1.6 M in hexanes, 1.02 mmol) was added dropwise *via* syringe. The mixture was stirred 1h at -78°C, then $ZnCl_2$ (165 mg, 1.21 mmol) was added. Stirred 1h at -78°C then 1h at 0°C, then **3.1a** (360 mg, 0.62 mmol) and $Pd(PPh_3)_4$ (81 mg, 0.070 mmol) were added. Stirred at 0°C for 1h then at ambient temperature for 40h, at which point the solvent was removed *in vacuo* and the residue partitioned between CH_2Cl_2 and water. Extracted twice with CH_2Cl_2, and the combined organic layers were dried using $MgSO_4$ and filtered. Purified on silica gel (3:1 hexanes: CH_2Cl_2 as eluent) to afford 310 mg **3.1** as a yellow solid (87% yield). ^{1}H NMR (400 MHz, CD_2Cl_2) δ 7.94 (d, J = 8.0 Hz, Ar, 1H), 7.89 (d, J = 8.0 Hz, Ar, 1H), 7.56 (t, J = 7.5 Hz, Ar, 2H), 7.44 (d, J = 7.0 Hz, Ar, 1H), 7.38 (d, J = 7.0 Hz, Ar, 1H), 7.18 (d, J = 8.0, Ar, 2H), 7.12 (d, J = 8.0 Hz, Ar, 2H), 6.94 (d, J = 8.5 Hz, Ar, 2H), 6.83 (s, Ar, 4H), 6.36 (d, J = 8.5 Hz, Ar, 2H), 2.86 (s, NMe_2, 6H), 2.32 (s, Me, 6H), 1.97 (s, Me, 12H) ppm; ^{13}C NMR (100 MHz, CD_2Cl_2) δ 148.7, 147.9, 141.6, 140.9, 140.6, 140.5, 138.2, 136.1, 135.8, 131.4, 131.2,130.6, 130.2, 129.2, 129.0, 128.5, 127.9, 127.1, 125.4, 124.9, 111.2, 39.9, 23.2, 20.8 ppm; HRMS (EI) calc'd for $C_{42}H_{42}BN$: 572.3489, found 572.3478.

3.2.3 X-Ray Diffraction Analysis

Single crystals of **3.1** were grown by slow evaporation from a solution of hexanes and CH_2Cl_2. Crystal data for this compound is listed in Table 3.1, and selected bond lengths and angles are given in Table 3.2. This crystal structure is available at pubs.acs.org and may be obtained free of charge via DOI 10.1021/ol102749y.

Table 3.1: Crystallographic data for compound 3.1

Compound	**2.1**
Formula	$C_{21}H_{21}B_{0.50}N_{0.50}$
FW	285.79
Space Group	Pca2(1)
a, Å	23.245(5)
b, Å	11.539(3)
c, Å	12.288(2)
α, °	90
β, °	90
γ, °	90
V, Å^3	3296.1(12)
Z	8
D_{calc}, g cm^{-1}	1.152
T, K	180(2)
μ, mm^{-1}	0.065
$2\theta_{max}$, °	56.82
Reflns measured	18482
Reflns used (R_{int})	6470 (0.2009)
Parameters	398
Final R Values [I > 2σ(I)]:	
R_1[a]	0.0625
wR_2[b]	0.1012
R values (all data):	
R_1[a]	0.2665
wR_2[b]	0.1420
Goodness-of-fit on F^2	0.719

[a] $R_1 = \Sigma[(|F_0| - |F_c|) / \Sigma |F_0|$

[b] $wR2 = [\Sigma w[(F_0^2-F_c^2)^2] / \Sigma[w(F_0^2)^2]]^{1/2}$

$w = 1 / [\sigma^2(F_0^2) + (0.075P)^2]$, where $P = [Max (F_0^2, 0) + 2F_c^2] / 3$

Table 3.2: Selected bond lengths (Å) and angles (°) for compound 3.1

Compound 3.1			
B(1)-C(20)	1.523(9)	C(1)-C(2)	1.341(7)
B(1)-C(25)	1.594(9)	C(1)-C(10)	1.459(7)
B(1)-C(34)	1.632(10)	C(1)-C(17)	1.478(7)
N(1)-C(14)	1.387(7)	C(8)-C(9)	1.374(7)
N(1)-C(23)	1.427(7)	C(9)-C(10)	1.437(8)
N(1)-C(24)	1.437(7)	C(9)-C(11)	1.471(8)
C(20)-B(1)-C(25)	117.9(6)	C(2)-C(1)-C(10)	119.1(6)
C(20)-B(1)-C(34)	119.1(6)	C(2)-C(1)-C(17)	117.4(6)
C(25)-B(1)-C(34)	122.8(6)	C(10)-C(1)-C(17)	123.0(6)
C(14)-N(1)-C(23)	121.8(6)	C(9)-C(8)-C(7)	122.6(7)
C(14)-N(1)-C(24)	119.1(6)	C(8)-C(9)-C(10)	117.9(6)
C(23)-N(1)-C(24)	116.5(6)	C(8)-C(9)-C(11)	115.3(6)

3.3 Results and Discussion

3.3.1 Synthesis and X-Ray Crystallography

This material is best prepared by sequential Negishi coupling of the donor and acceptor chromophores to 1,8-diiodonaphthalene, involving one-pot metal-halogen exchange and formation of an organozinc intermediate, followed by palladium-catalyzed C-C bond formation with the appropriate aryl halide. (Figure 3.2) This method was found to proceed in much higher yield than more commonly used Suzuki coupling reactions, and it is possible that the steric demands of the substrate play a role in the efficiency of this coupling step. The steric congestion in this molecule is apparent from the crystal structure of **3.1**, with torsion angles of 57.2° and 47.4° and bend angles of 118.02° and 115.22° between the naphthyl linker and the phenyl rings of the donor and acceptor chromophores, respectively. (Figure 3.3) Incorporation of a rigid linker forces the donor and acceptor atoms into close proximity, with a B···N separation distance of 5.55 Å.

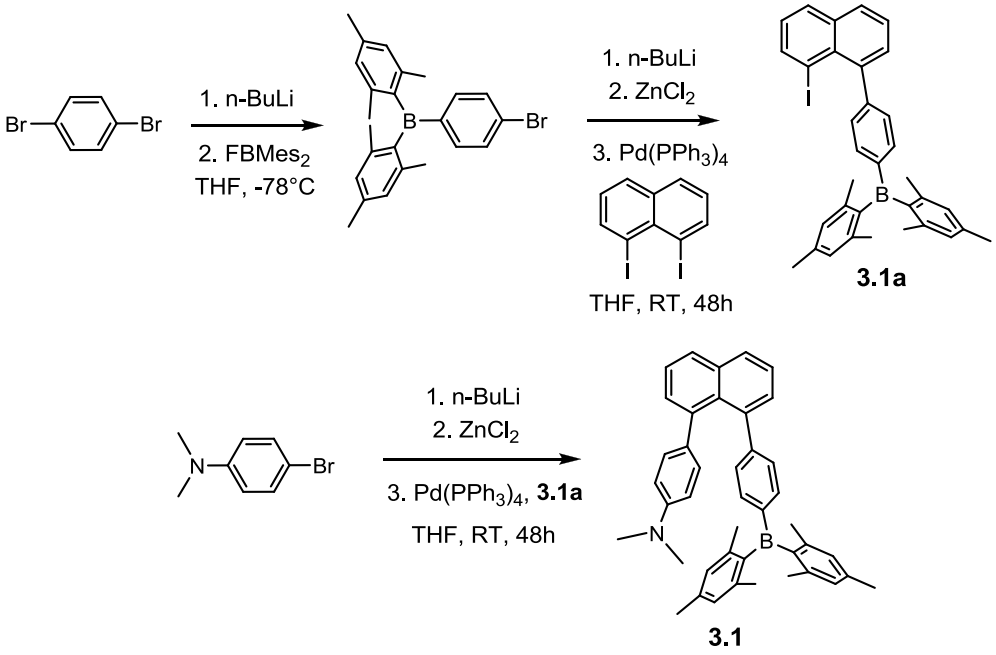

Figure 3.2: Negishi coupling route to compound **3.1**.

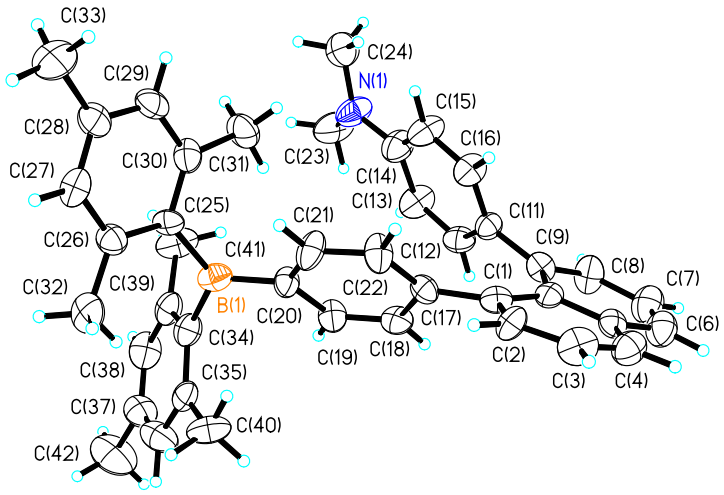

Figure 3.3: Crystal structure of **3.1** with 35% thermal ellipsoids.

3.3.2 Photophysical Properties

The through-space donor-acceptor charge-transfer transition may be observed as a weak low-energy band centered at ~386 nm in the UV-visible absorption spectrum of **3.1** in CH_2Cl_2. This spectrum also features an intense band at 333 nm, attributed to charge-transfer from the filled π orbitals on the mesityl and naphthyl rings to the boron centre. (Figure 3.4) These assignments have been corroborated by theoretical absorption spectra calculated using time-dependent density functional theory, confirming that the intense absorption band is not in fact due to donor-acceptor charge-transfer as is commonly seen in directly conjugated systems.[5] Due to the ambipolar nature of **3.1**, this compound undergoes both reversible reduction and oxidation by cyclic voltammetry, at potentials of $E_{1/2}^{red}$ = -2.41 V and $E_{1/2}^{ox}$ = +0.34 V vs. $FeCp_2^{0/+}$ in DMF.

Compound **3.1** exhibits bright green charge-transfer fluorescence (λ_{max} = 529 nm in CH_2Cl_2) with a quantum efficiency of 0.43, the highest observed to date for a molecule displaying through-space charge transfer to boron.[3] (Figure 3.4) This considerable increase in quantum efficiency over previously reported non-conjugated donor-acceptor triarylboron compounds is likely due to both the improved donor strength

of the dialkylamine as well as the close donor-acceptor spacing imposed by the naphthyl linker. The charge-transfer nature of this transition is consistent with the significant solvent dependence of the emission wavelength, exhibiting a strong red-shift in polar solvents and consistent with a highly polar excited state.

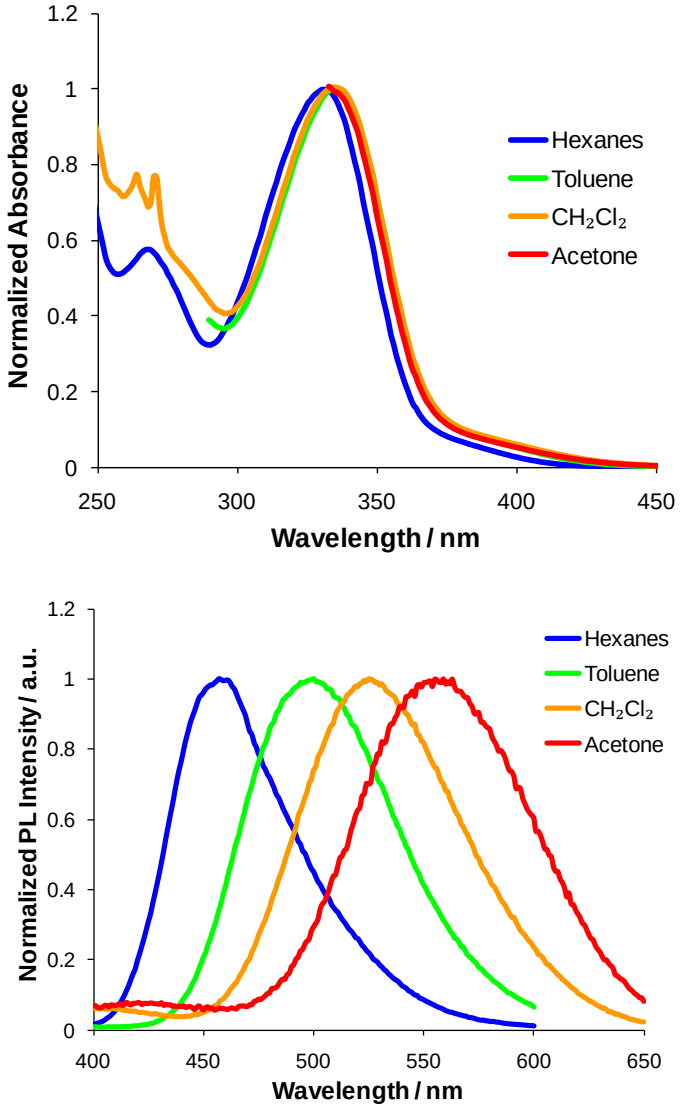

Figure 3.4: Absorbance (top) and fluorescence (bottom) spectra of 10^{-5} M solutions of **3.1**. λ_{ex} = 330 nm.

3.3.3 Fluorescent Switching with H^+ and F^-

When tetrabutylammonium fluoride (TBAF) is added to a solution of **3.1**, the emission colour is observed to rapidly switch from green to sky blue with similar quantum efficiency (λ_{max} = 469 nm, Φ = 0.42). (Figure 3.5) This is accompanied by an increase in intensity of the strong 333 nm band in the UV-visible spectrum of **3.1**, likely due to a reduction in the CT contributions of this transition and increase in π-π^* character, improving the overall overlap between participating MOs. Approximately 20 equivalents of fluoride are required to achieve complete color switching, higher than most organoboranes but comparable to similar sterically congested materials reported previously,[3,6] corresponding to a binding constant *K* of $(1.7 \pm 0.5) \times 10^4$ M^{-1}. ^{1}H and ^{19}F NMR titrations of **3.1** with TBAF indicate the quantitative conversion of **3.1** to [**3.1·F**]$^-$ without intermediates (see Appendix, section 3.6). Conversely, addition of strong acid (HBF_4 or $HBAr^F_4$) to a CH_2Cl_2 solution of **1** results in quantitative protonation after addition of ~1.5 eq. of acid, switching the emission colour of the sample to bright purple (λ_{max} = 398 nm). (Figure 3.5) This is accompanied by a large increase in quantum yield of the sample (Φ = ~1.0), which is consistent with other triarylboron compounds conjugated to highly electron rich π systems.[6,7] As with [**3.1·F**]$^-$**,** NMR data indicate clean formation of [**3.1·H**]$^+$ on addition of acid (section 3.6).

Remarkably, the fluorescent responses to both acid and fluoride in this system are fully reversible by applying the opposite trigger. Despite possessing receptor sites for both ions, the compound exists instead as free **3.1** when treated with both stimuli, and the green fluorescence is preserved. Similarly, after treatment of **3.1** with excess acid or fluoride, the CT emission can be restored by titration with the other trigger (Figure 3.5b and d). No sample degradation is observed in either case, and these processes can be cycled several times in either direction without loss of fluorescent intensity. These results are in constrast with previous studies, in which it was shown that protonation of a proximal tertiary amine could promote hydrolysis of an adjacent triarylborane.[8] The removal of fluoride ions from triarylboranes using protic acids including water has been reported previously.[9]

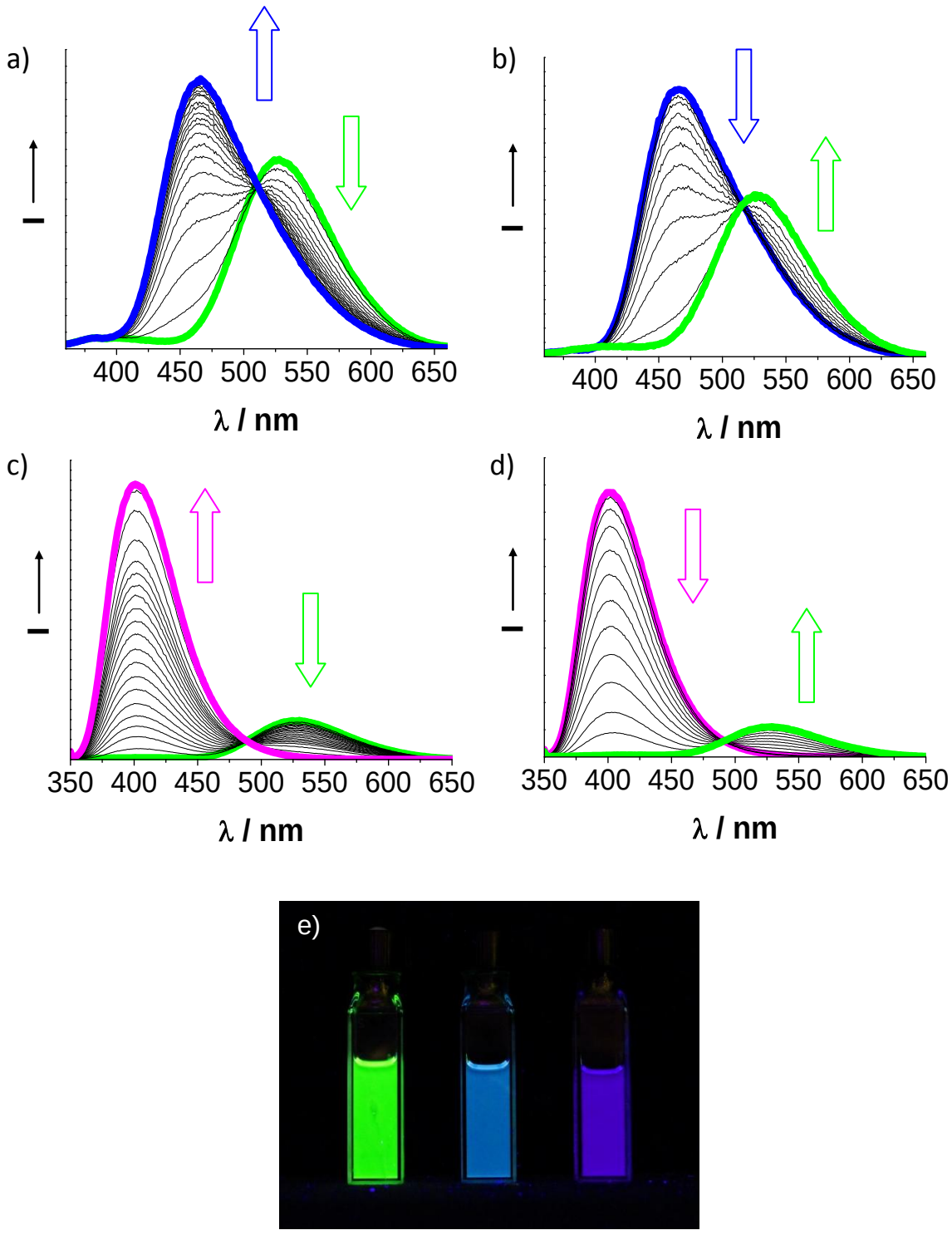

Figure 3.5: Fluorescent titration spectra for 1.0×10^{-5} M solutions of **3.1** in CH_2Cl_2 (λ_{ex} = 365 nm): (a) **3.1** titrated with 20 equiv. of TBAF; (b) 21 equiv. of TBAF added to **3.1** and then titrated with 14 equiv. of HBF_4; (c) **3.1** titrated with 1.8 equiv of HBF_4; (d) 1.8 equiv of HBF_4 added to **3.1** and then titrated with 3.0 equiv of TBAF. e) Photos of 10^{-5} M solutions of (from left to right) **3.1**, [**3.1**·**F**]$^-$ and [**3.1**·**H**]$^+$ under 365 nm UV irradiation.

While the selectivity of dimesitylboranes for fluoride ions over Cl^-, Br^- and others is well documented, these compounds are well known to be responsive to cyanide ions as well.[10] Titration with tetraethylammonium cyanide (TEACN) in CH_2Cl_2 thus triggers a similar fluorescent spectral change to that induced by F^- (λ_{max} = 466 nm, $K = (1.6 \pm 0.5) \times 10^4\ M^{-1}$). As the response to both anions is similar, these studies will focus on fluoride as a trigger for fluorescent change here.

3.3.4 DFT Calculations

DFT calculations on compound **3.1** and its H^+ and F^- adducts at the B3LYP/6-31G* level of theory provide insight into the nature of fluorescence in each of these emissive states. Calculations indicate that the donor and acceptor chromophores make the largest contributions to the HOMO and LUMO, respectively, consistent with through-space *p*(N) ← *p*(B) charge transfer as the lowest-energy emission pathway. However, once the *p* orbital on boron is blocked using fluoride, the lowest energy transition of [**3.1**·**F**]$^-$ becomes a charge transfer from the (F)BMes_2-phenyl (HOMO) to the naphthyl (LUMO), producing blue fluorescence. If instead the filled p orbital on nitrogen is blocked using acid, the lowest energy transition of [**3.1**·**H**]$^+$ is from the BMes_2phenylnaphthyl (HOMO) to the phenyl-naphthyl (LUMO), producing purple fluorescence with some charge transfer character. The trend of the emission energy observed for these species agrees with that of the calculated HOMO-LUMO gaps shown in Figure 3.6.

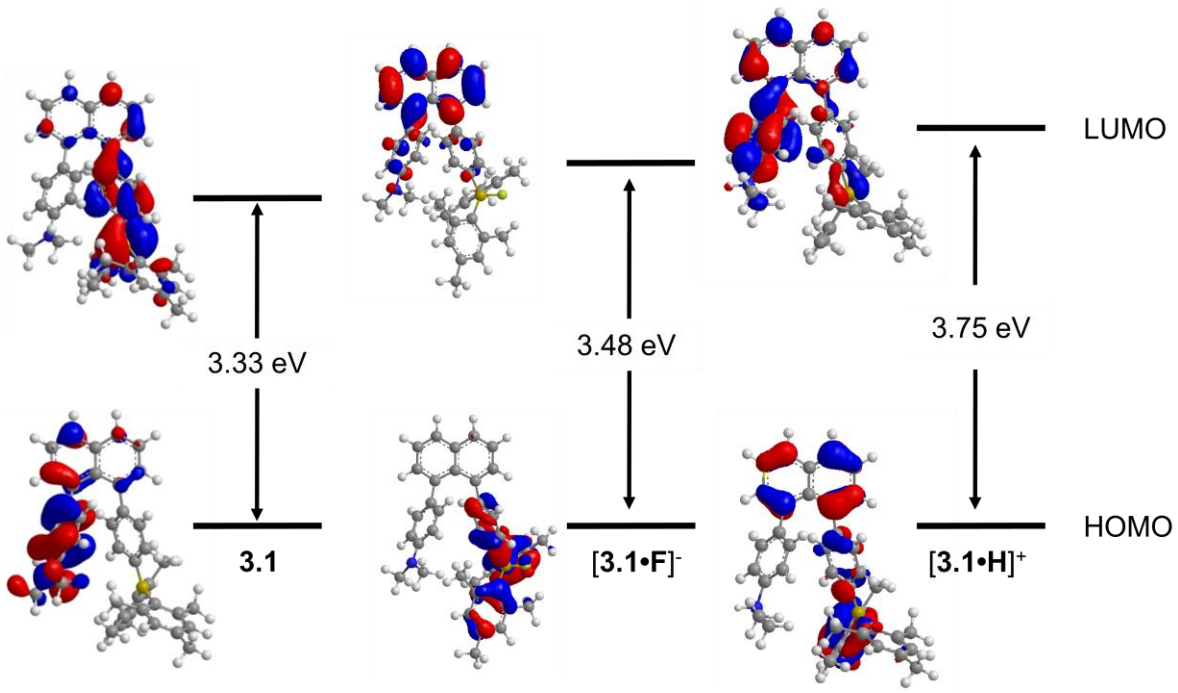

Figure 3.6: Calculated MO surfaces and HOMO-LUMO gaps for **3.1** and its H^+ and F^- adducts.

3.3.5 ^{1}H and ^{19}F NMR Titrations

^{1}H and ^{19}F NMR titrations of [**3.1·F**]$^-$ with acid or [**3.1·H**]$^+$ with fluoride provide insight into these processes. While chelation of HF by a compound with spatially proximate phosphine and borane groups has been recently reported,[11] the 5.55 Å B···N separation distance in this case is too long to support chelation of HF in the presence of both analytes. Instead, it appears that fluoride abstraction from [**3.1·F**]$^-$ occurs *via* a B-F···H intermediate when acid is added, as evidenced by the appearance of a broad peak from -146 to -153 ppm in the ^{19}F NMR spectrum of [**3.1·F**]$^-$ on titration with HBF_4. This is similar in chemical shift to previously studied hydrogen bond adducts of fluoride.[12] Once sufficient acid is added to completely switch the emission color back to green, this peak disappears, indicating restoration of the material to the original form of **3.1**.

A similar intermediate is observed in the ^{19}F NMR spectrum of [**3.1**·**H**]$^{+}$ titrated with F^{-}, though the peak is much sharper, appearing further upfield between -181 to -185 ppm and likely arising from a N-H···F intermediate. Once again, after a sufficient amount of fluoride has been added, compound **3.1** is restored to its original form. Though the deprotonation of a dialkylarylamine by fluoride may not seem intuitively favourable due to their stronger basicities in water, this is in fact consistent with the dramatically higher basicity of fluoride in anhydrous aprotic solvent.[13]

3.4 Conclusions

In summary, we have demonstrated a highly luminescent, nonconjugated donor-acceptor triarylboron compound that can rapidly and reversibly be switched between three fluorescent states using either acid or fluoride. Moreover, each of these stimuli can also be used to reverse the effects of the other, making it possible to cycle compound **3.1** between the three fluorescent colors using only two simple triggers.

3.5 Notes and References

The work described in this chapter has been published as:

- Z. M. Hudson, X.-Y. Liu and S. Wang. *Org. Lett.*, **2011**, *13*, 300.

References

(1) For recent reviews, see: a) C. R.Wade, A. E. J. Broomsgrove, S. Aldridge, F. P. Gabbaï, *Chem. Rev.* **2010**, *110*, 3958. b) T. W. Hudnall, C.-W. Chiu, F. P. Gabbaï, *Acc. Chem. Res.* **2009**, *42*, 388. c) Z. M. Hudson, S. Wang, *Acc. Chem. Res.* **2009**, *42*, 1584. d) S. Yamaguchi, A. Wakamiya, *Pure Appl. Chem.* **2006**, *78*, 1413. e) C. D. Entwistle, T. B. Marder, *Chem. Mater.* **2004**, *16*, 4574. f) Jaekle, F. *Chem. Rev.* **2010**, *110*, 3985, and references therein.

(2) a) J. D. Hoefelmeyer, F. P. Gabbaï, *Organometallics* **2002**, *21*, 982. b) J. D. Hoefelmeyer, S. Sole, F. P. Gabbaï, *Dalton Trans.* **2004**, 1254. c) C. L. Dorsey, P. Jewula, T. W. Hudnall, J. D. Hoefelmeyer, T. J. Taylor, N. R. Honesty, C.-W. Chiu, M. Schulte, F. P. Gabbaï, *Dalton Trans.* **2008**, 4442. d) M. Melaimi, S. Sole, C.-W. Chiu, H. Wang, F. P. Gabbaï, *Inorg. Chem.* **2006**, *45*, 8136. e) M. Melaimi, F. P. Gabbaï, *J. Am. Chem. Soc.* **2005**, *127*, 9680. f) S. Sole, F. P. Gabbaï, *Chem. Commun.* **2004**, 1284. g) M. H. Lee, F. P. Gabbaï, *Inorg. Chem.* **2007**, *46*, 8132. h) C.-W. Chiu, F. P. Gabbaï, *J. Am. Chem. Soc.* **2006**, *128*, 14248.

(3) a) X. Y. Liu, D. R. Bai, S. Wang, *Angew. Chem., Int. Ed.* **2006**, *45*, 5475. b) D. R. Bai, X. Y. Liu, S. Wang, *Chem. Eur. J.* **2007**, *13*, 5713.

(4) K.A. Connors, Binding Constants: The Measurement of Molecular Complex Stability Constants, John Wiley and Sons, 1987.

(5) For example, see: a) W.-L. Jia, X.-D. Feng, D. R. Bai, Z.-H. Lu, S. Wang, G. Vamvounis, *Chem. Mater.* **2005**, *17*, 164. b) Y. Sun, S. Wang, *Inorg. Chem.* **2010**, *49*, 4394.

(6) S.-B. Zhao, P. Wücher, Z. M. Hudson, T. M. McCormick, X. Y. Liu, S. Wang, X.-D. Feng, Z.-H. Lu, *Organometallics* **2008**, *27*, 6446.

(7) N. Wang, Z. M. Hudson, S. Wang, *Organometallics* **2010**, *29*, 4007.

(8) A. E. J. Broomsgrove, D. A. Addy, A. Di Paolo, I. R. Morgan, C. Bresner, V. Chislett, I. A. Fallis, A. L. Thompson, D. Vidovic, S. Aldridge, *Inorg. Chem.* **2010**, *49*, 157.

(9) a) Y. Sun, N. Ross, S.-B. Zhao, K. Huszarik, W.-L. Jia, R.-Y. Wang, D. Macartney, S. Wang, *J. Am. Chem. Soc.* **2007**, *129*, 7510. b) S. Yamaguchi, S. Akiyama, K. Tamao, *J. Am. Chem. Soc.* **2001**, *123*, 11372.

(10) a) C. R. Wade, F. P. Gabbaï, *Inorg. Chem.* **2009**, *49*, 714. b) C.-W. Chiu, F. P. Gabbaï, *Dalton Trans.* **2008**, 814. c) T. W. Hudnall, F. P. Gabbaï, *J. Am. Chem. Soc.* **2007**, *129*, 11978. d) A. E. J. Broomsgrove, D. A. Addy, C. Bresner, I. A. Fallis, A. L. Thompson, S. Aldridge, *Chem. Eur. J.* **2008**, *14*, 7525.

(11) S. Moebs-Sanchez, N. Saffon, G. Bouhadir, L. Maron, D. Bourissou, *Dalton Trans.* **2010**, *39*, 4417.

(12) a) T. W. Hudnall, M. Melaimi, F. P. Gabbaï, *Org. Lett.* **2006**, *8*, 2747. b) I. G. Shenderovich, S. N. Smirnov, G. S. Denisov, V. Gindin, N. S. Golubev, A. Dunger, R. Reibke, S. Kirpekar, O. L. Malkina, H.-H. Limbach, *Ber. Bunsenges. Phys. Chem.* **1998**, *102*, 422.

(13) K. O. Christe, W. W. Wilson, R. D. Wilson, R. Bau, J. A. Feng, *J. Am. Chem. Soc.* **1990**, *112*, 7619.

3.6 Appendix: NMR Titrations

3.6.1 ^{1}H NMR Titrations of 3.1 and its F^- and H^+ Adducts

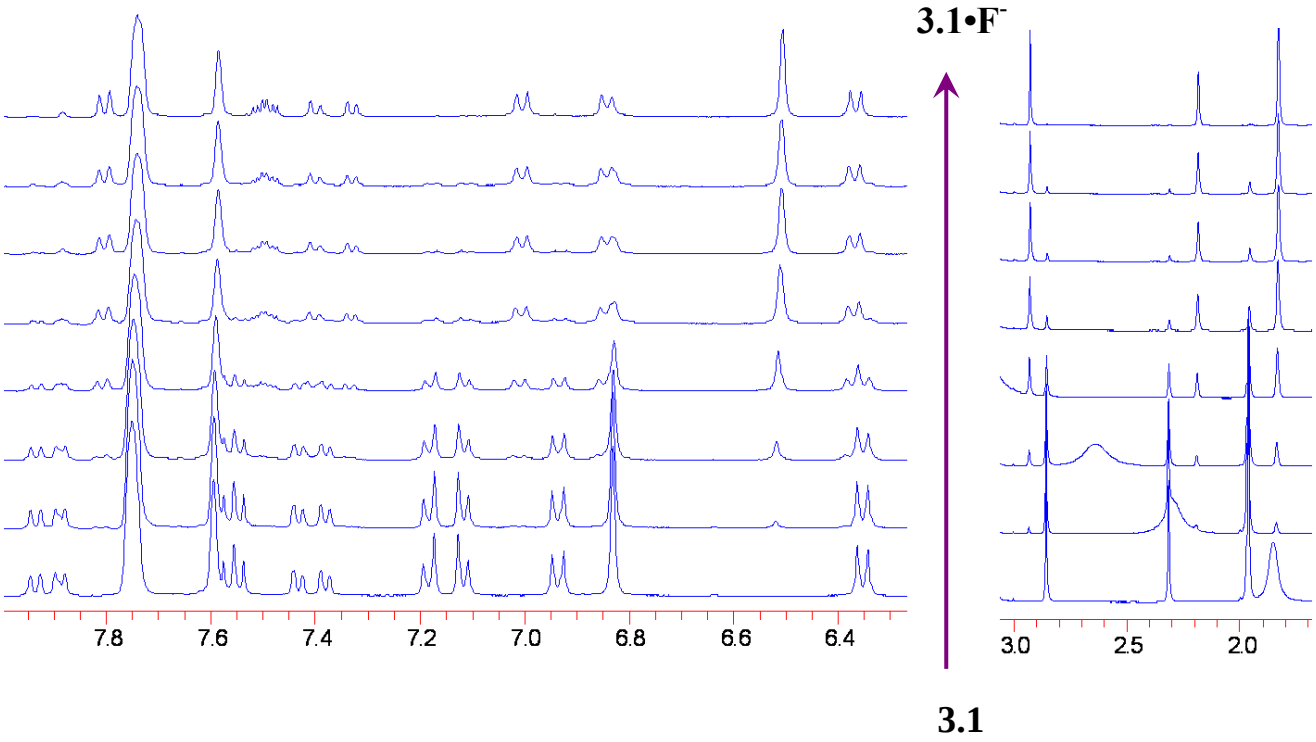

Figure 3.7: ^{1}H NMR Titration of **3.1** with 0-20 equivalents of TBAF to give **3.1•F**$^-$ in CD_2Cl_2.

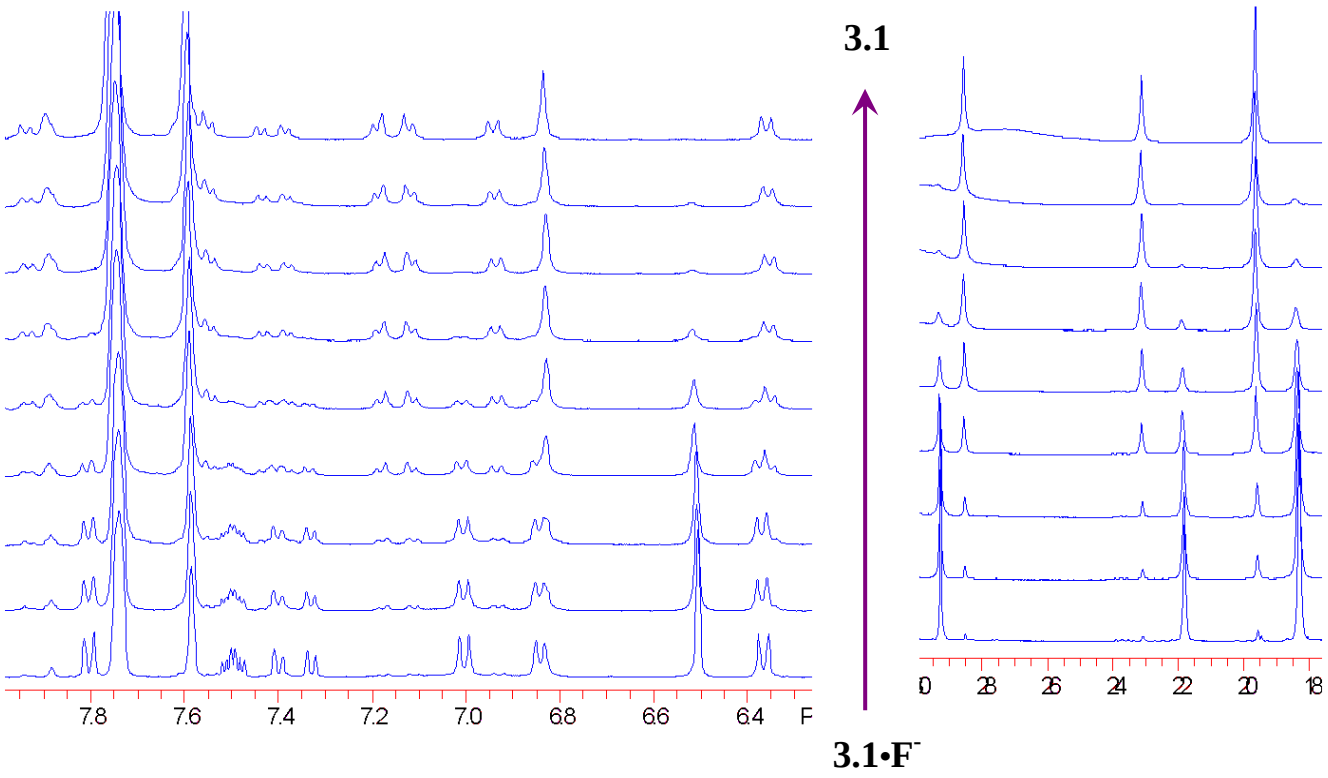

Figure 3.8: ^{1}H NMR Titration of [**3.1**•F^-] with 0-14 equivalents of $HBAr^f_4$ to give **3.1** in CD_2Cl_2.

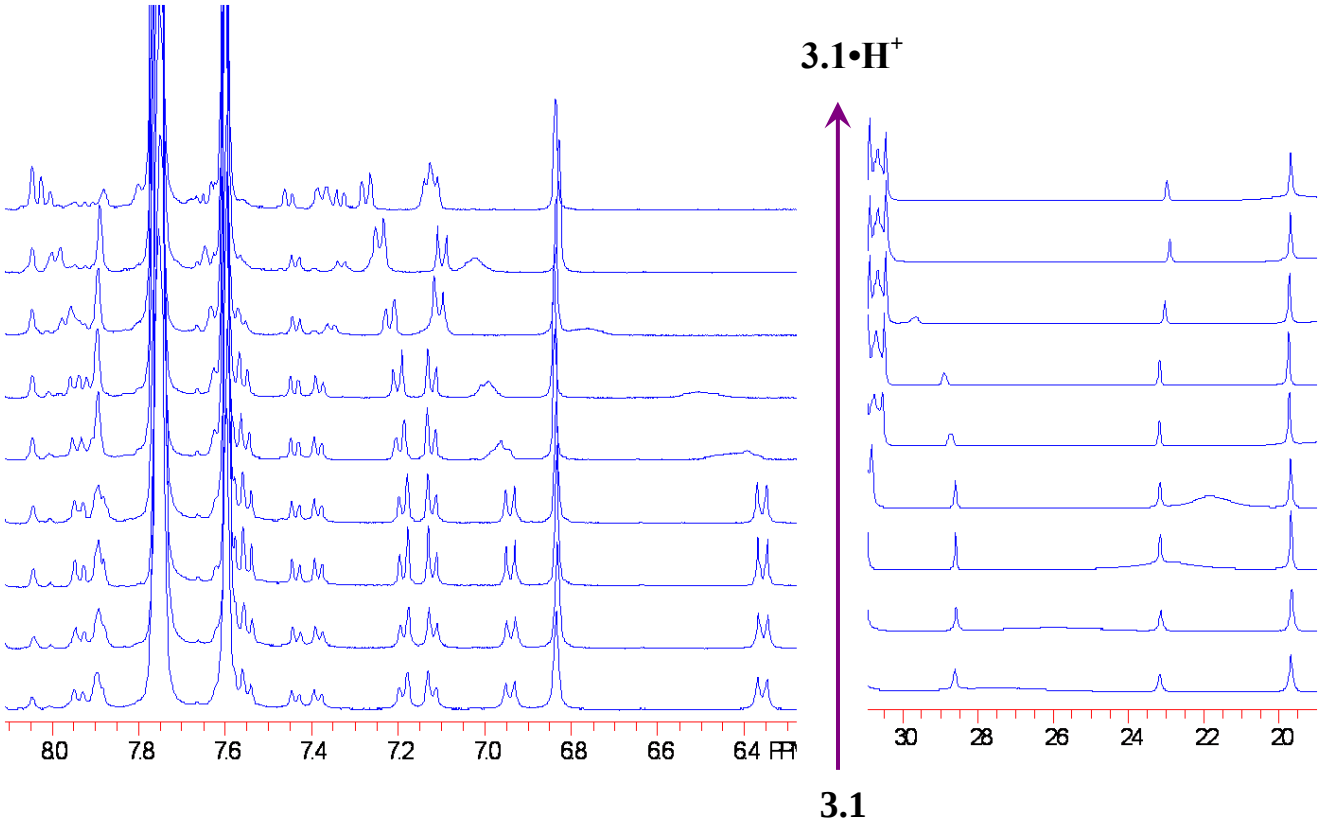

Figure 3.9: ^{1}H NMR Titration of **3.1** with 0-1.8 equivalents of $HBAr^{f}_{4}$ to give [**3.1•H**$^{+}$] in CD_2Cl_2.

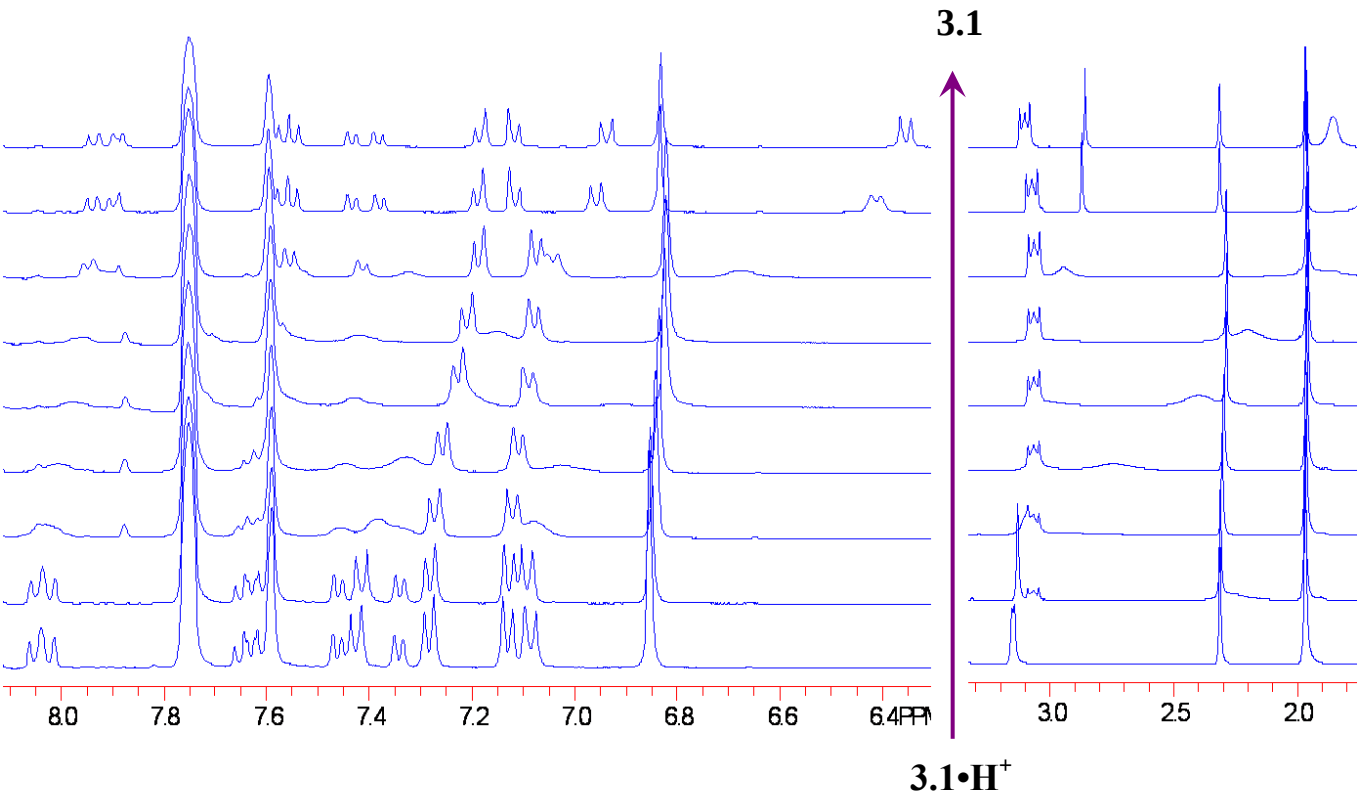

Figure 3.10: ^{1}H NMR Titration of [**3.1•H^{+}**] with 0-3.0 equivalents of TBAF to give **3.1** in CD_2Cl_2.

3.6.2 ^{19}F NMR Titrations of 3.1 and its F^- and H^+ Adducts

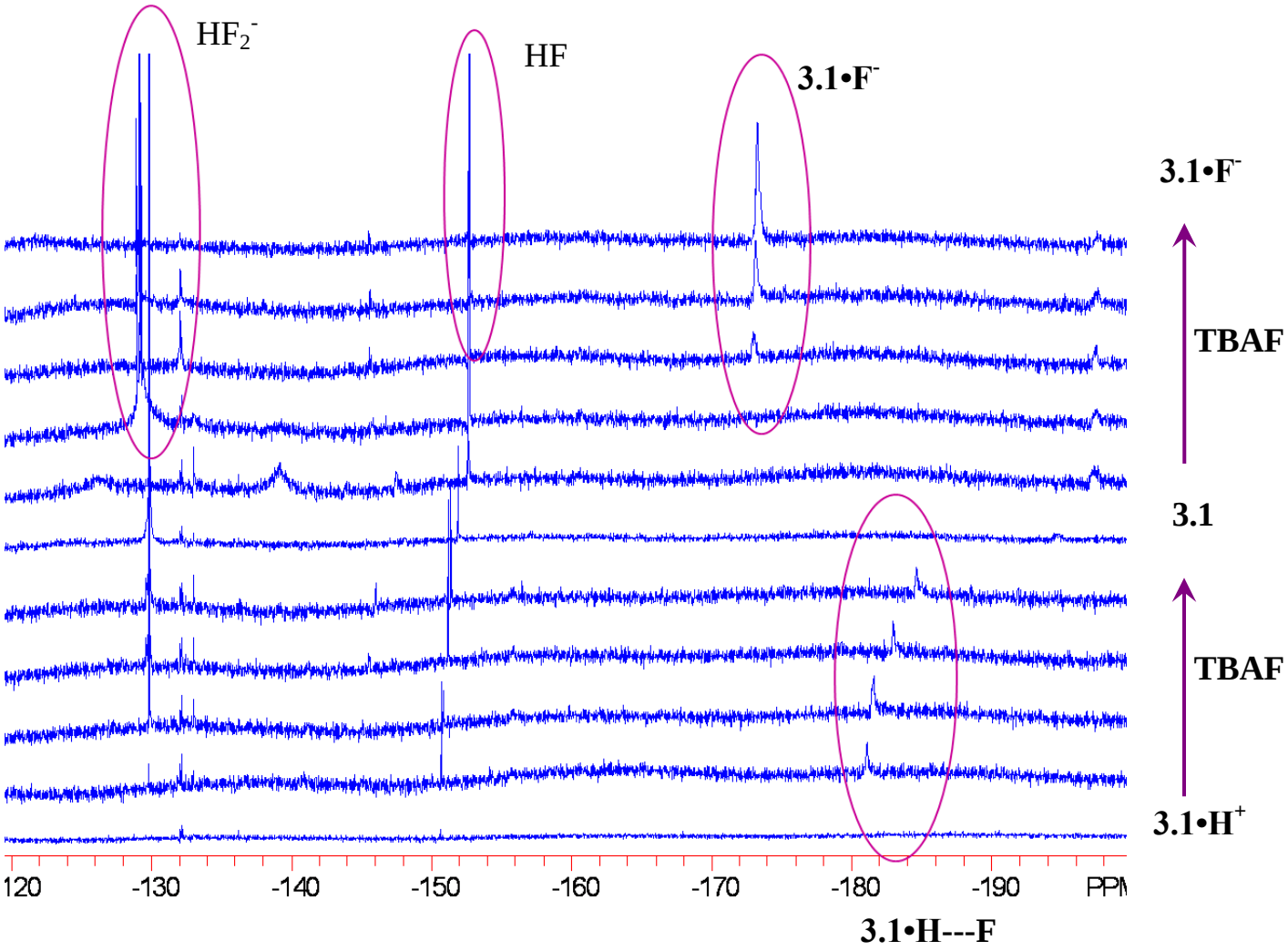

Figure 3.11: ^{19}F NMR Titration of [**3.1•H$^+$**] with 0-24 equivalents of TBAF to give **3.1**, followed by [**3.1•F$^-$**] in CD_2Cl_2.

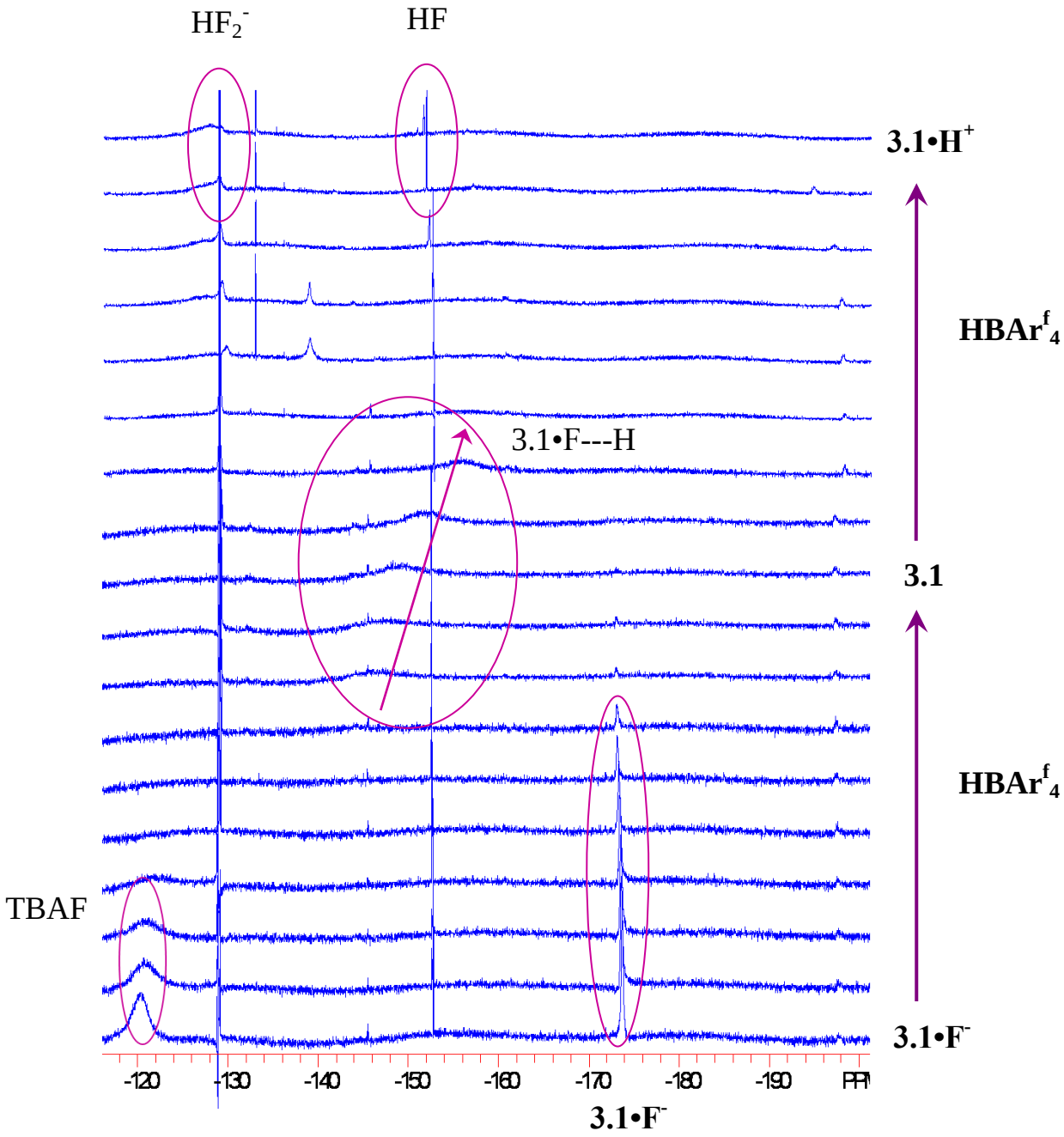

Figure 3.12: ^{19}F NMR Titration of [**3.1•F**$^-$] with 0-16 equivalents of $HBAr^f_4$ to give **3.1**, followed by [**3.1•H**$^+$] in CD_2Cl_2.

Chapter 4

Enhancing the Phosphorescence and Electrophosphorescence Efficiencies of Cyclometalated Pt(II) Compounds with Triarylboron

4.1 Introduction

As described in Chapter 1, triarylboron compounds have been the subject of much recent research activity due to their ability to act as powerful electron acceptors, facilitated by the empty p_π orbital on the boron centre. This feature allows triarylboranes to readily undergo reversible reduction to form a stable radical anion, making them particularly attractive for use as electron-transport materials (ETMs) in organic light-emitting diodes (OLEDs). When protected from nucleophilic attack and hydrolysis by appropriate bulky substituents, highly stable materials can be synthesized with impressive charge-transporting properties. In addition, triarylboranes may also be used in OLEDs as emitters. The electron-accepting boron centre readily facilitates intramolecular charge-transfer in the presence of an appropriate electron donor, providing highly luminescent compounds with impressive quantum yields.[1]

More recently, we have sought to determine if similarly efficient luminescence could be achieved in arylboron compounds using a metal centre as the electron donor. Complexes that display efficient phosphorescence are of great interest as triplet emitters for OLEDs, as these materials can harvest both singlet and triplet excitons in electroluminescent (EL) devices, giving internal quantum efficiencies that can approach 100%.[2] Early investigations in our group in 2007 revealed that the presence of a triarylboron group could greatly improve the phosphorescence of Pt(II) and Cu(I) complexes of *N*-(2'-pyridyl)-7-azaindole (NPA), suggesting that such an improvement in the MLCT phosphorescence of metal complexes was indeed possible.[3]

Triarylboron-containing metal complexes are thus promising candidates for use as emitters in electrophosphorescent devices due to this enhancement in emission brightness. Furthermore, metal chelation has recently been shown to improve the electron-accepting ability of a triarylboron group on the backbone of a metal chelate,[4] which should improve the electron-transporting properties of the boron centre. Since electron mobilities in organic EL devices are typically 1 to 2 orders of magnitude lower than hole mobilities, emitters based on organometallic triarylboranes have the potential to improve device efficiency due to improved carrier balance and charge recombination.[5] Finally, the bulky triarylboron group has been shown to reduce intermolecular aggregation and promote the formation of amorphous films,[1] reducing excimer formation and nonradiative energy transfer in optoelectronic devices.

Despite these considerable advantages, only a single example had been reported of an EL device based on a triarylboron-containing metal complex at the outset of this research, based on Ir(III).[6] In contrast to cyclometalated Ir(III) compounds, which have been extensively studied and produced many highly efficient EL devices,[7] cyclometalated Pt(II) complexes have found comparatively limited use in OLEDs due to their typically weaker luminescence and the tendency to produce excimer emission as a result of their square planar geometry.[8] We therefore decided to examine the impact of triarylboron on a range of *N*,*C*-chelate Pt(II) complexes, and investigate their performance in EL devices.

Our investigations have shown that the triarylboron moiety is capable of significantly enhancing the quantum efficiency and electron-transporting properties of these Pt(II) complexes, which in turn can be used to improve the brightness, efficiency, and electron mobility of EL devices based on Pt(II) electrophosphors. Using these materials, we demonstrate efficient green electrophosphorescence using a bifunctional boron-containing Pt(II) complex,[9] and efficient orange electrophosphorescence using a trifunctional donor-acceptor Pt(II) compound.[10] Finally, with improvements in device structure we demonstrate for the first time a Pt(II)-based OLED with an external quantum efficiency > 20%.[11]

4.2 Experimental

4.2.1 General Procedures

Experimental techniques and instruments used follow those described in section 2.2. The syntheses of BppyA, BppyB,[12] *p*-(diphenylamino)phenyl pinacolborane,[13] and PtCl(acac)(DMSO)[14] have been reported previously.

4.2.2 Electroluminescent Device Fabrication

Devices were fabricated in a Kurt J. Lesker LUMINOS® cluster tool with a base pressure of ~10^{-8} Torr without breaking vacuum. The ITO anode is commercially patterned and coated on glass substrates 50 x 50 mm^2 with a sheet resistance less than 15 Ω. Substrates were ultrasonically cleaned with a standard regiment of Alconox®, acetone, and methanol followed by UV ozone treatment for 15 min. The active area for all devices was 2 mm^2. The film thicknesses were monitored by a calibrated quartz crystal microbalance and were further verified for single-carrier devices using capacitance-voltage measurements (Agilent 4294A). I-V characteristics were measured using a HP4140B picoammeter in ambient air. Luminance measurements and EL spectra were taken using a Minolta LS-110 luminance meter and an Ocean Optics USB200 spectrometer with bare fiber, respectively. The external quantum efficiency of EL devices was calculated following standard procedures.[15] After deposition, single carrier devices were transferred to a homebuilt variable temperature cryostat for measurement at 298K. UPS measurements were performed using a PHI 5500 MultiTechnique system, with attached organic deposition chamber with a base pressure of 10^{-10} Torr. Additional details regarding device fabrication, characterization and UPS measurements have been described elsewhere.[16]

4.2.3 Synthesis of Brominated Intermediates

General synthesis of brominated intermediates: To a 250 mL Schlenk flask with stir bar and condenser was added boronic acid (5.6 mmol), 2,5-dibromopyridine (5.6 mmol), $Pd(PPh_3)_4$ (0.17 mmol), K_2CO_3 (28

mmol), and 120 mL degassed THF:H_2O (1:1). The mixture was heated to 55°C under N_2 and allowed to stir overnight, after which the THF was evaporated *in vacuo* and the aqueous layer extracted with CH_2Cl_2. The combined organic layers were dried with $MgSO_4$, concentrated, and the residue purified by column chromatography on silica (hexanes:CH_2Cl_2 as eluent) to produce the desired brominated ligand.

5'-bromo-(2-(2'-pyridyl)benzothiophene) (Brbtp): (Yield: 82%). ^{1}H NMR (600 MHz, $CDCl_3$): δ 8.67 (d, J = 2.3 Hz, 1H, pyridine), 7.88-7.78 (m, 4H), 7.67 (d, J = 8.3 Hz, 1H, thianaphthene), 7.36 (t, J = 6.4 Hz, 1H, thianapthene), 7.35 (t, J = 6.1 Hz, 1H, thianapthene) ppm; ^{13}C NMR (100 MHz, $CDCl_3$): δ 151.1, 150.7, 143.5, 140.7, 140.4, 139.2, 125.4, 124.7, 124.2, 122.6, 121.8, 120.7, 119.4 ppm; HRMS calc'd for $C_{13}H_8BrNS$ $[M]^+$: 288.9561, found 288.9561.

5'-bromo-(2-(2'-pyridyl)benzofuran) (Brbzf): (Yield 56%). ^{1}H NMR (400 MHz, CD_2Cl_2): δ 8.73 (d, J = 2.4 Hz, 1H, pyridine), 7.97 (dd, J = 8.4 Hz, J = 2.4 Hz, 1H, pyridine), 7.83 (d, J = 8.4 Hz, pyridine), 7.69 (d, J = 7.6 Hz, benzofuran), 7.58 (d, J = 8.0 Hz, 1H, benzofuran), 7.47 (s, 1H, benzofuran), 7.39 (td, J = 7.2 Hz, J = 1.2 Hz, 1H, benzofuran), 7.30 (td, J = 7.6 Hz, J = 0.8 Hz, 1H, benzofuran) ppm; ^{13}C NMR (100 MHz, CD_2Cl_2): δ 155.7, 154.8, 151.3, 147.9, 139.6, 129.0, 125.7, 123.6, 122.1, 120.9, 119.9, 111.7, 105.5. HRMS calc'd for $C_{13}H_9NOBr$ $[M+H]^+$: 273.9867, found 273.9875.

5-bromo-3'-methoxy-(2-phenylpyridine) (Brmeop): (Yield 73%). ^{1}H NMR (600 MHz, $CDCl_3$) δ 8.73 (d, J = 2.4 Hz, 1H, pyridine), 7.87 (dd, J = 8.5 Hz, J = 2.4 Hz, 1H, pyridine), 7.61 (d, J = 8.5 Hz, 1H, pyridine), 7.55 (t, J = 1.9 Hz, 1H, phenyl), 7.50 (d, J = 7.1 Hz, 1H, phenyl), 7.37 (t, J = 7.9 Hz, 1H, phenyl), 6.98 (dd, J = 8.2 Hz, J = 2.5 Hz, 1H, phenyl), 3.88 (s, 3H, methoxy) ppm; ^{13}C NMR (125 MHz, $CDCl_3$) δ 160.1, 155.6, 150.6, 139.6, 139.2, 129.8, 121.7, 119.4, 119.1, 115.3, 111.9, 55.3 ppm; HRMS calc'd for $C_{12}H_{10}BrNO$ $[M]^+$: 262.9946, found 262.9925.

5-bromo-2',3'-difluoro-(2-phenylpyridine) (Brdfp): (Yield 88%). ^{1}H NMR (400 MHz, C_6D_6): δ 8.59 (d, J = 1.90 Hz, 1H, pyridine), 7.79 (tt, J = 7.9 Hz, J = 1.7 Hz, 1H, phenyl), 7.18 (dd, J = 8.5 Hz, J = 1.5 Hz, 1H, pyridine), 7.11(dd, J = 8.5 Hz, J = 2.4 Hz, 1H, pyridine), 6.63 (m, 2H, phenyl) ppm; ^{13}C NMR (100 MHz, C_6D_6): δ 151.5, 151.0, 149.0, 138.9, 128.7, 125.8, 125.4, 124.3, 124.26, 120.3, 117.6 ppm; ^{19}F NMR (376 MHz, C_6D_6): δ -139.3 (ddd, J = 19.5 Hz, J = 9.8 Hz, J = 4.6 Hz), -143.5 (td, J = 19.5 Hz, J = 6.9 Hz) ppm; HRMS calc'd for $C_{11}H_6BrF_2N$ [M^+]: 268.9652, found 268.9641.

5-bromo-4'-(*N,N*-diphenylamino)-(2-phenylpyridine) (BrNppy): (Yield 89%). ^{1}H NMR (600 MHz, $CDCl_3$): δ 8.67 (d, J = 2.4 Hz, 1H, pyridine), 7.82 (d, J = 8.4 Hz, 2H, *p*-Ph), 7.81 (dd, J = 8.5 Hz, J = 2.4 Hz, 1H, pyridine), 7.55 (d, J = 8.5 Hz, 1H, pyridine), 7.27 (t, J = 7.7 Hz, 4H, N-*Ph*) 7.13 (d, J = 7.7 Hz, 4H, N-*Ph*), 7.12 (d, J = 8.3 Hz, 2H, *p*-Ph), 7.05 (t, J = 7.8 Hz, 2H, N-*Ph*) ppm; ^{13}C NMR (125 MHz, $CDCl_3$): δ 155.4, 150.5, 149.0, 147.3, 139.1, 131.6, 129.3, 127.5, 124.9, 123.4, 122.8, 120.8, 118.3 ppm; HRMS calc'd for $C_{23}H_{17}BrN_2$ [M^+]: 400.0575, found 400.0580.

5-bromo-4'-(*N*-(1-naphthyl)-*N*-phenylamino)-(2-phenylpyridine) (Yield 86%). ^{1}H NMR (400 MHz, $CDCl_3$) δ 8.76 (s, 1H), 8.05 (d, J = 8.4Hz, 1H), 7.99 (d, J = 8.2 Hz, 1H), 7.92-7.85 (m, 3H), 7.84 (d, J = 8.5 Hz, 1H), 7.60-7.50 (m, 3H), 7.46 Hz (d, J = 7.5 Hz, 1H), 7.45 (t, J = 7.3 Hz, 1H), 7.34 (d, J = 7.3 Hz, 1H), 7.32 (d, J = 8.1 Hz, 1H), 7.24 (d, J = 7.9 Hz, 2H), 7.14 (d, J = 8.7 Hz, 2H), 7.10 (t, J = 8.1 Hz, 1H) ppm; ^{13}C NMR (75 MHz, $CDCl_3$) δ 155.5, 150.4, 149.6, 147.7, 143.0, 139.0, 135.2, 131.1, 130.6, 129.2, 128.4, 127.5, 127.3, 126.8, 126.5, 126.3, 126.2, 124.1, 122.9, 122.7, 120.63, 120.59, 118.1 ppm; HRMS calc'd for $C_{27}H_{19}BrN_2$: 450.0732, found 450.0743.

4.2.4 Synthesis of Boron-Functionalized Cyclometalating Ligands

General synthesis of N,C-chelate ligands: To a 250 mL Schlenk flask with stir bar was added the desired brominated intermediate (3.5 mmol) and 80 mL dry THF. The mixture was cooled to -78°C under N_2 and

allowed to stir for 30 min, at which point *n*-BuLi (3.85 mmol, 1.6 M in hexanes) was added dropwise. The mixture was stirred for 40 min, then $FBMes_2$ (3.9 mmol) in 20 mL THF was added dropwise *via* cannula. The mixture was stirred 1h at -78°C, then allowed to warm slowly to room temperature and stirred overnight. The mixture was then concentrated and the residue partitioned between CH_2Cl_2 and water. The aqueous layer was extracted twice with CH_2Cl_2, and the combined organic layers were dried with $MgSO_4$, concentrated, and purified by column chromatography on silica (hexanes:CH_2Cl_2 as eluent) to afford the desired borylated ligand. A reaction temperature of -100°C was used for the preparation of Bdfp, Bbtp, and Bbzf.

5'-(dimesitylboryl)-(2-(2'-pyridyl)benzothiophene) (Bbtp): (Yield 63%). ^{1}H NMR (500 MHz, $CDCl_3$): δ 8.66 (s, 1H, pyridine), 7.93 (s, br, 1H, thianaphthene), 7.89-7.85 (m, 1H, thianaphthene), 7.84-7.79 (m, 2H, thianaphthene/pyridine), 7.77 (d, J = 7.9 Hz, pyridine), 7.37 (t, J = 3.6 Hz, 1H, thianaphthene), 7.35 (t, J = 3.6 Hz, 1H, thianaphthene), 2.32 (s, 6H, mesityl), 2.05 (s, 12H, mesityl) ppm. ^{13}C NMR (125 MHz, $CDCl_3$) δ 157.3, 154.7, 144.8, 144.2, 141.2, 140.7, 140.4, 139.3, 138.9, 128.41, 128.36, 125.4, 124.6, 124.3, 122.6, 122.4, 118.9, 23.5, 21.2 ppm. HRMS calc'd for $C_{31}H_{30}BNS$ $[M]^+$: 459.2192, found 459.2201.

5'-(dimesitylboryl)-(2-(2'-pyridyl)benzofuran) (Bbzf): (Yield 31%). ^{1}H NMR (600 MHz, $CDCl_3$): δ 8.70 (s, 1H, pyridine), 7.87 (d, J = 7.9 Hz, 1H, benzofuran), 7.86 (d, J = 7.9 Hz, 1H, benzofuran), 7.66 (d, J = 8.1 Hz, 1H, pyridine), 7.56 (d, J = 8.1 Hz, 1H, pyridine), 7.53 (s, 1H, benzofuran), 7.34 (t, J = 7.5 Hz, 1H, benzofuran), 7.26 (t, J = 7.6 Hz, 1H, benzofuran), 6.84 (s, 4H, mesityl), 2.31 (s, 6H, mesityl), 2.04 (s, 12H, mesityl) ppm. ^{13}C NMR (100 MHz, $CDCl_3$): δ 157.3, 155.5, 155.1, 151.2, 144.4, 140.8, 140.7, 139.3, 139.1, 128.7, 128.4, 125.6, 123.3, 121.9, 119.1, 111.5, 106.4, 23.5, 21.2 ppm. HRMS calc'd for $C_{31}H_{31}BNO$ $[M+H]^+$: 444.2500, found 444.2521.

5-(dimesitylboryl)-3'-methoxy-(2-phenylpyridine) (Bmeop): (Yield 58%).^{1}H NMR (600 MHz, $CDCl_3$) δ 8.81 (s, 1H, pyridine), 7.89 (d, J = 7.9 Hz, 1H, phenyl), 7.79 (s, 1H, phenyl), 7.78 (d, J = 8.0 Hz, 1H, pyridine), 7.69 (d, J = 7.7 Hz, 1H, phenyl), 7.41 (t, J = 7.9 Hz, 1H, phenyl), 7.03 (d, J = 8.0 Hz, 1H, pyridine), 6.90 (s, 4H, mesityl), 3.91 (s, 3H, methoxy), 2.36 (s, 6H, mesityl), 2.12 (s, 12H, mesityl) ppm. ^{13}C NMR (150 MHz, $CDCl_3$) δ 160.0, 159.1, 156.9, 144.4, 140.8, 140.6, 140.1, 139.0, 138.2, 129.6, 128.3, 119.9, 119.5, 115.8, 112.0, 55.2, 23.4, 21.1 ppm. HRMS calc'd for $C_{30}H_{33}BNO$ $[M+H]^+$: 434.2655, found 434.2661.

5-(dimesitylboryl)-2',3'-difluoro-(2-phenylpyridine) (Bdfp): (Yield 66%). ^{1}H NMR (500 MHz, C_6D_6): δ 9.90 (s, 1H, pyridine), 8.12 (dd, J = 8.0 Hz, J = 6.5 Hz, 1H, phenyl), 7.70 (d, J = 7.9 Hz, 1H, pyridine), 7.66 (dd, J = 7.9 Hz, J = 1.7 Hz, 1H, pyridine), 6.77 (s, 4H, mesityl), 6.65 (multiplet, 2H, phenyl), 2.19 (s, 6H, mesityl), 2.06 (s, 12 H, mesityl) ppm. ^{13}C NMR (125 MHz, C_6D_6): δ 157.3, 154.8, 151.7, 148.7, 144.3, 141.4, 140.9, 139.5, 139.4, 129.6, 129.0, 126.3, 124.3, 124.2, 117.8, 23.7, 21.3 ppm. ^{19}F NMR (376 MHz, C_6D_6): δ -139.4 (ddd, J = 20.7 Hz, J = 9.2 Hz, J = 4.6 Hz), -142.8 (dt, J = 20.7 Hz, J = 6.9 Hz) ppm. HRMS calc'd for $C_{29}H_{28}BF_2N$ $[M^+]$: 439.2283, found 439.2263.

5-(dimesitylboryl)-4'-(*N*,*N*-diphenylamino)-(2-phenylpyridine) (BNppy): (Yield 77%). ^{1}H NMR (600 MHz, CD_2Cl_2): δ 8.66 (d, J = 1.9 Hz, 1H, pyridine), 8.02 (d, J = 8.8 Hz, 2H, *p*-Ph), 7.79 (dd, J = 8.0 Hz, J = 1.9 Hz, 1H, pyridine), 7.73 (d, J = 8.0 Hz, 1H, pyridine), 7.33 (t, J = 7.6 Hz, 4H, N-*Ph*), 7.17 (d, J = 7.7 Hz, 4H, N-*Ph*), 7.13 (d, J = 8.8 Hz, 2H, *p*-Ph), 7.11 (t, J = 7.4 Hz, 2H, N-*Ph*), 6.89 (s, 4H, mesityl), 2.34 (s, 6H, mesityl), 2.07 (s, 12H, mesityl) ppm. ^{13}C NMR (150 MHz, CD_2Cl_2): δ 159.0, 157.3, 149.4, 147.4, 144.4, 141.1, 140.8, 139.1, 137.4, 132.2, 129.4, 128.4, 128.0, 125.1, 123.6, 122.4, 118.8, 23.3, 21.0 ppm. HRMS calc'd for $C_{41}H_{39}BrN_2$ $[M^+]$: 570.3206, found 570.3234.

5-(dimesitylboryl)-4'-(*N*-(1-naphthyl)-*N*-phenylamino)-(2-phenylpyridine) (BNPB2): (Yield 80%). ^{1}H NMR (400 MHz, $CDCl_3$) δ 8.73 (d, J = 1.7 Hz, 1H), 8.01-7.96 (m, 3H), 7.93 (d, J = 8.2 Hz, 1H), 7.84 (d, J = 8.6 Hz, 1H), 7.81 dd, J = 8.1 Hz, J = 1.7 Hz, 1H), 7.66 (d, J = 8.1 Hz, 1H), 7.52 (t, J = 7.5 Hz, 1H), 7.50 (t, J = 8.2 Hz, 1H), 7.40 (d, J = 8.1 Hz, 1H), 7.39 (t, J = 8.1 Hz, 1H), 7.29 (d, J = 8.4 Hz, 1H), 7.27 (d, J = 7.3 Hz, 1H), 7.19 (d, J = 7.6 Hz, 2H), d, J = 8.9 Hz, 2H), 7.05 (t, J = 7.3 Hz, 1H), 6.88 (s, 4H), 2.36 (s, 6H), 2.10 (s, 12H) ppm; ^{13}C NMR (100 MHz, $CDCl_3$) δ 159.1, 157.3, 149.9, 147.7, 144.4, 143.0, 141.0, 140.7, 139.0, 137.2, 135.3, 131.1, 129.2, 128.4, 128.3, 128.1, 127.3, 126.9, 126.8, 126.5, 126.3, 126.2, 124.1, 123.1, 122.8, 120.5, 118.8, 23.5, 21.2 ppm; HRMS calc'd for $C_{45}H_{41}BN_2$: 620.3363, found 620.3381.

4.2.5 Synthesis of Cyclometalated Pt(II) Complexes

General procedure for the preparation of cyclometalated Pt complexes: To a 100 mL Schlenk flask with stir bar and condenser was added N,C-chelate ligand (0.17 mmol), PtCl(DMSO)(acac) (0.17 mmol) and NaOAc (0.17 mmol) in 25 mL degassed MeOH. The mixture was heated at reflux for two days, concentrated, then purified on silica (hexanes:CH_2Cl_2 as eluent) to afford the desired cyclometalated Pt complex.

Pt(*N*^*C*-BppyA)(*O*^*O*-acetylacetonate) (Pt-BppyA): (Yield 22%). ^{1}H NMR (400 MHz, CD_2Cl_2) δ 9.02 (d, sat, J = 1.4 Hz, J_{Pt-H} = 39.9 Hz, 1H, pyridine), 7.91 (dd, J = 8.1 Hz, J = 1.4 Hz, 1H, pyridine), 7.64 (d, J = 8.0 Hz, 1H, pyridine), 7.58-7.52 (m, 2H, phenyl), 7.21 (t, J = 7.4 Hz, 1H, phenyl), 7.12 (t, J = 7.6 Hz, 1H, phenyl), 6.92 (s, 4H, mesityl), 5.45 (s, 1H, acac), 2.34 (s, 6H, mesityl), 2.11 (s, 12H, mesityl), 1.99 (s, 3H, acac), 1.69 (s, 3H, acac) ppm. ^{13}C NMR (150 MHz, C_6D_6) δ 185.5, 184.1, 171.5, 156.2, 146.0, 144.8, 143.2, 141.1, 139.4, 136.6, 132.1, 130.5, 129.0, 124.5, 123.7, 117.8, 102.5, 27.6, 27.0, 23.8, 21.2 ppm. Anal. calc'd. for $C_{34}H_{36}BNO_2Pt$: C 58.63, H 5.21, N 2.01, found: C 58.32, H 5.62, N 1.86.

Pt(*N*^*C*-BppyB)(*O*^*O*-acetylacetonate) (Pt-BppyB): (Yield 22%).^{1}H NMR (400 MHz, CD_2Cl_2) δ 9.01 (d, sat, J = 5.7 Hz, J_{Pt-H} = 38.5 Hz, 1H, pyridine), 7.88 (t, J = 7.9 Hz, 1H, pyridine), 7.72 (d, J = 7.9 Hz, 1H, pyridine), 7.63 (s, sat, J_{Pt-H} = 35.5 Hz, 1H, phenyl), 7.45 (d, J = 7.6 Hz, 1H, phenyl), 7.23 (d, J = 7.7 Hz, 1H, phenyl), 7.20(dd, J = 7.9 Hz, J = 5.7 Hz, 1H, pyridine), 6.87 (s, 4H, mesityl), 5.46 (s, 1H, acac), 2.32 (s, 6H, mesityl), 2.10 (s, 12H, mesityl), 2.01 (s, 3H, acac), 1.73 (s, 3H, acac) ppm. ^{13}C NMR (100 MHz, CD_2Cl_2) δ 186.0, 184.1, 167.7, 148.0, 147.6, 146.3, 142.2, 140.7, 138.7, 138.41, 138.35, 138.1, 131.8, 128.0, 122.1, 119.3, 102.1, 28.1, 26.4, 23.3, 20.9 ppm. Anal. calc'd. for $C_{34}H_{36}BNO_2Pt$: C 58.63, H 5.21, N 2.01, found: C 58.50, H 5.26, N 2.00.

Pt(*N*^*C*-Bbtp)(*O*^*O*-acetylacetonate) (Pt-Bbtp): (Yield 43%). ^{1}H NMR (600 MHz, C_6D_6) δ 9.38 (s, 1H, pyridine), 9.37 (d, J = 8.0 Hz, 1H, thianaphthene), 7.73 (d, J = 7.8 Hz, 1H, pyridine), 7.46 (d, J = 7.9 Hz, 1H, pyridine), 7.42 (t, J = 8.0 Hz, 1H, thianaphthene), 7.21 (t, J = 8.0 Hz, 1H, thianaphthene), 6.81 (s, 4H, mesityl), 6.81 (d, J = 8.0 Hz, 1H, thianaphthene), 5.13 (s, 1H, acac), 2.20 (s, 6H, mesityl), 2.09 (s, 12H, mesityl), 1.64 (s, 3H, acac), 1.51 (s, 3H, acac) ppm. ^{13}C NMR (150 MHz, C_6D_6) δ 185.2, 183.7, 167.5, 156.2, 147.2, 146.5, 146.0, 144.2, 141.1, 140.8, 139.2, 138.6, 128.9, 128.3, 127.6, 126.7, 124.5, 122.9, 117.6, 102.6, 27.3, 26.2, 23.8, 21.2 ppm. Anal. calc'd. for $C_{36}H_{36}BNO_2PtS$: C 57.45, H 4.82, N 1.86, found C 57.29, H 4.68, N 1.86.

Pt(*N*^*C*-Bbzf)(*O*^*O*-acetylacetonate) (Pt-Bbzf): (Yield 15%). ^{11}H NMR (600 MHz, CD_2Cl_2) δ 8.92 (s, 1H, pyridine), 8.07 (d, J = 7.8 Hz, 1H, pyridine), 7.85 (d, J = 7.9 Hz, 1H, pyridine), 7.48 (d, J = 8.2 Hz, 1H, benzofuran), 7.39 (t, J = 8.2 Hz, 1H, benzofuran), 7.36 (d, J = 8.0 Hz, 1H, benzofuran), 7.27 (t, J = 7.4 Hz, 1H, benzofuran), 6.92 (s, 4H, mesityl), 5.54 (s, 1H, acac), 2.34 (s, 6H, mesityl), 2.14 (s, 12H, mesityl), 2.05 (s, 3H, acac), 1.72 (s, 3H, acac) ppm. ^{13}C NMR (100 MHz, C_6D_6) δ 184.8, 183.8, 160.2, 158.9, 158.2, 157.1, 147.4, 141.0, 140.8, 139.2, 134.5, 134.2, 128.9, 127.0, 125.3, 124.6, 123.3, 115.9, 111.8, 102.5, 27.3, 26.2, 23.8, 21.2 ppm. Anal. calc'd. for $C_{36}H_{36}BNO_3Pt$: C 58.70, H 4.93, N 1.90, found:

C 57.27, H 4.72, N 1.82 (The low carbon content may be caused by the presence of CH_2Cl_2 solvent molecules in the crystal lattice. Calc'd for 0.2 CH_2Cl_2 per molecule: C 57.70, H, 4.87, N, 1.86).

Pt(*N*^*C*-Bmeop)(*O*^*O*-acetylacetonate) (Pt-Bmeop): (Yield 23%).^{1}H NMR (400 MHz, CD_2Cl_2) δ 9.00 (d, sat, J = 1.5 Hz, J_{Pt-H} = 40.0 Hz, 1H, pyridine), 7.90 (dd, J = 8.1 Hz, J = 1.5 Hz, 1H, pyridine), 7.60 (d, J = 8.1 Hz, 1H, pyridine), 7.43 (d, J = 8.4 Hz, 1H, phenyl), 7.12 (d, J = 2.6 Hz, 1H, phenyl), 6.94-6.89 (m, 5H, mesityl/phenyl), 5.44 (s, 1H, acac), 3.85 (s, 3H, methoxy), 2.33 (s, 6H, mesityl), 2.11 (s, 12H, mesityl), 1.97 (s, 3H, acac), 1.67 (s, 3H, acac) ppm. ^{13}C NMR (125 MHz, C_6D_6) δ 185.3, 183.9, 171.4, 157.7, 156.2, 146.0, 145.2, 141.1, 140.8, 139.4, 133.2, 132.7, 129.0, 117.8, 117.1, 110.2, 109.8, 102.6, 55.0, 27.6, 27.0, 23.9, 21.3 ppm. Anal. calc'd. for $C_{35}H_{38}BNO_3Pt$: C 57.86, H 5.27, N 1.93, found: C 57.86, H 5.07, N 1.92.

Pt(*N*^*C*-Bdfp)(*O*^*O*-acetylacetonate) (Pt-Bdfp): (Yield 16 %). ^{1}H NMR (600 MHz, C_6D_6): δ 9.46 (s, 1H, pyridine), 7.76 (dd, 1H, J = 8.2 Hz, J = 4.9 Hz, phenyl), 7.61, (d, 1H, J = 8.1 Hz, pyridine), 7.45 (d, 1H, J = 8.1, pyridine), 7.02 (dt, J = 10.5 Hz, J = 8.2 Hz, 1H, phenyl) 6.79 (s, 4H, mesityl), 5.02 (s, 1H, acac), 2.19 (s, 6H, mesityl), 2.02 (s, 12H, mesityl), 1.64 (s, 3H, acac), 1.51 (s, 3H, acac) ppm. ^{13}C NMR (150 MHz, $CDCl_3$) δ 185.7, 184.3, 155.8, 149.4, 147.7, 146.6, 141.1, 140.6, 139.6, 137.2, 137.0, 133.6, 129.0, 126.4, 122.5, 118.3, 114.5, 102.6, 27.4, 26.9, 23.8, 21.2. ^{19}F NMR (376 MHz, C_6D_6): δ -142.4 (dd, J = 19.5 Hz, J = 8.1 Hz), -147.6 (ddd, J = 19.5 Hz, J = 10.4 Hz, J = 4.6 Hz) ppm. Anal. calc'd. for $C_{34}H_{34}BF_2NO_2Pt$: C 55.75, H 4.68, N 1.91, found: C 55.15, H 4.70, N 1.83.

Pt(*N*^*C*-BNppy)(*O*^*O*-acetylacetonate) (Pt-BNppy): (Yield 20%). ^{1}H NMR (400 MHz, CD_2Cl_2): δ 8.90 (d, sat, J = 1.6 Hz, J_{Pt-H} = 37.1 Hz, 1H, pyridine), 7.81 (dd, J = 8.1 Hz, J = 1.6 Hz, 1H, pyridine), 7.47 (d, J = 8.1 Hz, 1H, pyridine), 7.39 (d, J = 8.5 Hz, 1H, phenyl), 7.34 (t, J = 7.4 Hz, 4H, N-*Ph*), 7.21 (d, J = 7.4 Hz, 4H, N-*Ph*), 7.12 (t, J = 7.3 Hz, 2H, N-*Ph*), 7.08 (d, J = 2.4 Hz, 1H, phenyl), 6.91 (s, 4H, mesityl), 6.75

(dd, J = 8.5 Hz, J = 2.4 Hz, 1H, phenyl), 5.37 (s, 1H, acac), 2.33 (s, 6H, mesityl), 2.12 (s, 12H, mesityl), 1.70 (s, 3H, acac), 1.66 (s, 3H, acac) ppm. ^{13}C NMR (100 MHz, CD_2Cl_2): δ 186.0, 183.8, 169.8, 155.9, 149.3, 147.2, 146.0, 142.6, 140.8, 139.2, 137.3, 135.1, 129.3, 128.4, 125.8, 125.1, 123.8, 122.3, 116.9, 116.8, 101.9, 27.4, 26.7, 23.4, 21.0 ppm. Anal. calc'd. for $C_{46}H_{45}BN_2O_2Pt$: C 63.96, H 5.25, N 3.24, found: C 64.19, H 5.32, N 3.03.

Pt(*N*^*C*-BNPB2)(*O*^*O*-acetylacetonate) (Pt-BNPB2): (Yield 23%). ^{1}H NMR (400 MHz, CD_2Cl_2) δ 8.89 (s, sat, J_{Pt-H} = 31.5 Hz, 1H), 8.04 (d, J = 8.4 Hz, 1H), 7.95 (d, J = 8.1 Hz, 1H), 7.87 (d, J = 7.87 Hz, 1H), 7.76 (d, J = 8.1 Hz, 1H), 7.56 (t, J = 7.4 Hz, 1H), 7.51 (t, J = 8.0 Hz, 1H), 7.47-7.39 (m, 3H), 7.33-7.23 (m, 5H), 7.06 (t, J = 7.0 Hz, 1H), 6.91 (s, 4H), 6.61 (dd, J = 8.6 Hz, J = 2.4 Hz, 1H), 5.33 (s, 1H), 2.33 (s, 6H), 2.12 (s, 12H), 1.65 (s, 3H), 1.61 (s, 3H) ppm; ^{13}C NMR (100 MHz, CD_2Cl_2) δ 186.3, 184.1, 170.2, 156.3, 150.1, 147.8, 146.3, 143.3, 143.1, 141.1, 140.8, 139.6, 136.9, 135.7, 135.2, 132.0, 129.4, 128.8, 128.5, 128.1, 127.3, 126.9, 126.7, 126.6, 125.6, 124.5, 124.2, 123.4, 120.6, 117.2, 115.4, 102.2, 27.7, 26.9, 23.8, 21.3 ppm; Anal. calc'd for $C_{50}H_{47}BN_2O_2Pt$: C 65.72, H 5.18, N 3.07, found C 65.74, H 5.41, N 3.02

4.2.6 X-Ray Diffraction Analysis

Single crystals of several of the above-listed cyclometalated Pt(II) complexes were grown by slow evaporation from solutions of CH_2Cl_2 and methanol. Crystal data for these compounds are listed in Table 4.1, and important bond lengths and angles are given in Table 4.2. These crystal structures have been deposited to the Cambridge Crystallographic Data Centre as CCDC 776137–776142, and may be obtained free of charge via www.ccdc.cam.ac.uk/data_request/cif.

Table 4.1: Crystallographic data

Compound	**Pt-BppyA**	**Pt-BppyB**	**Pt-Bdfp**	**Pt-Bmeop**	**Pt-Bbtp**
Formula	$C_{34}H_{36}BNO_2Pt$	$C_{34}H_{36}BNO_2Pt$	$C_{34}H_{34}BF_2NO_2Pt$	$C_{35}H_{38}BNO_3Pt$	$C_{72}H_{72}B_2N_2O_6Pt_2$
FW	696.54	696.54	732.52	726.56	1473.10
Space Group	P2(1)/n	P2(1)/c	P-1	P2(1)/c	P-1
a, Å	10.5936(2)	19.803(3)	8.2719(8)	19.1103(12)	8.151(2)
b, Å	15.9635(3)	7.9816(13)	11.2458(11)	10.5928(7)	10.669(3)
c, Å	35.0945(5)	19.404(3)	17.0385(17)	17.0223(11)	18.158(5)
α, °	90	90	71.7150(10)	90	104.878(4)
β, °	93.3660(10)	108.100(10)	88.8380(10)	115.218(4)	90.091(4)
γ, °	90	90	78.1980(10)	90	100.131(4)
V, $Å^3$	5924.63(18)	2915.4(8)	1471.5(3)	3117.4(3)	1500.5(7)
Z	8	4	2	4	1
D_{calc}, g cm^{-1}	1.562	1.587	1.653	1.548	1.630
T, K	180(2)	180(2)	180(2)	180(2)	180(2)
μ, mm^{-1}	4.767	4.844	4.812	4.536	4.713
$2\theta_{max}$, °	54.26	54.38	54.32	54.40	53.80
Reflns measured	35177	11699	16210	18500	15987
Reflns used (R_{int})	13038 (0.0595)	6377 (0.1363)	6387 (0.0364)	6845 (0.1220)	6375 (0.0954)
Parameters	719	360	378	374	411
Final R Values [I > 2σ(I)]:					
R_1[a]	0.0547	0.0800	0.0288	0.0650	0.1389
wR_2[b]	0.0993	0.1742	0.0639	0.1248	0.3154
R values (all data):					
R_1[a]	0.0977	0.1744	0.0361	0.1609	0.1820
wR_2[b]	0.1123	0.2252	0.0667	0.1596	0.3322
Goodness-of-fit on F^2	1.031	0.960	1.020	0.938	1.191

[a] $R_1 = \Sigma[(|F_0| - |F_c|) / \Sigma |F_0|$

[b] $wR2 = [\Sigma w[(F_0^2-F_c^2)^2] / \Sigma[w(F_0^2)^2]]^{1/2}$

$w = 1 / [\sigma^2(F_0^2) + (0.075P)^2]$, where $P = [Max (F_0^2, 0) + 2F_c^2] / 3$

Table 4.2: Selected bond lengths (Å) and angles (°) for several Pt(II) complexes.

		Pt-BppyA	
Pt(1)-C(1)	1.967(8)	N(1)-C(7)	1.359(9)
Pt(1)-N(1)	1.995(6)	B(1)-C(17)	1.567(13)
Pt(1)-O(1)	1.997(5)	B(1)-C(26)	1.576(12)
Pt(1)-O(2)	2.081(5)	B(1)-C(10)	1.589(12)
N(1)-C(11)	1.340(9)		
C(1)-Pt(1)-N(1)	81.4(3)	C(11)-N(1)-C(7)	120.2(6)
C(1)-Pt(1)-O(1)	93.5(3)	C(11)-N(1)-Pt(1)	123.7(5)
N(1)-Pt(1)-O(1)	174.5(2)	C(7)-N(1)-Pt(1)	116.2(5)
C(1)-Pt(1)-O(2)	174.3(3)	C(17)-B(1)-C(26)	124.7(7)
N(1)-Pt(1)-O(2)	93.2(2)	C(17)-B(1)-C(10)	118.7(7)
O(1)-Pt(1)-O(2)	91.9(2)	C(26)-B(1)-C(10)	116.5(8)
		Pt-BppyB	
Pt(1)-C(1)	1.965(16)	N(1)-C(7)	1.41(2)
Pt(1)-N(1)	1.998(12)	B(1)-C(12)	1.52(3)
Pt(1)-O(1)	1.999(9)	B(1)-C(21)	1.59(3)
Pt(1)-O(2)	2.093(10)	B(1)-C(3)	1.62(2)
N(1)-C(11)	1.336(17)		
C(1)-Pt(1)-N(1)	81.7(6)	C(12)-B(1)-C(21)	126.6(15)
C(1)-Pt(1)-O(1)	91.5(5)	C(12)-B(1)-C(3)	120.3(16)
N(1)-Pt(1)-O(1)	173.0(5)	C(21)-B(1)-C(3)	113.0(15)
C(1)-Pt(1)-O(2)	176.6(5)	C(11)-N(1)-C(7)	119.2(13)
N(1)-Pt(1)-O(2)	95.2(5)	C(11)-N(1)-Pt(1)	124.1(12)
O(1)-Pt(1)-O(2)	91.7(4)	C(7)-N(1)-Pt(1)	116.8(9)
		Pt-Bdfp	
Pt(1)-C(7)	1.966(4)	F(1)-C(10)	1.362(5)
Pt(1)-N(1)	1.988(3)	F(2)-C(11)	1.365(4)
Pt(1)-O(1)	1.999(3)	C(2)-B(1)	1.572(6)
Pt(1)-O(2)	2.076(3)	C(12)-B(1)	1.577(6)
N(1)-C(1)	1.353(5)	C(21)-B(1)	1.582(6)

C(7)-Pt(1)-N(1)	81.84(14)	C(5)-N(1)-Pt(1)	116.5(2)
C(7)-Pt(1)-O(1)	93.17(13)	C(30)-O(1)-Pt(1)	124.5(3)
N(1)-Pt(1)-O(1)	174.74(11)	C(33)-O(2)-Pt(1)	123.9(3)
C(7)-Pt(1)-O(2)	174.55(13)	C(2)-B(1)-C(12)	118.4(4)
N(1)-Pt(1)-O(2)	93.03(12)	C(2)-B(1)-C(21)	116.3(4)
O(1)-Pt(1)-O(2)	91.91(11)	C(12)-B(1)-C(21)	125.3(4)
C(1)-N(1)-C(5)	119.8(3)	F(1)-C(10)-C(9)	120.9(4)
C(1)-N(1)-Pt(1)	123.7(3)	F(2)-C(11)-C(6)	121.4(4)

Pt-BMeop

Pt(1)-C(1)	1.985(12)	O(2)-C(34)	1.283(14)
Pt(1)-N(1)	1.997(8)	O(3)-C(4)	1.382(13)
Pt(1)-O(1)	2.001(7)	O(3)-C(12)	1.440(14)
Pt(1)-O(2)	2.095(8)	B(1)-C(22)	1.541(18)
N(1)-C(11)	1.352(13)	B(1)-C(10)	1.571(17)
N(1)-C(7)	1.353(13)	B(1)-C(13)	1.600(18)
O(1)-C(32)	1.289(13)		

C(1)-Pt(1)-N(1)	81.1(4)	C(22)-B(1)-C(10)	119.5(11)
C(1)-Pt(1)-O(1)	93.2(4)	C(22)-B(1)-C(13)	123.7(10)
N(1)-Pt(1)-O(1)	174.1(4)	C(10)-B(1)-C(13)	116.7(11)
C(1)-Pt(1)-O(2)	175.3(4)	C(11)-N(1)-C(7)	120.1(9)
N(1)-Pt(1)-O(2)	94.5(3)	C(11)-N(1)-Pt(1)	123.3(8)
O(1)-Pt(1)-O(2)	91.2(3)	C(7)-N(1)-Pt(1)	116.6(7)
C(4)-O(3)-C(12)	117.2(10)		

Pt-Bbtp

Pt(1)-C(6)	1.963(4)	N(1)-C(18)	1.353(6)
Pt(1)-N(1)	1.990(4)	N(1)-C(14)	1.356(6)
Pt(1)-O(1)	1.995(3)	B(1)-C(17)	1.570(6)
Pt(1)-O(2)	2.057(3)	B(1)-C(28)	1.574(7)
S(1)-C(12)	1.731(5)	B(1)-C(19)	1.578(6)
S(1)-C(13)	1.751(5)		

C(6)-Pt(1)-N(1)	81.73(18)	C(12)-S(1)-C(13)	89.5(2)
C(6)-Pt(1)-O(1)	94.37(17)	C(18)-N(1)-C(14)	119.2(4)

N(1)-Pt(1)-O(1)	175.55(15)	C(18)-N(1)-Pt(1)	124.8(3)
C(6)-Pt(1)-O(2)	172.33(17)	C(17)-B(1)-C(28)	117.7(4)
N(1)-Pt(1)-O(2)	91.55(14)	C(17)-B(1)-C(19)	116.2(4)
O(1)-Pt(1)-O(2)	92.19(13)	C(28)-B(1)-C(19)	126.1(4)

4.3 Results and Discussion

4.3.1 Synthesis and Molecular Design

To study the impact of boryl substitution on cyclometalated complexes of Pt(II), a series of *N,C*-chelate ligands with well-documented photophysical properties were selected and functionalized with a dimesitylboron ($BMes_2$) group. Acetylacetonate (acac) was chosen as the ancillary ligand for these complexes, offering improved solution and solid-state stability over previously reported triarylboron-containing *N,C*-chelate platinum complexes containing phenyl, SMe_2 or DMSO ancillary ligands.[3,12] In addition, the acetylacetonate ligand has a high triplet energy, and should not interfere with phosphorescent emission from the boron chromophore.[17,18] Furthermore, this ligand offers improved rigidity of the complexes compared to the non-chelating SMe_2, phenyl or DMSO ancillary ligands previously studied by our group, decreasing energy loss *via* radiationless vibrational decay. Finally, this design facilitates direct comparison with non-boron functionalized *N,C*-chelate-Pt(acac) phosphors, which have been extensively investigated by Thompson and coworkers.[18a] The π skeletons of the cyclometalates were selected to exemplify both a range of colors and functionalization, including electron donating and withdrawing groups, heteroatoms, and constitutional isomers. Due to the improved electron-accepting ability of triarylboron centres attached to the π skeleton *via* a pyridine ring,[12] the majority of these materials were prepared with the boron centre on the pyridine site. The *N,C*-chelate ligands **BppyA** and **BppyB** were obtained by previously published procedures.[12] All other *N,C*-chelate ligands have not been previously reported and were prepared first by Suzuki coupling of 2,5-dibromopyridine with the appropriate boronic acids to produce the brominated intermediates as shown in Figure 4.1, which proceed in good yields with excellent selectivity for the 2-position of the pyridine ring under mild conditions. Subsequent treatment of these intermediates with *n*-BuLi followed by the addition of Mes_2BF gives the target ligands also in good yields, although lower temperatures (-100°C) are necessary for the benzofuryl and benzothienyl species to minimize deprotonation at the 3-position and subsequent formation of four-coordinate boron side products.

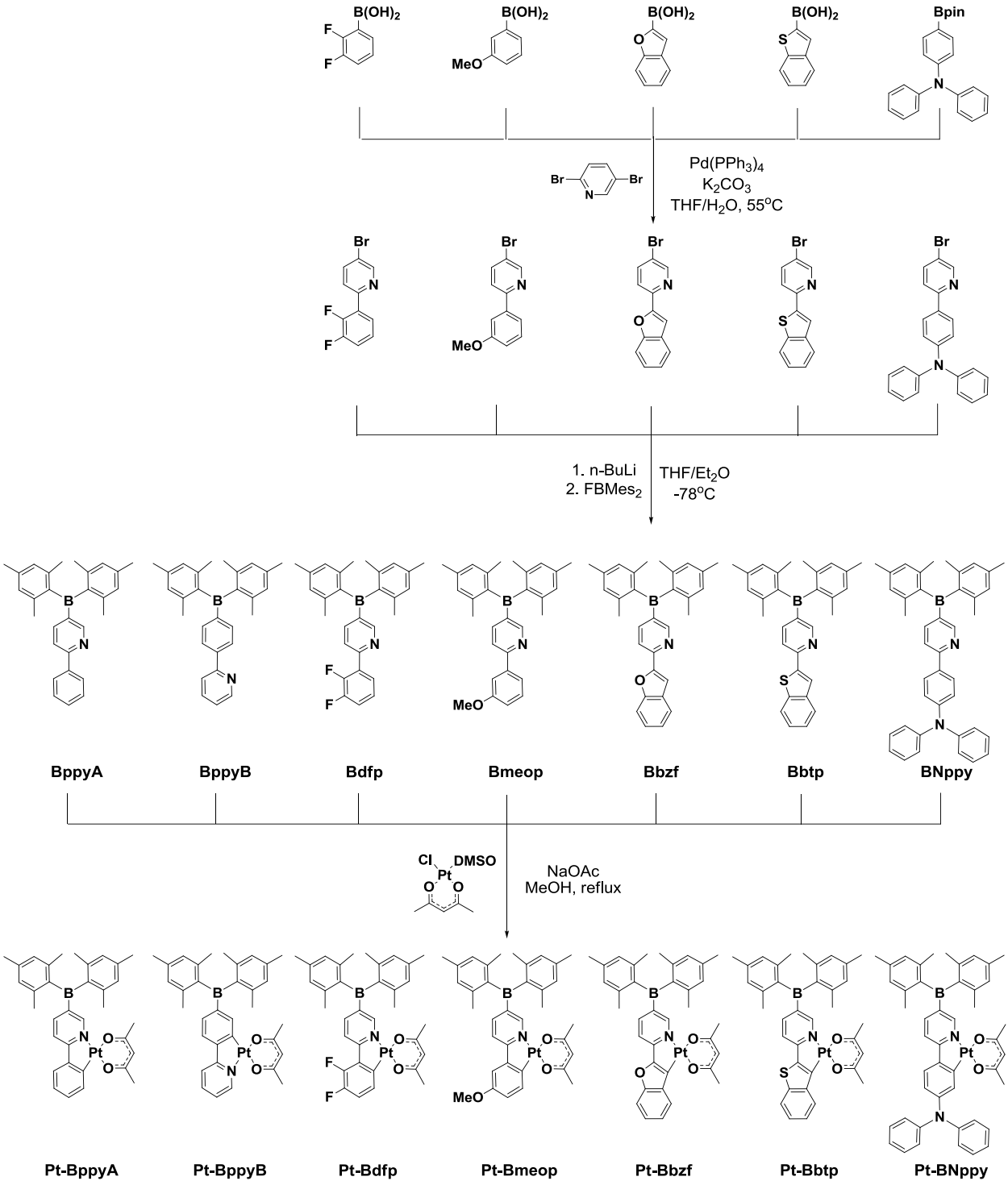

Figure 4.1: Synthesis of boron-functionalized *N,C*-chelate Pt(II) acetylacetonates. (**Pt-BNPB2** not shown)

The synthesis of cyclometalated acetylacetonate complexes of Pt(II) is well documented in literature, typically involving heating 2-3 equivalents of the *N,C*-chelate ligand in the presence of K_2PtCl_4 to form first the chloride-bridged dinuclear species, then cleavage of the dimer at high temperature (≥80°C) with Na(acac) to form the desired complex.[18] This method, however, is unsuitable for the pyridine-functionalized $BMes_2$ ligands shown in Figure 4.1 because of their poor stability at high temperature in solution. We therefore developed an alternative strategy based on the method of Crespo and coworkers,[19] involving the reaction of 1 equivalent of ligand with PtCl(DMSO)(acac) in the presence of NaOAc in refluxing methanol. The resulting Pt(II) complexes can then be purified by column chromatography and isolated in high purity. Though overall yields were often low due to incomplete reaction, this procedure is a versatile method for the synthesis of cyclometalated Pt(II) complexes requiring mild temperatures. Furthermore, the previously reported cyclometalation methods[18] employ excess ligand, giving yields with respect to the ligand that are extremely low, a situation best avoided if the cyclometalating ligands themselves are of value.

All complexes have been fully characterized by NMR and elemental analyses. Furthermore, crystal structures of many of these complexes have been obtained by single-crystal X-ray diffraction analyses, which provide insight on intermolecular interactions in the solid state and can be used as starting points for theoretical investigations of their electronic structures.

4.3.2 Crystal Structures

The structures of **Pt-BppyA**, **Pt-BppyB**, **Pt-Bdfp**, **Pt-Bmeop**, and **Pt-Bbtp** are shown in Figure 4.2. The Pt(II) center in all complexes has a typical square planar geometry with similar Pt-C, Pt-N and Pt-O bond lengths. The two Pt-O bonds in each complex show considerable differences, with those *trans* to the Pt-C bonds significantly longer (2.08 Å on average) than those *trans* to the Pt-N bond (2.00 Å on average), owing to the greater *trans* effect exerted by the carbanion ligand. **Pt-Bdfp** forms a stacked dimer in the

crystal lattice with a Pt···Pt separation distance of 3.404(1) Å (Figure 4.2). Similarly short Pt···Pt distances have been well documented in literature.[20] Dimeric packing is also observed for **Pt-Bbtp** with a Pt···Pt separation distance of 3.692(1) Å. Notably, no significant intermolecular stacking interactions are evident for **Pt-BppyA**, **Pt-BppyB** and **Pt-Bmeop** in the solid state, and thus these compounds are likely to be less prone to excimer emission, which can significantly shift emission energy and reduce emission efficiency.

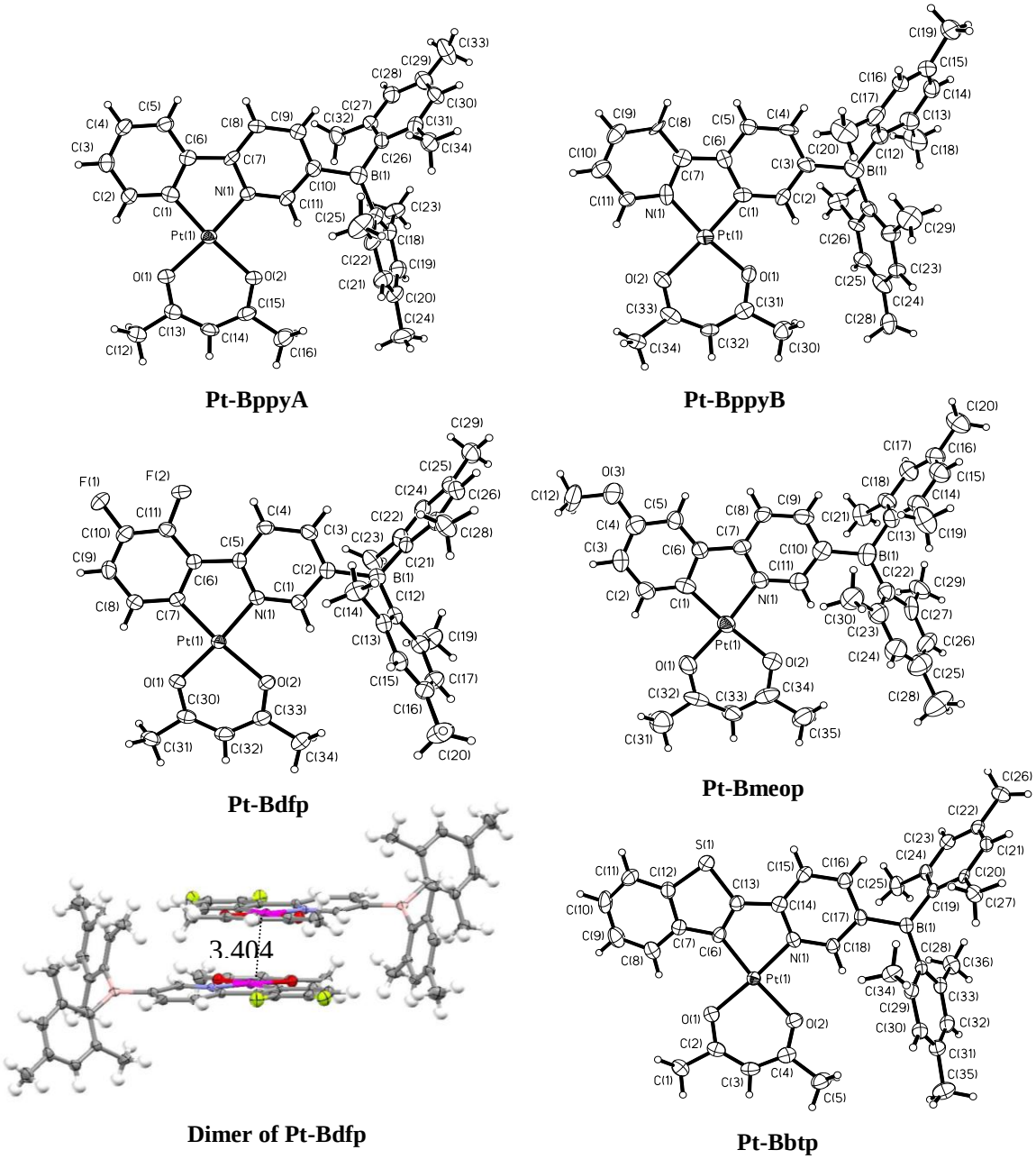

Pt-BppyA **Pt-BppyB**

Pt-Bdfp **Pt-Bmeop**

Dimer of Pt-Bdfp **Pt-Bbtp**

Figure 4.2: Crystal structures of several *N,C*-chelate Pt(II) acetylacetonates

4.3.3 Photophysical and Electrochemical Properties: Ligands

These ligands are all luminescent in solution and the solid state (Table 4.3). In the absence of a metal atom, these boron-containing cyclometalating ligands all exhibit relatively strong, broad absorption bands above 325 nm. This can be attributed to charge-transfer to boron from the pendant mesityl groups, and is common in compounds containing the dimesitylboron moiety without strong external donors.[21] This is supported by the emission spectra of the ligands, which show nearly identical emission maxima (406-422 nm) despite substantial variation in the electronic nature of the π-skeleton to which the boron group is attached (Figure 4.3).

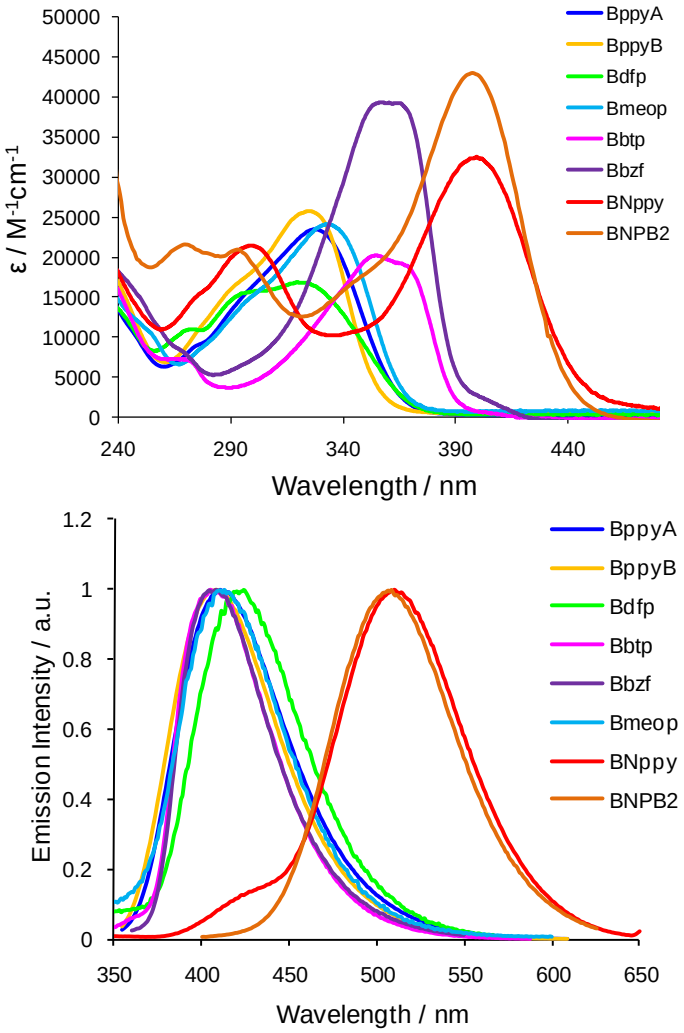

Figure 4.3: Absorption (top) and emission (bottom) spectra of the boron-functionalized ligands at 10^{-5} M in CH_2Cl_2. λ_{ex} = 365 nm.

Table 4.3: Photophysical properties of *N,C*-chelate ligands.

Ligand	Absorbance, λ (nm) ε (10^4 cm^{-1} M^{-1})[a]	Emission λ_{max} (nm)[a]	Φ_P[b]	$E_{1/2}^{red}$ (mV)[c]	HOMO (eV)[d]	LUMO (eV)[d]
BppyA	233 (1.88), 329 (2.34)	411	0.16	-2.12	-5.99	-2.68
BppyB	232 (2.12), 327 (2.57)	409	0.01	-2.16	-3.01	-2.64
Bdfp	232 (1.74), 289 (1.57), 323 (1.68)	424	0.07	-1.98	-6.11	-2.82
Bbtp	233 (1.96), 355 (2.02), 367 (1.91)	405	0.42	-1.93	-5.90	-2.87
Bbzf	233 (2.13), 358 (3.93), 3.66 (3.91)	408	0.63	-1.93	-5.84	-2.87
Bmeop	232 (2.08), 335 (2.40)	413	0.39	-2.10	-6.00	-2.70
BNppy	232 (2.39), 301 (2.14), 401 (3.24)	510	0.94	-2.08	-5.41	-2.72
BNPB2	271 (2.13), 298 (1.96), 396 (4.27)	509	1.0	-2.19	-5.35	-2.61

[a] Measured in CH_2Cl_2 at $1x10^{-5}$ M, [b] In CH_2Cl_2 relative to anthracene ($\Phi = 0.36$)[14] All QYs are ± 5%. [c] In DMF relative to $FeCp^{0/+}$. [d] Determined using the reduction potential and optical energy gap.

The **BNppy** and **BNPB2** ligands containing diarylamine donor groups are exceptions to this trend. These compounds show red shifted absorption and emission bands that are highly sensitive to solvent polarity, due to donor-acceptor charge transfer from nitrogen to boron. This results in highly polarized excited states which emit light with near-unit quantum efficiency, similar to examples of donor-acceptor triarylboranes previously reported by us and others.[1,21] By varying the polarity of the solvent, the emission of these compounds in solution is tunable through the blue-violet (λ_{max} = ~430 nm in hexanes) to yellow (λ_{max} = ~535 in MeOH) region of the visible spectrum (Figure 4.4). It is interesting to note that the 5-methoxy substituent in **Bmeop** does not have the same effect, presumably due to its weaker donor strength or the improved electronic communication offered by the *para* geometry in **BNppy** and **BNPB2**.

These ligands all show reversible reduction waves by cyclic voltammetry attributable to reduction of the boron centre, and some electronic effects are apparent. **Bdfp** has the least negative reduction potential among the phenylpyridines (-1.98 V relative to $FeCp^{0/+}$), rendered the strongest electron acceptor by the electron-withdrawing fluorine atoms. **Bbtp** and **Bbzf** undergo reduction at -1.93 V, consistent with the smaller HOMO-LUMO gap imparted by more extensive conjugation apparent from the absorption spectra. **BNppy, BNPB2** and **Bmeop** undergo reduction at ca. 150 mV lower potentials, an anticipated

consequence of functionalization of the π system with electron donor groups. In addition, **BNppy** and **BNPB2** also undergo quasi-reversible oxidation at +0.58 and +0.56 V, due to oxidation of the diarylamine moieties.

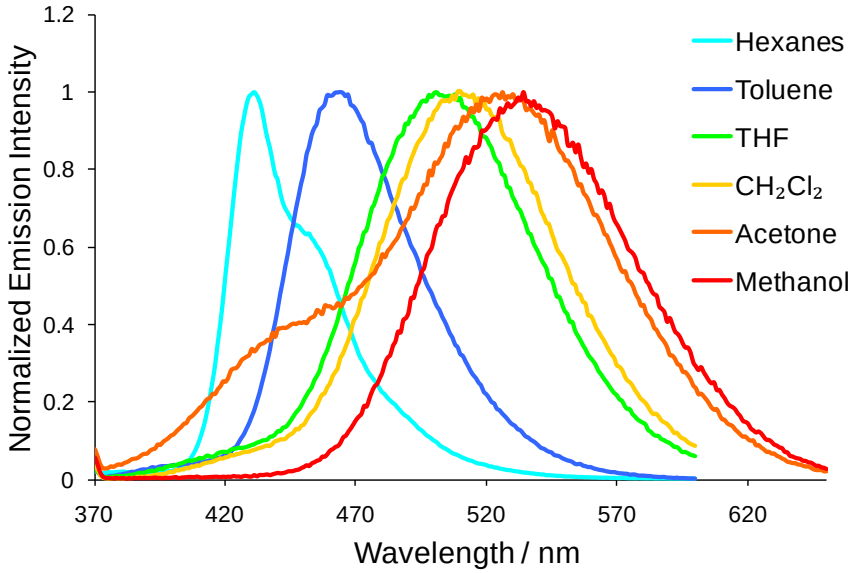

Figure 4.4: (Top): Normalized emission spectra for **BNppy** at 10^{-5} M in various solvents. Bottom: Solutions of BNppy at ca. 10^{-5} M under irradiation with UV light (365 nm). From left to right: hexanes, toluene, THF, CH_2Cl_2, acetone, MeOH, MeCN.

4.3.4 Photophysical and Electrochemical Properties: Complexes

Functionalization of the *N,C*-chelate ligands with Pt(acac) gives rise to low-energy absorption bands in the UV-vis spectra of all complexes. This transition is particularly intense in the case of **Pt-Bbtp**, **Pt-Bbzf**, **Pt-BNppy** and **Pt-BNPB2**, attributable to a primarily LC transition in these molecules ($\varepsilon \approx$ 20,000-40,000) that appears to completely overshadow the MLCT transition band (Figure 4.5), while this transition may be considered as MLCT in nature for the nonborylated Pt(II) phenylpyridine derivatives.[18a] The lowest energy absorption bands are red shifted by 15-40 nm and have higher molar absorptivities (by a factor of ca. 1.5 - 4) relative to the corresponding non-borylated Pt(II) complexes reported in literature.[18] **Pt-BNppy** and **Pt-BNPB2** however show particularly large red shifts of >50 nm, due to the availability of low-energy ligand-based charge transfer pathways from the diarylamine to the boron moiety. All complexes are emissive under UV irradiation at room temperature in solid state and in solution with good color tunability from green to red. (Figure 4.6)

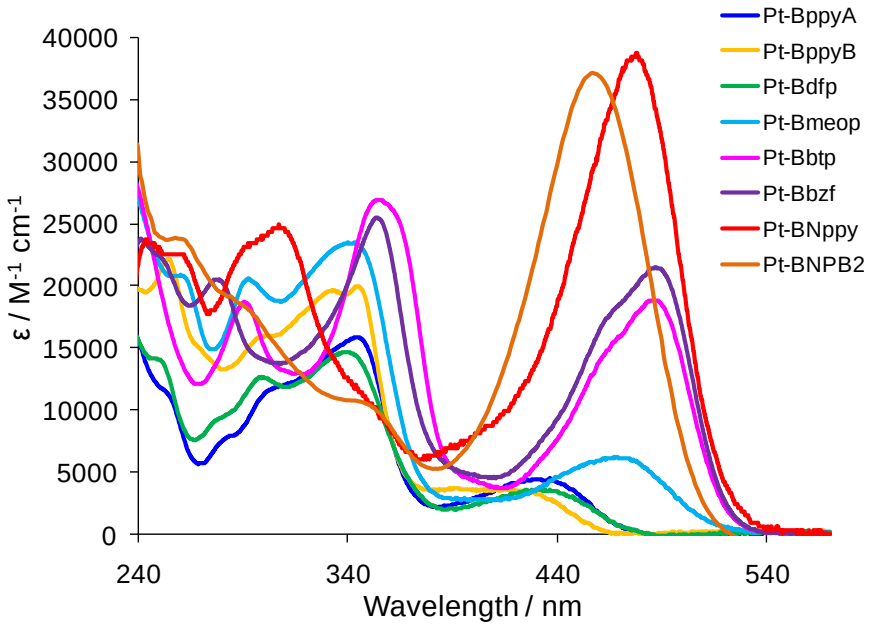

Figure 4.5: Absorption spectra of the boron-functionalized Pt(II) complexes at 10^{-5} M in CH_2Cl_2.

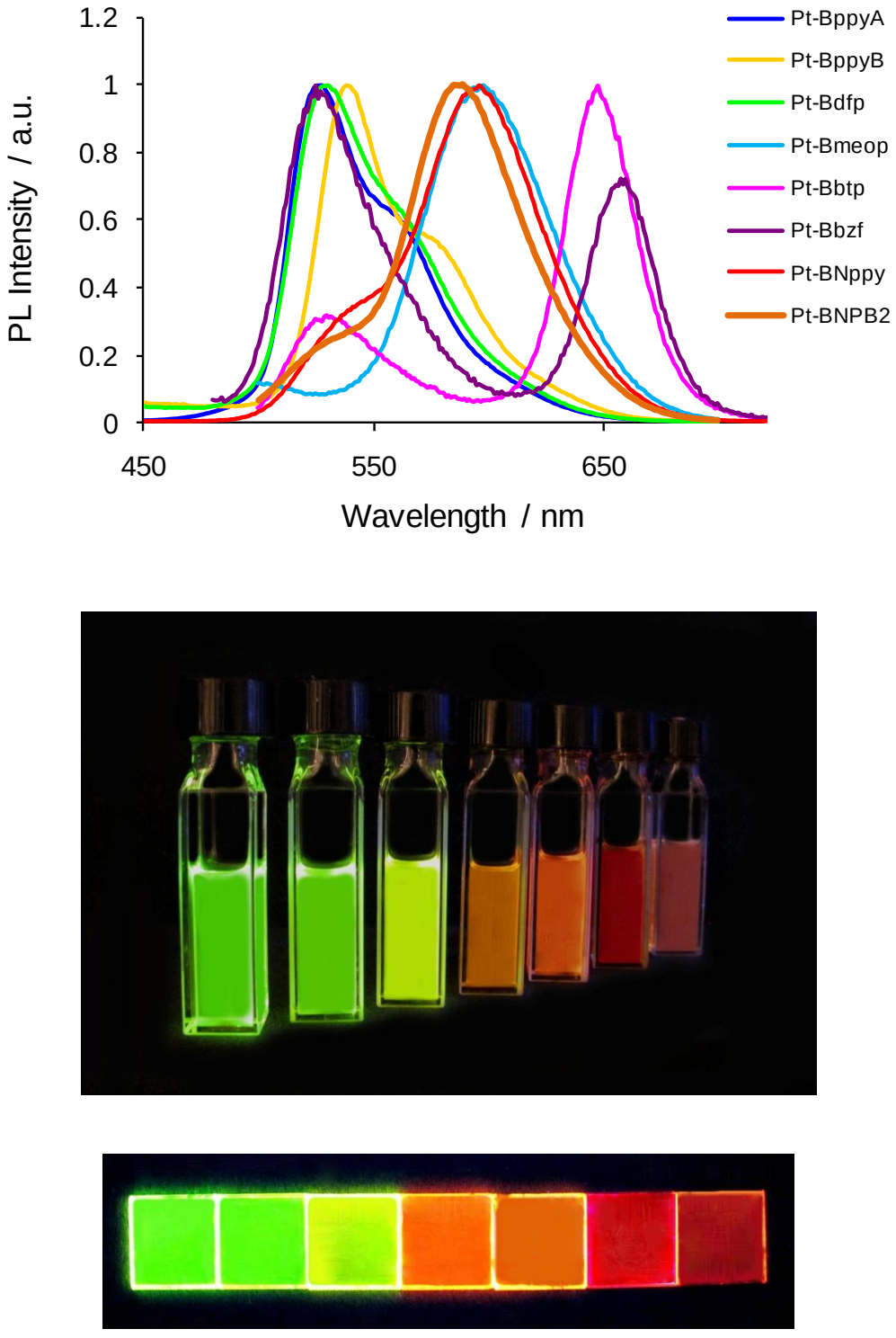

Figure 4.6: Top: Emission spectra of the boron-functionalized ligands at 10^{-5} M in CH_2Cl_2. λ_{ex} = 365 nm. Bottom: Photos showing the colors of the Pt(II) complexes under 365 nm UV irradiation in CH_2Cl_2 solution at 10^{-5} M (top) and in PMMA at 10 wt. % on quartz substrates. From left to right: **Pt-BppyA**, **Pt-Bdfp**, **Pt-BppyB**, **Pt-Bmeop**, **Pt-BNppy**, **Pt-Bbtp**, **Pt-Bbzf**.

These borylated Pt(II) complexes show bright, oxygen-sensitive phosphorescence, with impressive quantum efficiencies ranging from 0.06-0.98 in degassed CH_2Cl_2 relative to $Ir(ppy)_3$ (Table 4.4). **Pt-BppyA** in particular has an emission efficiency on par with that of $Ir(ppy)_3$, making it among the brightest reported Pt(II) phosphors. Compared to that of Pt(ppy)(acac), the emission energy of **Pt-BppyA** is about 50 nm red shifted and its quantum efficiency is about 3 times higher, demonstrating the phosphorescent enhancement produced by incorporation of the $BMes_2$ group. Furthermore, when doped into a PMMA matrix at 10% by weight, these complexes are similarly bright with only minor changes in emission profile and lifetime. Consistent with the trends observed in solution, **Pt-BppyA** has the highest quantum efficiency in the solid state (0.57), making it an attractive candidate for use in OLEDs. As pure solids, the complexes display similar PL spectra as those in solution, with the exception of **Pt-Bdfp**. The emission profile of **Pt-Bdfp** is red shifted by 100 nm in the pure solid due to the close Pt-Pt stacking observed in the crystal structure, a phenomenon that has been frequently observed in Pt(II) complexes.[20] In contrast, doped PMMA films of this compound emit green light similar to that from solution upon UV irradiation.

Table 4.4: Photophysical properties of the Pt(II) complexes.

Complex	Absorption, λ_{max} ε (10^4 cm^{-1} M^{-1})[a]	λ_{max} (nm) Solution/Solid[b]	τ_P (μs)	Φ_P[c]	$E_{1/2}^{red}$ (V)[d]
Pt-BppyA	304 (1.22), 339 (1.55), 426 (0.43)	527 / 526	9.5	0.95/0.57	-1.84
Pt-BppyB	293 (1.52), 340 (1.94), 421 (0.34)	538 / 536	10.2	0.75 /0.38	-2.02
Pt-Bdfp	293 (1.19), 334 (1.45), 425 (0.36)	530 / 527	7.9	0.54/0.32	-1.71
Pt-Bbtp	350 (2.48), 461 (1.67), 483 (2.10)	525, 648 / 535, 648	14.5	0.12 / 0.03	-1.77
Pt-Bbzf	349 (2.60), 459 (1.37), 481 (1.83)	525, 654 / 519, 658	9.5	0.06 / 0.02	-1.76
Pt-Bmeop	289 (1.99), 337 (2.33), 463 (0.61)	598 / 590	14.1	0.45 / 0.27	-1.83
Pt-BNppy	287 (2.22), 302 (2.43), 474 (3.81)	596 / 588	67.4	0.76 / 0.42	-1.86
Pt-BNPB2	353 (1.02), 456 (3.71)	590 / 581	40.0	0.91 / 0.46	-1.97

[a] Measured in CH_2Cl_2 at $1x10^{-5}$ M, [b] Doped into PMMA at 10 wt%. [c] Phosphorescence quantum efficiency measured in CH_2Cl_2, relative to $Ir(ppy)_3$ = 0.97.[20] Solid state quantum yields were measured using an integration sphere. All QYs are ± 10%. [d] In DMF relative to $FeCp^{0/+}$.

The phosphorescence in these complexes is attributed to a mixture of ^{3}LC-^{1}MLCT character,[17] with the relative amount of MLCT character increasing from green to red. The emission spectra of **Pt-BppyA**, **Pt-**

BppyB and **Pt-Bdfp** show broad vibrational features, indicative of substantial mixing with a ^{3}LC state, while **Pt-Bmeop**, **Pt-BNppy** and **Pt-BNPB2** show featureless emission bands. **Pt-Bbtp** and **Pt-Bbzf** are the most weakly emissive of the series, and show dual emission bands (a high energy peak at 525 nm and a low energy peak at 648 nm or 654 nm) with similar excitation profiles. In both cases, the higher energy peak is insensitive to the presence of O_2 and may thus be attributed to emission from a singlet state. Similar dual emission for these two compounds was also observed in doped PMMA films. The high energy band in **Pt-Bbzf** is particularly pronounced in solution, giving rise to a pinkish-red emission color for this complex in solution and red emission in the doped film.

Several important observations can be made from comparison with previously reported analogous non-borylated molecules. It is clear that the presence of the boron centre strongly promotes phosphorescence, producing large increases in the quantum yield of the complex in some cases. While enhancement in charge-transfer by triarylboron has also been observed in systems containing other metals[6,23] such as Ir(III) and Re(I), the enhancement in Φ_P appears particularly pronounced for the *N*,*C*-chelate Pt(acac) phosphors. Although enhancements in the quantum yield of MLCT phosphorescence by a triarylboron unit has been frequently observed, it does not necessarily guarantee an improvement in the quantum yield of a metal complex. For example, *N*,*N*-chelate 5,5'-$(BMes_2)_2$-2,2'-bipyridine complexes of Pt(II) are very weak emitters,[4,23] indicating that multiple factors are indeed at play.[17]

This phosphorescent enhancement is considerably more pronounced when the boron centre is added to a pyridine site on the phenylpyridine chelate, rather than the phenyl ring. Comparison of constitutional isomers **Pt-BppyA** and **Pt-BppyB** shows that the quantum efficiency of the pyridine-functionalized isomer is significantly higher than that of the phenyl-functionalized compound, which may be associated with the greater MLCT promoted by the synergistic coupling of the boron center with an electron-accepting pyridine ring. It is also noteworthy that functionalization with triarylboron does not

significantly alter the HOMO level of these complexes, indicating that changes in the LUMO are primarily responsible for the changes in emission behaviour.[18a] Of all the compounds for which comparison is available in this series, the greatest phosphorescent enhancement is exhibited by **Pt-BNppy**, in which the quantum efficiency is increased more than tenfold relative to the analogous complex lacking the boron moiety.[24] It is clear that the emission in this case occurs from a ligand-centered excited state involving intramolecular charge transfer from the amino donor to the boron acceptor. Such phosphorescence enhancement *via* intramolecular charge transfer has been previously demonstrated in complexes of Pt(II) and Os(II).[23,25,26] Thus, both intra-ligand donor-acceptor charge transfer and the MLCT transition promoted by the $BMes_2$ unit are likely the key factors contributing to the phosphorescence enhancement observed for these Pt(II) complexes.

Due to the stabilization of the radical anion by the triarylboron centre, these compounds all undergo reversible reduction at -1.7 to -2.0 V relative to $FeCp^{0/+}$. The complexes functionalized with the boryl group on the pyridine ring have reduction potentials 0.47 to 0.66 V more positive than the corresponding non-borylated Pt(II) analogues,[18a] demonstrating a significant enhancement in the electron-accepting abilities of these molecules. Though the effect is less pronounced, the phenyl-substituted **Pt-BppyB** still undergoes reversible reduction at 0.37 V more positive potential than its non-borylated parent complex. These results demonstrate that the boron centre is capable of enhancing not only the phosphorescence but also the electron-accepting ability of cyclometalated complexes of Pt(II).

4.3.5 Electronic Structures and Theoretical Calculations

The frontier molecular orbitals of many platinum phenylpyridines have been described previously in literature,[18] and it is known that the HOMO in similar systems has significant electron density on the 4-position of the phenyl ring, while the phenyl 3- and 5-positions make significant contributions to the LUMO. As described by Thompson and others these electronic features can be used to predictably control

the optical band gaps in these systems.[17,18a] In the borylated complexes, we observed that substitution of the phenyl 4-position with an electron-donating methoxy group raises the HOMO level of the molecule, producing a 72 nm red shift in the emission maximum and changing the luminescence color of the complex from green (**Pt-BppyA**) to orange (**Pt-Bmeop**). Furthermore, substitution of both HOMO and LUMO sites with fluorine atoms in **Pt-Bdfp** improves the electron accepting ability of the complex relative to **Pt-BppyA** (ΔE = 130 mV) without significantly altering either the optical bandgap or emission color, attributable to the competing inductively withdrawing and π-donating effects of the fluorine atoms in the 3- and 4- positions, respectively. It is also possible to reduce the bandgap and emission energies of these complexes by increasing the conjugation length of the π-system, as in the case of **Pt-Bbzf**, and **Pt-Bbtp**. It is interesting to note that there is little difference between the sulphur-containing **Pt-Bbtp** and the oxygen-containing **Pt-Bbzf** in reduction potentials, emission maxima, frontier orbital energy levels, and optical bandgaps, despite the pronounced differences in electronegativity of these two atoms.

To further explain the photophysical properties of these materials, we have examined their electronic structures in detail using TD-DFT calculations and Mulliken population analysis. We note that the $S_0 \rightarrow S_1$ transitions arise predominantly from the HOMO and LUMO with reasonable oscillator strengths (Table 4.5). Hence, our discussion will focus on these orbitals (Figure 4.7). The trends in the calculated and observed energy gaps are in reasonable agreement. **Pt-BppyB** has the largest HOMO-LUMO gap of the series, due primarily to the high LUMO level in this molecule caused by substitution of the borane on a phenyl rather than the more electronegative pyridine ring.

Table 4.5: Experimental HOMO-LUMO energy and DFT calculation results

Complex	HOMO (eV)[a]	LUMO (eV)[b]	%Pt in HOMO	%B in LUMO	% H →L in $S_0 \rightarrow S_1$	$S_0 \rightarrow S_1$ Oscillator Strength
Pt-BppyA	-5.51	-2.96	33	29	91	0.101
Pt-BppyB	-5.45	-2.78	33	18	83	0.054
Pt-Bbtp	-5.34	-3.03	16	23	85	0.283
Pt-Bbzf	-5.40	-3.04	17	23	82	0.413
Pt-Bdfp	-5.66	-3.09	31	27	91	0.078
Pt-Bmeop	-5.32	-2.97	26	29	92	0.079
Pt-BNppy	-5.27	-2.94	1	28	88	0.651
Pt-BNPB2[c]	-5.22	-2.83	--	--	87	0.681

[a] Calculated using the LUMO level and the optical energy gap. [b] Calculated using the reduction potential relative to the ferrocene HOMO level (-4.80 eV). [c] Population analysis was not conducted for this molecule, though calculated values are expected to be similar to Pt-BNppy.

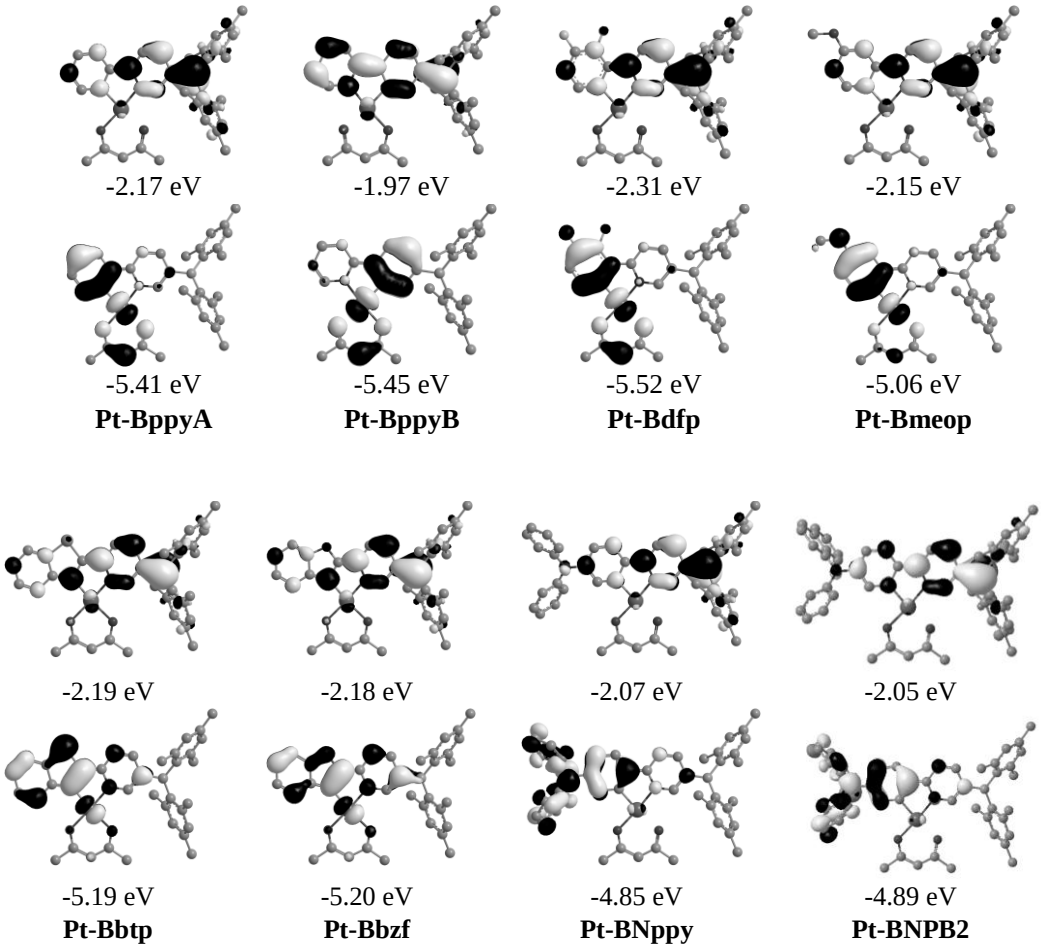

Figure 4.7: Molecular orbital diagrams for the LUMO (top) and HOMO (bottom) for each Pt(II) complex with calculated orbital energy levels. Isocontour value = 0.03 au.

As anticipated, the LUMOs of these molecules include large contributions from the $BMes_2$ group, and in particular the boron atom itself (Table 4.5). While the Pt(II) centre makes a significant contribution to the HOMO of **Pt-BppyA**, **Pt-BppyB**, **Pt-Bdfp**, and **Pt-Bmeop** (26-33%), its involvement is lower for **Pt-Bbtp** and **Pt-Bbzf** (16% and 17%), and very small for **BNppy** (1%), which instead has large contributions from the $–NAr_2$ groups to the HOMO level. This is consistent with UV-visible spectral data, which suggest that the lowest energy excited states in these molecules possess greater LC character, and with the long decay lifetime of **Pt-BNppy**. It should be noted that the boron centre also promotes efficient phosphorescence in **Pt-BNppy** and **Pt-BNPB2**, due not to an enhancement in metal-to-ligand charge transfer, but rather the introduction of a highly favourable donor-acceptor ^{3}LC state. To firmly establish the exact role of the triarylboron unit in the phosphorescence enhancement of *N,C*-chelate Pt(II) complexes, however, more detailed theoretical and photophysical work are necessary.

4.3.6 Electroluminescence of Pt-BppyA

Due to its high quantum yield and strong electron accepting ability, the performance of **Pt-BppyA** in electroluminescent devices was evaluated. Because of their relatively long decay lifetimes, these Pt(II) complexes are better used as doped emissive layers to prevent exciton quenching by triplet-triplet annihilation. To optimize EL performance, we first prepared multilayer devices on ITO-coated glass substrates using *N,N'*-di-[(1-naphthalenyl)-*N,N'*-diphenyl]-(1,1'-biphenyl)-4,4'-diamine (NPB) as the hole transport layer (HTL), 4,4'-*N,N'*-dicarbazolebiphenyl (CBP) as the host material, and 1,3,5-tris(*N*-phenylbenzimidazole-2-yl)benzene (TPBI) as the electron-transport layer (ETL), as shown in Figure 4.8, varying the doping concentration from 10 to 30%. The EL spectra of these devices (A-D) are shown in Figure 4.8. Though the efficiency of these initial devices was relatively poor, several important observations can be made from these data. The most efficient device was achieved with a doping concentration of 15% **Pt-BppyA** by weight in the active layer, giving peak current and power efficiencies of 5.31 cd/A and 5.21 lm/W, and green electroluminescence with CIE coordinates of (0.35, 0.61). The EL

spectra of devices A to C match very well with the PL spectrum of **Pt-BppyA**. Excimer emission is observed at doping levels above 20%, resulting in a broad EL profile and a reduction in device efficiency. This is likely a result of the use of a square-planar Pt(II) complex as the electrophosphor, as these molecules tend to have strong intermolecular interactions in the solid state. It can also be seen that as the doping concentration increases, the driving voltage decreases, indicating that the dopant is indeed effective at transporting charge. In addition, a very small emission peak from NPB at 442 nm can be seen at higher doping levels, indicating that the recombination zone moves toward the anode as the dopant concentration increases. This led us to suggest that the device may be hole-deficient. To address this, similar devices were fabricated with the addition of a WO_3 hole-injection layer, which has been shown to improve the injection of holes into NPB.[27] However, this had almost no effect on device performance, indicating that a deficiency of holes was not a factor.

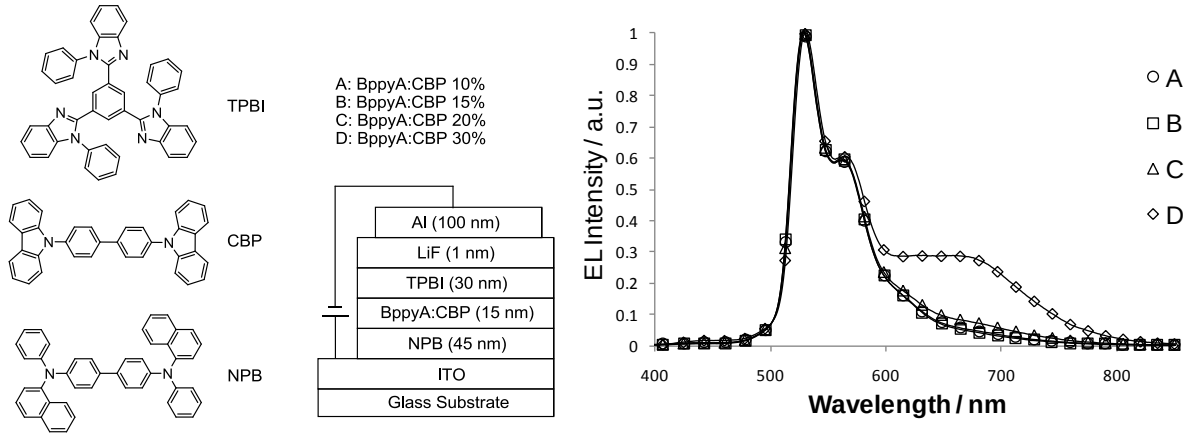

Figure 4.8: OLED device structures A-D and their electroluminescence spectra.

The HOMO level of **Pt-BppyA** was then measured directly using UV photoelectron spectroscopy (UPS, see ESI) using a 3 nm thick layer of material deposited on highly-oriented pyrolytic graphite (HOPG) *in situ*. The UPS measured HOMO level of **Pt-BppyA**, 5.66 eV, matches well with that obtained from CV and absorption spectra. This energy level is significantly lower than that of NPB (5.40 eV) and the well

known triplet emitter $Ir(ppy)_3$ (5.40 eV) suggesting that the energetic barrier to direct charge injection from NPB to the dopant may be limiting device performance. Build-up of NPB^+ radical cations at the hole transport-active layer interface provides a means by which excitons in the active layer can be quenched by nonradiative decay. Furthermore, the triplet level of NPB (2.3 eV) is lower than that of the emitter in this case (2.5 eV), suggesting that triplet energy transfer from the dopant to the adjacent NPB layer may also be occurring.

It has recently been shown that incorporation of a thin layer of non-doped CBP between these two layers can move the recombination zone away from NPB and reduce charge buildup at the NPB interface, thus reducing nonradiative quenching.[28] Based on this consideration, a new set of devices with a 15 nm thick 15% **Pt-BppyA**:CBP active layer were fabricated, with a 5 nm CBP layer between the active layer and HTL. The improvement in device efficiency afforded by this simple structural modification was truly impressive, as shown by the performance of device E (ITO/NPB(45 nm)/CBP(5nm)/15%**Pt-BppyA**:CBP (15nm)/TPBI(30nm)/LiF(1nm)/Al(100nm)), which gives peak current and power efficiencies of 34.5 cd/A and 29.8 lm/W, the highest of any triarylboron-based OLED reported in literature and among the brightest Pt(II) electrophosphorescent devices. In addition, this new device gave a maximum luminance of 31,510 cd/m^2 at only 9.8 V, as shown in Figure 4.9 and Figure 4.10.

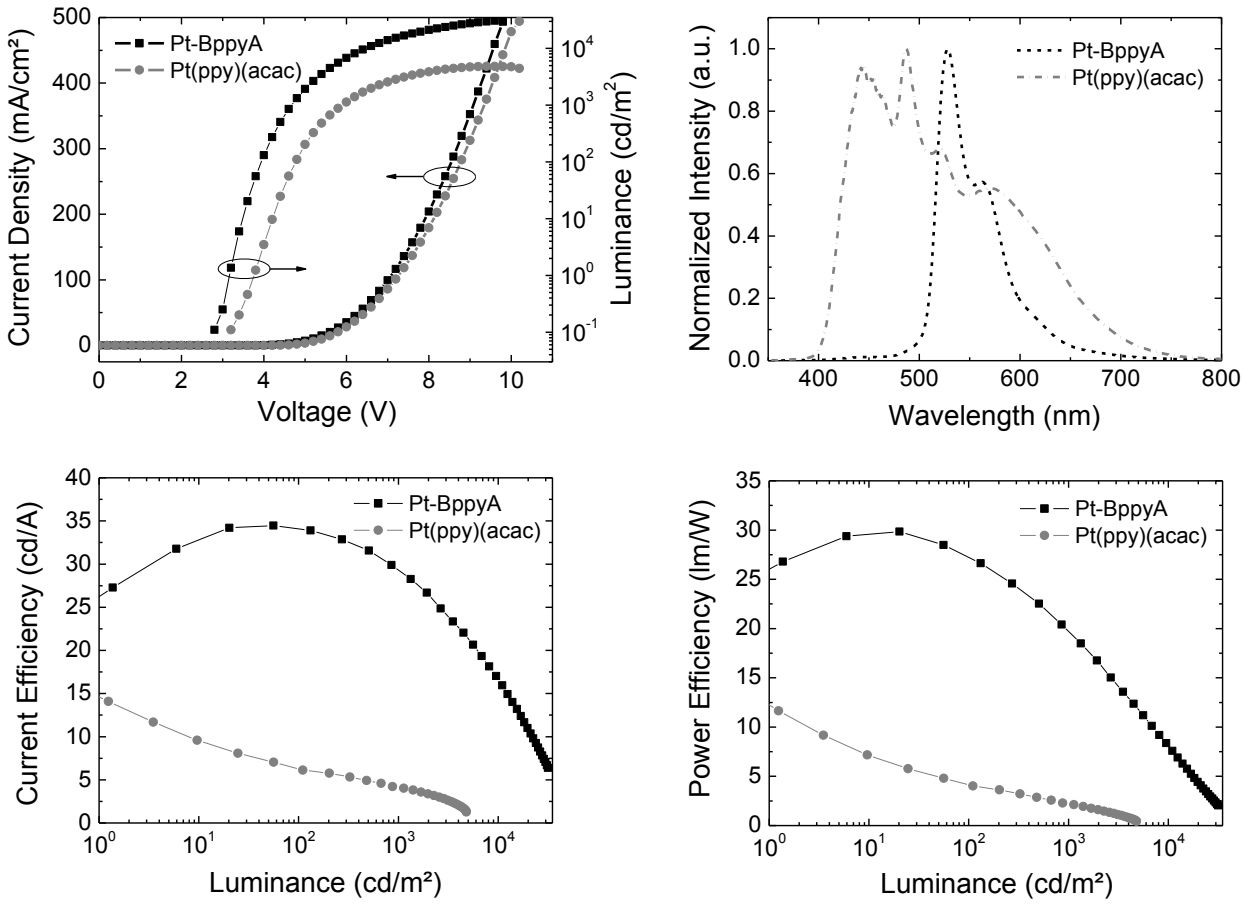

Figure 4.9: *L–V–J* diagrams, current and power efficiency vs. luminance characteristics, and EL spectra at 9V for devices E (**Pt-BppyA**) and F (Pt(ppy)(acac)).

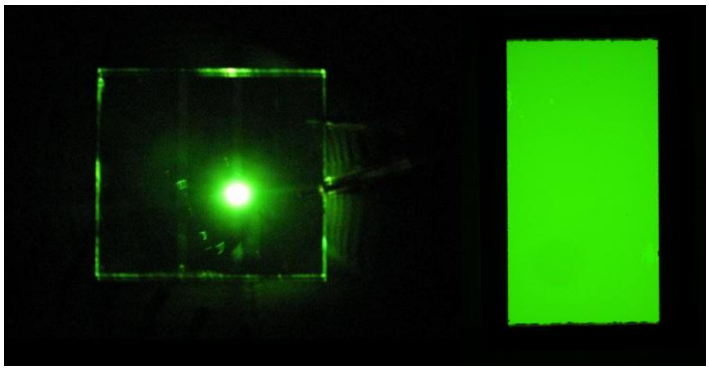

Figure 4.10: Left: photo of the **Pt-BppyA** -based device E, operating at 9 V. Right: Photo of a single pixel of device E.

To clearly isolate the impact of the boron centre, a control device F was fabricated with a structure identical to device E, but with Pt(ppy)(acac), which lacks the triarylboron group, replacing **Pt-BppyA** in

the active layer. UPS measurements indicated that Pt(ppy)(acac) has a HOMO energy of 5.64 eV, very similar to that of **Pt-BppyA**, and thus that the benefit afforded through the use of the CBP buffer layer should be similar. The EL efficiencies of device F are considerably lower, showing maximum current and power efficiencies of 14.1 cd/A and 11.7 lm/W, with a maximum luminance of 4823 cd/m^2 (Figure 4.9). The maximum external quantum efficiency of this device is also lower, 6.9% at only 1 cd/A versus 8.9% at 100 cd/A for the **Pt-BppyA** based device. Furthermore, the EL spectrum of the control device shows broad white electroluminescence with substantial emission in the UV region from TPBI, with CIE coordinates of (0.30, 0.33) at low luminance. This can be clearly attributed to excimer formation, which becomes dominant even in dilute doped films in this case. This illustrates the desirable film-forming properties provided by the bulky boron centre, which reduces aggregation and excimer formation in devices based on **Pt-BppyA**. In addition, the emission from TPBI indicates that the recombination zone in device F has moved significantly toward the cathode, consistent with the substantially lower electron mobility of the active layer in the control device. In contrast, the **Pt-BppyA** device has not only high color purity, but also a high efficiency. In fact, the current and power efficiencies of these **Pt-BppyA** devices were found to be comparable to those of reference devices fabricated using $Ir(ppy)_3$ as the emissive material, which is a well known and extensively studied efficient green emitter.[17]

To more thoroughly examine the electron-transporting ability afforded by the triarylboron group, we fabricated single-carrier devices G and H (Figure 4.11) designed to transport electrons only.[28] **Pt-BppyA** and Pt(ppy)(acac) doped at 10 wt. % into CBP were used as the active layer in the two devices, respectively. As shown in Figure 4.11, the **Pt-BppyA** device G has a current density 3-4 orders of magnitude higher than that of the Pt(ppy)(acac) device H, establishing unambiguously that the triarylboron centre indeed can greatly enhance electron mobility in organic EL devices. The superior performance of electroluminescent device E relative to that of device F can thus be attributed in part to the improved electron transport due to the boron centre.

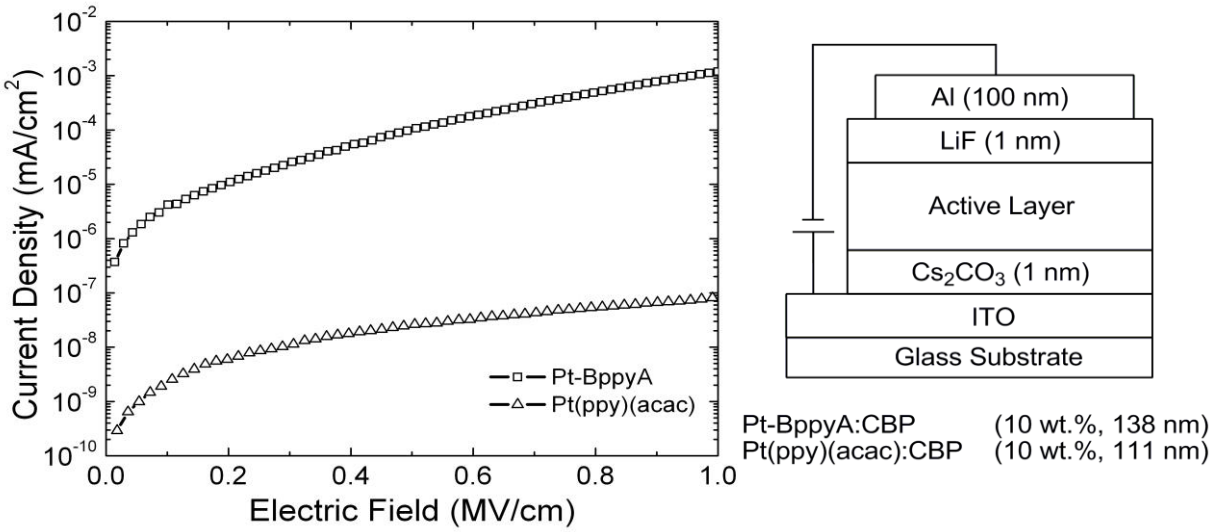

Figure 4.11: Left: Plots of current density as a function of average electric field for the electron-only devices G (**Pt-BppyA**) and device H (Pt(ppy)(acac)). Right: The device structure.

4.3.7 Electroluminescence of Pt-BNPB2

Pt-BNPB2 was designed as a successor to the highly fluorescent 4-(dimesitylboryl)-4'-(*N*-(1-naphthyl)-*N*-phenylamino)biphenyl (BNPB),[1h] able to take advantage of the much higher efficiencies achievable using triplet emitters in OLEDs due to spin statistics. Replacement of the phenyl spacer adjacent to the boron centre with an electron-deficient pyridine moiety not only enhances donor-acceptor charge-transfer, but also allows this compound to act as a cyclometalating ligand to Pt(II). Like **Pt-BppyA**, this compound incorporates a boron centre to facilitate electron transport and a metal centre to promote phosphorescence. However, this trifunctional material additionally incorporates a triarylamine moiety to facilitate reversible oxidation and hole transport. The donor group was incorporated from the well-known hole-transport material NPB, perhaps the most widely used hole transport material used in OLEDs to date. In addition, this moiety promotes charge-transfer to triarylboron with a high quantum efficiency that is also preserved in the metal complex despite the large red shift in the emission spectrum.

This compound shows impressive performance when doped into a host material and used as the emissive layer in phosphorescent OLEDs. Multilayer EL devices were prepared by vacuum vapour deposition on ITO-coated glass substrates, with structures shown in Figure 4.12. Lu and coworkers have recently shown that transition metal oxide hole injection layers, such as MoO_3 raise the work function of the ITO anode sufficiently so as to allow direct charge injection into the host material, eliminating the need for a discrete hole-transport layer (HTL) entirely.[29] Using CBP as HTL and host and TPBI as the electron-transport layer (ETL), we first evaluated the EL performance of **Pt-BNPB2** by fabricating a series of devices in which the position of the doped emission zone between the electrodes was varied.

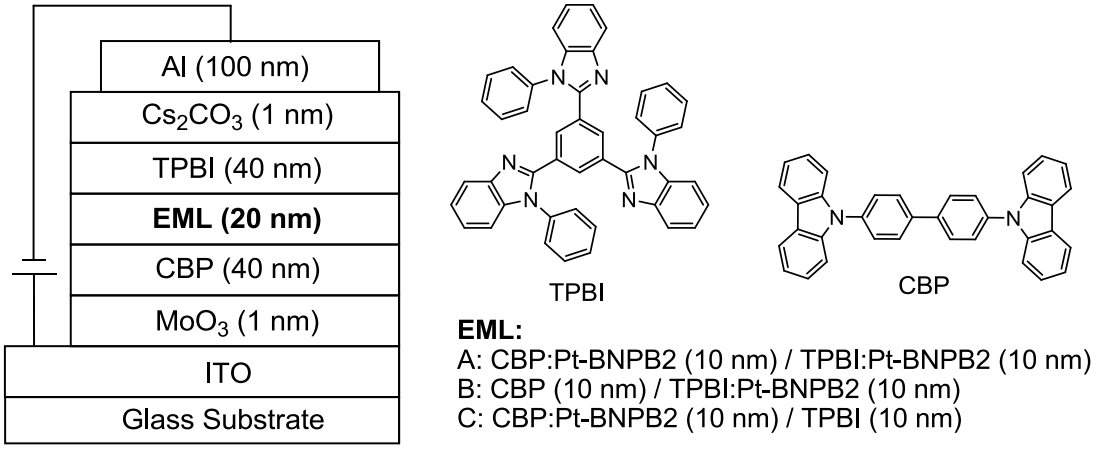

Figure 4.12: Device structure and energy level diagram of OLEDs fabricated using **Pt-BNPB2** as the emitter at a doping concentration of 10 wt%.

We evaluated CBP and TPBI as hosts for **Pt-BNPB2** in the EML as well as a double emission zone architecture of **Pt-BNPB2** doped into both CBP and TPBI. Devices with **Pt-BNPB2** doped into TPBI had lower efficiencies, most likely due to poor carrier balance. The highest efficiency devices were thus obtained using a single layer of doped CBP. With this structure, high-efficiency orange electrophosphorescence was achieved with maximum current and power efficiencies of 35.0 cd/A and 36.6 lm/W and a maximum external quantum efficiency of 10.6%, the highest reported for a device using a triarylboron-based EML and among the highest reported using Pt(II) in OLEDs.[8e,f] (Figure 4.13 and

Figure 4.14) Furthermore, these devices continue to show impressive performance at higher luminance, giving this device design potential for use in commercial OLEDs.

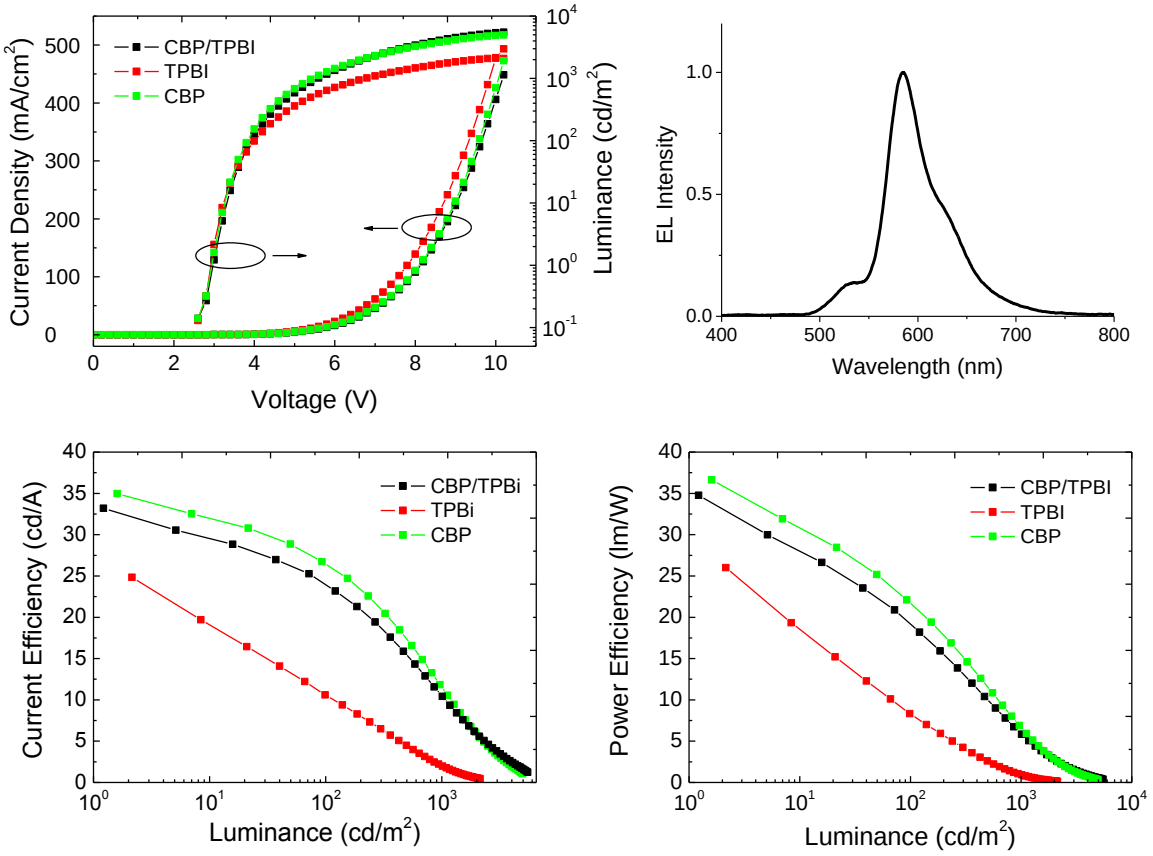

Figure 4.13: Luminance-current density-voltage characteristics, efficiency data, and EL spectrum of devices based on **Pt-BNPB.**

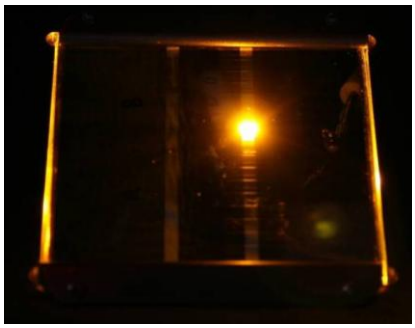

Figure 4.14: OLED using **Pt-BNPB** doped into CBP operating at 5V.

4.3.8 Pt(II)-Based OLEDs with External Quantum Efficiencies above 20%

Using the device structure employed in the fabrication of **Pt-BNPB2** OLEDs, we were also able to significantly improve the performance of EL devices based on **Pt-BppyA**. As described in section 4.3.7, a traditional hole transport layer such as NPB was omitted in favour of direct charge injection into CBP. Devices were fabricated with a structure of ITO / MoO_3 (1 nm) / CBP (35 nm) / emissive layer (15 nm) / TPBI (65 nm) / LiF (1 nm) / Al (100 nm), with both CBP (device A) and TPBI (device B) used as host for Pt-BppyA at a doping level of 8%. Figure 4.15 compares the current efficiency and power efficiency of PHOLEDs using different hosts for the Pt-BppyA emitter. The peak current efficiency reaches 44.0 cd/A using CBP as host (device A) and 55.8 cd/A using TPBI (device B). A high power efficiency is also achieved, reaching 64 and 49 lm/W at 10 cd/m^2 and remaining as high as 41 and 29 lm/W at 1000 cd/m^2 for devices A and B, respectively. The higher current efficiency and power efficiency of device B indicates that the internal quantum efficiency (IQE) of the device is higher using TPBI as host.

Interestingly, the turn on voltage of both devices was >3 V, which is substantially higher than the photon energy of 2.5 eV for the electroluminescence (EL) from Pt-BppyA. Using an identical device structure, the turn-on voltage using $Ir(ppy)_2(acac)$ as emitter was measured to be only 2.6 eV, just slightly above the photon energy of 2.4 eV, due to direct charge trapping and subsequent exciton formation on the dopant.[30] The much higher turn on voltage for the Pt-BppyA device therefore suggests that the excitons are not directly formed on the dopant, but rather on the CBP or TPBI host and then transferred to the electrophosphor.

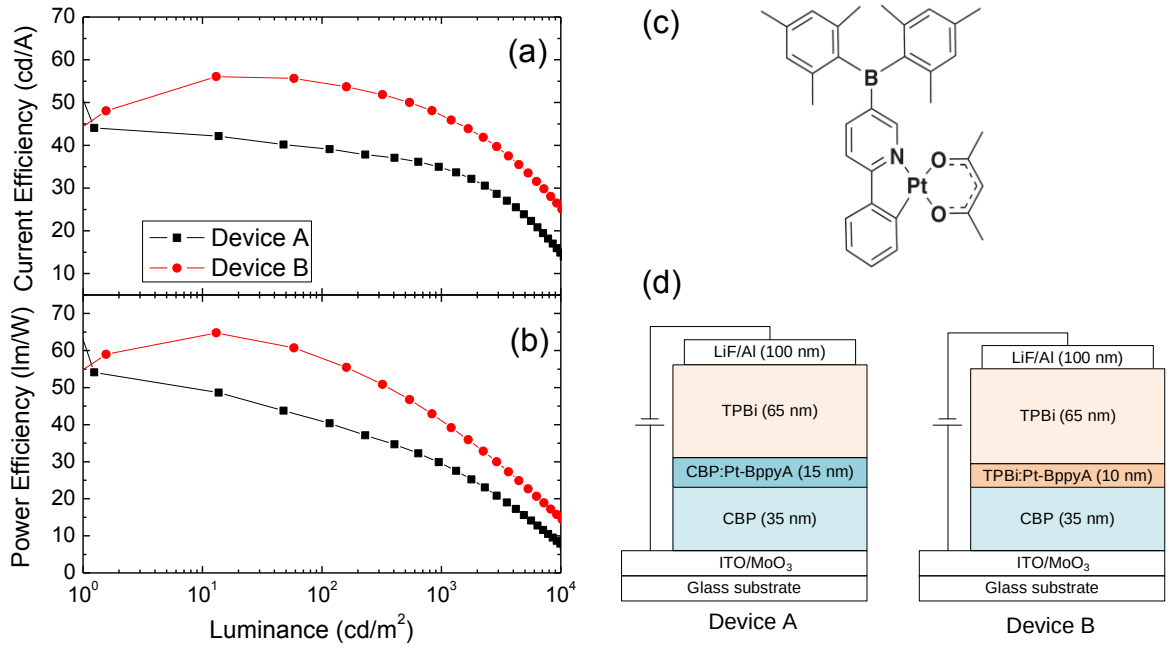

Figure 4.15: (a) Current efficiency and (b) power efficiency of device A and B. (c) Structure of Pt-BppyA. (d) Schematic diagram of the structures of devices A and B.

However, since CBP is a poor electron-transporting material and TPBI a poor hole transporter, one would expect exciton formation at the CBP/TPBI interface to be more efficient than on either layer alone. With this exciton formation mechanism, higher efficiency should be expected from a double emission zone structure, in which Pt-BppyA is doped into adjacent layers of both CBP and TPBI. Devices were then fabricated using a structure of ITO / MoO_3 / CBP (35 nm) / CBP:Pt-BppyA (15 nm) / TPBI:Pt-BppyA (10 nm) / TPBI (55 nm) / LiF / Al, denoted as device C (Figure 4.16a). Using this structure, the peak current and power efficiencies are further increased to 64.8 cd/A and 79.3 lm/W respectively, significantly higher than those of either device A or B. Furthermore, the maximum EQE of this device reaches 20.9%, remaining as high as 17.0% at 1,000 cd/m^2. (Figure 4.16b) This represents to our knowledge the highest efficiency Pt(II)-based PHOLED reported to date, and exhibits performance comparable to that of Ir(III) complexes such as $Ir(ppy)_3$.

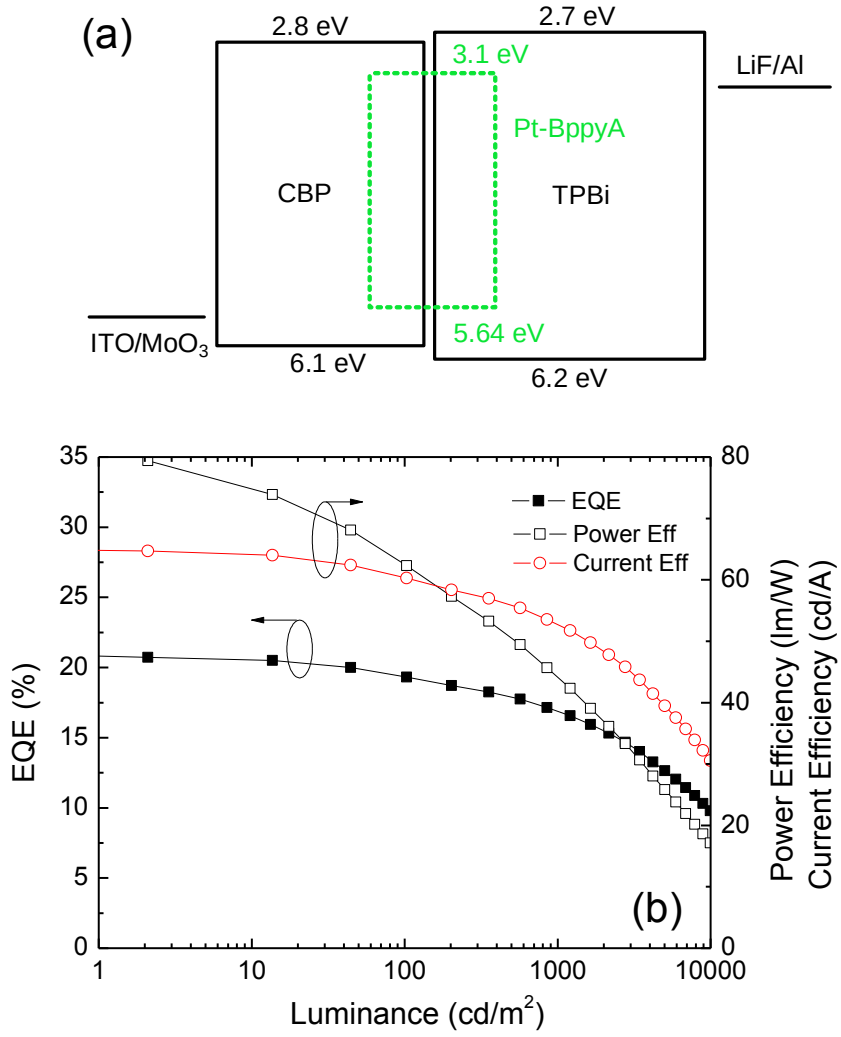

Figure 4.16: (a) Schematic energy-level diagrams of device C. (b) Current efficiency, power efficiency and EQE of device C.

4.4 Conclusions

Herein we have described the first synthesis of *N*,*C*-cyclometalated Pt(acac) complexes bearing the triarylboron functional group, and have applied this strategy to a range of chromophores, giving complexes with good color tunability and high phosphorescence quantum yields. The photophysical and electrochemical properties of these complexes have been studied in detail, and show excellent agreement

with theoretical predictions. These data support that the triarylboron moiety promotes increased participation of the MLCT state in the lowest energy emission pathway, and greatly enhances the phosphorescent quantum yield of many of these complexes. We have further demonstrated that the electron-accepting properties and steric bulkiness of this boron functionality can be harnessed to significantly enhance the brightness, efficiency and electron mobility of electroluminescent devices based on Pt(II) phosphors, as highly efficient EL devices based on **Pt-BppyA** and **Pt-BNPB** have been achieved, including the highest efficiency Pt(II)-based OLED reported in literature. The high efficiency of these devices demonstrates that the performance of Pt(II)-based OLEDs can approach that of Ir(III)-based devices, and that using the triarylboron moiety is an effective means by which Pt(II) complexes with high quantum efficiency may be achieved.

4.5 Notes and References

The work described in this chapter includes contributions from the following publications:

- Z. M. Hudson, C. Sun, M. G. Helander, H. Amarne, Z.-H. Lu and S. Wang, *Adv. Funct. Mater.*, **2010**, *20*, 3426.
- Z. M. Hudson, M. G. Helander, Z.-H. Lu and S. Wang. *Chem. Commun.* **2011**, *47*, 755.
- Z. B. Wang, M. G. Helander, Z. M. Hudson, J. Qiu, S. Wang and Z.-H. Lu. *Appl. Phys. Lett.*, **2011**, *98*, 213301.

References

(1) a) T. Noda, Y. Shirota, *J. Am. Chem. Soc.* **1998**, *120*, 9714. b) Y. Shirota, *J. Mater. Chem.* **2005**, *15*, 75. c) T. Noda, H. Ogawa, Y. Shirota, *Adv. Mater.* **1999**, *11*, 283. d) Y. Shirota, M. Kinoshita, T. Noda, K. Okumoto, T. Ohara, *J. Am. Chem. Soc.* **2000**, *122*, 1102. e) H. Doi, M. Kinoshita, K. Okumoto, Y. Shirota, Yasuhiko, *Chem. Mater.* **2003**, *15*, 1080. f) W. L. Jia, D. R. Bai, T. McCormick, Q. D. Liu, M. Motala, R. Wang, C. Seward, Y. Tao, S. Wang, *Chem. Eur. J.* **2004,** *10*, 994. g) W. L. Jia, M. J. Moran, Y. Y. Yuan, Z. H. Lu, S. Wang, *J. Mater. Chem.* **2005**, *15*, 3326. h) W. L. Jia, X. D. Feng, D. R. Bai, Z. H. Lu, S. Wang, G. Vamvounis, *Chem. Mater.* **2005**, *17*, 164. i)

F. H. Li, W. L. Jia, S. Wang, Y. Q. Zhao, Z. H. Lu, *J. Appl. Phys.* **2008**, *103*, 034509/1. j) A. Wakamiya, K. Mori, S. Yamaguchi, *Angew. Chem. Int. Ed.* **2007**, *46*, 4237. k) A. Steffen, M. G. Tay, A. S. Batsanov, J. A. K. Howard, A. Beeby, K. Q. Vuong, X.-Z. Sun, M. W. George, T. B. Marder, *Angew. Chem. Int. Ed.* **2010**, *49*, 2349.

(2) a) M. E. Thompson, *MRS Bulletin*, **2007**, *32*, 694 and references therein. b) K. Chen, C. H. Yang, Y. Chi, C. S. Liu, C. H. Chang, C. C. Chen, C. C. Wu, M. W. Chung, Y. M. Cheng, G. H. Lee and P. T. Chou, *Chem. Eur. J.* **2010**, *16*, 4315. c) Y. Chi and P. T. Chou, *Chem. Soc. Rev*. **2010**, *39*, 638.

(3) S. B. Zhao, T. McCormick and S. Wang, *Inorg. Chem.*, **2007**, *46*, 10965.

(4) Y. Sun, N. Ross, S. B. Zhao, K. Huszarik, W. L. Jia, R. Y. Wang, D. Macartney, S. Wang, *J. Am. Chem. Soc.* **2007**, *129*, 7510.

(5) H. Aziz, Z. D. Popovic, N. X. Hu, A. M. Hor, and G. Xu, *Science*, **1999**, *283*, 1900.

(6) G. J. Zhou, C. L. Ho, W. Y. Wong, Q. Wang, D. G. Ma, L. X. Wang, Z. Y. Lin, T. B. Marder, A. Beeby, *Adv. Funct. Mater.* **2008**, *18*, 499.

(7) For representative examples, see: a) M. E. Thompson, *MRS Bulletin*, **2007**, *32*, 694 and references therein. b) K. Chen, C. H. Yang, Y. Chi, C. S. Liu, C. H. Chang, C. C. Chen, C. C. Wu, M. W. Chung, Y. M. Cheng, G. H. Lee, P. T. Chou, *Chem. Eur. J.* **2010**, *16*, 4315. c) T. C. Lee, J. Y. Hung, Y. Chi, Y. M. Cheng, C. H. Lee, P. T. Chou, C. C. Chen, C. H. Chang, C. C. Wu, *Adv. Funct. Mater*. **2009,** *19*, 2639. d) Y. H. Song, Y. C. Chiu, Y. Chi, Y. M. Cheng, C. H. Lai, P. T. Chou, K. T. Wong, M. H. Tsai, C. C. Wu, *Chem. Eur. J.* **2008**, *14*, 5423. e) C. F. Chang, Y. M. Cheng, Y. Chi, Y. C. Chiu, C. C. Lin, G. H. Lee, P. T. Chou, C. C. Chen, C. H. Chang, C. C. Wu, *Angew. Chem. Int. Ed.*, **2008**, *47*, 4542.

(8) For examples, see: a) V. Adamovich, J. Brooks, A. Tamayo, A. M. Alexander, P. I. Djurovich, B. W. D'Andrade, C. Adachi, S. R. Forrest, M. E. Thompson, *New J. Chem.* **2002**, *26*, 1171. b) B. W. D'Andrade, J. Brooks, V. Adamovich, M. E. Thompson, S. R. Forrest, *Adv. Mater*. **2002**, 14, 1032.

c) B. Ma, P. I. Djurovich, S. Garon, B. Alleyne, M. E. Thompson, *Adv. Funct. Mater.* **2006**, *16*, 2438. d) A. F. Rausch, H. H. H. Homeier, P. I. Djurovich, M. E. Thompson, H. Yersin, *Proc. SPIE*, **2007**, *6655*, 66550F/1. e) M. Cocchi, D. Virgili, V. Fattori, D. L. Rochester, J. A. G. Williams, *Adv. Funct. Mater.* **2007**, *17*, 285. f) J. A. G. Williams, S. Develay, D. L. Rochester, L. Murphy, *Coord. Chem. Rev.*, **2008**, *252*, 2596. g) X. H. Yang, Z. X. Wang, S. Madakuni, J. Li, G. E. Jabbour, *Adv. Mater.* **2008**, *20*, 2405. h) W. Mróz, C. Botta, U. Giovanella, E. Rossi, A. Colombo, C. Dragonetti, D. Roberto, R. Ugo, A. Valore, J.A.G. Williams, *J. Mater. Chem.* **2011**, *21*, 8653.

(9) Z. M. Hudson, C. Sun, M. G. Helander, H. Amarne, Z.-H. Lu and S. Wang, *Adv. Funct. Mater.*, 2010, **20**, 3426;

(10) Z. M. Hudson, M. G. Helander, Z.-H. Lu and S. Wang. *Chem. Commun.* 2011, **47**, 755.

(11) Z. B. Wang, M. G. Helander, Z. M. Hudson, J. Qiu, S. Wang and Z.-H. Lu. *Appl. Phys. Lett.*, **2011**, *98*, 213301.

(12) Y. L. Rao, S. Wang, *Inorg. Chem.*, **2009**, *48*, 7698.

(13) A. Medina, C. G. Claessens, G. M. A. Rahman, A. M. Lamsabhi, O. Mo, M. Yanez, D. M. Guldi, T. Torres, *Chem. Commun.* **2008**, *15*, 1759.

(14) S. A. De Pascali, P. Papadia, A. Ciccarese, C. Pacifico, F. P. Fanizzi, *Eur. J. Inorg. Chem.* **2005**, 788.

(15) S. R. Forrest, D. D. C. Bradley, and M. E. Thompson, *Adv. Mater.* **2003**, *15*, 1043.

(16) a) M. G. Helander, Z. B. Wang, M. T. Greiner, J. Qiu, Z. H. Lu, *Rev. Sci. Instrum.* **2009**, *80*, 033901. b) M. G. Helander, M. T. Greiner, Z. B. Wang, and Z. H. Lu, *Appl. Surf. Sci.* **2010**, *256*, 2602.

(17) Y. You, S. Y. Park, *Dalton Trans.*, **2009**, 1267. (b) Y. Chi, P. T. Chou, *Chem. Soc. Rev.* **2010**, *39*, 638 and references therein.

(18) a) J. Brooks, Y. Babayan, S. Lamansky, P. I. Djurovich, I. Tsyba, R. Bau, M. E. Thompson, *Inorg. Chem.*, **2002**, *41*, 3055. b) B. Yin, F. Niemeyer, J. A. G. Williams, J. Jiang, A. Boucekkine, L. Toupet, H. Le Bozec, V. Guerchais, *Inorg. Chem.* **2006**, 45, 8584. c) D. N. Kozhevnikov, V. N. Kozhevnikov, M. M. Ustinova, A. Santoro, D. W. Bruce, B. Koenig, R. Czerwieniec, T. Fischer, M. Zabel, H. Yersin, *Inorg. Chem.* **2009**, *48*, 4179.

(19) M. Crespo, C. M. Anderson, J. M. Tanski, *Can. J. Chem.*, **2009**, 80-87.

(20) For example, see: T. Sajoto, P. I. Djurovich, A. B. Tamayo, J. Oxgaard, W. A. Goddard III, M. E. Thompson, *J. Am. Chem. Soc.*, **2009**, *131*, 9813.

(21) Z. M. Hudson, S. Wang, *Acc. Chem. Res.* **2009**, *42*, 1584 and references therein.

(22) a) C. R. Wade, F. P. Gabbai, *Inorg. Chem.*, **2010**, *49*, 714. b) S. T. Lam, N. Zhu, V. W. W. Yam, *Inorg. Chem.* **2009**, *48*, 9664. c) Y. M. You, S. Park, *Adv. Mater.* **2008**, *20*, 3820. d) Q. Zhao, F. Y. Li, S. J. Liu, M. X. Yu, Z. Q. Liu, T. Yi, C. H. Huang, *Inorg. Chem.* **2008**, *47*, 9256.

(23) Y. Sun, S. Wang, *Inorg. Chem.* **2009**, *48*, 3755.

(24) Z. He, W. Y. Wong, X. Yu, H. S. Kwok, Z. Lin, *Inorg. Chem.* **2006**, *45*, 10922.

(25) Y. Sun, S. Wang, *Inorg. Chem.* **2010**, *49*, 4394

(26) J. K. Yu, Y. M. Cheng, Y. H. Hu, P. T. Chou, Y. L. Chen, S. W. Lee, Y. Chi, *J. Phys. Chem. B*, **2004**, *108*, 19908.

(27) Z. B. Wang, M. G. Helander, M. T. Greiner, J. Qiu, and Z. H. Lu, *Phys. Rev. B* **2009**, *80*, 235325.

(28) Z. B. Wang, M. G. Helander, Z. W. Liu, M. T. Greiner, J. Qiu, and Z. H. Lu, *Appl. Phys. Lett.* **2009**, *96*, 043303.

(29) Z.B. Wang, M.G. Helander, J. Qiu, Z.W. Liu, M.T. Greiner, and Z.H. Lu, *J. Appl. Phys.*, **2010**, *108*, 024510.

(30) a) C. Adachi, M. A. Baldo, M. E. Thompson, and S. R. Forrest, *J. Appl. Phys.* **2001**, *90*, 5048. b) Z. B. Wang, M. G. Helander, J. Qiu, D. P. Puzzo, M. T. Greiner, Z. W. Liu, and Z. H. Lu, *Appl. Phys. Lett.* **2011**, *98*, 073310.

Chapter 5

Nonconjugated Dimesitylboryl-Functionalized Phenylpyridines and Their Cyclometalated Pt(II) Complexes

5.1 Introduction

Optoelectronic materials containing a triarylboron group have been the subject of considerable recent research due to the electron-accepting ability of the boron centre. When accompanied by appropriate electron donors such as amines, the triarylboron centre promotes intense donor-acceptor charge transfer luminescence in π-conjugated materials.[1] The empty p_π orbital of triarylboranes stabilizes the formation of radical anions, and has led to their successful use in nonlinear optical materials,[2] and as emissive and electron-transport materials in organic light-emitting diodes (OLEDs).[3]

Triarylboranes have also been extensively investigated as chemical sensors for anions. While bulky mesityl groups protect the boron centre from most nucleophiles, small anions such as fluoride and cyanide are capable of binding to the boron centre despite this steric protection.[4-6] As the empty *p* orbital on boron typically makes a large contribution to the LUMO of the molecule, this binding event may be observed by colorimetric, luminescent, or electrochemical changes. Luminescent sensing is particularly attractive, as it allows the detection of an analyte with high sensitivity. Directly conjugated donor-acceptor boranes typically act as "switch-off" luminescent sensors, as binding of an anion to the boron centre blocks the empty p orbital, deactivating any charge-transfer emission. (Compound A, Figure 5.1)

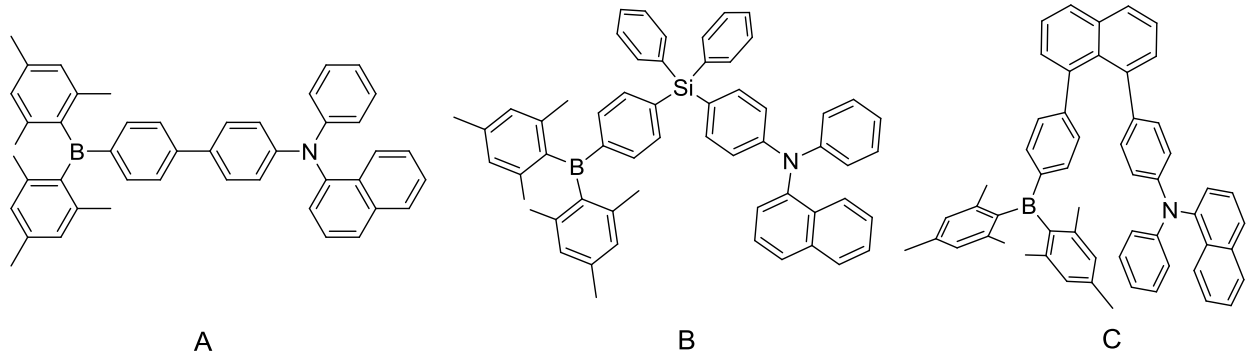

Figure 5.1: Donor-acceptor triarylboranes with varying geometry

We have recently shown, however, that non-conjugated donor-acceptor triarylboranes can act as effective "switch-on" sensors, in which binding of an analyte may be clearly observed by a change in luminescence from one colour to another.[5] For example, compounds B and C incorporate distinct donor and acceptor chromophores connected by rigid and non-rigid linkers, respectively. In the absence of fluoride, both exhibit through-space charge-transfer as broad green emission. When fluoride is added, this emission readily switches to the blue fluorescence of the arylamine chromophore.

More recent research has shown that the triarylboron group is capable of greatly enhancing metal-to-ligand charge transfer (MLCT) in transition-metal compounds, leading to higher luminescent quantum yields and brighter phosphorescent emission.[7] In combination with the improved electron-transporting and film-forming properties afforded by the triarylboron group, this enhanced phosphorescence has allowed for the fabrication of OLEDs with exceptional performance.[7c-f] Furthermore, several reports have described the use of organometallic triarylboranes for phosphorescent sensing,[6] in which interference from background fluorescence or scattering may be removed by time-gated detection.

Despite advances in related organic systems, however, non-conjugated triarylboranes incorporating a metal centre as donor have not been widely studied, and little is known about the through-space interaction between metal centres and the boron group. Only one example of such a compound, Pt(*N*,*C*-

2.1)(SMe_2)Ph, is known to date, and this material was found to exhibit simultaneous singlet and triplet dual emission from both chromophores.[5c] To further investigate these systems, we designed ligands **5.1** and **5.2**, incorporating a flexible silane and a rigid naphthyl linker for $BMes_2$-C_6H_4- and Pt(ppy)(acac) units (ppy = 2-phenylpyridine), which may readily serve as cyclometalating ligands to a variety of transition-metal atoms. Herein we report the synthesis and photophysical properties of these compounds and their Pt(II) complexes.

5.2 Experimental

5.2.1 General Procedures

Experimental techniques and instruments used follow those described in section 2.2. The synthesis of (*p*-dimesitylborylphenyl)-(*p*-bromophenyl)diphenylsilane ,[5] 1-(*p*-dimesitylborylphenyl)-8-iodonaphthalene,[5] 2-(4'-bromophenyl)pyridine,[7d] and PtCl(DMSO)(acac) have been reported previously.[8]

5.2.2 Synthesis of (*p*-dimesitylborylphenyl)-(*p*-(2-pyridylphenyl))diphenylsilane (5.1):

To a 50 mL Schlenk flask with stir bar and condenser was added (*p*-dimesitylborylphenyl)-(*p*-bromophenyl)diphenylsilane (150 mg, 0.23 mmol), $Pd(PPh_3)_4$ (13.1 mg, 0.011 mmol) and 30 mL degassed THF. 2-tributylstannylpyridine (0.35 mL, 0.91 mmol) was then added *via* syringe, and the mixture was heated at reflux for 48 h. The solvent was removed under reduced pressure, and the residue purified on silica (2:1 hexanes:CH_2Cl_2 as eluent) to give 76 mg **5.1** as a white solid (51% yield). ^{1}H NMR (400 MHz, $CDCl_3$) δ 8.72 (d, J = 4.7 Hz, 1H, *Py*), 8.00 (d, J = 8.1 Hz, 2H, - C_6H_4-), 7.80 (t, J = 7.6 Hz, 1H, *Py*), 7.76 (d, J = 7.7 Hz, 1H, *Py*), 7.68 (d, J = 8.1 Hz, 2H, -C_6H_4-), 7.62-7.56 (m, 6H, -*Ph*, - C_6H_4-), 7.48 (d, J = 7.8 Hz, 2H, - C_6H_4-), 7.44 (t, J = 7.3 Hz, 2H, -*Ph*), 7.37 (t, J = 7.4 Hz, 4H, -*Ph*), 7.28 (dd, J = 6.5 Hz, J = 4.7 Hz, 1H, *Py*), 6.80 (s, 4H, *Mes*), 2.29 (s, 6H, *Mes*), 2.01 (s, 12H, *Mes*) ppm; ^{13}C NMR (100 MHz, $CDCl_3$) δ 156.9, 149.2, 147.2, 141.7, 140.8, 139.7, 138.7, 138.2, 137.4, 136.9, 135.8, 135.5, 135.0,

134.0, 133.8, 129.7, 128.1, 127.9, 126.4, 122.5, 121.0, 23.4, 21.2 ppm; HRMS calc'd for $C_{47}H_{44}BNSi$: 661.3345, found 661.3347.

5.2.3 Synthesis of 1-(*p*-dimesitylborylphenyl)-8-(*p*-(2-pyridylphenyl))naphthalene (5.2):

To a 50 mL Schlenk flask with stir bar was added 2-(4'-bromophenyl)pyridine (181 mg, 0.77 mmol) and 30 mL dry, degassed THF. The solution was cooled to -78ºC, then n-BuLi (0.53 mL, 0.85 mmol, 1.6 M in hexanes) was added dropwise *via* syringe. After stirring for 1h, anhydrous $ZnCl_2$ (137 mg, 1.01 mmol) was added. The mixture was stirred 1 h at -78ºC, then 1 h at 0ºC, then $Pd(PPh_3)_4$ (45 mg, 0.39 mmol) and 1-(*p*-dimesitylborylphenyl)-8-iodonaphthalene (300 mg, 0.52 mmol) were added. The mixture was stirred 1 h at 0ºC, then allowed to warm slowly to room temperature and stirred for 48 h. After removal of the solvent under reduced pressure, the residue was purified on silica (30:1 hexanes:EtOAc as eluent) to give 253 mg **5.2** as a white solid (81% yield). ^{1}H NMR (500 MHz, $CDCl_3$) δ 8.66 (d, J = 4.1 Hz, 1H, *Py*), 7.95 (d, J = 7.9 Hz, 2H, -*C*$_6$*H*$_4$-), 7.68 (t, J = 7.6 Hz, 1H, *Py*), 7.64 (d, J = 8.3 Hz, 2H, -*C*$_6$*H*$_4$-), 7.59 (d, J = 6.1 Hz, 2H, *Naph*), 7.56 (d, J = 7.2 Hz, 1H, *Py*), 7.45 (t, J = 7.8 Hz, 2H, *Naph*), 7.23-7.14 (m, 5H, *Py*, *Naph*, -*C*$_6$*H*$_4$-), 7.09 (d, J = 7.9 Hz, 2H, -*C*$_6$*H*$_4$-), 6.72 (s, 4H, *Mes*), 2.27 (s, 6H, *Mes*), 1.75 (s, 12H, *Mes*) ppm; ^{13}C NMR (125 MHz, $CDCl_3$) δ 157.0, 149.5, 147.6, 144.1, 141.5, 140.6, 140.2, 139.9, 138.1, 136.6, 136.5, 136.3, 135.6, 131.6, 131.2, 130.0, 129.2, 129.0, 128.8, 128.6, 127.9, 127.9, 125.9, 125.4, 125.2, 121.8, 23.4, 21.1 ppm; HRMS calc'd for $C_{45}H_{40}BN$: 605.3254, found 605.3248.

5.2.4 Synthesis of Pt(*N*^*C*-5.1)(*O*^*O*-acetylacetonate) (Pt-5.1):

To a 50 mL Schlenk flask with stir bar and condenser was added **5.1** (70 mg, 0.11 mmol), PtCl(DMSO)(acac) (43 mg, 0.11 mmol), NaOAc (8.7 mg, 0.11 mmol) and 20 mL degassed 1:1 THF:MeOH. The mixture was heated at reflux for 3 days, then the solvent was removed under reduced pressure and the residue purified on silica (1:1 hexanes:CH_2Cl_2 as eluent) to give 38 mg **Pt-5.1** as a

yellow solid (38% yield). ^{1}H NMR (400 MHz, C_6D_6) δ 9.06 (d, sat, J = 5.4 Hz, 1H, *Py*), 8.67 Hz (s, sat, 1H, Py-*Ph*), 7.95 (d, J = 7.5 Hz, 2H, -*C*$_6$*H*$_4$-), 7.93-7.89 (m, 4H), 7.69 (d, J = 7.6 Hz, 2H, -*C*$_6$*H*$_4$-), 7.63 (d, J = 7.6 Hz, 1H, Py-*Ph*), 7.34-7.24 (m, 7H), 6.91 (d, J = 7.8 Hz, 1H, Py-*Ph*), 6.86 (s, 4H, *Mes*), 6.83 (t, J = 7.2 Hz, 1H, *Py*), 6.23 (t, J = 7.2 Hz, 1H, *Py*), 5.25 (s, 1H, *acac*), 2.27 (s, 6H, *Mes*), 2.21 (s, 12H, *Mes*), 1.79 (s, 3H, *acac*), 1.63 (s, 3H, *acac*) ppm; ^{13}C NMR (100 MHz, C_6D_6) δ 185.7, 184.7, 169.0, 147.9, 147.7, 146.7, 142.7, 141.4, 140.6, 140.3, 140.2, 139.1, 138.0, 137.5, 137.1, 136.0, 135.9, 135.6, 132.1, 130.0, 129.1, 128.3, 122.9, 121.4, 118.8, 102.9, 28.5, 27.3, 24.1, 21.7 ppm; Anal. Calc'd for $C_{52}H_{50}BNO_2PtSi$: C 65.40, H 5.28, N 1.47, found C 64.30, H 4.80, N 1.43.

5.2.5 Synthesis of Pt(*N*^*C*-5.2)(*O*^*O*-acetylacetonate) (Pt-5.2):

To a 50 mL Schlenk flask with stir bar and condenser was added **2** (50 mg, 0.083 mmol), PtCl(DMSO)(acac) (34 mg, 0.083 mmol), NaOAc (6.8 mg, 0.083 mmol) and 20 mL degassed 1:1 THF:MeOH. The mixture was heated at reflux for 3 days, then the solvent was removed under reduced pressure and the residue purified on silica (2:1 hexanes:CH_2Cl_2 as eluent) to give 27 mg **Pt-5.2** as a yellow solid (36% yield). ^{1}H NMR (500 MHz, $CDCl_3$) δ 9.09 (d, J = 5.4 Hz, 1H, *Py*), 8.04 (s, 1H, Py-*Ph*), 7.72 (d, J = 8.5 Hz, 1H, *Naph*), 7.71 (d, J = 8.5 Hz, 1H, *Naph*) 7.68 (d, J = 6.6 Hz, 1H, Py-*Ph*), 7.54 (d, J = 7.7 Hz, 1H, *Naph*), 7.43 (d, J = 7.7 Hz, 1H, *Naph*), 7.41 (d, J = 6.6 Hz, 1H, Py-*Ph*), 7.36-7.28 (m, 4H), 6.87 (t, J = 7.4 Hz, 1H, *Py*), 6.85-6.79 (m, 3H), 6.73 (s, 4H), 6.26 (t, J = 6.2 Hz, 1H, *Py*), 5.11 (s, 1H, *acac*), 2.15 (s, 6H, *Mes*), 2.01 (s, 12H, *Mes*), 1.69 (s, 3H, *acac*), 1.53 (s, 3H, *acac*) ppm; ^{13}C NMR (125 MHz, C_6D_6) δ 185.7, 184.7, 169.0, 147.9, 147.7, 146.7, 142.7, 141.4, 140.6, 140.2, 139.1, 138.0, 137.5, 137.1, 136.0, 135.6, 132.1, 130.0, 129.1, 122.9, 121.4, 118.8, 102.9, 28.5, 27.3, 24.1, 21.7 ppm (Several quaternary carbons could not be detected due to poor solubility.); Anal. Calc'd for $C_{50}H_{46}BNO_2Pt$: C 66.82, H 5.16, N 1.56, found C 66.62, H 5.31, N 1.46.

5.2.6 X-ray Diffraction Analysis

Single crystals of **5.1** and **5.2** were grown by slow evaporation from solutions of and CH_2Cl_2 and hexanes. Crystal data for these compounds are listed in Table 5.1, and important bond lengths and angles are given in Table 5.2. These crystal structures have been deposited to the Cambridge Crystallographic Data Centre as CCDC 830933 and 830934, and may be obtained free of charge via www.ccdc.cam.ac.uk/data_request/cif.

Table 5.1: Crystallographic data for compounds 5.1 and 5.2

Compound	**5.1**	**5.2**
Formula	$C_{47}H_{44}BNSi$	$C_{45}H_{40}BN$
FW	661.73	605.59
Space Group	P-1	P-1
a, Å	11.148(8)	12.377(3)
b, Å	13.357(10)	15.585(4)
c, Å	13.864(11)	19.596(5)
α, °	72.748(9)	93.572(3)
β, °	75.411(10)	104.934(3)
γ, °	87.040(10)	110.558(3)
V, $Å^3$	1907(2)	3370.5(13)
Z	2	4
D_{calc}, g cm^{-1}	1.152	1.193
T, K	180(2)	180(2)
μ, mm^{-1}	0.095	0.067
$2\theta_{max}$, °	53.00	53.00
Reflns measured	19543	35767
Reflns used (R_{int})	7856 (0.0828)	13890 (0.0650)
Parameters	457	859
Final R Values [I > 2σ(I)]:		
R_1[a]	0.0942	0.0668
wR_2[b]	0.2315	0.1622
R values (all data):		
R_1[a]	0.1591	0.1205
wR_2[b]	0.2854	0.1960
Goodness-of-fit on F^2	1.015	1.003

[a] $R_1 = \Sigma[(|F_0| - |F_c|) / \Sigma |F_0|$

[b] $wR2 = [\Sigma w[(F_0^2-F_c^2)^2] / \Sigma[w(F_0^2)^2]]^{1/2}$

$w = 1 / [\sigma^2(F_0^2) + (0.075P)^2]$, where $P = [Max (F_0^2, 0) + 2F_c^2] / 3$

Table 5.2: Selected bond lengths (Å) and angles (°) for compounds 5.1 and 5.2.

Compound 5.1			
Si(1)-C(13)	1.855(4)	N(1)-C(29)	1.368(8)
Si(1)-C(1)	1.863(4)	B(1)-C(4)	1.570(5)
Si(1)-C(7)	1.868(4)	B(1)-C(30)	1.571(6)
Si(1)-C(19)	1.871(4)	B(1)-C(39)	1.572(6)
N(1)-C(25)	1.361(7)		
N(1)-C(25)	1.361(7)		
C(13)-Si(1)-C(1)	108.36(15)	C(7)-Si(1)-C(19)	108.74(18)
C(13)-Si(1)-C(7)	108.55(18)	C(4)-B(1)-C(30)	116.2(3)
C(1)-Si(1)-C(7)	109.46(16)	C(4)-B(1)-C(39)	120.4(3)
C(13)-Si(1)-C(19)	114.20(17)	C(30)-B(1)-C(39)	123.4(3)
C(1)-Si(1)-C(19)	107.46(16)	C(25)-N(1)-C(29)	116.3(6)
Compound 5.2			
N(1)-C(45)	1.345(3)	B(1)-C(16)	1.584(4)
N(1)-C(41)	1.348(3)	C(4)-C(25)	1.486(3)
C(1)-B(1)	1.552(4)	C(33)-C(36)	1.490(4)
B(1)-C(7)	1.581(4)		
C(1)-B(1)-C(7)	116.5(2)	C(2)-C(4)-C(25)	120.3(2)
C(1)-B(1)-C(16)	119.0(2)	C(45)-N(1)-C(41)	117.5(2)
C(7)-B(1)-C(16)	124.4(2)	C(32)-C(33)-C(34)	118.3(2)
C(5)-C(4)-C(2)	118.0(2)	C(32)-C(33)-C(36)	117.4(2)
C(5)-C(4)-C(25)	121.5(2)	C(34)-C(33)-C(36)	124.1(2)

5.3 Results and Discussion

5.3.1 Synthesis

The syntheses of compounds **Pt-5.1** and **Pt-5.2** are shown in Figure 5.2. **Pt-5.1** incorporates a silane linker with a high degree of rotational flexibility, while **Pt-5.2** includes a more rigid naphthyl spacer that both decreases the metal-boron separation distance and increases the steric congestion of the molecule. **5.1** is prepared by first introducing the boryl substituent to di(*p*-bromophenyl)diphenylsilane by lithium-halogen exchange and substitution with $FBMes_2$. Subsequent Stille coupling with the appropriate pyridyl stannane gives **5.1** in good yield. It should be noted that more common Suzuki coupling reactions should be avoided once the dimesitylboron group is introduced, as the basic conditions required for this reaction can lead to unwanted side products in the presence of Pd catalyst.[9] Ligand **5.2** is most efficiently prepared by synthesis of first the arylboron and phenylpyridine arms of the molecule, followed by their stepwise coupling to 1,8-diiodonaphthalene. This is readily achieved in both cases by Negishi coupling *via* organozinc intermediates. The Pt(II) acetylacetonate (acac) complexes of these ligands were prepared under mild conditions on stirring with PtCl(DMSO)(acac) in the presence of NaOAc in refluxing methanol.[7c-d,8b] The use of acac as an ancillary ligand has several advantages, giving stable complexes that may be isolated in high purity by column chromatography. In addition, the rigidity and high triplet level of the acac ligand minimize its impact on the quantum yield of the phosphorescent phenylpyridine Pt(II) unit.[10]

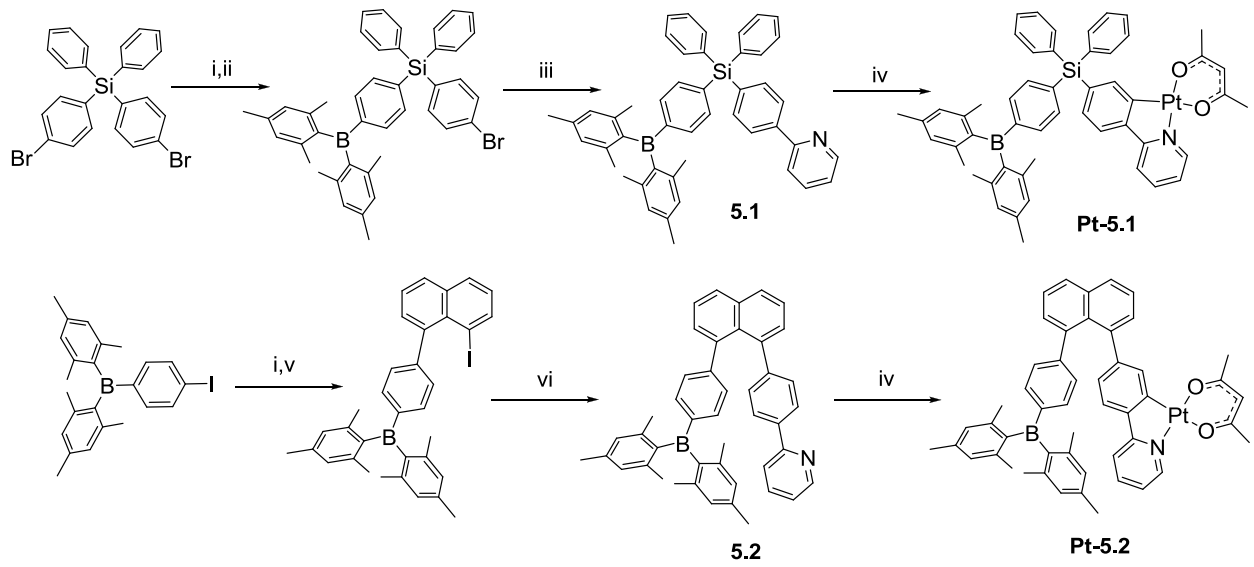

Figure 5.2: Synthesis of Pt(II) complexes. Reagents and Conditions: i) n-BuLi, THF, -78°C; ii) $FBMes_2$, -78°C to RT; iii) 2-($SnBu_3$)pyridine, $Pd(PPh_3)_4$, THF, reflux; iv) PtCl(DMSO)(acac), NaOAc, THF/MeOH, reflux; v) $ZnCl_2$, 0°C, then 1,8-diiodonaphthalene, $Pd(PPh_3)_4$, 0°C to RT; vi) 4-(2'-ppy)phenylzinc bromide, $Pd(PPh_3)_4$, THF, RT.

5.3.2 Crystal Structures

Single-crystals suitable for X-ray diffraction analysis were obtained for the free ligands **5.1** and **5.2** by slow evaporation from CH_2Cl_2/hexanes, while efforts to obtain single crystals of the Pt(II) complexes were unsuccessful. The large difference in steric congestion between ligand **5.1** and **5.2** is readily apparent on comparison of these structures (Figure 5.3). In the crystal structure of **5.1**, the boron and phenylpyridine arms of the molecule show no intramolecular steric interaction, with the shortest separation distance being 9.89 Å from the boron atom to the pyridyl ring. In contrast, in ligand **5.2** this distance is much shorter (5.55 Å on average for the two independent molecules in the lattice). The crystal structure of **5.2** reveals considerable strain, with the naphthyl linker being out of coplanarity by approximately 14°. Though joined by a contiguous path of sp^2-hybridized atoms, the boron and phenylpyridine arms of **5.2** show torsion angles of 40.8° and 44.8° with the naphthyl ring, expected to greatly reduce electronic communication through the linker. The C-C bond distances between the phenyl groups and the naphthyl ring are 1.486(4) and 1.490(4) Å, respectively, further supporting this poor

conjugation. Molecules of **5.2** pack in such a manner in the crystal lattice that the $BMes_2$ groups are all on the same side while the pyridylphenyl groups are parallel to each other (Figure 5.3).

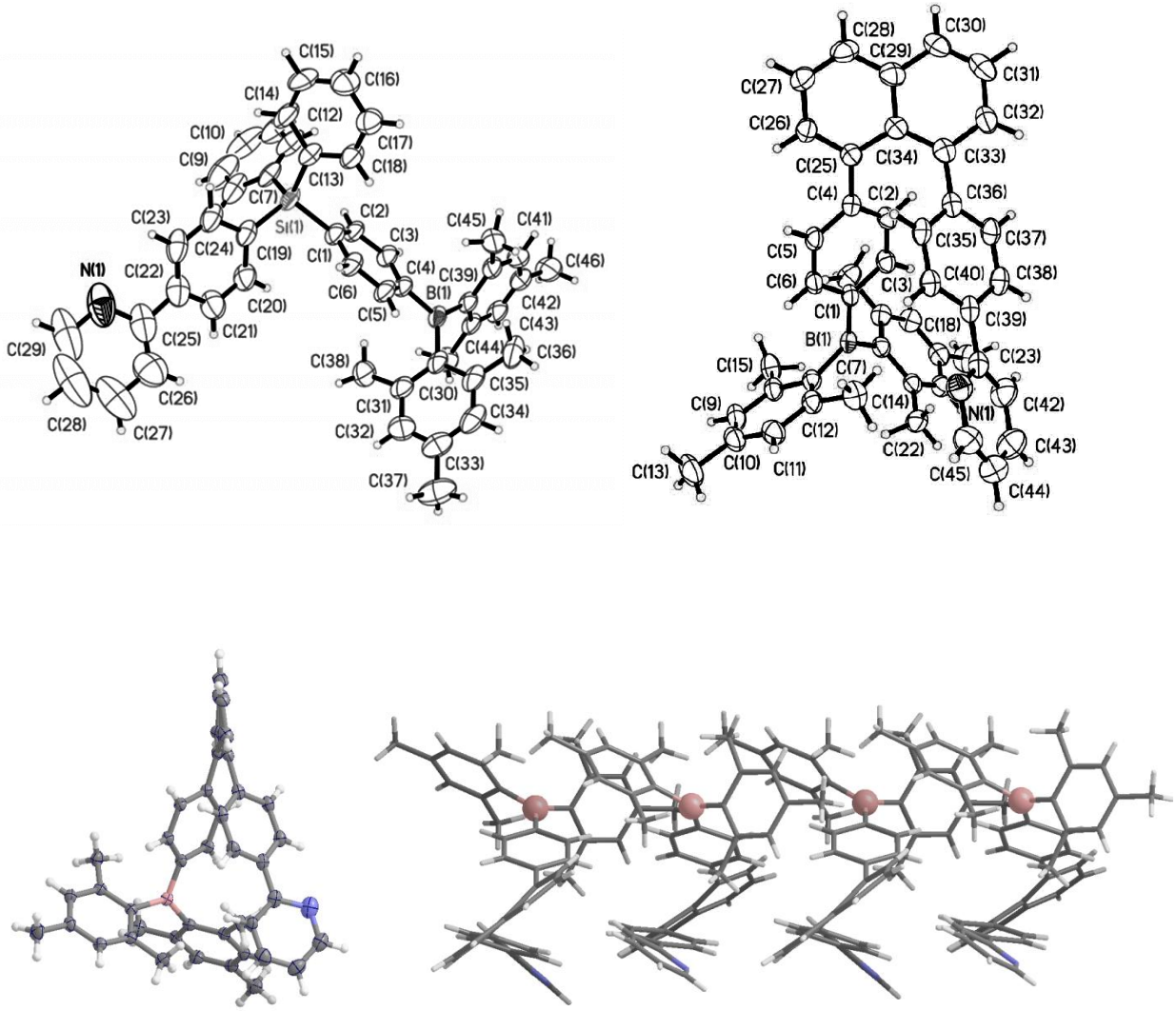

Figure 5.3: Top: Crystal structures of **5.1** (left) and **5.2** (right). Bottom left: side view of **5.2** showing the bending of the naphthyl ring. Bottom right: A diagram showing the orientation and packing of molecules of **5.2** in the crystal lattice.

5.3.3 Photophysical and Electrochemical Properties

Ligands **5.1** and **5.2** both display broad absorptions centered around 325 nm, characteristic of charge transfer from the filled π orbitals of adjacent aryl groups to the empty *p* orbital on the boron centre. The molar extinction coefficient of this band in **5.2** is more than twice as intense as that in **5.1**, owing to the additional contribution from the electron-rich naphthyl ring (Figure 5.4). Chelation to Pt(II) introduces a distinct low-energy absorption band in both cases, characteristic of MLCT from the Pt(II) centre to the phenylpyridine chelate.[7]

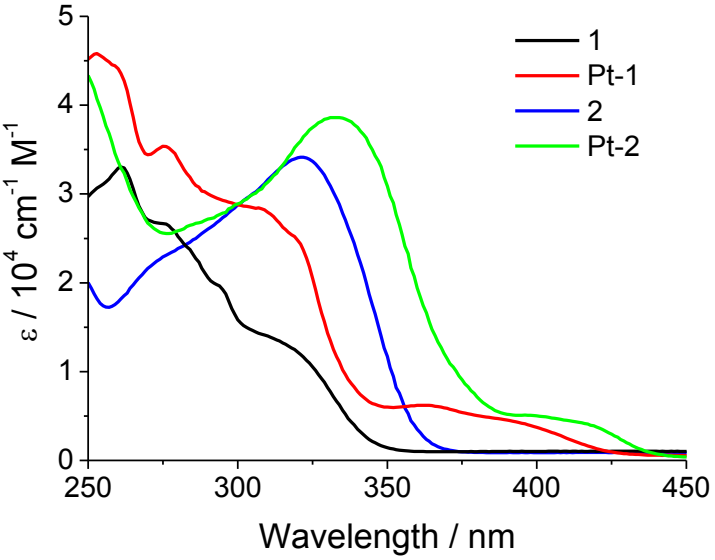

Figure 5.4: UV-Vis absorption spectra of the boryl ligands and their Pt(acac) compounds in CH_2Cl_2.

The CV diagrams of both ligands and their Pt(II) complexes are shown in Figure 5.5. Ligand **5.2** and its Pt(II) complex have very poor solubility in DMF, resulting in weak reduction peaks. Nonetheless, the data show that ligand **5.1** has a more positive reduction potential than **5.2** (by ~50 mV). This may be attributed to the close proximity of the boron center to a relatively electron rich naphtyl and ppy group in **5.2**. The Pt(acac) compounds have a more negative reduction potential, compared to the corresponding free ligand, an indication that the Pt(II) chelation has a significant impact on the electronic properties of

the $BMes_2$ center despite the lack of direct conjugation between these two portions of the molecule. This is in contrast to the effect observed in fully conjugated systems, where it has been shown that metal chelation can substantially improve the electron-accepting ability of triarylboranes by Coulombic and inductive effects.[7,11]

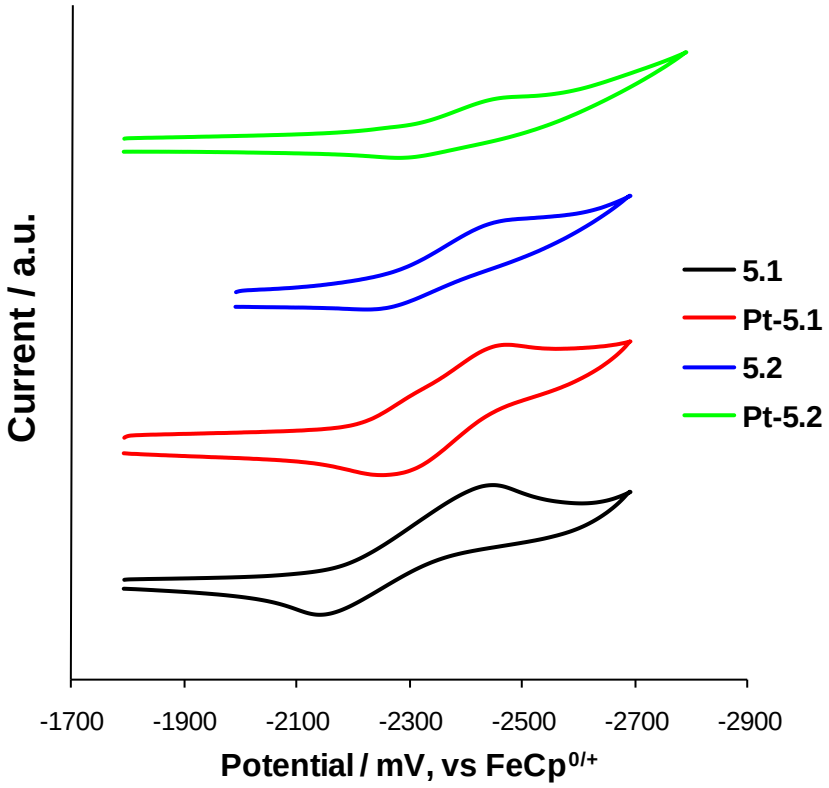

Figure 5.5: Cyclic voltammetry diagrams of the boryl ligands and their Pt(acac) compounds in DMF with NBu_4PF_6 as the electrolyte.

To understand the impact exerted by Pt(II) chelation, we performed DFT calculations at the B3LYP level of theory using LANL2DZ as the basis set for Pt, and 6-31G* for all other atoms. The computational results show that while both ligands possess a distinct boron-centered LUMO, their respective Pt complexes show closely spaced LUMO and LUMO+1 levels with the LUMO being on the ppy-chelate while the LUMO+1 lies on the triarylboron group (Figure 5.6). The HOMO for **5.1** is localized on the

mesityl π orbitals, while the HOMO of **5.2** is localized mostly on the naphthyl ring. The energy of the MO based on the empty *p* orbital on boron (LUMO+1) is destabilized considerably upon chelation to Pt(II) compared to the free ligands. Introduction of the metal centre is found to have the largest impact on the HOMO energy of both molecules, raising the HOMO level by approximately 0.5 eV. This results in a clear change in the lowest energy electronic transition for both nonconjugated boranes, from one based on the triarylboron group itself, to a transition that is largely based on the metal chelate site. It is possible that the increased electron density of the ppy chelate in the complex increases repulsive interactions between the two different arms, thus increasing the π* energy level of the triarylboron arm.

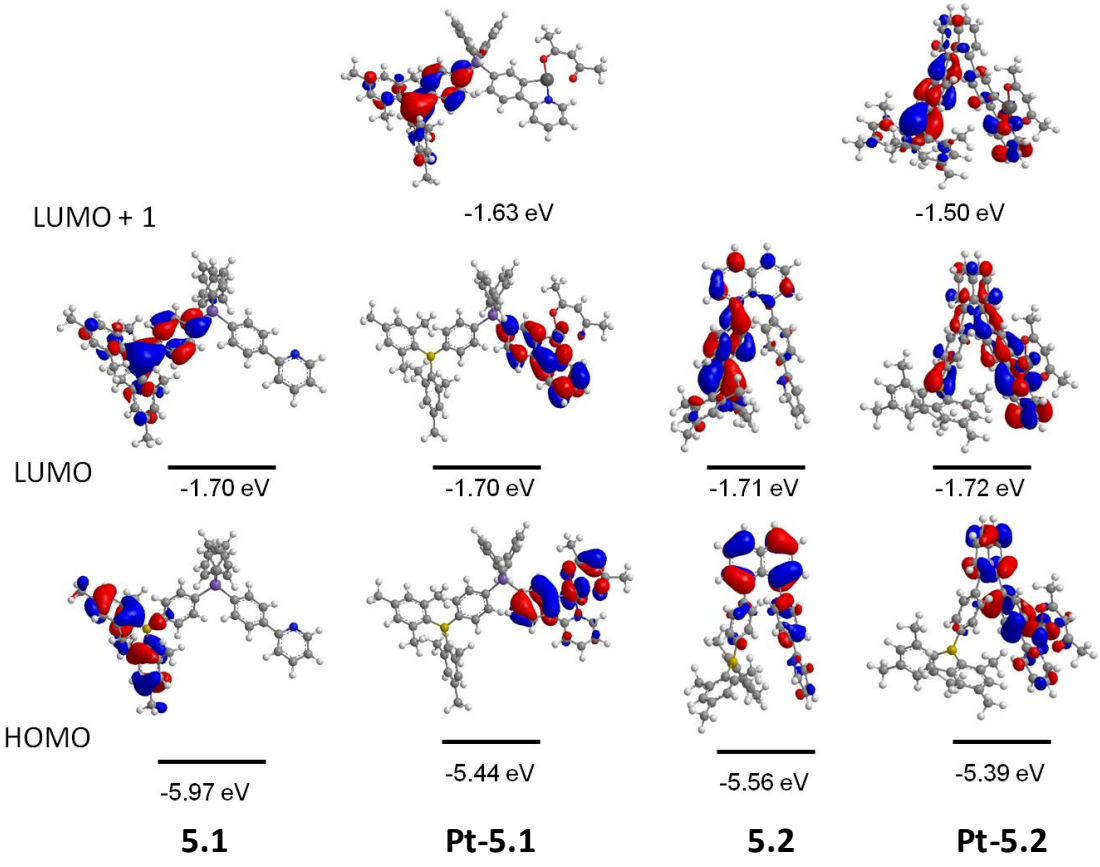

Figure 5.6: Molecular orbital diagrams and energy levels obtained from DFT calculations.

5.3.4 Luminescence

Ligands **5.1** and **5.2** both show high-energy purple fluorescence upon irradiation with UV light, with little change in emission maximum despite considerable differences in structure (Figure 5.7). However, while **5.1** displays only a moderate fluorescence quantum yield of 0.21, that of **5.2** is near unity, consistent with previously reported naphthyl-functionalized triarylboranes.[12] Despite the similarities in the fluorescence of the ligands, the phosphorescent properties of **Pt-5.1** and **Pt-5.2** are dramatically different. Both display long-lived phosphorescent emission, with decay lifetimes of 6.3 and 5.7 μs, respectively. **Pt-5.1** shows bright blue-green emission in the solid state and solution (λ_{em} = 490 nm), similar to that of Pt(ppy)(acac),[10] with a remarkable quantum yield of 0.66 in degassed CH_2Cl_2. The vibrational features clearly visible in the emission spectrum of **Pt-5.1** indicate that this phosphorescence may be attributed to a mixture of ligand-centered (LC) and MLCT excited states. **Pt-5.2**, however, exhibits only very weak, broad orange phosphorescence (λ_{em} = 567 nm), with a quantum yield of approximately 0.005, attributable to the considerable strain in this molecule.

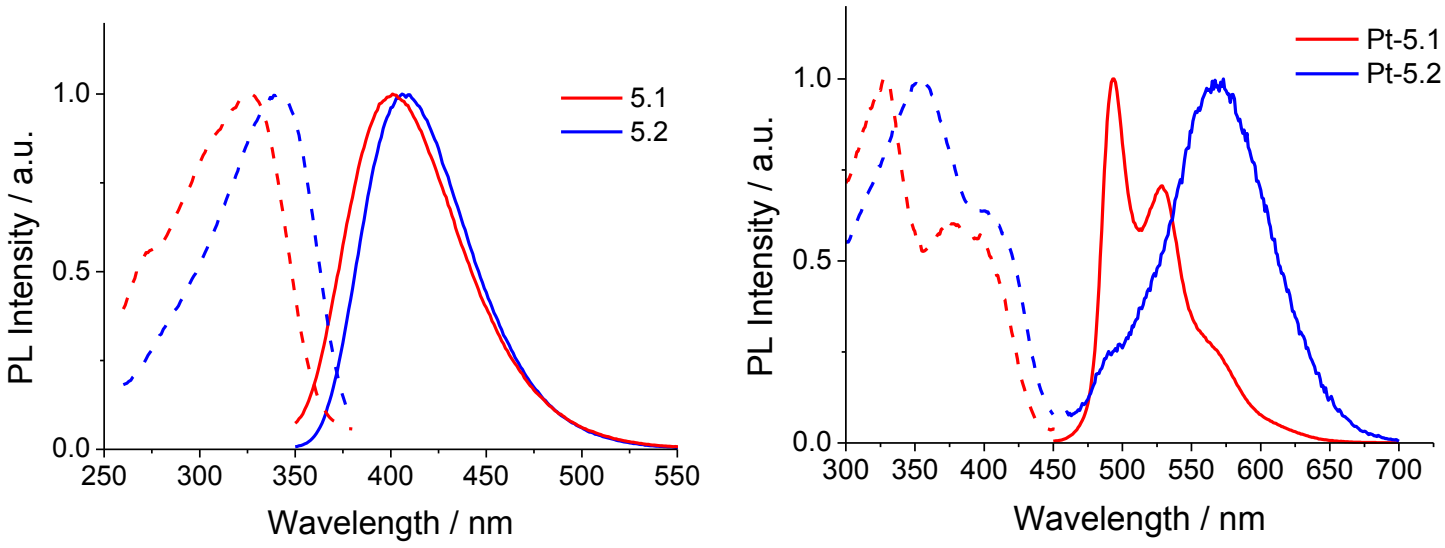

Figure 5.7: Excitation spectra (dashed) and emission spectra (solid) for **5.1** and **5.2** (left) and their Pt(II) complexes (right), obtained at 10^{-5} M in CH_2Cl_2 at 298 K.

This low energy emission likely has contributions from through-space intramolecular charge transfer from the Pt(ppy)(acac) unit to the $BMes_2Ph$ unit, since there are considerable contributions from the $BMes_2$ arm to the LUMO level of **Pt-5.2** (Figure 5.6) while no similar contributions are present for **Pt-5.1**. The distinct phosphorescence of the two Pt(II) complexes illustrates the importance of donor-acceptor geometry on modulating phosphorescent color and efficiency. The photophysical properties of all compounds are summarized in Table 5.3.

Table 5.3: Photophysical properties of 5.1, 5.2 and their Pt(II) complexes

Compound	Absorption, λ_{max} (nm), (ε, [10^4 M^{-1} cm^{-1}])[a]	$\lambda_{em,}$ (nm)	Φ[b]	τ_P (μs)
5.1	285 (2.63), 304 (1.95), 325 (1.32)	401	0.21	--
Pt-5.1	262 (4.57), 285 (3.55), 325 (2.67)	494	0.66	6.3
5.2	286 (2.29), 331 (3.41), 400 (0.45)	406	1.0	--
Pt-5.2	287 (2.67), 333 (3.86), 413 (0.44)	473	0.005	5.7

[a] Obtained at 1.0 x 10^{-5} M in CH_2Cl_2 at 298K. [b] All quantum yields ±10%.

To further explore the electronic structure of these non-conjugated molecules, we performed luminescent titration experiments using NBu_4F (TBAF) in CH_2Cl_2. Both boryl ligands **5.1** and **5.2** display a fluorescent quenching response with the addition of fluoride (Figure 5.8), thus confirming that the fluorescence of these two molecules do not involve through-space charge transfer between the two different legs of the molecules, in agreement with the DFT calculation results. In contrast to diarylamino groups that are excellent electron donors and promote through-space intramolecular charge transfer in non-conjugated systems, as we reported previously,[5a,5b] the ppy ligand cannot serve as an appropriate electron donor in molecules **5.1** and **5.2**. In the case of **5.1**, the fluorescent emission is completely quenched on saturation with F^-, while **5.2** experiences only ~60% emission quenching. This is consistent with titrations of both molecules in absorption mode. Compound **5.1** displays complete quenching of the

325 nm absorption band, indicating that the boryl unit is the sole contributor to this electronic transition. Compound **5.2** however only shows partial quenching of the 325 nm band, confirming that the naphthyl linker plays a role in the fluorescent emission of the molecule.

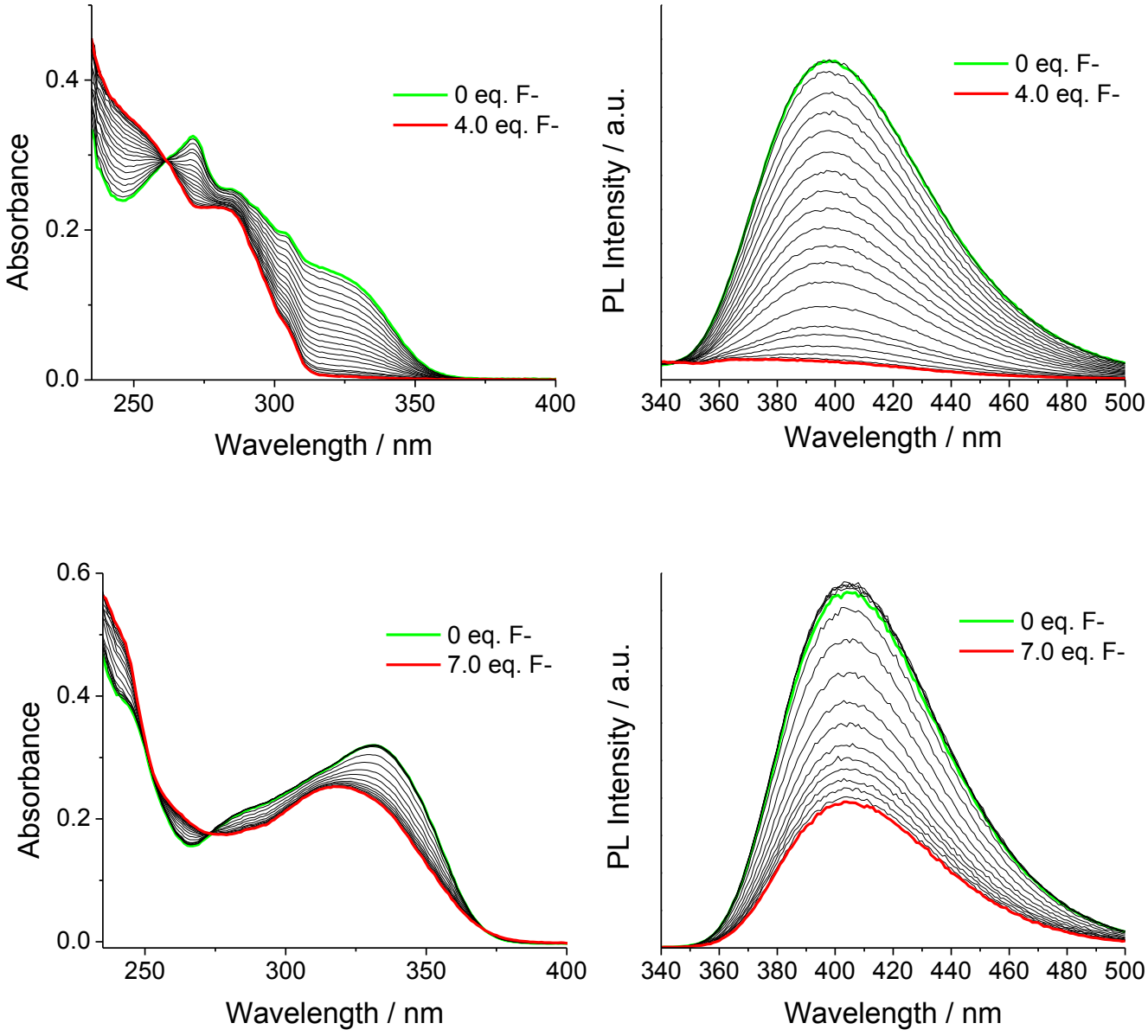

Figure 5.8: UV-visible and fluorescent titrations of 5.1 (top) and 5.2 (bottom) with TBAF at 10^{-5} M in CH_2Cl_2. λ_{ex} = 330 nm.

When metal complexes **Pt-5.1** and **Pt-5.2** are titrated with fluoride, however, both show partial quenching of the broad absorption at 325 nm, while the MLCT band is in both cases totally unaffected (Figure 5.9). This is in contrast to directly conjugated systems, suggesting that the presence of a spatially proximate but electronically separated boryl acceptor does not perturb electronic excited states at lower energy elsewhere in the molecule. Indeed, the low energy phosphorescence displayed by **Pt-5.1** and **Pt-5.2** is totally unaffected by saturation of the $BMes_2$ binding site with fluoride. (Figure 5.10) These results are somewhat unexpected, and represent to our knowledge the first case in which the phosphorescence of $BMes_2$-containing metal compounds could not be affected by anion binding. These results also support that the phosphorescence of both **Pt-5.1** and **Pt-5.2** is mostly localized on the Pt(ppy)(acac) portion of the molecule. The phosphorescent response of **Pt-5.1** toward fluoride ions is in sharp contrast with that of the closely related V-shaped molecule Pt(*N*,*C*-**2.1**)(SMe_2)Ph we reported recently[5c] where a $BMes_2$-C_6H_4-arm and a Pt(*N*,*C*-NPA)(SMe_2)Ph unit (NPA = *N*-(2'-pyridyl)-7-azaindole) are linked together by a diphenylsilane linker. Pt(*N*,*C*-**2.1**)(SMe_2)Ph displays simultaneous singlet and triplet dual emission originating from the boryl and Pt arms of the molecule, respectively, and has a distinct response to the addition of fluoride ions.[5c] Compounds **Pt-5.1** and **Pt-5.2**, however, demonstrate that the dual emissive properties of a non-conjugated system are highly dependent on the nature and the energetic state of the chelate group around the metal center. It is likely that in these cases, the arms of both molecules were too close together to disrupt energy transfer from the boryl arm to the metal chromophore.

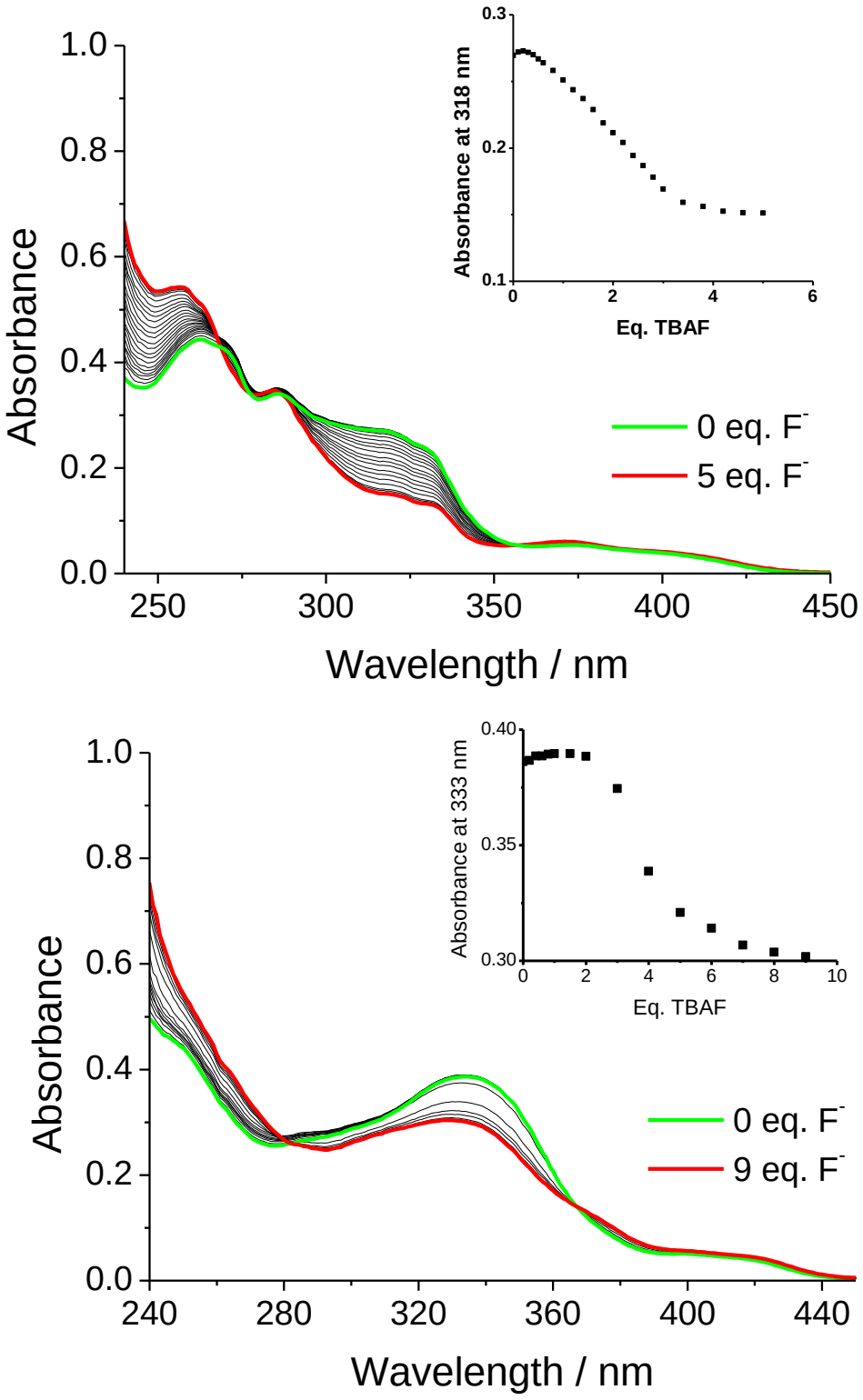

Figure 5.9: UV-visible absorption titrations of **Pt-5.1** (top) and **Pt-5.2** (bottom) with TBAF at 10^{-5} M in CH_2Cl_2. Inset: The absorption intensity at the quenched absorption maximum for each compound.

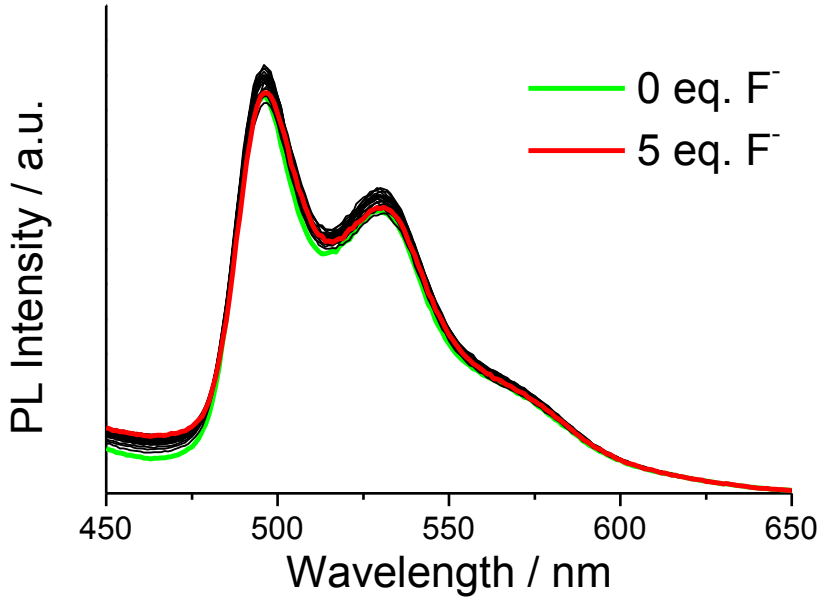

Figure 5.10: Phosphorescent titration of **Pt-5.1** with TBAF at 10^{-5} M in CH_2Cl_2 under air. **Pt-5.2** is not detectably emissive in aerated solution and also showed no change in PL intensity on addition of F^-.

5.4 Conclusions

A pair of non-conjugated dimesitylboron-containing Pt(II) phosphors have been prepared with remarkably different properties based on the nature of the linker. The V-shaped **Pt-5.1** shows bright green phosphorescence at room temperature, while the U-shaped **Pt-5.2** is almost non-emissive under ambient conditions, indicating that the molecular geometry and shape have a significant impact on the phosphorescence of $BMes_2$-functionalized Pt(II) compounds. With an improved understanding of their synthesis and photophysical properties, future studies will examine the impact of the spatially proximate Lewis acidic boron centre on the reactivity of Pt(II) complexes.

5.5 Notes and References

The work described in this chapter has been published as:

- Z.M. Hudson and S. Wang. *Organometallics*, **2011**, *30*, 4695-4701.

References

(1) For recent reviews, see: a) C. D. Entwistle, T. B. Marder, *Angew. Chem., Int. Ed.* **2002**, *41*, 2927. b) F. Jäkle, *Coord. Chem. Rev.* **2006**, *250*, 1107. c) Z. M. Hudson, S. Wang, *Acc. Chem. Res.* **2009**, *42*, 1584. d) F. Jäkle, *Chem. Rev.* **2010**, *110*, 3985. e) C. R. Wade, A. E. J. Broomsgrove, S. Aldridge, F. P. Gabbaï, *Chem. Rev.* **2010**, *110*, 3958.

(2) a) M. Lequan, R. M. Lequan, K. C. Ching, *J. Mater. Chem.* **1991**, *1*, 997. b) C. D. Entwistle, T. B. Marder, *Chem. Mater.* **2004**, *16*, 4574. c) Z. Q. Liu, Q. Fang, D. X. Cao, D. Wang, G. B. Xu, *Org. Lett.* **2004**, *6*, 2933. d) Z. Yuan, C. D. Entwistle, J. C. Collings, D. Albesa-Jové, A. S. Batsanov, J. A. K. Howard, H. M. Kaiser, D. E. Kaufmann, S.-Y. Poon, W.-Y. Wong, C. Jardin, S. Fathallah, A. Boucekkine, J.-F. Halet, N. J. Taylor, T. B. Marder, *Chem. Eur. J.* **2006**, *12*, 2758. e) R. Stahl, C. Lambert, C. Kaiser, R. Wortmann, R. Jakober, *Chem. Eur. J.* **2006**, *12*, 2358. f) L. M. Tao, Y. H. Guo, X. M. Huang, C. K. Wang, *Chem. Phys. Lett*. **2006**, *425*, 10.

(3) a) T. Noda, Y. Shirota, *J. Am. Chem. Soc.* **1998**, *120*, 9714. b) Y. Shirota, *J. Mater. Chem.* **2005**, *15*, 75. c) T. Noda, H. Ogawa, Y. Shirota, *Adv. Mater.* **1999**, *11*, 283. d) Y. Shirota, M. Kinoshita, T. Noda, K. Okumoto, T. Ohara, *J. Am. Chem. Soc.* **2000**, *122*, 1102. e) W. L. Jia, D. R. Bai, T. McCormick, Q. D. Liu, M. Motala, R. Wang, C. Seward, Y. Tao, S. Wang, *Chem. Eur. J.* **2004**, *10*, 994. f) W. L. Jia, X. D. Feng, D. R. Bai, Z.-H. Lu, S. Wang, G. Vamvounis, *Chem. Mater.* **2005**, *17*, 164. g) F. H. Li, W. L. Jia, S. Wang, Y. Q. Zhao, Z. H. Lu, *J. Appl. Phys.* **2008**, *103*, 034509/1.

(4) For representative examples, see: a) S. Yamaguchi, T. Shirasaka, S. Akiyama, K. Tamao, *J. Am. Chem. Soc.* **2002**, *124*, 8816. b) S. Solé, F. P. Gabbaï, *Chem. Commun.* **2004**, 1284. c) M. Melaïmi, F. P. Gabbaï, *J. Am. Chem. Soc.* **2005**, *127*, 9680. d) C. W. Chiu, F. P. Gabbaï, *J. Am. Chem. Soc.* **2006**, *128*, 14248. e) M. H. Lee, F. P. Gabbaï, *Inorg. Chem.* **2007**, *46*, 8132. f) T. W. Hudnall, F. P.

Gabbaï, *J. Am. Chem. Soc.* **2007**, *129*, 11978. g) T. W. Hudnall, Y.-M. Kim, M. W. P. Bebbington, D. Bourissou, F. P. Gabbaï, *J. Am. Chem. Soc.* **2008**, *130*, 10890.

(5) a) X. Y. Liu, D. R. Bai, S. Wang, *Angew. Chem. Int. Ed.* **2006**, *45*, 5475. b) D. R. Bai, X. Y. Liu, S. Wang, *Chem. Eur. J.* **2007**, *13*, 5713. c) Z. M. Hudson, S. B. Zhao, S. Wang, *Chem. Eur. J.* **2009**, *15*, 6081.

(6) a) Y. Sun, S. Wang, *Inorg. Chem.* **2009**, *48*, 3755. b) Y. Sun, S. Wang, *Inorg. Chem.* **2010**, *49*, 4394. c) Q. Zhao, F. Y. Li, S. J. Liu, M. X. Yu, Z. Q. Liu, T. Yi, C. H. Huang, *Inorg. Chem.* **2008**, *47*, 9256. d) S. T. Lam, N. Zhu, V. W. W. Yam, *Inorg. Chem.* **2009**, *48*, 9664. e) Y. You, S. Y. Park, *Dalton Trans.* **2009**, 1267. f) J. K. Day, C. Bresner, N. D. Coombs, I. A. Fallis, L. L. Ooi, S. Aldridge, *Inorg. Chem.* **2008**, *47*, 793.

(7) a) E. Sakuda, A. Funahashi, N. Kitamura, *Inorg. Chem.* **2006**, *45*, 10670. b) S. B. Zhao, T. McCormick, S. Wang, *Inorg. Chem.* **2007**, *46*, 10965. c) G. J. Zhou, C. L. Ho, W. Y. Wong, Q. Wang, D. G. Ma, L. X. Wang, Z. Y. Lin, T. B. Marder, A. Beeby, *Adv. Funct. Mater.* **2008**, *18*, 499. d) Z. M. Hudson, C. Sun, M. G. Helander, H. Amarne, Z.-H. Lu, S. Wang, *Adv. Funct. Mater.* **2010**, *20*, 3426. e) Z. M. Hudson, M. G. Helander, Z.-H. Lu, S. Wang, *Chem. Commun*. **2011**, *47*, 755. f) Z. B. Wang, M. G. Helander, Z. M. Hudson, S. Wang, Z.-H. Lu, *Appl. Phys. Lett*, **2011**, *98*, 213301.

(8) a) S. A. De Pascali, P. Papadia, A. Ciccarese, C. Pacifico, F. P. Fanizzi, *Eur. J. Inorg. Chem.* **2005**, 788. b) M. Crespo, C. M. Anderson, J. M. Tanski, *Can. J. Chem.*, **2009**, *87*, 80.

(9) N. Wang, Z. M. Hudson, S. Wang, *Organometallics*, **2010**, *29*, 4007.

(10) J. Brooks, Y. Babayan, S. Lamansky, P. I. Djurovich, I. Tsyba, R. Bau, M. E. Thompson, *Inorg. Chem.*, **2002**, *41*, 3055.

(11) a) Y. Sun, N. Ross, S. B. Zhao, K. Huszarik, W. L. Jia, R. Y. Wang, D. Macartney, S. Wang, *J. Am. Chem. Soc.* **2007**, *129*, 7510. b) C. R. Wade, F. P. Gabbaï, *Inorg. Chem.* **2010**, *49*, 714.

(12) S. B. Zhao, P. Wucher, Z. M. Hudson, T. M. McCormick, X. Y. Liu, S. Wang, X. D. Feng, Z.-H. Lu, *Organometallics*, **2008**, *27*, 6446.

Chapter 6

Efficient One-Pot Synthesis of Cyclometalated Platinum(II) β-Diketonates at Ambient Temperature

6.1 Introduction

Cyclometalated platinum complexes are among the most efficient phosphorescent materials, and have been widely explored for use in chemical sensors[1] and organic light-emitting diodes (OLEDs).[2] In particular, cyclometalated platinum (II) β-diketonates have been the subject of considerable research[3] due to the excellent stability and high triplet energy level of typical diketonate ancillary ligands. As a result, this moiety has been incorporated into materials with many fascinating structures, including bimetallic complexes,[4] photochromic materials,[5] liquid crystals,[6] and metallahelicenes.[7] Furthermore, the efficient phosphorescence of cyclometalated platinum β-diketonates has led to many applications in biological imaging,[8] nonlinear optics,[9] oxygen sensing,[10] and most notably electroluminescent devices.[2b-h] Despite this broad research activity, however, an efficient synthetic method for producing these compounds has remained elusive. This is of particular concern due to the high cost of platinum-based starting materials, increasing the cost of research and seriously limiting the commercial viability of these compounds.

Cyclometalated platinum β-diketonates are typically prepared by a modified method of Lewis and coworkers,[3a,11] a two-step process in which 2 to 2.5 equivalents of cyclometalating ligand are heated with K_2PtCl_4 to give a chloro-bridged platinum dimer, which is then heated with Na_2CO_3 and β-diketone to give the final product (Figure 6.1). This process has several disadvantages, requiring long reaction times at high temperature and giving typical yields of only 20-40% over two steps. The need for excess ligand is particularly problematic, as the organic ligands used for many applications in advanced materials are often of considerable value themselves. Furthermore, the high temperature reaction conditions limit the

scope of cyclometalating ligands that can be used to prepare these complexes. Although recent reports have described stoichiometric reactions of cyclometalating ligands using PtCl(DMSO)(acac) as starting material, long reaction times and low yields are typical of this method as well.[2b-c,12]

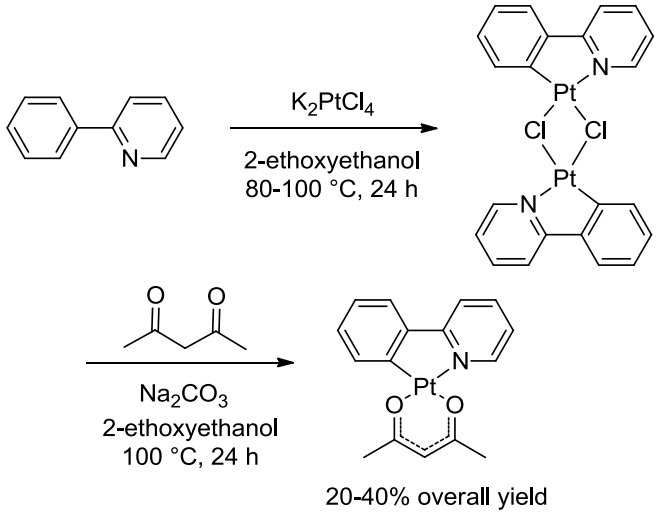

Figure 6.1: The traditional preparation method for cyclometalated Pt(II) *β*-diketonates

Seeking to address this challenge, we have developed an efficient one-pot synthesis of cyclometalated platinum *β*-diketonates under mild conditions. This method requires only stoichiometric equivalents of the *N^C*-chelate ligand, with typical yields of 80-90% after 3 hours reaction time at ambient temperature. The results of our studies are reported herein.

6.2 Experimental

6.2.1 General Procedures

Experimental techniques and instruments used follow those described in section 2.2. All reactions were carried out under air unless otherwise noted. 2-phenylphyridine, 2-phenylquinonline, and benzo[h]quinolone were purchased from Aldich chemical company. 4-dimethylamino-2-phenylpyridine,[13]

5-(dimesitylboryl)-2-phenylpyridine,[2b] 5-dimesitylboryl-4-(*N*-(1-naphthyl)-*N*-phenylamino)phenyl pyridine,[2c] 2-(2-pyridyl)indole,[14] 1-naphthyldiphenylphosphine,[15] (1-methyl-3-phenylimidazol-2-ylidine)silver iodide[16] and $[PtMe_2(SMe_2)]_2$[17] starting materials were prepared according to literature procedures. 2-(2-pyridyl)benzothiophene, 2-(2-pyridyl)benzofuran, and all other substituted phenylpyridines were prepared by Suzuki coupling of 2-bromopyridine with commercially available boronic acids.[18] Pt complexes **6.1a**,[3a] **6.1b**,[3a] **6.1c**,[19] **6.2a**,[3a] **6.3**,[3a] **6.6**,[3a] **6.7**,[3a] **6.8a**,[2b] **6.8b**,[2f] **6.8c**,[2c] **6.9b**[3a] and **6.11**[20] are previously known compounds, which are characterized by ^{1}H NMR and elemental analysis. The remaining novel complexes have been characterized by ^{1}H and ^{13}C NMR and elemental analysis.

6.2.2 General Procedure for the Synthesis of Cyclometalated Pt(II) Complexes

To a 20 mL screw-cap vial with stir bar is added one equivalent of cyclometalating ligand (0.35 mmol), $[PtMe_2(SMe_2)]_2$ dimer (100 mg, 0.17 mmol) and 3 mL of THF. The reaction is allowed to stir 1 hr at ambient temperature, then a solution of organic acid (1 mL, 0.35 M in THF) is added dropwise. The mixture is stirred for 30 minutes, then a solution of Na(*β*-diketonate) (0.70 mmol in 2 mL MeOH) is added. The mixture is stirred for 1.5 hours, then partitioned between water and CH_2Cl_2. The organic layer is washed with brine, dried over $MgSO_4$, filtered, and concentrated. The residue is then purified on a plug of silica gel (hexanes:CH_2Cl_2 as eluent) to give analytically pure material.

6.2.3 Synthetic and Characterization Data

Compounds **6.1** through **6.9** were prepared according to the general procedure described above. Compounds **6.10** and **6.11** were prepared by a modified version of this procedure, which is described herein. The structures of all complexes are given in Table 6.1.

6.1a: ^{1}H NMR (400 MHz, $CDCl_3$) δ 9.00 (d, sat, J_{Pt-H} = 41.8 Hz, J = 5.8 Hz, 1H), 7.80 (t, J = 7.8 Hz, 1H), 7.71 – 7.55 (m, 2H), 7.45 (d, J = 7.6 Hz, 1H), 7.21 (t, J = 7.4 Hz, 1H), 7.15 – 7.06 (m, 2H), 5.48 (s, 1H), 2.01 (s, 6H) ppm, Anal. calc'd for $C_{16}H_{15}NO_2Pt$: C 42.86, H 3.37, N 3.12; found C 43.56, H 3.39, N 2.98.

6.1b: ^{1}H NMR (400 MHz, $CDCl_3$) δ 9.00 (d, sat, J_{Pt-H} = 40.9 Hz, J = 5.8 Hz, 1H), 7.81 (t, J = 7.7 Hz, 1H), 7.67 (d, J = 7.6 Hz, 1H), 7.63 (d, J = 8.1 Hz, 1H), 7.45 (d, J = 7.6 Hz, 1H), 7.22 (t, J = 7.4 Hz, 1H), 7.16 – 7.07 (m, 2H), 5.82 (s, 1H), 1.29 (s, 9H), 1.28 (s, 9H) ppm, Anal. calc'd for $C_{22}H_{27}NO_2Pt$: C 49.62, H 5.11, N 2.63; found C 49.86, H 5.05, N 2.59.

6.1c: ^{1}H NMR (400 MHz, $CDCl_3$) δ 9.15 (d, sat, J_{Pt-H} = 39.0 Hz, J = 5.8 Hz, 1H), 8.11 (d, J = 7.3 Hz, 2H) 8.08 (d, J = 7.1 Hz, 2H), 8.01 (d, J = 7.1 Hz, 1H), 7.85 (t, J = 7.7 Hz, 1H), 7.80 (d, J = 7.3 Hz, 1H), 7.69 (d, J = 8.1 Hz, 1H), 7.57 (t, J = 7.3 Hz, 2H), 7.51 (t, J = 7.8 Hz, 4H), 7.29 (t, J = 8.3 Hz, 1H), 7.20 (t, J = 6.1 Hz, 1H), 7.15 (t, J = 7.5 Hz, 1H), 6.79 (s, 1H) ppm, Anal. calc'd for $C_{26}H_{19}NO_2Pt$: C 54.54, H 3.35, N 2.45, found C 55.05, H 2.92, N 2.40.

6.2a: ^{1}H NMR (400 MHz, $CDCl_3$) δ 8.97 (d, sat, J_{Pt-H} = 42.3 Hz, J = 5.8 Hz, 1H), 7.77 (t, J = 7.7 Hz, 1H), 7.57 (d, J = 8.0 Hz, 1H), 7.42 (s, 1H), 7.34 (d, J = 7.8 Hz, 1H), 7.07 (dd, J = 7.4, 5.8 Hz, 1H), 6.92 (d, J = 7.8 Hz, 1H), 5.48 (s, 1H), 2.41 (s, 3H), 2.03 (s, 3H), 2.01 (s, 3H) ppm; Anal. calc'd for $C_{17}H_{17}NO_2Pt$: C 44.16, H 3.71, N 3.03; found C 44.99, H 3.61, N 2.98.

6.2b: ^{1}H NMR (400 MHz, $CDCl_3$) δ 9.00 (d, sat, J_{Pt-H} = 40.5 Hz, J = 5.8 Hz, 1H), 7.82 (t, J = 7.8 Hz, 1H), 7.64 – 7.47 (m, 2H), 7.36 (d, J = 8.3 Hz, 1H), 7.14 (t, J = 6.6 Hz, 1H), 7.10 (dd, J = 8.2, 2.1 Hz, 1H) 5.50 (s, 1H), 2.04 (s, 3H), 2.02 (s, 3H) ppm; ^{13}C NMR (100 MHz, $CDCl_3$) δ 185.8, 184.4, 167.3, 147.3, 143.1, 141.0, 138.3, 134.8, 130.0, 124.0, 123.6, 121.4, 118.5, 102.6, 28.2, 27.1 ppm; Anal. calc'd for $C_{16}H_{14}ClNO_2Pt$: C 39.80, H 2.92, N 2.90; found C 40.29, H 2.91, N 2.68; m.p. > 300 °C.

6.2c: ^{1}H NMR (400 MHz, $CDCl_3$) δ 8.99 (d, sat, J_{Pt-H} = 39.6 Hz, J = 5.8 Hz, 1H), 7.82 (t, J = 7.8 Hz, 1H), 7.72 (d, J = 1.8 Hz, 1H), 7.58 (d, J = 8.1 Hz, 1H), 7.32-7.23 (m, 2H), 7.15 (t, J = 6.5 Hz, 1H), 5.49 (s, 1H), 2.04 (s, 3H), 2.02 (s, 3H) ppm; ^{13}C NMR (100 MHz, $CDCl_3$) δ 185.8, 184.3, 167.3, 147.3, 143.5, 141.4, 138.3, 132.8, 126.5, 124.2, 123.9, 121.5, 118.5, 102.6, 28.2, 27.1 ppm, Anal. calc'd for $C_{16}H_{14}BrNO_2Pt$: C 36.45, H 2.68, N 2.66; found C 36.89, H 2.63, N 2.56; m.p. > 300 °C.

6.3: ^{1}H NMR (400 MHz, $CDCl_3$) δ 9.07 (d, sat, J_{Pt-H} = 40.7 Hz, J = 5.8 Hz, 1H), 8.04 (d, J = 8.1 Hz, 1H), 7.88 (t, J = 8.1 Hz, 1H), 7.32 (dd, J = 8.4, 4.9 Hz, 1H), 7.24 – 7.17 (m, 1H), 7.14 – 7.04 (dt, J = 10.9, 8.3 Hz, 1H), 5.49 (s, 1H), 2.02 (s, 3H), 2.01 (s, 3H) ppm; Anal. calc'd for $C_{16}H_{13}NO_2FPt$: C 39.68, H 2.71, N 2.89; found C 40.11, H 2.70, N 2.78.

6.4: ^{1}H NMR (400 MHz, $CDCl_3$) δ 9.00 (d, sat, J_{Pt-H} = 39.8 Hz, J = 5.8 Hz, 1H), 7.80 (t, J = 7.8 Hz, 1H), 7.58 (d, J = 8.1 Hz, 1H), 7.51 (d, J = 8.4 Hz, 1H), 7.10 (dd, J = 7.3, 5.6 Hz, 1H), 7.04 (d, J = 2.7 Hz, 1H), 6.91 (dd, J = 8.3, 2.7 Hz, 1H), 5.47 (s, 1H), 3.85 (s, 3H), 2.00 (s, 6H) ppm; ^{13}C NMR (100 MHz, $CDCl_3$) δ 185.6, 183.9, 168.0, 157.1, 147.3, 145.0, 138.1, 131.1, 128.9, 121.3, 118.3, 115.6, 108.8, 102.5, 55.4, 28.3, 27.1 ppm, Anal. calc'd for $C_{17}H_{17}NO_3Pt$: C 42.68, H 3.58, N 2.93; found C 43.19, H 3.55, N 2.79; m.p. 227-228 °C.

6.5: ^{1}H NMR (400 MHz, $CDCl_3$) δ 8.41 (d, J = 6.9 Hz, 1H), 7.58 (d, J = 7.3 Hz, 1H), 7.37 (d, J = 7.6 Hz, 1H), 7.15 (t, J = 7.4 Hz, 1H), 7.05 (t, J = 7.4 Hz, 1H), 6.74 (d, J = 3.0 Hz, 1H), 6.34 (dd, J = 7.0, 3.0 Hz, 1H), 5.43 (s, 1H), 3.11 (s, 6H), 1.97 (s, 3H), 1.96 (s, 3H) ppm; ^{13}C NMR (100 MHz, $CDCl_3$) δ 185.1, 183.8, 166.7, 155.1, 146.0, 145.8, 138.1, 130.5, 128.3, 123.0, 121.9, 103.8, 102.3, 100.2, 39.4, 28.2, 27.2 ppm; Anal. calc'd for $C_{18}H_{20}N_2O_2Pt$: C 43.99, H 4.10, N 5.70; found C 44.99, H 4.15, N 5.68; m.p. 265-266 °C.

6.6: ^{1}H NMR (400 MHz, $CDCl_3$) δ 9.14 (d, J = 5.4 Hz, 1H), 8.26 (d, J = 8.0 Hz, 1H), 7.85 – 7.73 (m, 2H), 7.63 – 7.57 (m, 2H), 7.53 (d, J = 8.8 Hz, 1H), 7.44 (dd, J = 8.0, 5.4 Hz, 1H), 5.54 (s, 1H), 2.07 (s, 6H) ppm; Anal. calc'd for $C_{18}H_{15}NO_2Pt$: C 45.76, H 3.20, N 2.97; found C 46.11, H 3.12, N 2.92.

6.7: ^{1}H NMR (400 MHz, $CDCl_3$) δ 9.57 (d, J = 8.9 Hz, 1H), 8.26 (d, J = 8.7 Hz, 1H), 7.85 – 7.72 (m, 4H), 7.59 (d, J = 7.7 Hz, 1H), 7.55 (dd, J = 8.1, 6.9 Hz, 1H), 7.23 (d, J = 7.5 Hz, 1H), 7.17 (t, J = 7.5 Hz, 1H), 5.58 (s, 1H), 2.06 (s, 3H), 2.05 (s, 3H) ppm; Anal. calc'd for $C_{20}H_{17}NO_2Pt$: C 48.19, H 3.44, N 2.81; found C 48.47, H 3.28, N 2.67.

6.8a: ^{1}H NMR (400 MHz, $CDCl_3$) δ 9.04 (s, sat, J_{Pt-H} = 38.4 Hz, 1H), 7.88 (d, J = 8.0 Hz, 1H), 7.63 (d, J = 7.6 Hz, 1H), 7.57 (d, J = 8.1 Hz, 1H), 7.50 (d, J = 7.8 Hz, 1H), 7.22 (t, J = 7.4 Hz, 1H), 7.10 (t J = 7.5 Hz, 1H), 6.87 (s, 4H), 5.40 (s, 1H), 2.32 (s, 6H), 2.09 (s, 12H), 1.98 (s, 3H), 1.66 (s, 3H) ppm; Anal. calc'd. for $C_{34}H_{36}BNO_2Pt$: C 58.63, H 5.21, N 2.01; found C 57.63, H 5.23, N 1.83.

6.8b: ^{1}H NMR (400 MHz, $CDCl_3$) δ 8.89 (d, sat, J_{Pt-H} = 39.6 Hz, J = 5.3 Hz, 1H), 7.72 (t, J = 7.6 Hz, 1H), 7.47 (d, J = 7.8 Hz, 1H), 7.32-7.24 (m, 6H), 7.24-7.18 (m, 4H), 7.04 (t, J = 7.2 Hz, 2H), 7.00 (d, J = 6.5 Hz, 1H), 6.69 (dd, J = 8.4, 2.4 Hz, 1H), 5.39 (s, 1H), 1.97 (s, 3H), 1.73 (s, 3H) ppm, Anal. calc'd for $C_{28}H_{24}N_2O_2Pt$: C 54.63, H 3.93, N 4.55; found C 55.31, H 3.94, N 4.35.

6.8c: ^{1}H NMR (400 MHz, $CDCl_3$) δ 8.90 (s, sat, J_{Pt-H} = 35.3 Hz, 1H), 8.01 (d, J = 8.5 Hz, 1H), 7.88 (d, J = 8.2 Hz, 1H), 7.79 (d, J = 8.2 Hz, 1H), 7.75 (d, J = 8.1 Hz, 1H), 7.52 – 7.40 (m, 3H), 7.40 – 7.31 (m, 2H), 7.23 (m, 6H), 6.99 (m, 1H), 6.85 (m, 5H), 6.55 (d, J = 8.5 Hz, 1H), 5.31 (s, 1H) 2.30 (s, 6H), 2.08 (s, 12H), 1.62 (s, 6H) ppm; Anal. calc'd for $C_{50}H_{47}BN_2O_2Pt$: C 65.72, H 5.18, N 3.07; found C 66.09, H 5.07, N 3.08.

6.9a: ^{1}H NMR (400 MHz, $CDCl_3$) δ 8.86 (d, sat, J_{Pt-H} = 42.8 Hz, J = 5.6 Hz, 1H), 8.08 (d, J = 7.8 Hz, 1H), 7.73 (t, J = 7.8 Hz, 1H), 7.44 (d, J = 8.3 Hz, 1H), 7.37-7.30 (m, 2H), 7.24 (t, J = 7.3 Hz, 1H), 7.03 (dd, J = 7.4, 5.8 Hz, 1H), 5.54 (s, 1H), 2.06 (s, 3H), 2.03 (s, 3H) ppm ^{13}C NMR (100 MHz, $CDCl_3$) δ 185.1, 183.6, 159.5, 156.6, 147.8, 138.9, 133.3, 125.4, 123.7, 122.8, 119.1, 116.6, 116.3, 111.1, 102.5, 28.1, 26.4 ppm; Anal. calc'd for $C_{18}H_{15}NO_3Pt$: C 44.27, H 3.10, N 2.87; found C 44.68, H 2.72, N 2.73; m.p. 247-248 °C.

6.9b: ^{1}H NMR (400 MHz, $CDCl_3$) δ 8.92 (d, sat, J_{Pt-H} = 40.0 Hz, J = 5.8 Hz, 1H), 8.83 – 8.76 (m, 1H), 7.86 – 7.78 (m, 1H), 7.72 (t, J = 7.8 Hz, 1H), 7.40 – 7.28 (m, 4H), 6.96 (dd, J = 7.3, 5.8 Hz, 1H), 5.56 (s, 1H), 2.10 (s, 3H), 2.03 (s, 3H) ppm; Anal. calc'd. for $C_{18}H_{15}NO_2PtS$: C 42.97, H 3.00, N 2.78; found C 42.97, H 2.71, N 2.76.

6.9c: ^{1}H NMR (400 MHz, $CDCl_3$) δ 8.92 (d, sat, J_{Pt-H} = 40.7 Hz, J = 5.8 Hz, 1H), 8.30 (d, J = 7.9 Hz, 1H), 7.57 (t, J = 7.3 Hz, 2H), 7.49 (t, J = 7.3 Hz, 1H), 7.43 (d, J = 7.3 Hz, 2H), 7.36 (t, J = 7.9 Hz, 1H), 7.19 (t, J = 7.5 Hz, 1H), 7.11 (t, J = 7.3 Hz, 1H), 7.02 (d, J = 8.3 Hz, 1H), 6.79 (dd, J = 7.3, 5.7 Hz, 1H), 6.38 (d, J = 8.2 Hz, 1H), 5.54 (s, 1H), 2.09 (s, 3H), 2.02 (s, 3H) ppm; ^{13}C NMR (100 MHz, $CDCl_3$) δ 184.9, 183.5, 159.7, 148.2, 142.6, 142.3, 138.6, 138.1, 132.7, 129.6, 128.2, 127.9, 124.2, 123.6, 120.3, 118.2, 117.2, 116.5, 110.0, 102.4, 28.3, 26.4 ppm, Anal. calc'd for $C_{24}H_{20}N_2O_2Pt$: C 51.15, H 3.58, N 4.97; found C 51.67, H 3.51, N 4.73; m.p. > 300 °C.

6.10: To a 20 mL screw-cap vial with stir bar is added 1-naphthyldiphenylphosphine (97 mg, 0.35 mmol), $[PtMe_2(SMe_2)]_2$ dimer (100 mg, 0.17 mmol) and 3 mL degassed THF. The reaction is stirred 4 hours at 55°C under an N_2 atmosphere, then TfOH (1 mL, 0.35 M in THF) is added dropwise. The mixture is stirred for 30 minutes at room temperature, then a solution of Na(acac)•H_2O (98 mg, 0.70 mmol in 2 mL MeOH) is added. The mixture is stirred for 1.5 hours, then partitioned between water and CH_2Cl_2. The organic layer is washed with brine, dried over $MgSO_4$, filtered, and concentrated. The residue is then

purified on a plug of silica gel (hexanes:CH_2Cl_2 as eluent) to give **6.10** as a white solid in 65% yield. ^{1}H NMR (400 MHz, $CDCl_3$) δ 8.24 (d, sat, J_{Pt-H} = 44.6 Hz, J = 7.1 Hz, 1H), 7.91-7.80 (m, 5H), 7.67 (dd, J = 10.5 Hz, 7.1 Hz, 1H), 7.58 (dd, J = 8.1, 1.8 Hz, 1H), 7.51-7.36 (m, 8H), 5.52 (s, 1H), 2.16 (s, 3H), 1.93 (s, 3H) ppm; ^{13}C NMR (100 MHz, $CDCl_3$) δ 186.10, 184.8 (d, J_{P-C} = 3.7 Hz), 151.3 (d, J_{P-C} = 30.4 Hz), 134.12 (d, J_{P-C} = 52.7 Hz), 133.81 (d, d, J_{P-C} = 16.8 Hz), 133.24 (d, d, J_{P-C} = 15.0 Hz), 132.93 (d, J_{P-C} = 11.7 Hz), 130.9 (d, J_{P-C} = 62.9 Hz), 131.1 (d, J_{P-C} = 2.6 Hz), 130.7 (d, J_{P-C} = 32.2 Hz), 128.8 (d, J_{P-C} = 1.8 Hz), 128.5, 128.4, 126.5, 125.0 (d, J_{P-C} = 10.3 Hz), 122.7, 101.6, 28.2, 28.1 (d, J_{P-C} = 6.6 Hz) ppm; ^{31}P NMR (169 MHz, CDCl3) δ 28.27 (s, sat, J_{Pt-P} = 4671 Hz) ppm; Anal. calc'd for $C_{27}C_{23}O_2PPt$: C 53.55, H 3.83, found C 53.59, H 3.70; m.p. 222-223 °C.

6.11: To a 20 mL screw-cap vial with stir bar is added 1-methyl-3-phenylimidazol-2-ylidine)silver chloride (100 mg, 0.35 mmol), $[PtMe_2(SMe_2)]_2$ dimer (100 mg, 0.17 mmol) and 3 mL degassed THF. The reaction is stirred for 1 hour, then filtered to remove AgI. The mixture is then heated to 55°C for two hours, then cooled to room temperature. TsOH (1 mL, 0.35 M in THF) is then added dropwise, and the mixture is stirred for 30 minutes at room temperature. After cooling the reaction to -40°C, a solution of Na(acac)•H_2O (49 mg, 0.35 mmol in 1 mL MeOH) is added dropwise. The mixture is stirred for 2 hours, then allowed to warm to room temperature. After partitioning between water and CH_2Cl_2, the organic layer is washed with brine, and the combined extracts are dried over $MgSO_4$. The solution is filtered and concentrated and the residue purified on a plug of silica gel (CH_2Cl_2 as eluent) to give **6.11** as a yellow solid in 61% yield. ^{1}H NMR (400 MHz, $CDCl_3$) δ 7.78 (dd, sat, J_{Pt-H} = 52.1 Hz, J = 5.3, 2.0 Hz, 1H), 7.24 (d, J = 2.0 Hz, 1H), 7.01 (m, 2H), 6.93 (dd, J = 6.8, 2.0 Hz, 1H), 6.80 (d, J = 2.0 Hz, 1H), 5.49 (s, 1H), 4.07 (s, 3H), 2.05 (s, 3H), 1.96 (s, 3H) ppm; Anal. calc'd for $C_{15}H_{16}N_2O_2Pt$: C 39.91, H 3.57, N 6.21, found C 40.34, H 3.60, N 6.08.

6.3 Results and Discussion

6.3.1 Methodology

We elected to use $[PtMe_2(SMe_2)]_2$ as starting material, which has been widely used as a precursor in C-H activation chemistry[21] and can be easily prepared on a multi-gram scale from K_2PtCl_4 in 85-90% overall yield. When treated with stoichiometric quantities of 2-phenylpyridine (ppy) in THF at ambient temperature, this starting material affords the cyclometalated $Pt(ppy)Me(SMe_2)$ complex with irreversible loss of CH_4. Treatment of this solution with one equivalent of trifluoromethane sulfonic acid (TfOH) leads to rapid loss of a second equivalent of CH_4, giving the corresponding $Pt(ppy)(OTf)(SMe_2)$ complex incorporating two labile ancillary ligands. Addition of a solution of sodium β-diketonate in methanol then gives clean conversion to the desired Pt(ppy)(acac) product, which is isolated as analytically pure material in 87% yield following column chromatography (Figure 6.2). This reaction sequence can be conveniently carried out at ambient temperature under an atmosphere of air in less than 3 hours.

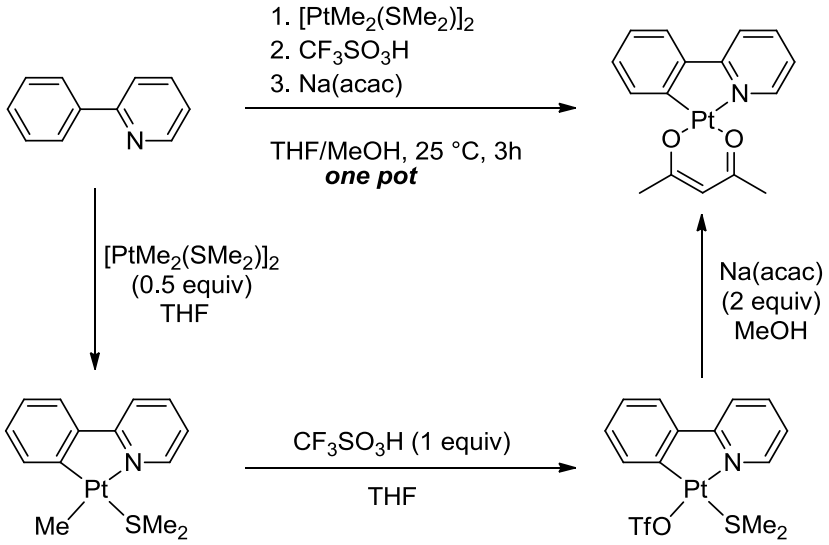

Figure 6.2: An improved one-pot synthesis of cyclometalated Pt(II) β-diketonates

6.3.2 Scope

This method shows broad substrate scope across *N^C*-chelate ligands incorporating a variety of structures and functional groups (Table 6.1). Clean conversion to the cyclometalated diketonate complex is observed for both electron-rich (R = -OMe, -NR_2) and electron deficient (R = F, Cl) arenes, with little change in overall yields observed in either case. The method is equally successful in the synthesis of heterocyclic *N^C*-chelate complexes, and can be used to synthesize benzofuran, benzothiazole, and *N*-phenylindole derivatives in 92, 89, and 83% yield, respectively (Table 6.1, entry **6.9**). Incorporation of extended π-systems is equally facile, as platinum *β*-diketonate complexes of 2-phenylquinoline and benzo[*h*]quinoline (entries **6.6**, **6.7**) are readily prepared in yields of 87 and 76%. Motivated by our own interest in boron chemistry, we also present an improved synthesis of several triarylboron-functionalized platinum phosphors (entries **8a**, **8c**), among the most efficient Pt-based emitter materials incorporated into OLEDs to date.[2b-c,22] The yields of these boryl-functionalized Pt(II) compounds are about 4 to 5 times greater than those (~20%) obtained using the PtCl(DMSO)(acac) precursor method described in Chapter 4.[2b,2c] Compounds **6.2b-c**, **6.4**, **6.5**, **6.9a**, **6.9c**, and **6.10** have not been previously reported, and are fully characterized by ^{1}H NMR, ^{13}C NMR, and elemental analysis, and the identity of all known compounds was confirmed by ^{1}H NMR and elemental analysis.

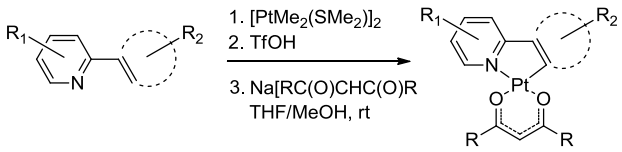

Table 6.1: Preparation of N^C chelate Pt(II) *β*-diketonates

Entry	Ligand	Complex	Yield [%][a]
6.1	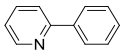	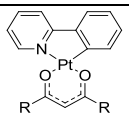	**6.1a**, R = Me: 87 **6.1b**, R = *t*-Bu: 87 **6.1c**, R = Ph: 83
6.2	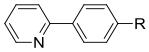	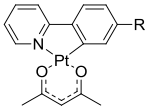	**6.2a**, R = Me: 81 **6.2b**, R = Cl: 85 **6.2c**, R = Br: 85
6.3	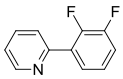	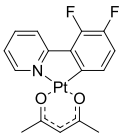	76
6.4	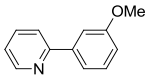	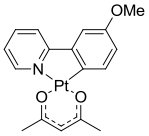	85
6.5	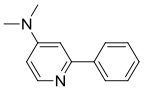	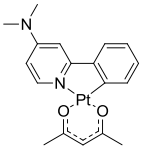	83
6.6	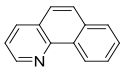	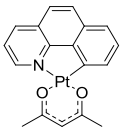	76
6.7	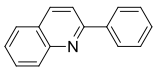	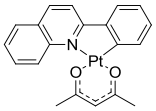	87
6.8[b]	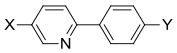	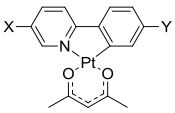	**6.8a**, X = $BMes_2$, Y = H, 94 **6.8b**, X = H, Y = NPh_2, 92 **6.8c**, X = $BMes_2$, Y = NAr_2, 88[c]
6.9	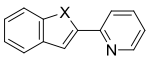	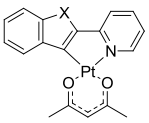	**6.9a**, X = O: 92 **6.9b**, X = S:89 **6.9c**, X = N-Ph: 83

[a] Yields are of analytically pure material. [b] Mes = Mesityl (2,4,6-trimethylphenyl), [c] Ar_2 = Ph(1-Naphthyl)

While functionalization of Pt(II) *β*-diketonates on the *N^C*-chelate backbone is more common, considerable research has also been devoted to the functionalization of Pt complexes on the *β*-diketonate itself.[2d-e,4a,6a] While acetylacetonate (acac) is by far the most widely used of these, dibenzoylmethane (dbm) and dipivaloylmethane (dpm) have also appeared in numerous studies, with notably different physical properties. Using these as representative examples in reaction with 2-phenylpyridine, this method is shown to be applicable using alternative *β*-diketonate ligands with no significant reduction in overall yield (Entry **6.1b**,**c**).

Our initial investigations made use of TfOH, due to the high lability of its conjugate base when acting as a ligand to metal centers. However, its high toxicity and difficulty in handling make it less than ideal for use on an industrial scale. We therefore studied the use of other strong organic acids, namely *p*-toluenesulfonic acid (TsOH) and trifluoroacetic acid (TFA) in the demethylation of Pt(ppy)Me(SMe_2). After reaction with acetylacetonate, these reactions gave product **6.1a** in 91 and 92% yield respectively, indicating that strong acids that are more easily handled may be used in a similar manner.

Encouraged by these results, we sought to determine if this method could be applied to other cyclometalated platinum systems. *P^C*-chelate phosphines have recently found use as highly efficient emitter materials for OLEDs,[2h,23] though platinum-containing examples are comparatively less well studied. In particular, very few reports describe the preparation of platinum *β*-diketonate P^C-chelate complexes,[24] presenting numerous opportunities for materials research. We thus examined the reaction of (1-naphthyl)diphenylphosphine with $[PtMe_2(SMe_2)]_2$, carried out under a nitrogen atmosphere to prevent oxidation of the phosphine. The cyclometalation of this ligand is readily achieved under mild heating at 55 °C for 4h, and following reaction with acid and acetylacetonate at room temperature, the corresponding Pt(*P^C*)(acac) complex was successfully obtained in 65% yield (Figure 6.3).

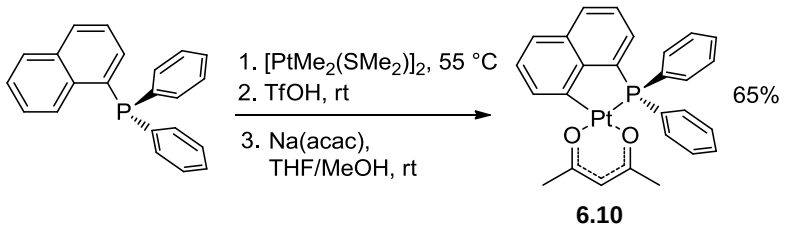

6.10

Figure 6.3: Synthesis of a *P^C* chelate Pt(II) *β*-diketonate complex.

Similarly, recent years have witnessed a surge of interest in platinum complexes of *N*-heterocyclic carbenes, with applications as broad as catalysis,[25] cancer therapy,[26] and organic electronics.[20,27] This presented a unique synthetic challenge, and we sought to determine if our methodology could be applied to the synthesis of *C^C*-chelate carbene complexes of platinum *β*-diketonates. Few examples of such products have appeared in literature, requiring several days at high temperature to prepare.[20,27a] Literature methods require initial formation of a silver(I) carbene species, followed by transmetalation with $Pt(COD)Cl_2$ (COD = 1,4-cyclooctadiene) at 100 °C for 16h, followed by reaction with *β*-diketone and Na(O-*t*-Bu) at 100 °C for a further 16 h.

Using *N*-methyl-*N*'-phenylimidazolium iodide as a representative example, we have found that our synthetic methods can be adapted successfully to give *C^C* chelate carbene complexes of platinum *β*-diketonates (Figure 6.4). These complexes remain most conveniently prepared *via* Ag(I) carbene starting materials, which can be easily isolated after reaction of imidazolium salt with Ag_2O at room temperature.[16,28] This species is then stirred for 1 hr with $[PtMe_2(SMe_2)]_2$, and filtered to remove precipitated AgI. Mild heating is then required for cyclometalation of the pendant phenyl group, with complete reaction observed after 2 hrs at 55 °C followed by reaction with acid at room temperature. Surprisingly, addition of Na(acac) as a neat solid or in methanol led to rapid decomposition, giving a complex mixture of products not isolable by column chromatography. This undesired reactivity in the

final step is readily avoided by cooling the reaction mixture to -40°C, and after 2 hrs the corresponding Pt(*C^C*)(acac) complex may be successfully isolated in 61% yield (Figure 6.4).

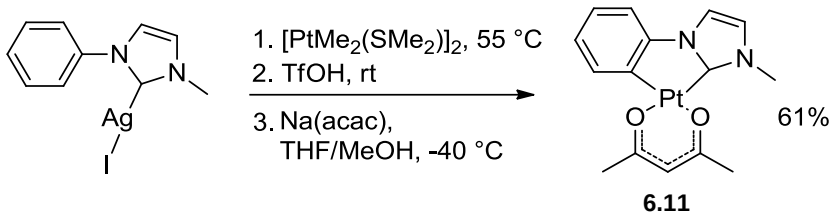

Figure 6.4: Synthesis of a Pt(II) *β*-diketonate complex using a *C^C* chelate carbene ligand.

6.4 Conclusions

In summary, we have described a simple one-pot method for the preparation of cyclometalated platinum *β*-diketonates in significantly higher yield at lower cost. This method requires only stoichiometric amounts of cyclometalating ligand, giving high yields after 3 hours' reaction time at ambient temperature. The method is versatile toward a broad array of functional groups and heterocyclic systems, and can be further adapted to the preparation of *P^C*-chelate phosphine compounds and *C^C*-chelate complexes of *N*-heterocyclic carbenes.

6.5 Notes and References

The work described in this chapter has been published as:

- Z. M. Hudson, B. A. Blight, S. Wang, *Org. Lett.* **2012**, *14*, 1700.

References

(1) a) S. W. Thomas III, S. Yagi, T. M. Swager, *J. Mater. Chem*. **2005**, *15*, 2829. b) S. W. Thomas III, K. Venkatesan, P. Müller, T. M. Swager, *J. Am. Chem. Soc.* **2006**, *128*, 16641. c) K. Li, Y. Chen, W. Lu, N. Zhu, C.-M. Che, *Chem. Eur. J.* **2011**, *17*, 4109. d) K. H. Wong, M. C. W. Chan, C.-M. Che, *Chem. Eur. J*. **1999**, *5*, 2845. e) Y. Rao, S. Wang, *Inorg. Chem.* **2009**, *48*, 7698. f) Z. M. Hudson, S. B. Zhao, R. Y. Wang, S. Wang, *Chem. Eur. J.* **2009**, *15*, 6131; g) M. Albrecht, G. van Koten, *Adv. Mater.* **1999**, *11*, 171; h) Z. M. Hudson, C. Sun, K. J. Harris, B. E. G. Lucier, R. W. Schurko, S. Wang, *Inorg. Chem.* **2011**, *50*, 3447; i) C. Huo, H. D. Zhang, H. Y. Zhang, H. Y. Zhang, B. Yang, P. Zhang, Y. Wang. *Inorg. Chem*. **2006**, *45*, 4735.

(2) For representative examples, see: a) M. Cocchi, D. Virgili, V. Fattori, D. L. Rochester, J. A. G. Williams, *Adv. Funct. Mater.* **2007**, *17*, 285. b) Z. M. Hudson, C. Sun, M. G. Helander, H. Amarne, Z.-H. Lu, S. Wang, *Adv. Funct. Mater.* **2010**, *20*, 3426. c) Z. M. Hudson, M. G. Helander, Z.-H. Lu, S. Wang, *Chem. Commun.* **2011**, *47*, 755. d) X. Yang, J. D. Froehlich, H. S. Chae, B. T. Harding, S. Li, A. Mochizuki, G. E. Jabbour, *Chem. Mater.* **2010**, *22*, 4776. e) M. Velusamy, C. Chen, Y. S. Wen, J. T. Lin, C. Lin, C. Lai, P. Chou, *Organometallics*, **2010**, *29*, 3912. f) Z. He, W. Wong, X. Yu, H. Kwok, Z. Lin, *Inorg. Chem.* **2006**, *45*, 10922. g) G. Zhou, Q. Wang, X. Wang, C. Ho, W. Wong, D. Ma, L. Wang, Z. Lin, *J. Mater. Chem.* **2010**, *20*, 7472. h) Y. Chi, P.-T. Chou, *Chem. Soc. Rev.* **2010**, *39*, 638, and references therein.

(3) a) J. Brooks, Y. Babayan, S. Lamansky, P. I. Djurovich, I. Tsyba, R. Bau, M. E. Thompson, *Inorg. Chem.* **2002**, *41*, 3055. b) M. D. Perez, P. I. Djurovich, A. Hassan, G. Y. Cheng, T. J. Stewart, K. Aznavour, R. Bau, M. E. Thompson, *Chem. Commun*. **2009**, 4215. c) M. Ghedini, T. Pugliese, M. La Deda, N. Godbert, I. Aiello, M. Amati, S. Belviso, F. Lelj, G. Accorsi, F. Barigelletti, *Dalton Trans.*

2008, *37*, 4303. d) D. N. Kozhevnikov, V. N. Kozhevnikov, M. Z. Shafikov, A. M. Prokhorov, D. W. Bruce, J. A. G. Williams, *Inorg. Chem.* **2011**, *50*, 3804. e) D. N. Kozhevnikov, V. N. Kozhevnikov, M. M. Ustinova, A. Santoro, D. W. Bruce, B. Koenig, R. Czerwieniec, T. Fischer, M. Zabel, H. Yersin, *Inorg. Chem.* **2009**, *48*, 4179.

(4) a) B. Ma, P. I. Djurovich, M. Yousufuddin, R. Bau, M. E. Thompson, *J. Phys. Chem. C.* **2008**, *112*, 8022. b) C. H. Shin, J. O. Huh, S. J. Baek, S. K. Kim, M. H. Lee, Y. Do, *Eur. J. Inorg. Chem.* **2010**, 3642; c) V. N. Kozhevnikov, M. C. Durrant, J. A. G. Williams, *Inorg. Chem.* **2011**, *50*, 6304.

(5) a) J. C. Chan, W. H. Lam, H. Wong, N. Zhu, W. Wong, V. W. W. Yam, *J. Am. Chem. Soc.* **2011**, *133*, 12690. b) Y. Rao, S. Wang, *Organometallics*, **2011**, *30*, 4453.

(6) a) J. Buey, L. Díez, P. Espinet, H.-S. Kitzerow, J. A. Miguel, *Chem. Mater.* **1996**, *8*, 2375. b) K. Venkatesan, P. H. J. Kouwer, S. Yagi, P. Müller, T. M. Swager, *J. Mater. Chem.* **2008**, *18*, 400. c) A. Santoro, A. C. Whitwood, J. A. G. Williams, V. N. Kozhevnikov, D. W. Bruce, *Chem. Mater.* **2009**, *21*, 3871. d) Y. Wang, Y. Liu, J. Luo, H. Qi, X. Li, M. Nin, M. Liu, D. Shi, W. Zhu, Y. Cao, *Dalton Trans.* **2011**, *40*, 5046.

(7) L. Norel, M. Rudolph, N. Vanthuyne, J. A. G. Williams, C. Lescop, C. Roussel, J. Autschbach, J. Crassous, R. Réau, *Angew. Chem. Int. Ed.* **2010**, *49*, 99.

(8) X. Mou, Y. Wu, S. Liu, M. Shi, X. Liu, C. Wang, S. Sun, Q. Zhao, X. Zhou, W. Huang, *J. Mater. Chem.* **2011**, *21*, 13951.

(9) a) W. Wu, H. Guo, W. Wu, S. Ji, J. Zhao, *Inorg. Chem.* **2011**, *50*, 11446. b) W. Wu, W. Wu, S. Ji, H. Guo, J. Zhao, *Dalton Trans.* **2011**, *40*, 5953.

(10) a) W. Wu, W. Wu, S. Ji, H. Guo, P. Song, K. Han, L. Chi, J. Shao, J. Zhao, *J. Mater. Chem.* **2010**, *20*, 9775. b) W. Wu, W. Wu, S. Ji, H. Guo, J. Zhao, *J. Organomet. Chem.* **2011**, *696*, 2388.

(11) B. N. Cockburn, V. Howe, T. Keating, B. F. G. Johnson, J. Lewis, *J. Chem. Soc., Dalton Trans.* **1973**, 404.

(12) M. Crespo, C. M. Anderson, J. M. Tanski, *Can. J. Chem.* **2009**, *87*, 80.

(13) D. Di Censo, S. Fantacci, F. De Angelis, C. Klein, N. Evans, K. Kalyanasundaram, H. J. Bolink, M. Gratzel, M. K. Nazeeruddin, *Inorg. Chem.* **2008**, *47*, 980-989.

(14) T. M. McCormick, Q. Liu, S. Wang, *Org. Lett.* **2007**, *9*, 4087-4090.

(15) C. Lin, Y. Chi, M. Chung, Y. Chen, K. Wang, G. Lee, P. Chou, W. Hung, H. Chiu, *Dalton Trans.* **2011**, *40*, 1132-1143.

(16) C. P. Newman, G. J. Clarkson, J. P. Rourke, *J. Organomet. Chem.* **2007**, *692*, 4962-4968.

(17) G. S. Hill, M. J. Irwin, C. J. Levy, L. M. Rendina, and R. J. Puddephatt, *Inorg. Synth.* **1998**, *32*, pp. 149-151.

(18) O. Lohse, P. Thevenin, E. Waldvogel, *Synlett* **1999**, *1*, 45-48.

(19) J. Liu, C. Yang, Q. Cao, M. Xu, J. Wang, H. Peng, W. Tan, X. Lü, X. Gao, *Inorg. Chim. Acta* **2009**, *362*, 575-579.

(20) Y. Unger, D. Meyer, O. Molt, C. Schildknecht, I. Münster, G. Wagenblast, T. Strassner, *Angew. Chem. Int. Ed.* **2010**, *49*, 10214-10216.

(21) a) J. D. Scott, R. J. Puddephatt, *Organometallics* **1983**, *2*, 1643. b) R. J. Puddephatt, M. A. Thomson, L. Manojlovic-Muir, K. W. Muir, A. A. Frew, M. P. Brown, *J. Chem. Soc. Chem. Commun.* **1981**, *15*, 805-806. c) F. B. Zhang, C. W. Kirby, D. W. Hairsine, M. C. Jennings, R. J. Puddephatt, *J. Am. Chem. Soc*. **2005**, *127*, 14196. d) D. T. Song, S. Wang, *Organometallics*, **2003**, *22*, 2187. e) S. B. Zhao, D. T. Song, W. L. Jia, S. Wang, *Organometallics*, **2005,** *24***,** 3290. f) D. D. Wick, K. I. Goldberg, *J. Am. Chem. Soc*. **1997**, *119*, 10235.

(22) Z. B. Wang, M. G. Helander, Z. M. Hudson, J. Qiu, S. Wang, Z.-H. Lu, *Appl. Phys. Lett*. **2011**, *98*, 213301.

(23) a) J.-Y. Hung, Y. Chi, I.-H. Pai, Y.-C. Yu, G. H. Lee, P. T. Chou, K. T. Wong, C. C. Chen, C. C. Wu, *Dalton Trans.* **2009**, *38*, 6472; b) Y. C. Chiu, J. Y. Hung, Y. Chi, C. C. Chen, C. H. Chang, C. C. Wu, Y. M. Cheng, Y. C. Yu, G. H. Lee, P.-T. Chou, *Adv. Mater*. **2009**, *21*, 2221.

(24) a) A. J. Cheney, B. L. Shaw, *J. Chem. Soc., Dalton Trans.* **1972**, 754. b) D. F. Gill, B. E. Mann, B. L. Shaw. *J. Chem. Soc., Dalton Trans.* **1973**, 270. c) J. M. Duff, B. E. Mann, B. L. Shaw, B. Turtle, *J. Chem. Soc. Dalton Trans.* **1974**, 139. d) H. D. Empsall, P. N. Heys, B. L. Shaw, *J. Chem. Soc. Dalton Trans.* **1978**, 257.

(25) a) H. Jullien, D. Brissy, R. Sylvain, P. Retailleau, J. V. Naubron, S. Gladiali, A. Marinetti, *Adv. Synth. Catal.* **2011**, *353*, 1109. b) D. Brissy, M. Skander, P. Retailleau, G. Frison, A. Marinetti, *Organometallics*, **2009**, *28*, 140. c) C. Lu, S. Gu, W. Chen, H. Qiu, *Dalton Trans.* **2010**, *39*, 4198.

(26) a) R. W.-Y. Sun, A. L-F. Chow, X.-H. Li, J. J. Yan, S. S.-Y. Chui, C.-M. Che. Chem. Sci. **2011**, 2, 728. b) M. Skander, P. Retailleau, B. Bourrié, L. Schio, P. Mailliet, A. Marinetti, *J. Med. Chem.* **2010**, *53*, 2146.

(27) a) S. Haneder, E. Da Como, J. Feldmann, J. M. Lupton, C. Lennartz, P. Erk, E. Fuchs, O. Molt, I. Münster, C. Schildknecht, G. Wagenblast. *Adv. Mater.* **2008**, *20*, 3325. b) Y. Wu, S. Wu, H. Li, Y. Geng, Z. Su, *Dalton Trans.* **2011**, *40*, 4480.

(28) Ag(I) carbenes have been reported both as linear L-Ag-X and ionic $[L_2Ag][AgX_2]$ formulations; for clarity, the former is depicted in this report.

Chapter 7

Efficient Blue Phosphorescence from Triarylboron-Functionalized Platinum(II) Complexes of *N*-Heterocyclic Carbenes

7.1 Introduction

Since the X-ray crystal structure of a stable *N*-heterocyclic carbene (NHC) was first determined by Arduengo in 1991,[1] these compounds have gone from highly specialized ligands to among the most widely used in organometallic chemistry.[2,3] Characterized by exceptionally strong σ-bonding and readily tunable steric and electronic properties, NHCs have found extensive use in both organic and transition-metal catalysis.[2] More recently, the rapid expansion of NHC research has led to their incorporation into a wide variety of functional materials, including antimicrobial agents,[4] liquid crystals,[5] supramolecular structures[6] and luminescent compounds.[7]

Phosphorescent transition-metal complexes are currently of great interest as biological imaging agents, chemical sensors, and emitters for organic light-emitting diodes (OLEDs),[8] though reports of phosphorescent NHC complexes are rare. High-energy blue phosphors in particular have presented a considerable challenge, as these compounds often suffer from poor stability and low emission quantum yields. NHCs are thus attractive for the preparation of blue phosphors, as the stability of metal-carbene complexes should increase the operational lifetime of these materials in organic electronic devices. Furthermore, the strong ligand field exhibited by the carbene can raise the energy of nonradiative *d-d* excited states on the metal centre, increasing their energy spacing with the phosphorescent excited state and improving quantum yields.[7b] Based on this principle, a handful of reports have described the use of NHC complexes of Pt(II) and Ir(III) as phosphorescent emitters for OLEDs.[9]

We and others have recently shown that the phosphorescence of many metal complexes may be dramatically enhanced by functionalization with a triarylboron group. This moiety is a powerful π-electron acceptor due to the empty *p* orbital on boron, facilitating both charge-transfer luminescence and electron transport. When protected from nucleophilic attack by appropriate bulky substituents, highly stable materials may be prepared with impressive quantum yields and charge-transporting properties. As a result, phosphorescent triarylboranes have found use as anion sensors,[10] vapochromic materials,[11] and as phosphorescent emitters in OLEDs,[12] including the most efficient Pt(II)-based OLED reported to date.

By combining the emissive and electron-transport properties of triarylboron with the strong ligand field of *N*-heterocyclic carbenes, we herein report the preparation of blue and blue-green phosphorescent Pt(II) compounds with quantum yields among the highest reported for carbene complexes to date. These complexes are stable to air, moisture and UV irradiation, and have been used to prepare high-efficienct electrophosphorescent devices.

7.2 Experimental

7.2.1 General Procedures

Experimental techniques and instruments used follow those described in section 2.2. Details regarding electroluminescent device fabrication and testing are described in section 4.2. *N*,*N*-dibenzyl-4-bromoaniline and *N*,*N*-dibenzyl-3-bromoaniline were prepared by literature methods.[13]

7.2.2 Synthesis of Boron-Functionalized Imidazolium Salts

***N*,*N*-dibenzyl-4-(dimesitylboryl)aniline (7.1a):** To a 250 mL Schlenk flask was added *N*,*N*-dibenzyl-4-bromoaniline (1.8 g, 5.1 mmol) and 80 mL dry THF. The mixture was cooled to -78°C, then *n*-BuLi (3.5

mL, 5.6 mmol, 1.6 M in hexanes) was added dropwise with stirring. The reaction was stirred for 1 h at -78°C, then $FBMes_2$ (1.6 g, 6.1 mmol) was added. The reaction was stirred at -78°C for 1 h, then allowed to warm slowly to room temperature and stirred for 16 h. After removal of the solvent *in vacuo*, the mixture was washed with sat. aq. NH_4Cl, then extracted with CH_2Cl_2 and water. The combined organic layers were dried using $MgSO_4$, filtered, and purified using flash chromatography on silica gel (4:1 hexanes:CH_2Cl_2 as eluent) to afford 2.4 g **7.1a** as a white solid (90% yield). ^{1}H NMR (400 MHz, $CDCl_3$) δ 7.43 (d, J = 8.2 Hz, 2H, -C_6H_4-), 7.35 (t, J = 7.1 Hz, 4H, -Ph), 7.32-7.22 (m, 6H, -Ph), 6.83 (s, 4H, Mes), 6.73 (d, J = 8.2 Hz, 2H, -C_6H_4-), 4.72 (s, 4H, -CH_2-), 2.32 (s, 6H, Mes), 2.12 (s, 12H, Mes) ppm; ^{13}C {^{1}H} NMR (100 MHz, $CDCl_3$) δ 152.5, 142.1, 140.6, 140.0, 137.8, 137.5, 133.0, 128.7, 127.9, 127.1, 126.7, 111.2, 53.8, 23.5, 21.1 ppm; HRMS calc'd for $C_{38}H_{40}BN$: 521.3254, found 321.3246.

4-dimesitylborylaniline (7.1b): To a 500 mL round-bottomed flask with stir bar was added **7.1a** (2.37 g, 4.5 mmol), palladium on carbon (0.50 g, 5 wt% Pd), p-toluenesulfonic acid (0.50 g, 2.9 mmol) and ethanol (200 mL). The reaction was bubbled with hydrogen gas for 16 h at room temperature, then passed through a pad of celite and concentrated *in vacuo*. The residue was washed with 1M aq. NaOH, then extracted with CH_2Cl_2 and water. The combined organic layers were dried using $MgSO_4$, filtered, and purified using flash chromatography on silica gel (1:1 hexanes:CH_2Cl_2 as eluent) to afford 1.31 g **7.1b** as a white solid (85% yield). ^{1}H NMR (300 MHz, $CDCl_3$) δ 7.39 (d, J = 8.4 Hz, 2H, -C_6H_4-), 6.82 (s, 4H, Mes), 6.61 (d, J = 8.4 Hz, 2H, -C_6H_4-), 4.03 (s, br, 2H, -NH_2), 2.32 (s, 6H, Mes), 2.07 (s, 12H, Mes) ppm; ^{13}C {^{1}H} NMR (75 MHz, $CDCl_3$) δ 150.5, 141.9, 140.7, 139.9, 137.7, 135.1, 128.0, 113.8, 23.4, 21.1 ppm; HRMS calc'd for $C_{24}H_{28}BN$: 341.2315, found 341.2309.

***N*-(4-dimesitylborylphenyl)imidazole (7.1c):** To a 100 mL round-bottomed flask with stir bar was added **7.1b** (1.12 g, 3.3 mmol), glyoxal (0.375 mL, 40 wt.%, 3.28 mmol) and 10 mL 1:1 THF:MeOH. The reaction was stirred for 16 h at room temperature, then NH_4Cl (0.35 g, 6.6 mmol), formaldehyde (0.45

mL, 37 wt.%, 6.6 mmol) and 25 mL MeOH were added. The reaction was heated to reflux for 1 h, then 0.5 mL 85% H_3PO_4 was added. The mixture was heated to reflux for an additional 8h, then poured over ice (25 g), washed with 2M aq. NaOH, and extracted with CH_2Cl_2 and water. The combined organic layers were dried using $MgSO_4$, filtered, and purified using flash chromatography on silica gel (4:1 ethyl acetate:hexanes as eluent) to afford 488 mg **7.1c** as a white solid (38% yield). ^{1}H NMR (400 MHz, $CDCl_3$) δ 7.94 (s, br, 1H, -Im), 7.63 (d, J = 8.2 Hz, 2H, -C_6H_4-), 7.37 (d, J = 8.2 Hz, 2H, -C_6H_4-), 7.35 (s, br, 1H, -Im), 7.21 (s, br, 1H, -Im), 6.84 (s, 4H, Mes), 2.31 (s, 6H, Mes), 2.02 (s, 12H, Mes) ppm; ^{13}C {^{1}H} NMR (100 MHz, $CDCl_3$) δ 144.8, 141.3, 140.7, 139.8, 139.0, 138.1, 135.4, 130.7, 128.3, 120.1, 117.7, 23.4, 21.2 ppm; HRMS calc'd for $C_{27}H_{29}BN_2$: 392.2424, found 392.2429.

***N*-(4-dimesitylborylphenyl)-*N*'-methylimidazolium iodide (7.1):** To a 25 mL round-bottomed flask with stir bar was added **7.1c** (400 mg, 1.01 mmol), methyl iodide (0.32 mL, 5.1 mmol) and 10 mL THF. After stirring at room temperature for 40 h under air, the white precipitate was filtered, washed with THF and dried to afford 433 mg **7.1** (80% yield). ^{1}H NMR (300 MHz, MeOH-d_4) δ 9.59 (s, 1H, Im), 8.15 (d, J = 2.1 Hz, 1H, Im), 7.81 (d, J = 2.1 Hz, 1H, Im), 7.76 (d, J = 8.6 Hz, 2H, -C_6H_4-), 7.69 (d, J = 8.6 Hz, 2H, -C_6H_4-), 6.86 (s, 4H, Mes), 4.06 (s, 3H, -CH_3), 2.30 (s, 6H, Mes), 1.99 (s, 12H, Mes) ppm; Anal. Calc'd for $C_{28}H_{33}BIN_2$: C 62.83, H 6.21, N 5.23, found C 62.82, H 5.99, N 5.12.

***N,N*-dibenzyl-3-(dimesitylboryl)aniline (7.2a):** Prepared in analogy with **7.1a** (83% yield). ^{1}H NMR (400 MHz, $CDCl_3$) δ 7.37 (t, J = 7.4 Hz, 1H, -C_6H_4-), 7.34-7.25 (m, 7H, -Ph, -C_6H_4-), 7.21-7.15 (m, 5H, -Ph, -C_6H_4-), 6.92 (s, 1H, -C_6H_4-), 6.77 (s, 4H, Mes), 4.59 (s, 4H, -CH_2-), 2.33 (s, 6H, Mes), 1.99 (s, 12H, Mes) ^{13}C {^{1}H} NMR (100 MHz, $CDCl_3$) δ 148.4, 146.4, 141.9, 140.6, 138.8, 138.0, 128.6, 128.5, 128.0, 126.9, 125.2, 121.0, 116.8, 112.5, 55.0, 23.2, 21.2 ppm; HRMS calc'd for $C_{38}H_{40}BN$: 521.3254, found 521.3260.

3-dimesitylborylaniline (7.2b): Prepared in analogy with **7.1b** (81% yield). ^{1}H NMR (400 MHz, $CDCl_3$) δ 7.15 (t, J = 7.5 Hz, 1H, -C_6H_4-), 6.94 (d, J = 7.2 Hz, 1H, -C_6H_4-), 6.86-6.78 (m, 6H, -C_6H_4-, Mes), 3.52 (s, br, 2H, -NH_2), 2.32 (s, 6H, Mes), 2.04 (s, 12H, Mes) ppm; ^{13}C {^{1}H} NMR (100 MHz, $CDCl_3$) δ 147.2, 145.9, 141.9, 140.8, 138.5, 128.8, 128.1, 126.8, 122.1, 118.7, 23.3, 21.2 ppm; HRMS calc'd for $C_{24}H_{28}BN$: 341.2315, found 341.2319.

***N*-(3-dimesitylborylphenyl)imidazole (7.2c):** Prepared in analogy with **7.1c** (73% yield). ^{1}H NMR (400 MHz, $CDCl_3$) δ 7.76 (s, br, 1H, -Im), 7.52-7.42 (m, 4H, -C_6H_4-), 7.21 (s, br, 1H, -Im), 7.15 (s, br, 1H, -Im), 6.83 (s, 4H, Mes), 2.31 (s, 6H, Mes), 2.00 (s, 12H, Mes) ppm; ^{13}C {^{1}H} NMR (75 MHz, $CDCl_3$) δ 148.2, 141.1, 140.8, 139.3, 137.2, 135.6, 135.1, 130.1, 129.5, 128.4, 128.2, 124.6, 118.4, 23.4, 21.2 ppm; HRMS calc'd for $C_{27}H_{29}BN_2$: 392.2424, found 392.2411.

***N*-(3-dimesitylborylphenyl)-*N*'-methylimidazolium iodide (7.2):** Prepared in analogy with **7.1** (70% yield). ^{1}H NMR (400 MHz, MeOH-d_4) δ 9.43 (s, 1H, Im), 7.98 (d, J = 2.1 Hz, 1H, Im), 7.87 (dt, J = 7.6 Hz, J = 1.7 Hz, 1H, -C_6H_4-), 7.74 (d, J = 2.1 Hz, 1H, Im), 7.68 (t, J = 7.7 Hz, 1H, -C_6H_4-), 7.66 (d, J = 1.7 Hz, 1H, -C_6H_4-), 7.65 (d, J = 7.9 Hz, 1H, -C_6H_4-), 6.86 (s, 4H, Mes), 4.00 (s, 3H, -CH_3), 2.29 (s, 6H, Mes), 1.99 (s, 12H, Mes) ppm; ^{13}C {^{1}H} NMR (100 MHz, MeOH-d_4) δ 150.5, 142.4, 142.2, 141.2, 138.5, 137.2, 136.7, 131.7, 129.7, 129.6, 126.9, 125.9, 123.0, 37.1, 23.9, 21.5 ppm; Anal. Calc'd for $C_{28}H_{33}BIN_2$: C 62.83, H 6.21, N 5.23, found C 62.92, H 6.53, N 4.58.

7.2.3 Synthesis of Boron-Functionalized Pt(II)-Carbene Complexes

Pt(*C*^*C*-7.1)(*O*^*O*-acetylacetonate) (BC1): To a 50 mL Schlenk flask with stir bar is added finely powdered **7.1** (300 mg, 0.56 mmol) and 15 mL dry, degassed THF. The resulting suspension is cooled to -78°C, then *n*-BuLi (0.37 mL, 0.59 mmol, 1.6 M in hexanes) is added dropwise with the appearance of a bright orange colour. After stirring for 1 h at -78°C, $[PtMe_2(SMe_2)]_2$ (161 mg, 0.28 mmol) is added. The mixture is stirred for 30 min at this temperature, then for 30 min at room temperature and finally at 55°C

for 30 min. After cooling to room temperature, a solution of *p*-toluenesulfonic acid (107 mg, 0.56 mmol) in 5 mL THF is added, and the reaction is stirred for 30 min. The mixture is then cooled to -78°C once more, and a solution of Na(acac)•H_2O (78 mg, 0.56 mmol) in 5 mL MeOH is added dropwise. After stirring for 1 h at -78°C and 1 h at room temperature, the solvent is removed *in vacuo* and the residue extracted with CH_2Cl_2/H_2O, then washed with brine. The organic layer is dried using $MgSO_4$, concentrated and purified on silica (1:1 hexanes:CH_2Cl_2 as eluent) to afford 99 mg **BC1** as a yellow solid (25% yield).^{1}H NMR (400 MHz, CD_2Cl_2) δ 7.82 (s, sat, J_{Pt-H} = 52.0 Hz, 1H), 7.31 (d, J = 2.0 Hz, 1H), 7.20 (d, J = 7.6 Hz, 1H), 6.94 (d, J = 7.8 Hz, 1H), 6.86 (d, J = 2.3 Hz, 1H), 6.83 (s, 4H), 5.45 (s, 1H), 4.04 (s, 3H), 2.29 (s, 6H), 2.07 (s, 12H), 1.95 (s, 3H), 1.73 (s, 3H) ppm; ^{13}C NMR (100 MHz, CD_2Cl_2) δ 185.7, 185.6, 152.1, 151.0, 142.8, 141.22, 141.20, 138.5, 134.4, 128.5, 124.6, 121.9, 115.1, 110.1, 102.1, 35.3, 28.3, 27.6, 23.9, 21.4 ppm; Anal. calc'd for $C_{33}H_{38}BN_2O_2Pt$: C 56.58, H 5.47, N 4.00, found C 55.58, H 5.00, N 3.73.

BC2: Prepared in analogy with **BC1** (17% yield). ^{1}H NMR (400 MHz, CD_2Cl_2) δ 7.75 (d, sat, J_{Pt-H} = 50.8 Hz, J = 7.6 Hz, 1H), 7.21 (d, J = 2.0 Hz, 1H), 7.05 (d, J = 7.6 Hz, 1H), 7.04 (s, 1H), 6.83 (d, J = 2.0 Hz, 1H), 6.82 (s, 4H), 5.53 (s, 1H), 4.05 (s, 3H), 2.30 (s, 6H), 2.03 (s, 12H), 1.98 (s, 3H), 1.52 (s, 3H), ppm; ^{13}C NMR (100 MHz, CD_2Cl_2) δ 185.82, 185.77, 150.0, 147.9, 142.6, 141.8, 141.3, 138.7, 135.1, 134.2, 131.8, 128.6, 121.6, 117.3, 115.0, 102.3, 35.3, 28.2, 23.76, 23.74, 21.5 ppm; Anal. calc'd for $C_{33}H_{38}BN_2O_2Pt$: C 56.58, H 5.47, N 4.00, found C 55.47, H 4.77, N 3.83.

7.2.4 X-Ray Diffraction Analysis

Single crystals of **BC1** and **BC2** were grown by slow evaporation from solutions of CH_2Cl_2 and methanol. Crystal data for these compounds are listed in Table 7.1, and important bond lengths and angles are given in Table 8.2.

Table 7.1: Crystallographic data for BC1 and BC2

Compound	**BC1**	**BC2**
Formula	$C_{33}H_{37}BN_2O_2Pt$	$C_{33}H_{37}BN_2O_2Pt$
FW	699.55	699.55
Space Group	P-1	P2(1)/c
a, Å	8.136(2)	17.450(3)
b, Å	11.030(3)	12.563(2)
c, Å	17.118(4)	13.497(2)
α, °	103.888(3)	90
β, °	90.285(3)	97.853(3)
γ, °	101.735(3)	90
V, $Å^3$	1457.8(6)	2931.1(8)
Z	2	4
D_{calc}, g cm^{-1}	1.594	1.585
T, K	180(2)	180(2)
μ, mm^{-1}	4.845	4.819
$2\theta_{max}$, °	52.00	52.00
Reflns measured	14895	11852
Reflns used (R_{int})	5693	5760
Parameters	361	361
Final R Values [I > 2σ(I)]:		
R_1 [a]	0.0272	0.0593
wR_2 [b]	0.0628	0.0720
R values (all data):		
R_1 [a]	0.0322	0.1750
wR_2 [b]	0.0653	0.1000
Goodness-of-fit on F^2	1.022	0.938

[a] $R_1 = \Sigma[(|F_0| - |F_c|) / \Sigma |F_0|$

[b] $wR2 = [\Sigma w[(F_0^2-F_c^2)^2] / \Sigma[w(F_0^2)^2]]^{1/2}$

$w = 1 / [\sigma^2(F_0^2) + (0.075P)^2]$, where $P = [Max (F_0^2, 0) + 2F_c^2] / 3$

Table 7.2: Selected bond lengths (Å) and angles (°) for BC1 and BC2.

		BC1	
Pt(1)-C(1)	1.947(4)	B(1)-C(16)	1.586(6)
Pt(1)-C(10)	1.989(4)	B(1)-C(25)	1.592(6)
Pt(1)-O(2)	2.040(3)	O(1)-C(14)	1.274(5)
Pt(1)-O(1)	2.095(3)	O(2)-C(12)	1.274(5)
B(1)-C(8)	1.567(6)		
C(1)-Pt(1)-C(10)	80.46(16)	C(8)-B(1)-C(16)	117.7(3)
C(1)-Pt(1)-O(2)	170.68(13)	C(8)-B(1)-C(25)	118.3(4)
C(10)-Pt(1)-O(2)	90.45(14)	C(16)-B(1)-C(25)	124.0(3)
C(1)-Pt(1)-O(1)	98.74(13)	C(14)-O(1)-Pt(1)	124.2(3)
C(10)-Pt(1)-O(1)	176.53(12)	C(12)-O(2)-Pt(1)	125.8(3)
O(2)-Pt(1)-O(1)	90.21(11)		
		BC2	
Pt(1)-C(1)	1.912(8)	B(1)-C(16)	1.58(2)
Pt(1)-C(5)	1.983(13)	B(1)-C(25)	1.63(2)
Pt(1)-O(2)	2.030(8)	O(1)-C(14)	1.239(14)
Pt(1)-O(1)	2.068(7)	O(2)-C(12)	1.247(13)
B(1)-C(8)	1.568(19)		
C(1)-Pt(1)-C(5)	81.2(5)	C(8)-B(1)-C(16)	118.5(17)
C(1)-Pt(1)-O(2)	172.5(4)	C(8)-B(1)-C(25)	118.2(15)
C(5)-Pt(1)-O(2)	91.3(4)	C(16)-B(1)-C(25)	123.2(14)
C(1)-Pt(1)-O(1)	97.5(4)	C(14)-O(1)-Pt(1)	125.6(10)
C(5)-Pt(1)-O(1)	175.6(4)	C(12)-O(2)-Pt(1)	125.7(9)
O(2)-Pt(1)-O(1)	90.0(3)		

7.3 Results and Discussion

7.3.1 Synthesis and X-Ray Crystallography

The synthesis of the boron-functionalized imidazolium salts 7.1 and 7.2 are readily achieved by Debus/Radziszewski cyclization of the phenylimidazole π-skeleton from the respective triarylboron-functionalized anilines, which were prepared by a modified method of Glogowski and coworkers.[14] (

Figure 7.1) Benzyl protection of the appropriate bromoanilines followed by metal-halogen exchange with *n*-butyllithium and substitution with $FBMes_2$ affords the desired amines in good overall yield after deprotection of the benzyl groups. Cyclization with glyoxal, ammonia, and formaldehyde provides the boron-functionalized phenylimidazoles, and upon stirring with methyl iodide at room temperature the asymmetric imidazolium salts **7.1** and **7.2** may be easily isolated as white precipitates.

The synthesis of **BC1** and **BC2** is challenging, as literature methods proved incompatible with ligands **7.1** and **7.2**. To date only two reports of similar [Pt(*C^C*)(*O^O*)] complexes have been reported in literature, prepared by first reacting the imidazolium salt of the NHC ligands with Ag_2O.[9c,f] In these cases, subsequent transmetallation at 80°C with [$PtCl_2$(COD)] followed by substitution with acetylacetone in the presence of potassium *tert*-butoxide at 100°C afforded the desired complexes. Unfortunately, ligands **7.1** and **7.2** were found to be unstable to Ag(I) as well as extended stirring at high temperature under basic conditions. However, we recently reported a simple one-pot procedure for the synthesis of platinum *β*-diketonates at ambient temperature,[15] which was readily adapted to the synthesis of **BC1** and **BC2**. Deprotonation of the imidazolium salts with *n*-butyllithium gives the corresponding free carbenes, which

are then coordinated to Pt(II) on addition of $[PtMe_2(SMe_2)]_2$ dimer. Mild heating at 55°C affords the corresponding Pt(*C*^*C*)Me(SMe_2) complexes with irreversible loss of CH_4. Addition of *p*-toluenesulfonic acid induces loss of a second equivalent of CH_4, and addition of Na(acac) at low temperature gives the desired complexes which can then be isolated by column chromatography as yellow solids.

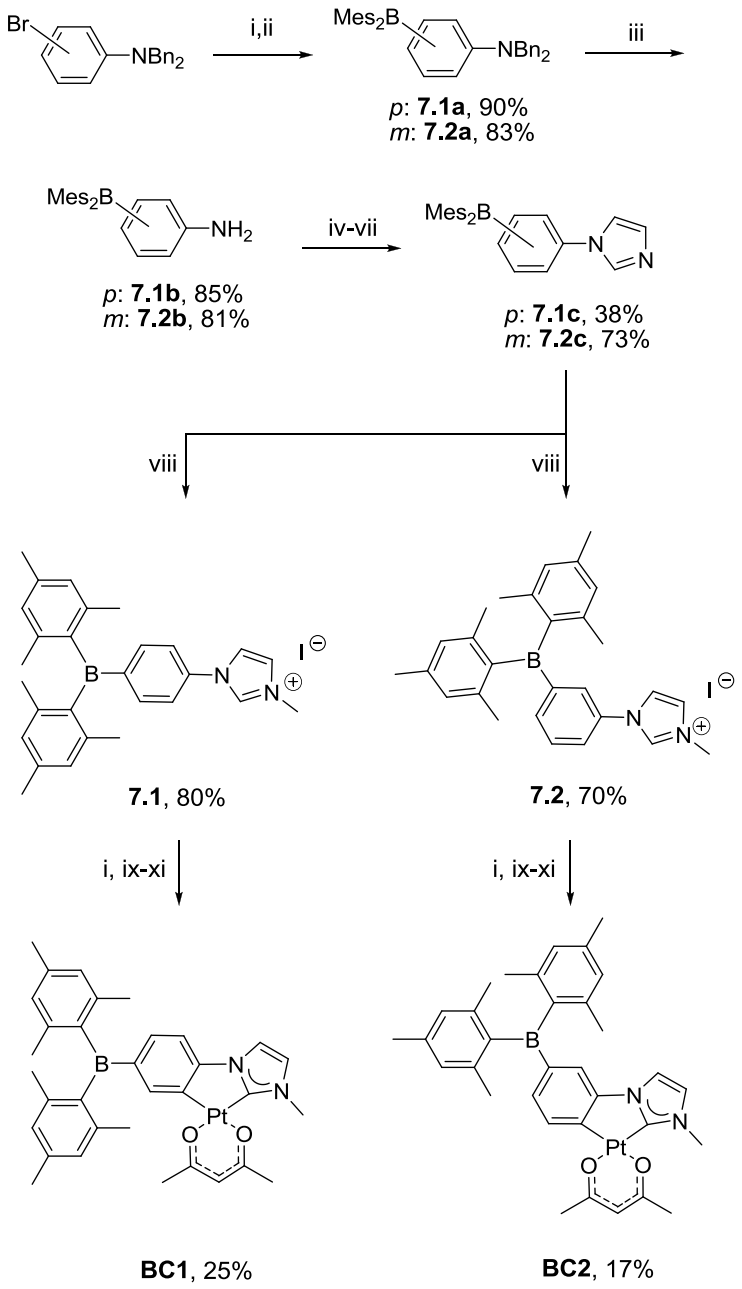

Figure 7.1: Synthesis of boron-functionalized *C^C*-chelate carbene complexes. Reagents and conditions: i) *n*-BuLi, THF, -78°C; ii) $FBMes_2$, THF, -78°C to RT; iii) Pd/C, TsOH, EtOH, 25°C; iv) glyoxal THF/MeOH, 25°C; v) H_2CO, NH_4Cl, 25°C; vi) H_3PO_4, reflux; vii) $NaOH_{(aq)}$, 0°C; viii) MeI, THF, 25°C; ix) $[PtMe_2(SMe_2)]_2$, -78°C to 55°C; x) TsOH, 25°C; xi) Na(acac), THF/MeOH, -78°C.

The molecular design of these complexes is intended to achieve high-energy blue phosphorescence with maximum quantum yield (Φ_P). The *C^C* chelate backbone presents a strong ligand field to the Pt(II) centre, raising the energy of nonradiative *d-d* transition states and reducing thermal quenching. The acetylacetonate (acac) ancillary ligand provides good solubility as well as solution and solid-state stability, while its rigid structure and high triplet energy level help to increase Φ_P. Complexes of Pt(II) and Ir(III) are among the most widely studied phosphorescent metal complexes, and the Pt(II) centre provides efficient phosphorescence *via* spin-orbit coupling in this case. Finally, the incorporation of triarylboron serves to greatly enhance metal-to-ligand charge-transfer phosphorescence.

Single crystals of both **BC1** and **BC2** were successfully obtained by slow evaporation of dichloromethane/hexane solutions, and have been examined by X-ray diffraction analyses. (Figure 7.2a) Both molecules display highly planar geometries about the Pt(II) centre with minimal strain apparent in either structure, important for the maximization of phosphorescent quantum yields. The strength of the carbene donor is evident in both cases, exhibiting C-Pt bond lengths shorter than those observed between the Pt(II) centre and the phenyl ring. The considerable *trans* influence of the carbene can also be observed, with the Pt-O bond *trans* to the carbene lengthened by as much as 0.05 Å relative to more common nitrogen donors in similar *N^C* chelate cyclometalated systems. The crystal structures of both **BC1** and **BC2** show dimeric Pt-Pt stacking, with short metal-metal distances of 3.389 and 3.505 Å, respectively. Some puckering of the Pt(II) square plane is evident in the crystal structure of both compounds as a result of this interaction (Figure 7.2b).

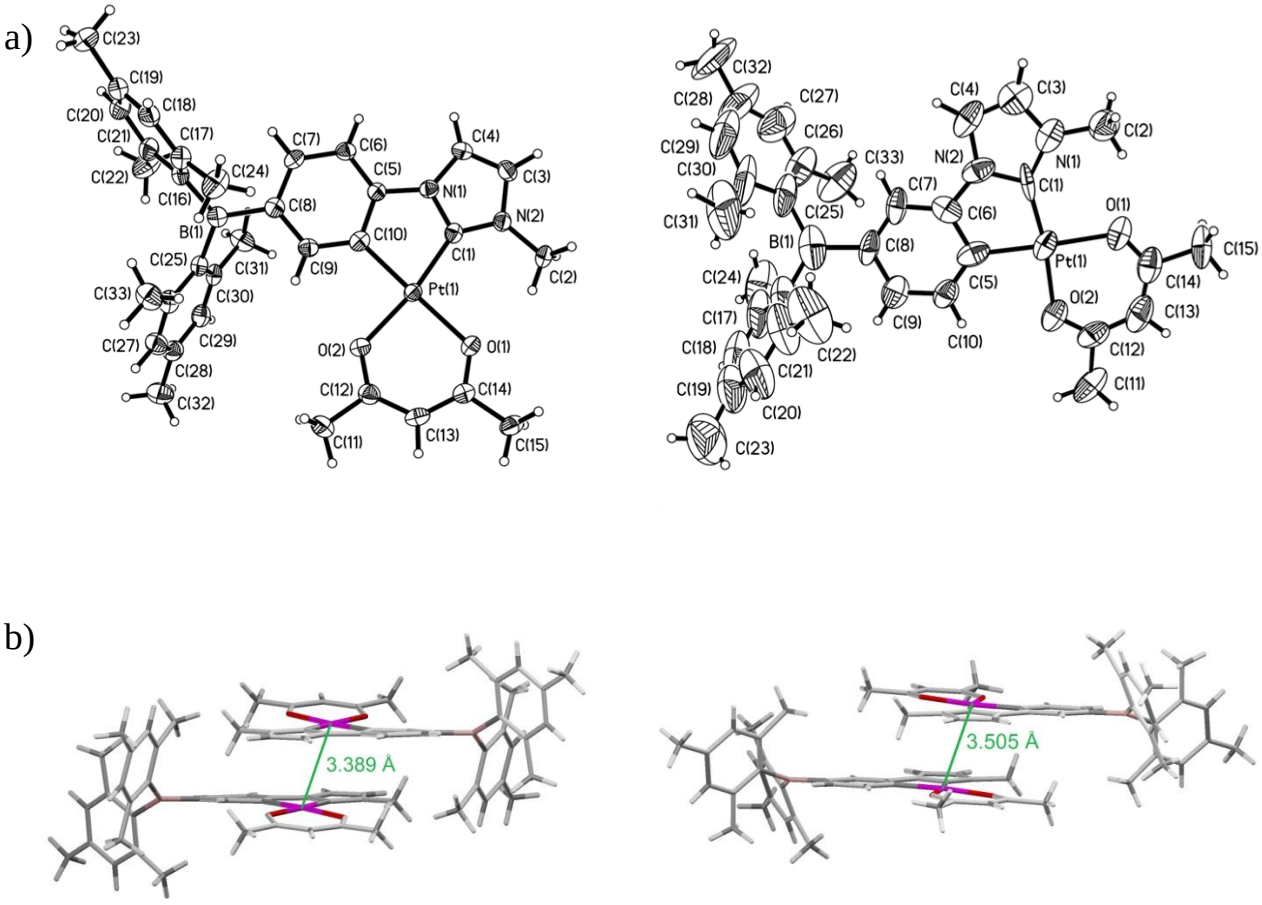

Figure 7.2: a) Crystal structures of **BC1** (left) and **BC2** (right) with 50% thermal ellipsoids. b) Dimeric stacking of **BC1** (left) and **BC2** (right) showing close Pt-Pt contacts.

7.3.2 Photophysical Properties

Both **BC1** and **BC2** display weak absorption bands around 375 nm (Figure 7.3a), which are absent in the parent phenylimidazole Pt(II) complex lacking the boron group.[9f] This band may thus be assigned to metal-to-ligand charge-transfer to boron. This is consistent with DFT calculations at the B3LYP level of

theory, which demonstrate that the HOMO includes significant electron density on the platinum centre, with the empty *p* orbital on boron making a large contribution to the LUMO. (Figure 7.4) It may thus be concluded that the presence of the triarylboron group significantly enhances MLCT in these *C^C* chelate systems.

This enhancement in MLCT is accompanied by a large increase in emission brightness and phosphorescent quantum yield for both complexes. Doped PMMA films of **BC1** and **BC2** exhibit impressive quantum yields of 90 and 86%, respectively, among the highest observed for metal-carbene complexes to date. Furthermore, this represents a dramatic increase over that observed for the parent *C^C*-chelate phenylimidazole in the absence of boron, which exhibits a phosphorescent quantum yield of only 7%.[9f] **BC1** exhibits blue-green phosphorescence in the solid state and solution, with an emission maximum of 482 nm in PMMA. This emission is blue-shifted 20 nm in its structural isomer **BC2**, resulting in sky-blue emission from the complex at λ_{max} = 464 nm. (Figure 7.3b,c) It has recently been shown that triarylboron substitution of the π-conjugated backbone of a metal complex at a site of electron density in the HOMO or the LUMO will lower the energy of either orbital, giving blue-shifted emission for the former and red-shifted emission for the latter. This is consistent with the observed emission colours of **BC1** and **BC2**, with the HOMO energy of **BC2** lower by 0.13 eV. In both cases the emission shows some vibronic character, indicative of phosphorescence from an excited state of both ligand-centered and MLCT character. Both **BC1** and **BC2** also undergo reversible reduction by cyclic voltammetry, indicative of electron-transporting functionality imparted by the triarylborane. The photophysical properties of both complexes are summarized in Table 7.3.

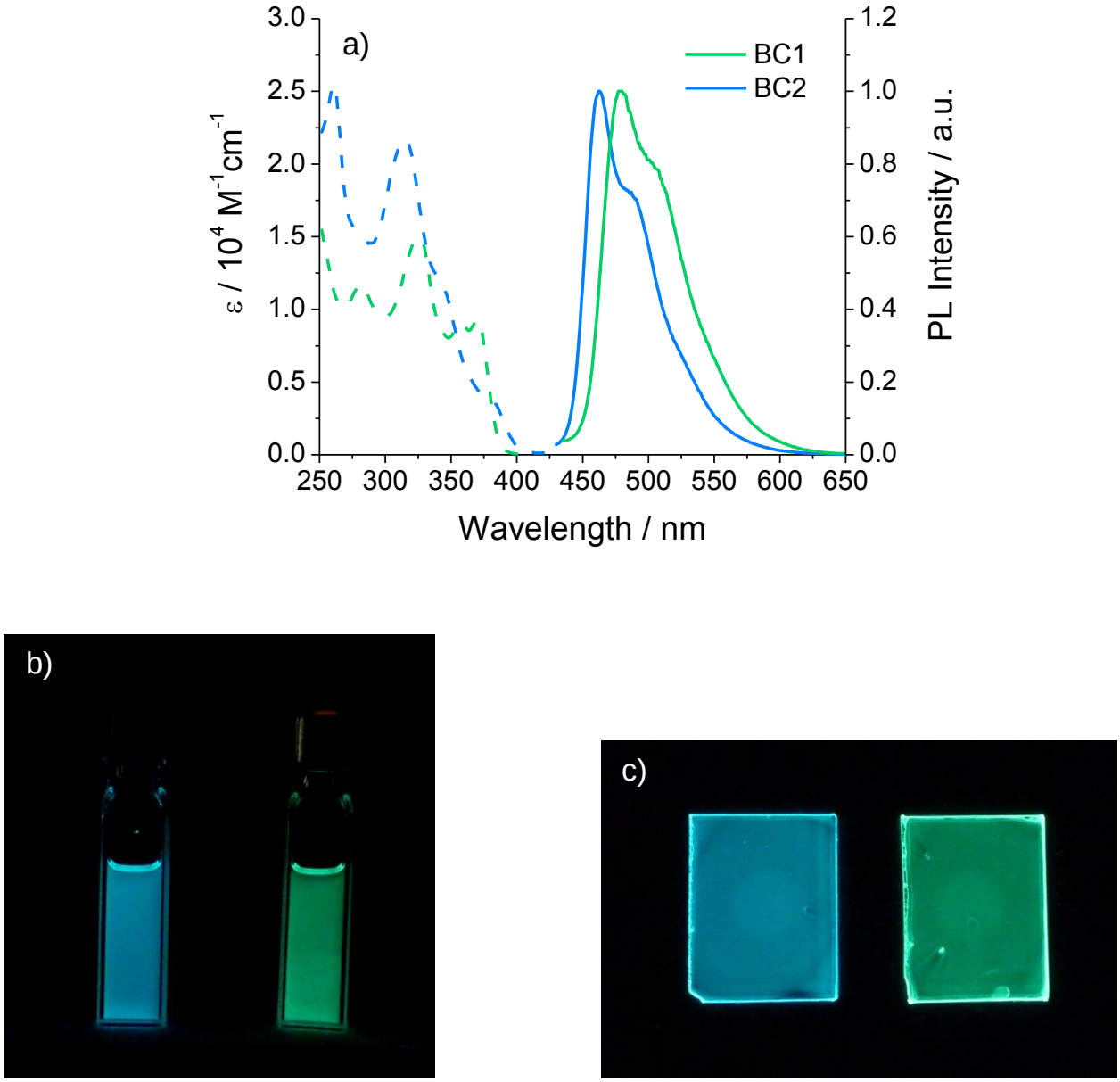

Figure 7.3: a) Absorption (dashed) and emission (solid) spectra of **BC1** and **BC2** at 10^{-5} M in CH_2Cl_2.b) Luminescence of 10^{-5} M solutions of **BC1** (green) and **BC2** (blue) in CH_2Cl_2. c) Luminescence of thin films of **BC1** and **BC2** on quartz substrates doped at 10 wt.% in PMMA. λ_{ex} = 365 nm.

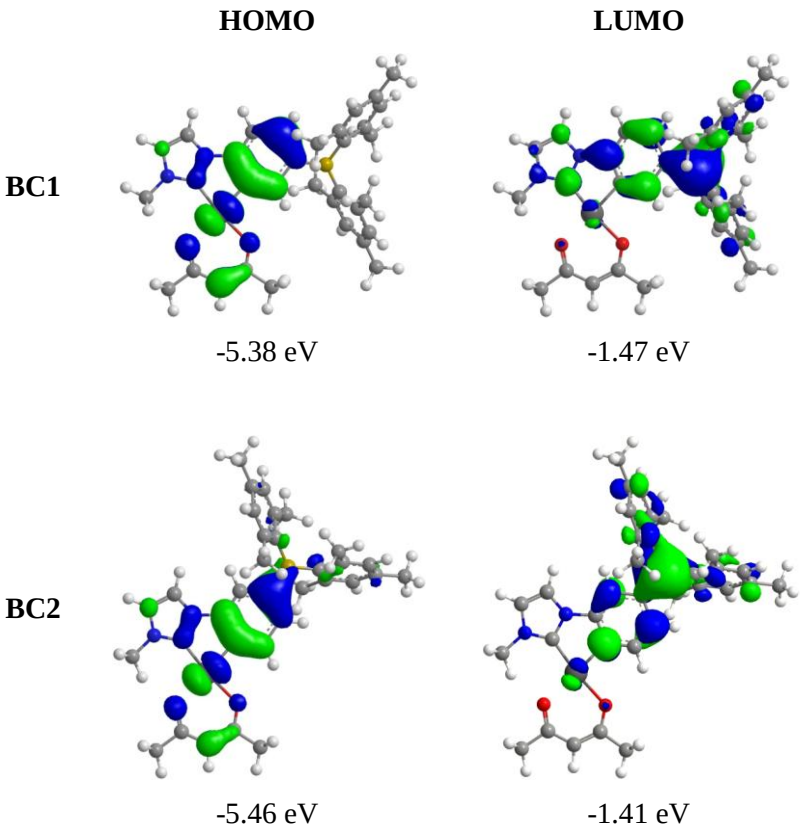

Figure 7.4: Calculated MO surfaces and energies for **BC1** and **BC2**. Isocontour = 0.03.

Table 7.3: Photophysical properties of BC1 and BC2.

Complex	Absorption, λ_{max} ε (10^4 cm^{-1} M^{-1})[a]	λ_{max} (nm) Solution[a]/Solid[b]	τ_P[a] (μs)	Φ_P[c] Solution[a]/Solid[b]	$E_{1/2}^{red}$ (V)[d]	HOMO (eV)[e]	LUMO (eV)[f]
BC1	381 (0.38), 344 (1.16), 316 (2.15)	478 / 482	6.9	0.87 / 0.90	-2.50	-5.73	-2.64
BC2	371 (0.76), 356 (0.80), 324 (1.48)	462 / 464	3.4	0.41 / 0.86	-2.49	-5.86	-2.65

[a] Measured in degassed CH_2Cl_2 at $1x10^{-5}$ M, [b] Doped into PMMA at 10 wt%. [c] Solution quantum efficiencies were measured in CH_2Cl_2 relative to $Ir(ppy)_3$ = 0.97.[16] Solid state quantum yields were measured using an integration sphere. All QYs are ± 10%. [d] In DMF relative to $FeCp^{0/+}$. [e] Measured in the solid state by UV photoelectron spectroscopy. [f] Calculated from the HOMO level and the optical energy gap.

7.3.3 Electroluminescent Devices

Based on the impressive quantum yields of these complexes, both **BC1** and **BC2** were evaluated as phosphorescent emitters for OLEDs. Devices were fabricated by vacuum vapor deposition on ITO-coated glass substrates, with structures shown in Figure 7.5. Due to the wide bandgaps of these materials, care was taken to ensure that the HOMO and LUMO energy levels of both emitters were contained within the bandgap of the host material, to ensure efficient trapping of both holes and electrons. Furthermore, it was necessary to employ a host material with a sufficiently high triplet level to ensure that excitons within the device were confined to the dopant. Based on these considerations, preliminary devices were fabricated using 4,4'-*N*,*N*'-dicarbazolylbiphenyl (CBP) as the hole-transport layer, 1,3,5-tris(*N*-phenylbenzimidazole-2-yl)benzene (TPBI) as the electron-transport layer, and *N*,*N*′-dicarbazolyl-3,5-benzene (mCP) as host. These devices had a structure of ITO/MoO_3 (1 nm)/CBP (35 nm)/mCP (5 nm)/mCP:emitter (12%, 15 nm)/TPBI (65 nm)/LiF (1 nm)/Al, as shown in Figure 7.5.

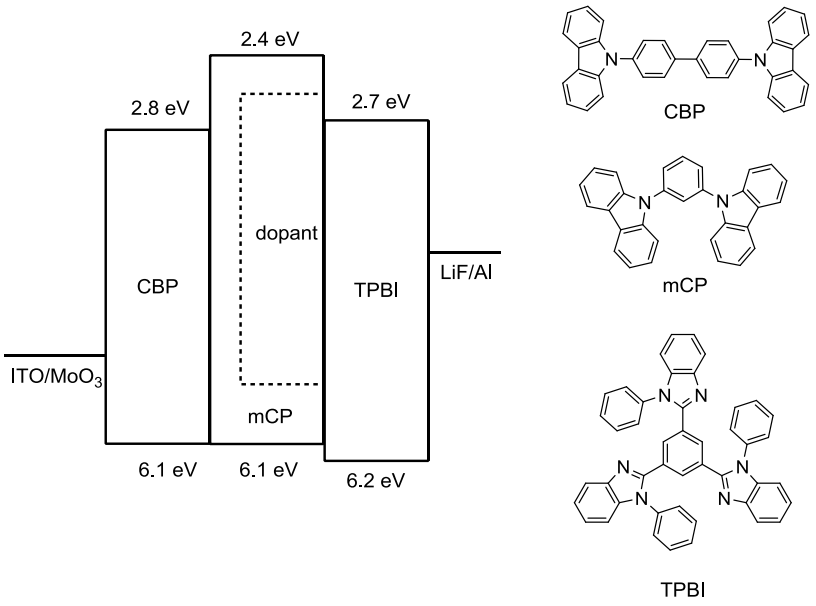

Figure 7.5: Schematic energy-level diagram for triple-layer **BC1** and **BC2** OLEDs.

The performance of both devices is shown in Figure 7.6. The device incorporating **BC1** as emitter shows peak current and power efficiencies of 53.0 cd/A and 41.6 lm/W, the highest reported to date for an OLED based on a platinum carbene complex. Furthermore, the efficiency remains as high as 49.6 cd/A and 33.6 lm/W at the display-relevant brightness of 100 cd/m^2. Devices based on the blue-emitting **BC2** also show impressive performance, with peak efficiencies of 25.8 cd/A and 22.5 lm/W, remaining at 19.2 cd/A and 13.6 lm/W at 100 cd/m^2.

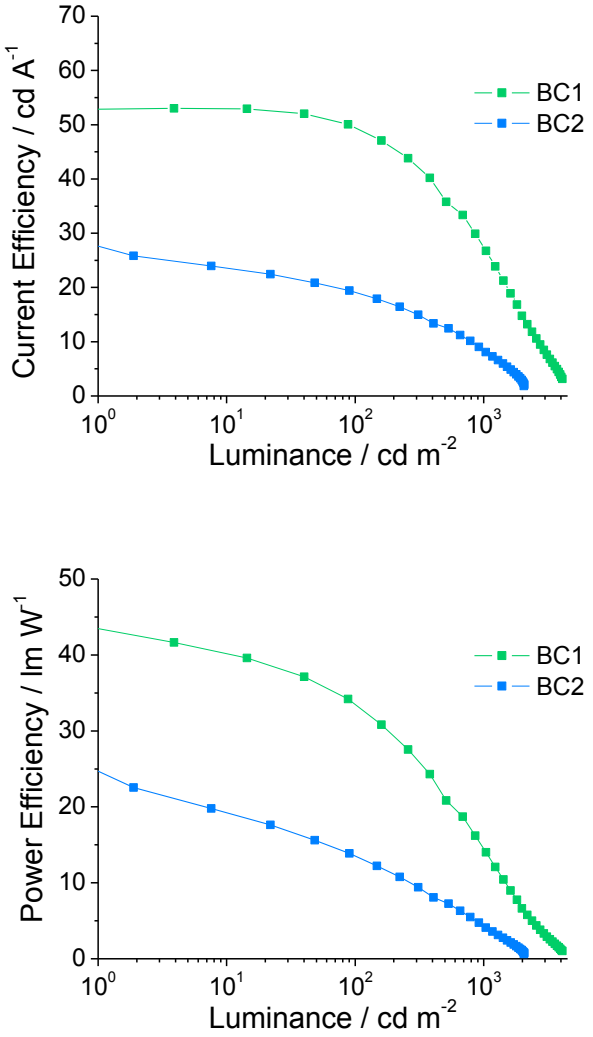

Figure 7.6: Current and power efficiencies for OLEDs based on **BC1** and **BC2**.

Surprisingly, these high device efficiencies are accompanied by a substantial red-shift in the electroluminescence spectrum of both devices relative to the solution or solid-state photoluminescence of either **BC1** or **BC2**. These data are shown in Figure 7.7 and correspond to Commission Internationale d'Éclairage (CIE) chromaticity coordinates of (0.34, 0.53) and (0.27, 0.50) for the devices based on **BC1** and **BC2** respectively.

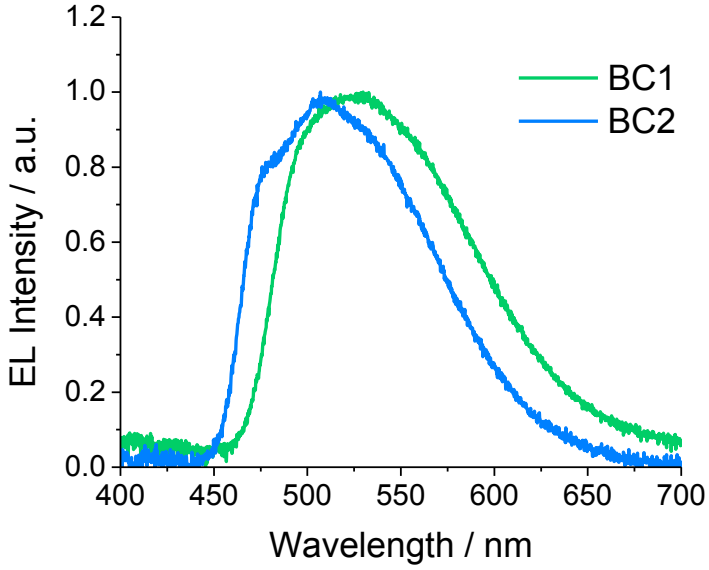

Figure 7.7: Electroluminescence spectra of devices based on BC1 and BC2, operating at 6.4 V.

The origin of this emission broadening is unknown. Varying the doping level of the carbene provided the same EL profile at doping levels of 0.5%, 1%, 2%, 4%, 8% and 12%, ruling out the formation excimers. Furthermore, vacuum-vapour deposition of a neat film of **BC1** on quartz gave yellow emission with λ_{max} = 548 nm, differing greatly from the EL profile of the **BC1**-based device. The EL profile was, however, found to vary according to the identity of the host material used, appearing different when doped into TPBI, CBP, TCTA (4,4′,4″-tris-(*N*-carbazolyl)-triphenlyamine) or CzSi (9-(4-tert-butylphenyl)-3,6-bis(triphenylsilyl)carbazole). (Figure 7.8) In the case of TPBI and CzSi, substantial emission from the host itself was also observed.

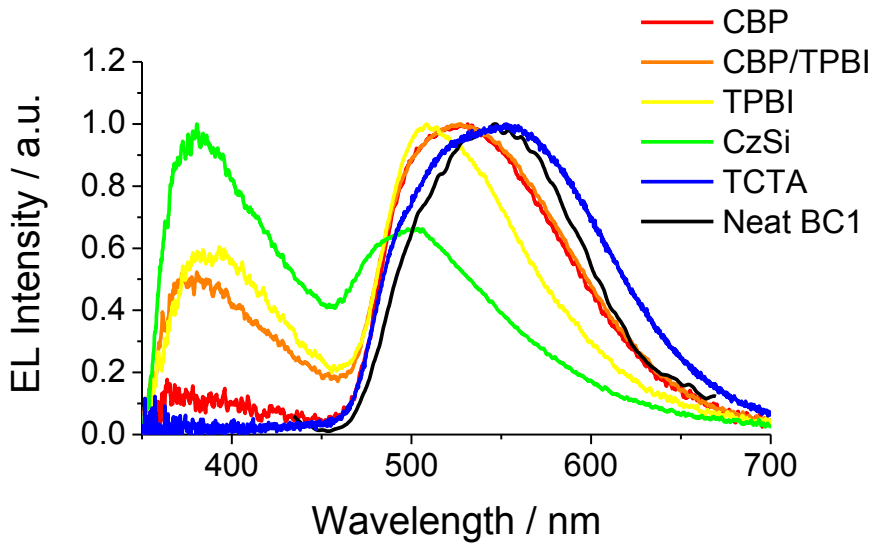

Figure 7.8: EL spectra of **BC1** in various hosts. Devices shown had a structure of ITO/MoO_3 (1 nm)/CBP (35 nm)/**host** (5 nm)/**host**:emitter (12%, 15 nm)/TPBI (65 nm)/LiF (1 nm)/Al. A doping concentration of 1% was used for the device in CzSi. The CBP/TPBI device was fabricated using 8 nm of doped CBP and 7 nm doped TPBI. The PL spectrum of a neat film of BC1 is shown for comparison.

To explore this further, a doped film of 8% **BC1** in CzSi was deposited on quartz, and the photoluminescence was measured. Curiously, the emission of this film exactly reproduces the solid-state photoluminescence of **BC1**, ruling out decomposition of the phosphor and indicating that only the electrical injection of excitons results in the observed emission broadening. While back-energy-transfer from dopant to host would seem an obvious explanation for this phenomenon, and is a common problem encountered during the use of high-energy phosphors, this appears unlikely for two reasons. First, such energy transfer processes typically result in extremely low electroluminescence efficiencies, yet remarkably efficient devices have been fabricated using both phosphors. Second, while the frontier orbital energy levels of **BC1** and **BC2** lie outside the HOMO-LUMO gaps of CBP and TPBI, similar emission broadening was observed when doped into mCP, TCTA and CzSi, all of which should adequately contain both the HOMO and LUMO levels of the dopants. It is noted that in the only previous example in literature describing OLEDs based on *C^C*-chelate Pt(II)-carbene complexes, no electroluminescence spectra were reported. We therefore speculate that the phenomena at play in this case are complex and deserving of further study.

7.4 Conclusions

In summary, we have developed a synthetic route to the first triarylboron-functionalized metal-carbene complexes, and have shown that the presence of the boron moiety greatly increases the phosphorescent quantum yield of these systems. Furthermore, the strong ligand field exerted by the carbene enables the preparation of Pt(II) complexes with efficient high-energy blue phosphorescence. The utility of these complexes has been further demonstrated in a series of preliminary electroluminescent devices, giving efficiencies among the highest reported to date for carbene-based OLEDs. However, the EL profiles of these devices showed unusual broadening, attributed to some interaction between dopant and host requiring further investigation.

7.5 Notes and References

The work described in this chapter has been published as:

- Z.M. Hudson, C. Sun, M.G. Helander, Y.-L. Chang, Z.-H. Lu and S. Wang. *J. Am. Chem. Soc.* **2012**, ASAP.

References:

(1) A. J. Arduengo, R. L. Harlow, M. Kline. *J. Am. Chem. Soc.* **1991**, *113*, 361.

(2) For recent reviews, see: a) X. Bugaut, F. Glorius, *Chem. Soc. Rev.* **2012**, *41*, 3511. b) G. C. Fortman, S. P. Nolan, *Chem. Soc. Rev.* **2011**, *40*, 5151. c) F. E. Hahn, M. C. Jahnke, *Angew. Chem. Int. Ed.*, **2008**, *47*, 3122. d) N. Marion, S. Diez-Gonzales, S. P. Nolan, *Angew. Chem. Int. Ed.*, **2007**, *26*, 2988. e) D. Enders, T. Balensiefer, *Acc. Chem. Res.* **2004**, *37*, 534.

(3) L. Mercs, M. Albrecht, *Chem. Soc. Rev.* **2010**, *39*, 1903.

(4) a) K. M. Hindi, M. J. Panzner, C. A. Tessier, C. L. Cannon, W. J. Youngs, *Chem. Rev.*, **2009**, *109*, 3859. b) A. Melaiye, R. S. Simons, A. Milsted, F. Pingitore, c) C. Wesdemiotis, C. A. Tessier, W.

J. Youngs, *J. Med. Chem*., **2004**, *47*, **973**. c) S. Patil, J. Claffey, A. Deally, M. Hogan, B. Gleeson, L. M. Menendez Mendez, H. Muller-Bunz, F. Paradisi, M. Tacke, *Eur. J. Inorg. Chem.*, **2010**, 1020. d) A. Melaiye, Z. Sun, K. Hindi, A. Milsted, D. Ely, D. H. Reneker, C. A. Tessier, W. J. Youngs, *J. Am. Chem. Soc*., **2005**, *127*, 2285.

(5) a) K. M. Lee, C. K. Lee, I. J. B. Lin, *Angew. Chem., Int. Ed*., **1997**, *36*, 1850. b) R. T. W. Huang, W. C. Wang, R. Y. Yang, J. T. Lu, I. J. B. Lin, *Dalton Trans*., **2009**, 7121. c) C. K. Lee, J. C. C. Chen, K. M. Lee, C. W. Liu, I. J. B. Lin, *Chem. Mater.*, **1999**, *11*, 1237. d) C. K. Lee, C. S. Vasam, T. W. Huang, H. M. J. Wang, R. Y. Yang, C. S. Lee, I. J. B. Lin, *Organometallics*, **2006**, *25*, 3768.

(6) a) A. K. Ghosh, V. J. Catalano, *Eur. J. Inorg. Chem.*, **2009**, 1832. b) F. E. Hahn, C. Radloff, T. Pape, A. Hepp, *Organometallics*, **2008**, *27*, 6408. c) C. Radloff, J. J. Weigand, F. E. Hahn, *Dalton Trans.*, **2009**, 9392. d) V. Lavallo, R. H. Grubbs, *Science*, **2009**, *326*, 559.

(7) a) S. U. Son, K. H. Park, Y.-S. Lee, B. Y. Kim, C. H. Choi, M. S. Lah, Y. H. Jang, D.-J. Jang, Y. K. Chung, *Inorg. Chem.*, **2004**, *43*, 6896. b) T. Sajoto, P. I. Djurovich, A. Tamayo, M. Yousufuddin, R. Bau, M. E. Thompson, R. J. Holmes, S. R. Forrest, *Inorg. Chem.*, **2005**, *44*, 7992. c) d) Y. Unger, A. Zeller, S. Ahrens, T. Strassner, *Chem. Commun.*, **2008**, 3263. e) W.-M. Xue, M. C.-W. Chan, Z.-M. Su, K.-K. Cheung, S.-T. Liu, C.-M. Che, *Organometallics*, **1998**, *17*, 1622. f) V. J. Catalano, M. A. Malwitz, A. O. Etogo, *Inorg. Chem.*, **2004**, *43*, 5714. g) Q.-X. Liu, F.-B. Xu, Q.-S. Li, H.-B. Song, Z.-Z. Zeng, *Organometallics*, **2004**, *23*, 610.

(8) See Chapter 1, references 8-10.

(9) a) R. J. Holmes, S. R. Forrest, T. Sajoto, A. Tamayo, P. I. Djurovich, M. E. Thompson, J. Brooks, Y.-J. Tung, B. W. D'Andrade, M. S. Weaver, R. C. Kwong, J. J. Brown, *Appl. Phys. Lett.*, **2005**, *87*, 243507. b) C.-F. Chang, Y.-M. Cheng, Y. Chi, Y.-C. Chiu, C.-C. Lin, G.-H. Lee, P.-T. Chou, C.-C. Chen, C.-H. Chang, C.-C. Wu, *Angew. Chem., Int. Ed.*, **2008**, *47*, 4542. c) S. Haneder, E. Da Como, J. Feldmann, J. M. Lupton, C. Lennartz, P. Erk, E. Fuchs, O. Molt, I. Munster, C. Schildknecht, G. Wagenblast, *Adv. Mater.* **2008**, *20*, 3325. d) C.-H. Hsieh, F.-I. Wu, C.-H. Fan, M.-

J. Huang, K.-Y. Lu, P.-Y. Chou, Y.-H. Ou Yang, S.-H. Wu, I-C. Chen, S.-H. Chou, K.-T. Wong, C.-H. Cheng. *Chem. Eur. J.* **2011**, *17*, 9180. e) H. Sasabe, J. Takamatsu, T. Motoyama, S. Watanabe, G. Wagenblast, N. Langer , O. Molt , E. Fuchs, C. Lennartz, J. Kido, *Adv. Mater.* **2010**, *22*, 5003. f) Y. Unger, D. Meyer, O. Molt, C. Schildknecht, I. Münster, G. Wagenblast, T. Strassner, *Angew. Chem. Int. Ed.* **2010**, *49*, 10214. g) K.-Y. Lu, H.-H. Chou, C.-H. Hsieh, Y.-H. Ou Yang, H.-R. Tsai, H.-Y. Tsai, L.-C. Hsu, C.-Y. Chen, I.-C. Chen, C.-H. Cheng, *Adv. Mater.* **2011**, *23*, 4933.

(10) For reviews, see C. R. Wade, A. E. J. Broomsgrove, S. Aldridge, F. P. Gabbaï, *Chem. Rev.* **2010**, 110, 3958, b) T. W. Hudnall, C.-W. Chiu, F. P. Gabbaï, *Acc. Chem. Res.* **2009**, *42*, 388.

(11) Z. M. Hudson, C. Sun, K. J. Harris, B. E. G. Lucier, R. W. Schurko, S. Wang, *Inorg. Chem.* **2011**, *50*, 3447

(12) a) G. J. Zhou, C. L. Ho, W.-Y. Wong, Q. Wang, D.-G. Ma, L.-X. Wang, Z.-Y. Lin, T. B. Marder, A. Beeby, *Adv. Funct. Mater.*, **2008**, 18, 499. b) Z. M. Hudson, C. Sun, M. G. Helander, H. Amarne, Z.-H. Lu, S. Wang, *Adv. Funct. Mater.*, **2010**, *20*, 3426. c) Z. M. Hudson, M. G. Helander, Z.-H. Lu, S. Wang, *Chem. Commun.* **2011**, *47*, 755. d) Z. B. Wang, M. G. Helander, Z. M. Hudson, J. Qiu, S. Wang and Z.-H. Lu. *Appl. Phys. Lett.*, **2011**, *98*, 213301.

(13) C. B. Singh, V. Kavala, A. K. Samal, B. K. Patel, *Eur. J. Org. Chem.* **2007**, 1369.

(14) M. E. Glogowski, N. Zumbulyadis, J. L. R. Williams, *J. Organomet. Chem.* **1982**, 97.

(15) Z. M. Hudson, B. A. Blight, S. Wang, *Org. Lett.* **2012**, *14*, 1700.

(16) T. Sajoto, P. I. Djurovich, A. B. Tamayo, J. Oxgaard, W. A. Goddard III, M. E. Thompson, *J. Am. Chem. Soc.*, **2009**, *131*, 9813.

Chapter 8

N-Heterocyclic Carbazole-Based Hosts for Simplified Single-Layer Phosphorescent OLEDs

8.1 Introduction

Organic light-emitting diodes (OLEDs) have attracted considerable research attention due to their applications in flat-panel displays and solid-state lighting.[1,2] Phosphorescent OLEDs (or PhOLEDs) employing late transition metal complexes as emitters are particularly attractive due to their ability to harvest both singlet and triplet excitons, making it possible to achieve internal quantum efficiencies of 100%.[1,2] However, due to the long excited-state lifetimes of phosphorescent materials, these emitters must be doped into host matrices to prevent exciton quenching by triplet-triplet annihilation. This doped emissive layer is then typically sandwiched between additional hole- and electron-transport layers (the HTL and ETL), which may be manipulated in order to achieve balanced charge injection into the emission zone. To date, nearly all development strategies for achieving high efficiencies in PhOLEDs have focused on such a multilayer strategy.

Unfortunately, the use of multiple organic layers in an OLED greatly increases the cost of the device, presenting a significant barrier to commercialization. The materials for each layer must be individually synthesized and carefully purified before being deposited sequentially on the substrate, resulting in an expensive and time-consuming fabrication process. Furthermore, care must be taken to match the appropriate energy levels of all adjacent layers, and to avoid exciplex formation and charge accumulation at every interface within the device. These present significant challenges to OLED mass production, making simplified device structures highly desirable.

Despite this strong motivation, only a small number of reports describe the preparation of simplified single-layer OLEDs, in which a single layer of organic material is required for device functionality.[3] Though recent work has shown that this design holds promise, the efficiency of all single-layer structures reported to date remains far behind those of more complex multilayer devices.[4] This is due primarily to the difficulty in developing a host material capable of balanced carrier transport that also possesses HOMO and LUMO levels well-matched to the work functions of the anode and cathode, respectively. Bipolar host materials containing both electron- and hole-transporting functionalities show promise in this regard, as careful selection and modification of the transporting moieties can provide good carrier balance.[5] Though such materials have been the subject of considerable recent research, examples of their use in single-layer OLEDs remain rare.[3c-e, i]

Carbazole-based molecules have been used extensively as host materials in OLEDs due to their high triplet energy and hole-transporting functionality.[6] In particular, 4,4'-*N*,*N*'-dicarbazolylbiphenyl (CBP) is perhaps the most widely used host material for phosphorescent emitters. It has also recently been demonstrated that CBP may be used directly as an HTL in both fluorescent and phosphorescent OLEDs.[7] For example, a phosphorescent OLED with > 20% external quantum efficiency (EQE) at a high luminance of > 10,000 cd/m^2 has been demonstrated in a bilayer device using CBP directly as hole transport layer as well as host.[7] Since no additional injection layers and exciton blocking layers were needed, the resultant device structure was highly simplified. The simple structure also helped to eliminate redundant organic/organic interfaces near the exciton formation zones, at which charge carriers could accumulate and ultimately quench excitons. Inspired by this, we sought to determine if similarly high performance could be achievable in an even more simplified device structure, employing a single material as HTL, ETL, and host.

Unfortunately, electron transport by CBP is relatively inefficient, resulting in poor electron injection from commonly used Cs_2CO_3/Al or LiF/Al cathodes. Thus, while CBP can be used to fabricate highly efficient double-layer devices, additional chemical modification to promote electron transport is required to achieve a new material capable of acting as HTL, ETL, and host. Following this device design strategy, we therefore sought to synthesize a material such that: (i) the LUMO level is lowered relative to CBP, reducing the barrier to electron injection at the cathode, ii) the HOMO energy is not significantly changed, preserving efficient hole injection at the anode, and iii) the triplet level remains significantly large for use with phosphorescent dopants.

Based on this concept, we herein describe the first examples of single-layer OLEDs with efficiencies competitive with traditional multilayer devices. In order to systematically lower the LUMO of CBP while leaving the HOMO level virtually unchanged, we have designed two novel host materials 4,5'-*N*,*N*'-dicarbazolyl-(2-phenylpyridine) (**CPPY**) and 4,5'-*N*,*N*'-dicarbazolyl-(2-phenylpyrimidine) (**CPHP**), which have been fully characterized and examined by ^{1}H and ^{13}C NMR spectroscopy, mass spectrometry, DFT calculations, X-ray crystallographic analysis, and ultraviolet photoelectron spectroscopy (UPS). We demonstrate that these simple structural changes are sufficient to drastically improve electron injection and transport, giving single layer OLEDs with by far the highest efficiencies reported to date. These devices have the structure ITO/MoO_3/host/host:dopant/host/Cs_2CO_3/Al, employing ITO/MoO_3 and Cs_2CO_3/Al as composite electrodes and $Ir(ppy)_2(acac)$ as phosphorescent emitter. With this structure, a peak EQE of 26.8% and current efficiency of 92.2 cd/A have been achieved, remaining as high as 21.3% and 73.3 cd/A at the practical brightness of 100 cd/m^{-2}.

8.2 Experimental

8.2.1 General Procedures

Experimental techniques and instruments used follow those described in section 2.2. Details regarding electroluminescent device fabrication and testing are described in section 4.2. The synthesis of 4,4'-dibromo-2-phenylpyridine has been reported previously.[8]

8.2.2 Synthesis of 4,4'-dibromo-2-phenylpyrimidine

To a 250 mL Schlenk flask with condenser and stir bar was added 4-bromophenylboronic acid (1.4 g, 7.0 mmol), 5-bromo-2-iodopyrimidine (2.0 g, 7.0 mmol), $Pd(PPh_3)_4$ (240 mg, 0.21 mmol) K_2CO_3 (2.9 g, 21 mmol) and 120 mL degassed 1:1 THF/H_2O. The mixture was heated to 55°C with stirring for 16 h, after which the THF was removed *in vacuo* and the aqueous layer extracted with CH_2Cl_2. The combined organic layers were dried with $MgSO_4$, concentrated, and the residue purified by column chromatography on silica (2:1 hexanes:CH_2Cl_2 as eluent) to give the above compound as a white solid (1.03 g, 53% yield). ^{1}H NMR (500 MHz, $CDCl_3$) δ 8.80 (s, 2H, *Pyr*), 8.27 (d, J = 8.5 Hz, 2H, *Ph*), 7.60 (d, J = 8.5 Hz, 2H, *Ph*) ppm; 162.0, 157.9, 132.5, 131.9, 129.7, 126.0, 118.5 ppm; HRMS Calc'd for $C_{10}H_6Br_2N_2$: 311.8898, found 311.8891.

8.2.3 Synthesis of Host Materials

Synthesis of host materials: To a 100 mL Schlenk flask with stir bar and condenser was added the desired dibromobiaryl (2.9 mmol), carbazole (1.44 g, 8.6 mmol), K_2CO_3 (3.2 g, 23 mmol), Cu powder (0.73 g, 11.5 mmol) 18-crown-6 (0.15 g, 0.58 mmol) and 30 mL degassed 1,2-dichlorobenzene. The mixture was heated to reflux at 185°C for 7 days, at which point the solvent was removed by vacuum distillation. The residue was then extracted with sat. aq. NH_4Cl and CH_2Cl_2. The combined organic layers were dried with

$MgSO_4$, filtered, concentrated and the residue purified on silica (3:2 $CHCl_3$:hexanes as eluent) to give the desired compound.

4,5'-*N,N*'-dicarbazolyl-(2-phenylpyridine) (CPPY): Yield 89%. ^{1}H NMR (400 MHz, $CDCl_3$) δ 9.02 (d, J = 2.4 Hz, 1H, *Py*), 8.35 (d, J = 8.4 Hz, 2H, *Ph*), 8.18 (d, J = 7.8 Hz, 2H, *Cz*), 8.17 (d, J = 7.6 Hz, 2H, *Cz*), 8.08 (d, J = 8.4 Hz, 1H, *Py*), 8.04 (dd, J = 8.4 Hz, 2.4 Hz, 1H, *Py*), 7.76 (d, J = 8.4 Hz, 2H, *Ph*), 7.53 (d, J = 8.1 Hz, 2H, *Cz*), 7.50-7.43 (m, 6H, *Cz*), 7.38-7.30 (m, 4H, *Cz*) ppm; ^{13}C {^{1}H}NMR (100 MHz, $CDCl_3$) δ 156.2, 148.3, 140.7, 140.6, 138.8, 137.4, 135.1, 133.4, 128.5, 127.3, 126.3, 126.1, 123.8, 123.6, 121.1, 120.64, 120.57, 120.4, 120.2, 109.8, 109.4 ppm; HRMS calc'd for $C_{35}H_{23}N_3$: 485.1892, found 485.1883.

4,5'-*N,N*'-dicarbazolyl-(2-phenylpyrimidine) (CPHP): Yield 93%. ^{1}H NMR (400 MHz, $CDCl_3$) δ 9.13 (s, 2H, *Pyr*), 8.80 (d, J = 8.6 Hz, 2H, *Ph*), 8.19 (d, J = 7.6 Hz, 2H, *Cz*), 8.17 (d, J = 7.6 Hz, 2H, *Cz*), 7.79 (d, J = 8.6 Hz, 2H, *Ph*), 7.55 (d, J = 8.2 Hz, 2H, *Cz*), 7.52-7.43 (m, 6H, *Cz*), 7.38 (t, J = 7.1 Hz, 2H, *Cz*), 7.32 (t, J = 7.5 Hz, 2H, *Cz*) ppm; ^{13}C {^{1}H} NMR (100 MHz, $CDCl_3$) δ 162.2, 155.4, 140.5, 140.4, 140.3, 135.6, 131.4, 130.0, 127.0, 126.6, 126.1, 124.1, 123.7, 121.2, 120.8, 120.4, 120.3, 109.9, 109.1 ppm; HRMS calc'd for $C_{34}H_{22}N_4$: 485.1892, found 485.1852.

8.2.4 X-ray Diffraction Analysis

Single crystals of **CPPY** and **CPHP** were grown by slow evaporation from solutions of hexanes and CH_2Cl_2. Molecules of CPHP co-crystallize with CH_2Cl_2 solvent molecules (0.5 CH_2Cl_2 per CPHP). Because of the disordering of the solvent molecules, they were removed using the Platon Squeeze routine[9] to improve the quality of the crystal data. Molecules of CPPY possess crystallographically imposed inversion center symmetry. As a result, the pyridyl nitrogen atom is disordered over two sites related by an inversion center. Crystal data for these compounds are listed in Table 8.1, and selected bond lengths

and angles are given in Table 8.2. These crystal structures have been deposited to the Cambridge Crystallographic Data Centre as CCDC 868871 and 868872 and may be obtained free of charge via www.ccdc.cam.ac.uk/data_request/cif.

Table 8.1: Crystallographic data for CPPY and CPHP

Compound	**CPPY**	**CPHP**
Formula	$C_{18}H_{12}N_{1.5}$	$C_{17}H_{11}N2$
FW	242.79	243.28
Space Group	P2(1)/c	C2/c
a, Å	8.174(3)	36.7389(17)
b, Å	16.122(5)	10.6986(5)
c, Å	10.280(3)	13.8150(7)
α, °	90	90
β, °	112.567(6)	99.949(4)
γ, °	90	90
V, $Å^3$	1251.0(7)	5348.4(4)
Z	4	16
D_{calc}, g cm^{-1}	1.414	1.209
T, K	296(2)	296(2)
μ, mm^{-1}	0.082	0.072
$2\theta_{max}$, °	52.00	54.44
Reflns measured	5636	25700
Reflns used (R_{int})	2429 (0.0419)	5913 (0.0519)
Parameters	182	344
Final R Values [I > 2σ(I)]:		
R_1 [a]	0.0513	0.0642
wR_2 [b]	0.1117	0.1860
R values (all data):		
R_1 [a]	0.1095	0.1120
wR_2 [b]	0.1400	0.2166
Goodness-of-fit on F^2	0.994	0.967

[a] $R_1 = \Sigma[(|F_0| - |F_c|) / \Sigma |F_0|$

[b] $wR2 = [\Sigma w[(F_0^2-F_c^2)^2] / \Sigma[w(F_0^2)^2]]^{1/2}$

$w = 1 / [\sigma^2(F_0^2) + (0.075P)^2]$, where $P = [Max (F_0^2, 0) + 2F_c^2] / 3$

Table 8.2: Selected bond lengths (Å) and angles (°) for CPPY and CPHP.

		CPPY	
C(1)-N(1)	1.405(3)	C(14)-N(2)	1.43(2)
C(19)-N(1)	1.423(3)	C(16)-N(2)	1.24(2)
C(12)-N(1)	1.401(3)	C(16)-C(16)A	1.479(4)
N(1)-C(12)-C(7)	108.5(2)	N(2)-C(14)-H(14A)	127.0
C(12)-N(1)-C(1)	107.88(18)	N(2)-C(16)-C(17)	118.1(9)
C(12)-N(1)-C(19)	125.48(19)	N(2)-C(16)-C(16)A	119.9(9)
C(1)-N(1)-C(19)	126.31(18)	C(17)-C(16)-C(16)A	122.0(3)
		CPHP	
N(1)-C(1)	1.403(3)	N(3)-C(13)	1.342(3)
N(1)-C(14)	1.410(3)	N(3)-C(16)	1.352(3)
N(1)-C(12)	1.411(3)	N(4)-C(15)	1.338(3)
N(2)-C(23)	1.399(3)	N(4)-C(16)	1.345(3)
N(2)-C(34)	1.411(3)	C(16)-C(17)	1.473(3)
N(2)-C(20)	1.421(3)		
C(1)-N(1)-C(14)	126.4(2)	C(34)-N(2)-C(20)	125.4(2)
C(1)-N(1)-C(12)	108.28(19)	C(13)-N(3)-C(16)	117.1(2)
C(14)-N(1)-C(12)	125.2(2)	C(15)-N(4)-C(16)	117.6(2)
C(23)-N(2)-C(34)	108.3(2)	N(4)-C(16)-N(3)	123.8(2)
C(23)-N(2)-C(20)	125.2(2)	C(22)-C(17)-C(18)	118.6(2)

8.3 Results and Discussion

8.3.1 Synthesis and Molecular Properties

CPPY and CPHP can be easily synthesized in two steps, first by palladium-catalyzed Suzuki coupling of 4-bromophenylboronic acid with the appropriate heteroaryl halide, followed by copper-catalyzed Ullman condensation in excellent yield (Figure 8.1). Both CPPY and CPHP show excellent thermal stability by thermogravimetric analysis, comparable to that of CBP (Table 8.3). As expected, the introduction of electronegative nitrogen atoms to the π-system of CBP lowers the LUMO energy, while leaving the HOMO level largely unchanged. Substitution of CBP with one or two nitrogen atoms was found to reduce the LUMO level by 0.19 and 0.33 eV respectively, with no significant change in the HOMO level in either case as measured by UPS.

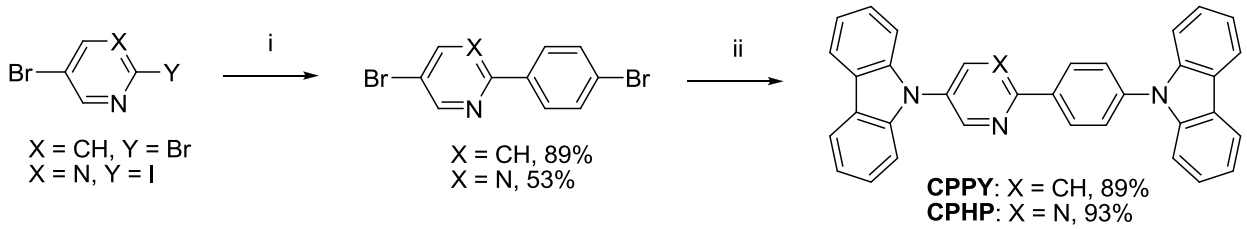

Figure 8.1: Synthesis of CPPY and CPHP. Reagents and conditions: i): 4-bromophenylboronic acid (1 equiv.), K_2CO_3 (3 equiv.), $Pd(PPh_3)_4$ (5 mol %), 1:1 THF:H_2O, 55°C, 16h; ii) Carbazole (3 equiv.), Cu powder (4 equiv.), 18-crown-6 (0.2 equiv.), K_2CO_3 (8 equiv.), *o*-dichlorobenzene, 185°C, 7d.

Table 8.3: Photophysical properties of host materials

Cmpd.	$\lambda_{max,\ abs}$ [nm][a]	$\lambda_{max,fluo.}$ [nm][a]	$\lambda_{max,phos.}$ [nm][b]	Φ_f [c]	E_T [eV]	T_d [°C]	HOMO [eV][d]	LUMO [eV][e]
CBP	241, 295, 319, 342	374	467	0.61	2.67	407	-6.05	-2.55
CPPY	238, 294, 343	399	474	0.70	2.62	395	-6.05	-2.74
CPHP	238, 258, 293, 343	425	475	0.24	2.61	403	-6.05	-2.88

[a] Measured at 10^{-5} M in CH_2Cl_2 at 298 K. [b] Measured in 2-MeTHF at 77K. [c] Relative to 9,10-diphenylanthracene (Φ=0.90), ±10%. [d] Measured in the solid state by UV photoelectron spectroscopy. [e] Calculated from the HOMO level and the optical energy gap.

X-ray crystal structural analysis confirmed that CPPY and CPHP have essentially identical structures to that of CBP with the two central aryl rings being virtually coplanar (Figure 8.2).[10] In fact, the crystals of CPPY and CBP are isomorphous with similar unit cell parameters and an identical space group, $P2_1/c$. This is possible due to two-site disordering of the pyridyl nitrogen atom of CPPY over two inversion center-related sites. Although the crystal of CPHP contains CH_2Cl_2 solvent molecules and is thus not readily comparable with CPPY and CBP, it is reasonable to suggest that intermolecular interactions of CPHP in the amorphous solid should be similar due to the similar molecular size and shape of these three molecules.

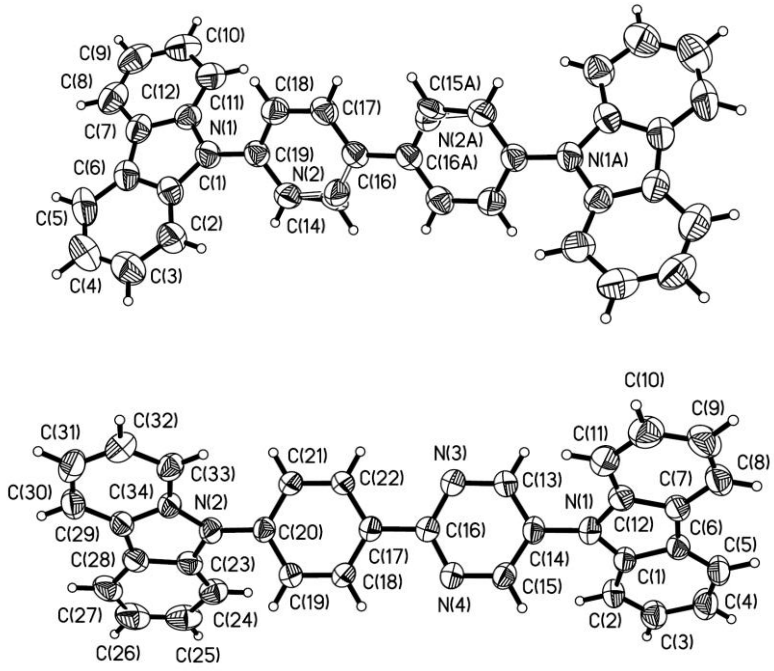

Figure 8.2: Crystal structures of **CPPY** (top, showing only one disordered site of the pyridyl N atom) and **CPHP** (bottom) with 50% thermal ellipsoids.

The absorption and emission spectra of CBP, CPPY and CPHP are shown in Figure 8.3, and show a clear progression to lower energy as the number of aromatic nitrogen atoms is increased. The triplet energies of these materials were also determined from the first vibronic peak in their time-resolved phosphorescent spectra at 77K, (Table 8.3) and suggest that these materials would be appropriate hosts for red, green, or even sky blue emitters.

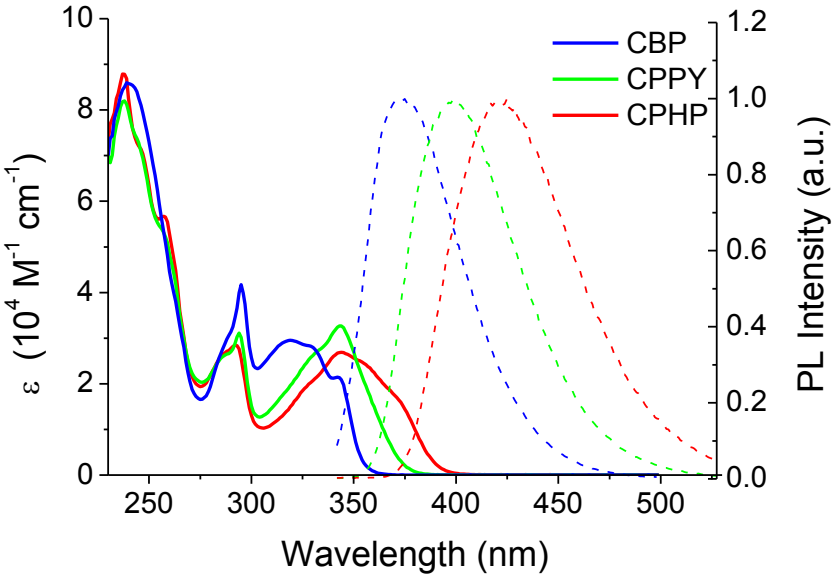

Figure 8.3: Absorption (solid) and emission (dashed) spectra at 10^{-5} M in CH_2Cl_2. λ_{ex} = 340 nm.

The electronic properties of CPPY and CPHP were also compared with that of CBP using DFT calculations at the B3LYP level of theory with 6-31G* as the basis set (Figure 8.4). Consistent with UPS data, almost no change is predicted in the HOMO level upon introduction of nitrogen atoms at the 2- and 6-positions of the CBP biphenyl ring system, as the electron density in the HOMO is primarily located on the carbazole functional groups. However, as the LUMO of CBP consists primarily of the π* orbitals of the biphenyl unit, the introduction of these electron-deficient nitrogen atoms is predicted to lower the LUMO level, as observed experimentally. This is further verified by cyclic voltammetry measurements in DMF solution, which indicate improved electron accepting ability in the order of CPHP>CPPY>CBP. Examination of the frontier MO surfaces of these three molecules also reveals increasing bipolar character moving from CBP to CPPY to CPHP. As the central biaryl unit becomes more electron-deficient, the HOMO exhibits increased electron density on the carbazole group farther from the central heteroaromatic ring, with the LUMO showing increased contribution from the *N*-heterocycle. This imparts more charge-transfer character to CPPY and CPHP, accounting for the larger Stokes shift observed for these molecules.

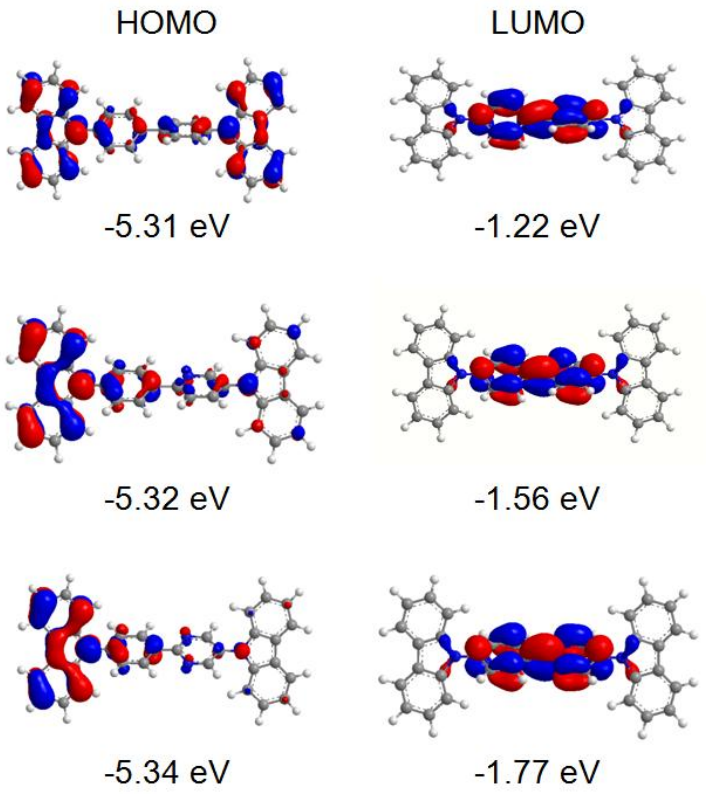

Figure 8.4: Frontier molecular orbital surfaces and calculated orbital energies for CBP (top), CPPY (middle) and CPHP (bottom). Isocontour value = 0.03.

8.3.2 Electroluminescent Devices

To evaluate the performance of these compounds in OLEDs, a series of devices were fabricated in which a thin layer of the doped host material was deposited between two undoped buffer layers of the same host, which act also as the ETL and HTL in this design (Figure 8.5). These devices have a structure of ITO/MoO_3 (1 nm)/host (35 nm)/host:$Ir(ppy)_2(acac)$ (8 wt %, 15 nm)/host (60 nm)/Cs_2CO_3 (1nm)/Al, with Device I, II and III incorporating CBP, CPPY and CPHP as host, respectively (see Table 8.4). All devices show green emission with a peak wavelength of 523 nm and Commision Internationale de l'Éclairage (CIE) coordinates of (0.32, 0.64), indicating that emission originates entirely from the $Ir(ppy)_2(acac)$ dopant in all cases.

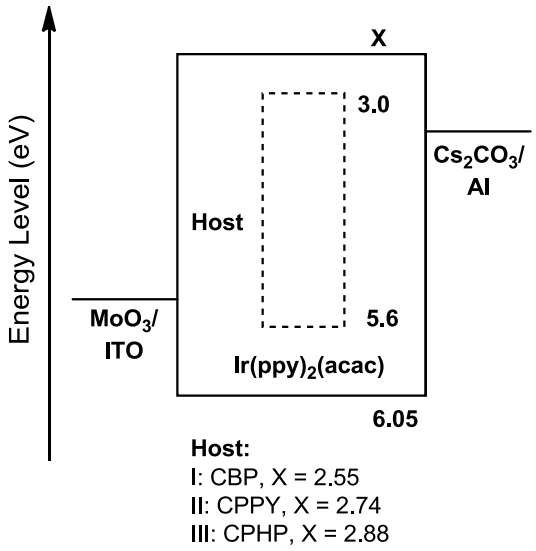

Figure 8.5: Schematic showing the structure of devices I-III.

The performance of the three devices is compared in Figure 8.6. Remarkably, after optimization of each layer thickness it was possible to achieve a reasonably high efficiency single-layer OLED simply using CBP as host. Device I shows a peak EQE of 13.3% and current efficiency of 54.4 cd/A at 438 cd/m^2, with a moderate turn-on voltage of 4.0 V. Device II incorporating CPPY as host outperforms the CBP-based device at low luminance, with a peak current efficiency of 74.9 cd/A, EQE of 21.5%, and turn-on voltage of 3.8 V. However, due to significant efficiency roll-off, Device I shows better performance at higher luminance (>200 cd/m^2). The performance of Device III, however, shows excellent performance at all voltages examined, giving an exceptionally high peak EQE and current efficiency of 26.8% and 92.2 cd/A, remaining as high as 21.3% and 73.3 cd/A at the practical brightness of 100 cd/m^2. Furthermore, this device shows a much lower turn-on voltage of 3.0 V, confirming that the lower LUMO level of CPHP does indeed reduce the barrier to electron injection at the cathode. This is to our knowledge the most efficient simplified single-layer OLED reported to date by a factor of two or more,[3] and most importantly, shows performance comparable to state-of-the-art devices based on conventional multilayer architectures.[4]

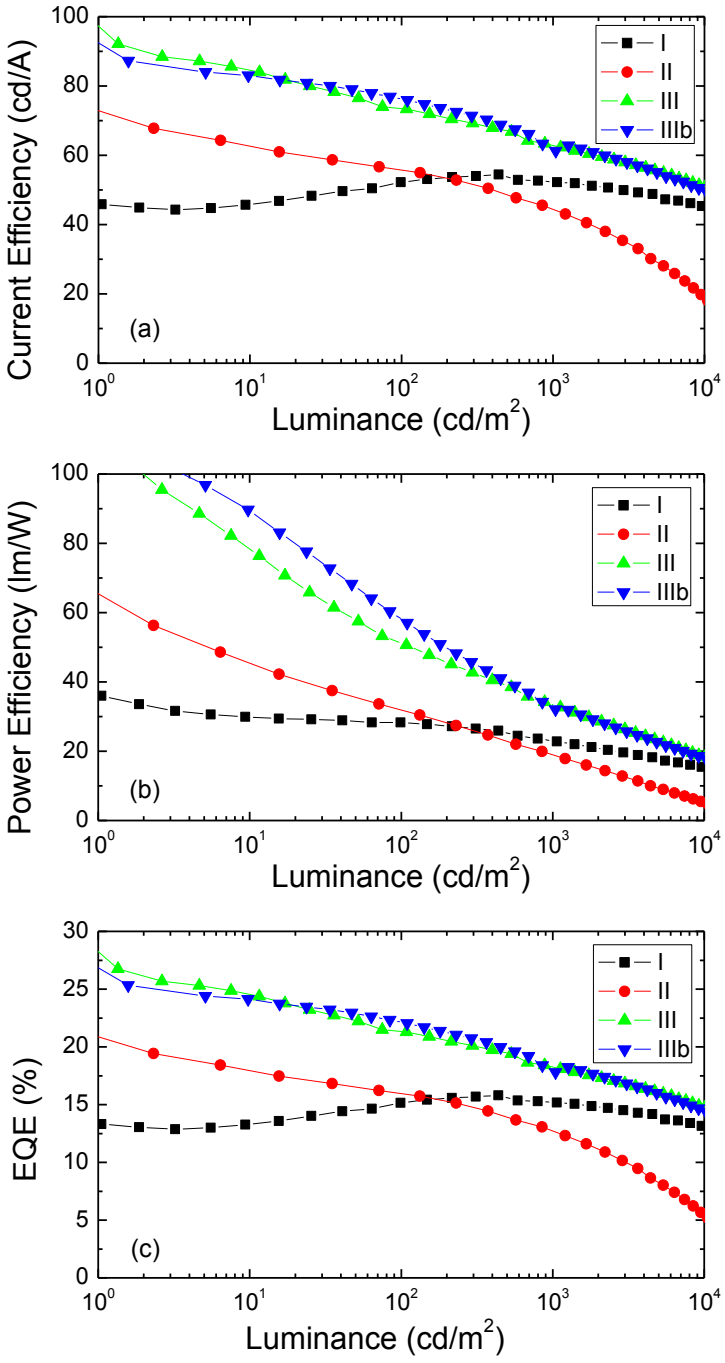

Figure 8.6: (a) Current efficiency, (b) power efficiency and (c) external quantum efficiency of devices I, II, III and IIIb.

Table 8.4: Device performance

Device	I	II	III	IIIb
V_{on} / V	4.0	3.8	3.0	2.8
CE_{max} / cd A^{-1}	54.4	74.9	92.2	87.3
PE_{max} / lm W^{-1}	36.0	56.3	106.1	107.7
EQE_{max} / %	13.3	21.5	26.8	25.3
CIE / (x, y)	(0.32, 0.64)	(0.32, 0.64)	(0.32, 0.64)	(0.32, 0.64)

Since no organic/organic heterojunctions are present to facilitate exciton formation in these single-layer devices, there should be a distribution of exciton formation in the host. We thus sought to determine if a broader emission zone doped with phosphorescent emitter could more effectively overlap with the exciton formation zone, thus further enhancing device efficiency. Device IIIb was fabricated with a structure of ITO/MoO_3 (1nm)/CPHP (35 nm)/CPHP:$Ir(ppy)_2(acac)$ (55 nm)/CPHP (20 nm)/Cs_2CO_3 (1 nm)/Al, using CPHP as host as in Device III but incorporating a much wider 55 nm doped region. The performance of this device is also shown in Figure 8.6, and is compared with Device III. No significant improvement was achieved by broadening the emission zone, indicating that doping in a wider region does not necessarily enhance the efficiency of an already optimized single-layer device.

Based on the HOMO and LUMO levels of CPPY it was expected that the performance of Device II should have been between that of CBP and CPHP. To determine the origins of the significant efficiency roll-off in Device II we fabricated single carrier hole-only devices to investigate the transport and injection of charge in the three different hosts. The performance of these three devices is compared in Figure 8.7. Surprisingly the electrical characteristics of the device with CPPY are markedly worse, which suggests either poor injection or transport of holes in this material. This most likely accounts for the significant efficiency roll-off in Device II due to poor electron-hole balance, particularly at high current and brightness. To determine if the poor electrical performance of CPPY was due to poor hole injection or

transport we measured the energy-level alignment at the interface with the ITO/MoO_3 anode using UPS. Figure 8.7 shows the UPS valance band spectrum of the frontier orbitals of the three different hosts deposited on MoO_3. Although the HOMO level relative to vacuum is the same for the three materials (-6.05 eV), the energy-level alignment is significantly different for CPPY. The HOMO derived peak in the valence band of CPPY is ~0.5 eV further from the Fermi level than for either CBP or CPHP, which indicates a significantly increased barrier to hole injection at the anode, consistent with the single carrier and OLED performance data. Owing to the similar structures of the three hosts, the reason for this radically different energy-level alignment is likely quite subtle. Among this series of materials, CPPY alone possesses a transverse dipole moment perpendicular to the molecular long axis, yet exhibits molecular packing isostructural with CBP by X-ray crystallography. However, the presence of this dipole moment may result in a preferred molecular orientation at the organic/MoO_3 interface, which may change the energy level alignment. Recent studies have shown that the dipole moments of structurally similar materials can have a dramatic effect on their performance in electroluminescent devices,[11] and we speculate that similar phenomena are at play here.

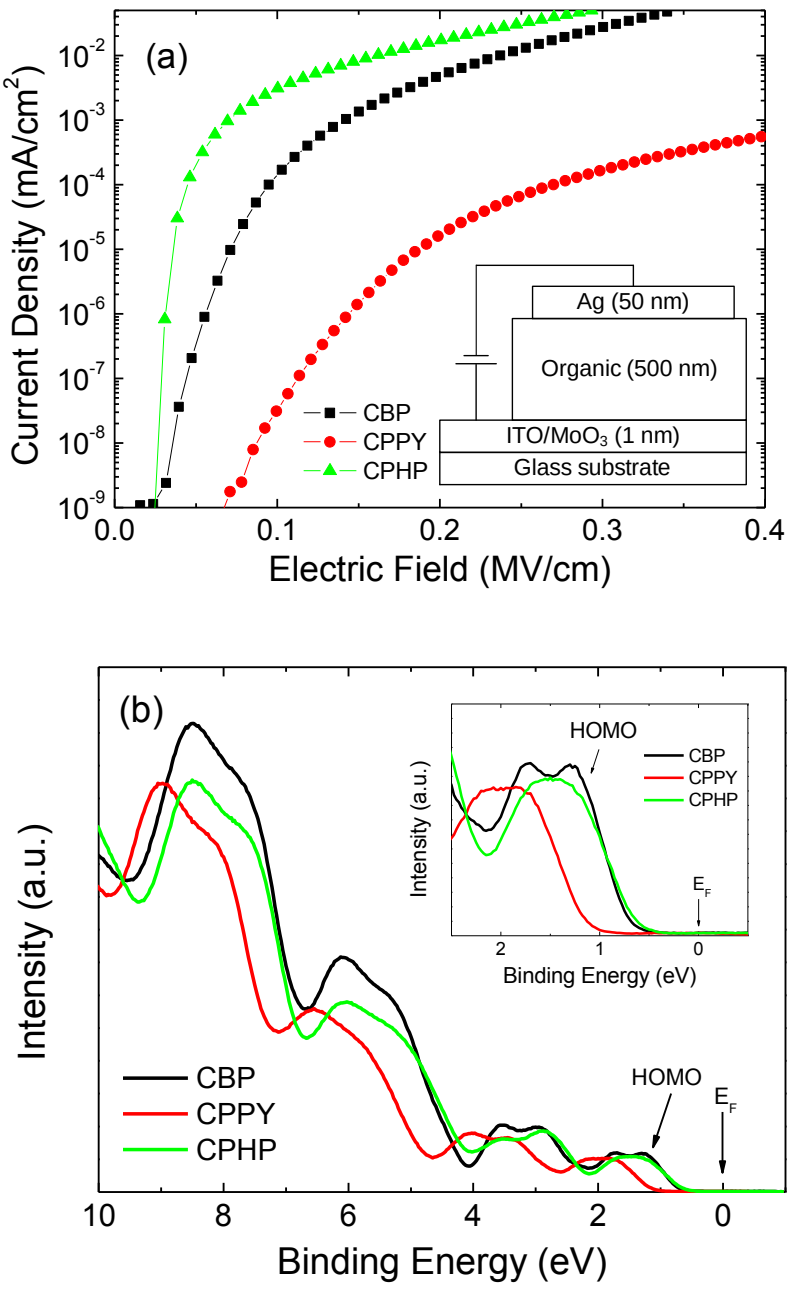

Figure 8.7: a) Charge-transport characteristics of hole-only devices incorporating CBP, CPPY and CPHP. Inset: Device structure. b) UPS spectral data for the host materials. Inset: Zoom region showing the energy level alignment of each host on ITO/MoO_3.

8.4 Conclusions

In summary, we have demonstrated new carbazole-based host materials 4,5'-*N*,*N*'-dicarbazolyl-(2-phenylpyridine) (**CPPY**) and 4,5'-*N*,*N*'-dicarbazolyl-(2-phenylpyrimidine) (**CPHP**), which can be used to give highly simplified single-layer OLEDs with unprecedented performance. Both materials are easily prepared in high yield by a two-step Suzuki coupling/Ullman condensation route. Devices based on these hosts using $Ir(ppy)_2(acac)$ as emitter exhibit maximum external quantum efficiencies of 21.5% and 26.8%, respectively, the highest reported to date for a simplified single-layer device. Experimental and theoretical studies confirm that the LUMO energies of these materials are notably lower than the commonly used host CBP, while the HOMO energies remain largely unchanged. This design facilitates improved electron injection and transport while preserving hole-transporting functionality, resulting in bipolar hosts with significantly improved device efficiencies. Based on these results we demonstrate that single-layer OLEDs with performance comparable to those of conventional multilayer devices can be achieved by careful control of charge transport within the host and the energy level alignment of the host material at metal/organic interfaces.

8.5 Notes and References

The work described in this chapter has been published as:

- Z. M. Hudson, Z. B. Wang, M. G. Helander, Z.-H. Lu, S. Wang. *Adv. Mater.* **2012**, **2012**, *24*, 2922-2928.

References

(1) a) L. Xiao, Z. Chen, B. Qu, J. Luo, S. Kong, Q. Gong, J. Kido, *Adv. Mater.* **2010**, *23*, 926-952. b) Y. Tao, C. Yang, J. Qin, *Chem. Soc. Rev.* **2011**, *40*, 2943-2970. c) Y. Shirota, H. Kageyama, *Chem. Rev.* **2007**, *107*, 953-1010. d) Y. Chi, P.-T. Chou, *Chem. Soc. Rev.*, **2010**, *39*, 638-655. d) Y. You, S. Y. Park, *Dalton Trans.*, **2009**, 1267-1272. e) J. A. G. Williams, S. Develay, D. L. Rochester, L. Murphy, *Coord. Chem. Rev.*, **2008**, *252*, 2596-2611.

(2) a) M. E. Thompson, *MRS Bulletin*, **2007**, *32*, 694 and references therein. b) M. A. Baldo, S. R. Forrest, M. E. Thompson in *Organic Electroluminescence*, Z. H. Kafafi ed., Ch. 6, p. 267. Taylor & Francis: New York, 2005. c) K. Chen, C. H. Yang, Y. Chi, C. S. Liu, C. H. Chang, C. C. Chen, C. C. Wu, M. W. Chung, Y. M. Cheng, G. H. Lee, P. T. Chou, *Chem. Eur. J.* **2010**, *16*, 4315. d) F.-M. Hwang, H. Y. Chen, P. S. Chen, C. S. Liu, Y. Chi, C. F. Shu, F. I. Wu, P. T. Chou, S. M. Peng, G. H. Lee, *Inorg. Chem*, **2005**, *44*, 1344. e) T. C. Lee, J. Y. Hung, Y. Chi, Y. M. Cheng, C. H. Lee, P. T. Chou, C. C. Chen, C. H. Chang, C. C. Wu, *Adv. Funct. Mater*. **2009,** *19*, 2639. f) Y. H. Song, Y. C. Chiu, Y. Chi, Y. M. Cheng, C. H. Lai, P. T. Chou, K. T. Wong, M. H. Tsai, C. C. Wu, *Chem. Eur. J.* **2008**, *14*, 5423. g) C. F. Chang, Y. M. Cheng, Y. Chi, Y. C. Chiu, C. C. Lin, G. H. Lee, P. T. Chou, C. C. Chen, C. H. Chang, C. C. Wu, *Angew. Chem. Int. Ed*., **2008**, *47*, 4542.

(3) a) K. R. J. Thomas, M. Velusamy, J. T. Lin, Y. T. Tao, C. H. Chuen, *Adv. Funct. Mater.* **2004**, *14*, 387-392. b) H. Zhang, C. Huo, J. Zhang, P. Zhang, W. Tian, Y. Wang, *Chem. Commun.* **2006**, 281-283. c) T. H. Huang, J. T. Lin, L. Y. Chen, Y. T. Lin, C. C. Wu, *Adv. Mater.* **2006**, *18*, 602-606. d) M. Lai, C. Chen, W. Huang, J. T. Lin, T. Ke, L. Chen, M. Tsai, C. Wu, *Angew. Chem. Int. Ed.* **2008**, *47*, 581-585. e) C. Chen, W. Huang, M. Lai, W. Tsao, J. T. Lin, Y. Wu, T. Ke, L. Chen, C.

Wu, *Adv. Funct. Mater.* **2009**, *19*, 2661-2670. f) Z. Liu, M. G. Helander, Z. Wang, Z. Lu, *Org. Electron.* **2009**, *10*, 1146-1151. g) Z. Liu, M. G. Helander, Z. Wang, Z. Lu, *J. Phys. Chem. C* **2010**, *114*, 11931-11935. h) N. C. Erickson, R. J. Holmes, *Appl. Phys. Lett.* **2010**, *97*, 083308. i) X. Qiao, Y. Tao, Q. Wang, D. Ma, C. Yang, L. Wang, J. Qin, F. Wang, *J. Appl. Phys*. **2010**, *108*, 034508.

(4) a) Y. Sun, N. C. Giebink, H. Kanno, B. Ma, M. E. Thompson, S. R. Forrest, Nature, 2006, 440, 908. b) S. Reineke, F. Lindner, G. Schwartz, N. Seidler, K. Walzer, B. Lussem, K. Leo. *Nature*, **2009**, 459, 234-238. c) Z. B. Wang, M. G. Helander, J. Qiu, D. P. Puzzo, M. T. Greiner, Z. M. Hudson, S. Wang, Z. W. Liu, Z. H. Lu. *Nature Photon.* **2011**, *5*, 753.

(5) a) Y. Tao, Q. Wang, C. Yang, Q. Wang, Z. Zhang, T. Zou, J. Qin, D. Ma, *Angew. Chem. Int. Ed.* **2008**, *47*, 8104-8107. b) F. Hsu, C. Chien, C. Shu, C. Lai, C. Hsieh, K. Wang, P. Chou, *Adv. Funct. Mater*. **2009**, *19*, 2834-2843. c) Z. Q. Gao, M. Luo, X. H. Sun, H. L. Tam, M. S. Wong, B. X. Mi, P. F. Xia, K. W. Cheah, C. H. Chen, *Adv. Mater*. **2009**, *21*, 688-692. d) H. Chou, C. Cheng, *Adv. Mater*. **2010**, *22*, 2468-2471. e) M. M. Rothmann, E. Fuchs, C. Schildknecht, N. Langer, C. Lennartz, I. Munster, P. Strohriegl, *Org. Electron.* **2011**, *12*, 1192-1197. f) C. Cai, S. Su, T. Chiba, H. Sasabe, Y. Pu, K. Nakayama, J. Kido, *Org. Electron.* **2011**, *12*, 843-850. g) A. Chaskar, H. Chen, K. Wong, *Adv. Mater.* **2011**, *23*, 3876-3895. h) Y. Chen, W. Hung, H. You, A. Chaskar, H. Ting, H. Chen, K. Wong, Y. Liu, *J. Mater. Chem.* **2011**, *21*, 14971-14978.

(6) a) K. Wong, Y. Chen, Y. Lin, H. Su, C. Wu, *Org. Lett.* **2005**, *7*, 5361-5364. b) M. H. Tsai, H. W. Lin, H. C. Su, T. H. Ke, C. C. Wu, F. C. Fang, Y. L. Liao, K. T. Wong, C. I. Wu, *Adv. Mater*. **2006**, *18*, 1216-1220. c) M. H. Tsai, Y. H. Hong, C. H. Chang, H. C. Su, C. C. Wu, A. Matoliukstyte, J. Simokaitiene, S. Grigalevicius, J. V. Grazulevicius, C. P. Hsu, *Adv. Mater.* **2007**, *19*, 862-866. d) S. Su, H. Sasabe, T. Takeda, J. Kido, *Chem. Mater.* **2008**, *20*, 1691-1693. e) T. Tsuzuki, S. Tokito, *Appl. Phys. Lett.* **2009**, *94*, 033302. f) J. He, H. Liu, Y. Dai, X. Ou, J. Wang, S. Tao, X. Zhang, P. Wang, D. Ma, *J. Phys. Chem. C* **2009**, *113*, 6761-6767. g) H. Fukagawa, N. Yokoyama, S. Irisa, S. Tokito, *Adv. Mater.* **2010**, *22*, 4775-4778. h) P. Schrogel, A. Tomkeviciene,

P. Strohriegl, S. T. Hoffmann, A. Kohler, C. Lennartz, *J. Mater. Chem.* **2011**, *21*, 2266-2273. i) T. Motoyama, H. Sasabe, Y. Seino, J. Takamatsu, J. Kido, *Chem. Lett.* **2011**, *40*, 306-308.

(7) Z. B. Wang, M. G. Helander, J. Qiu, D.P. Puzzo, M. T. Greiner, Z. W. Liu, Z. H. Lu, *Appl. Phys. Lett.* **2011**, *98*, 073310.

(8) A. S. Voisin-Chiret, M. Muraglia, G. Burzicki, S. Perato, F. Corbo, J. Sopkova-de Oliveira Santos, C. Franchini, S. Rault, *Tetrahedron* **2010**, *66*, 8000-8005.

(9) A. L. Spek, Acta Cryst. 1990, A46, C34. PLATON – a Multipurpose Crystallographic Tool, Utrecht University, Utrecht, The Netherlands, A. L. Spek (2006).

(10) P. J. Low, M. A. J. Paterson, D. S. Yufit, J. A. K. Howard, J. C. Cherryman, D. R. Tackley, R. Brook, B. Brown, *J. Mater. Chem.* **2005**, *15*, 2304-2315.

(11) C.-L. Chiang, S.-M. Tseng, C.-T. Chen, C.-P. Hsu, C.-F. Shu, *Adv. Funct. Mater.* **2008**, *18*, 248-257.

Chapter 9

Probing the Structural Origins of Vapochromism of a Triarylboron-Functionalized Pt(II) Acetylide by Optical and Multinuclear Solid-State NMR Spectroscopy

9.1 Introduction

There has been considerable interest in recent years in the development of vapochromic sensor materials for the detection of volatile organic compounds (VOCs).[1-3] Such materials reversibly show changes in absorption and/or luminescence colour on exposure to VOCs, and are attractive due to their ability to provide a highly sensitive and rapid response to volatile contaminants, as well as their potential for use in portable fibre-optic devices.[3c,3d,4] Vapochromic materials based on Au(I)[3] and Pt(II)[1,2a-h] are the most extensively investigated of these, and usually take advantage of metal-metal (or 'metallophilic') interactions in the solid state. The enhancement or disruption of this interaction upon adsorption of VOCs can thereby alter the HOMO-LUMO gap, leading to distinct absorption or emission colour changes.

Luminescent materials based on triarylboranes have also been the focus of much recent research activity, though until now towards entirely different applications. Due to the electron-accepting empty p_π orbital on the boron centre, these compounds have been developed into a wide range of functional materials.[5] These include highly efficient luminescent and electron-transport materials for organic light-emitting diodes (OLEDs),[6] compounds with nonlinear optical properties,[7] and highly sensitive and selective chemical sensors for fluoride and cyanide.[8] Furthermore, the triarylboron group has recently been shown to greatly enhance MLCT phosphorescence in complexes of Pt(II) and Ir(III), making this functionality attractive for use in phosphorescent materials as well.[9]

Herein we report the first example of a vapochromic material based on triarylboron and Pt(II), which shows a distinct luminescent response to a wide variety of VOCs (Compound **9.1,** Figure 9.1). Furthermore, extensive investigations into the structural origins of vapochromism in this system using optical and multinuclear solid-state ^{195}Pt, ^{13}C, ^{11}B and ^{1}H NMR spectroscopy have indicated that the mechanism of this vapochromic behaviour arises not from differences in metallophilic or π-π stacking interactions, but instead from modulations of excited state energy levels on individual molecules due to interactions with adsorbed VOC analyte. We report herein the first comprehensive solid-state NMR study on a vapochromic material, and demonstrate that the vapochromism of this material differs in origin from those of all previously reported examples.

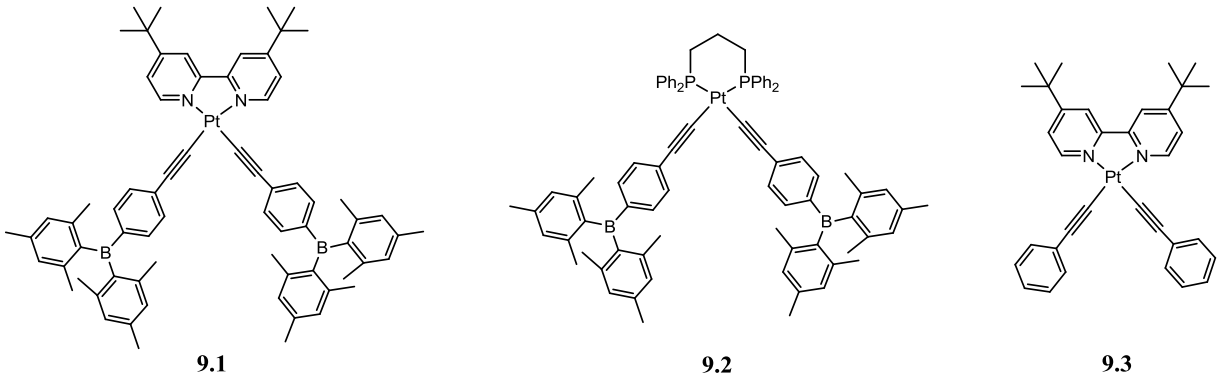

9.1 **9.2** **9.3**

Figure 9.1: Structures of Pt(II) complexes used in this study.

9.2 Experimental

9.2.1 General Procedures

Experimental techniques and instruments used follow those described in section 2.2. Powder X-ray diffraction patterns were acquired using a Bruker D8 Discover diffractometer using Cu-Kα radiation (λ = 1.54056 Å); samples of **9.1** were exposed to the vapour of each solvent for a minimum of 8 hours in a sealed chamber and then packed into glass capillaries which were sealed with silicon grease.

Photoluminescent quantum yields were measured using the optically dilute method ($A \approx 0.1$) at room temperature in degassed CH_2Cl_2 using *fac*-Ir(ppy)$_3$ in 2-MeTHF as the standard ($\Phi_r = 0.97$).[10] Vapour-dependent solid-state emission spectra were obtained by exposing a powdered film of **9.1** in a quartz cuvette to a drop of solvent vapour. Films of **9.1** were prepared by manually applying small amounts of powdered material to the quartz surface. Phosphorescent decay lifetimes were below the measurement limit for our instrument (≤ 2 μs). Molecular orbital calculations were performed using the Gaussian 03 program suite using crystal structures as the starting point for geometry optimizations where possible. The theoretical absorption spectrum of **9.1** was generated using the Gausssum 2.1.6 software package.[11] Calculations were performed at the B3LYP level of theory using LANL2DZ as the basis set for Pt, and 6-31G* for all other atoms.[12] The syntheses of *p*-(dimesitylboryl)phenylacetylene,[13] Pt(dbbpy)Cl_2 (dbbpy = 4,4'-di-*tert*-butyl-2,2'-bipyridine),[14] Pt(dppp)Cl_2 (dppp = 1,3-diphenylphosphinopropane)[15] and Pt(dbbpy)(C≡CC_6H_5)$_2$ (compound **9.3**)[16] have been reported previously.

9.2.2 Synthesis of Pt(dbbpy)(C≡CC_6H_4BMes_2)$_2$ (9.1):

To a 100 mL Schlenk flask with stir bar and condenser was added *p*-(dimesitylboryl)phenylacetylene (143 mg, 0.408 mmol, 2.2 eq.), dichloro(dbbpy)platinum(II) (99 mg, 0.185 mmol, 1.0 eq.), CuI (8 mg, 0.041 mmol, 0.1 eq.) and 55 mL degassed THF/NEt_3 (10:1 v/v). The mixture was heated to reflux under N_2 for 16h, then concentrated *in vacuo* and partitioned between CH_2Cl_2 and water. The aqueous layer was further extracted with 2 x 30 mL CH_2Cl_2, dried with $MgSO_4$, filtered, and concentrated to 5 mL with the appearance of a brown precipitate. The mother liquor was decanted, and the precipitate washed further with 3 mL CH_2Cl_2 and 3 mL Et_2O, affording compound **9.1** as an orange powder (188 mg, 87%). ^{1}H NMR (400 MHz, C_6D_6) δ 9.60 (d, br, J = 4.7 Hz, 2H, *bpy*), 7.90 (d, J = 7.9 Hz, 4H, -*Ph*-), 7.82 (d, J = 8.1 Hz, 4H, -*Ph*-), 7.59 Hz (s, br, 2H, *bpy*), 6.92 (s, 8H, *Mes*), 6.61 (d, J = 4.7 Hz, 2H, *bpy*), 2.32 (s, 12H, *Mes*), 2.31 (s, 24H, *Mes*), 1.09 (s, 18H, *t-Bu*) ppm; ^{13}C NMR (100 MHz, C_6D_6) δ 162.1, 156.7, 150.4, 143.2, 142.5, 141.1, 138.6, 137.1, 134.2, 132.0, 128.8, 128.2, 127.9, 124.2, 119.8, 35.4, 30.1, 23.9, 21.3

ppm; Anal. Calc'd for $C_{70}H_{76}B_2N_2Pt$: C 72.35, H 6.59, N 2.41, found C 72.38, H 6.55, N 2.25. Single crystals of **9.1** · $4CH_2Cl_2$ were dried under vacuum prior to analysis, though may contain residual solvent.

9.2.3 Synthesis of Pt(dppp)(C≡CC_6H_4BMes_2)$_2$ (9.2):

Prepared similarly to **9.1**, using *p*-(dimesitylboryl)phenylacetylene (135 mg, 0.386 mmol, 2.2 eq.), Pt(dppp)Cl_2 (119 mg, 0.175 mmol, 1.0 eq.), CuI (7 mg, 0.039 mmol, 0.1 eq.) and 55 mL degassed THF/NEt_3 (10:1 v/v). Purified by column chromatography on silica (hexanes, then CH_2Cl_2) then concentrated *in vacuo* to afford compound **9.2** as a white powder (129 mg, 56%). ^{1}H NMR (400 MHz, acetone-d_6) δ 7.95 (m, br, 8H, *dppp*), 7.42 (m, 8H, *dppp*), 7.40 (m, 4H, *dppp*), 7.14 Hz (d, J = 7.2 Hz, 4H, -*Ph*-), 6.78 (s, 8H, *Mes*), 6.77 (d, *J* = 7.2 Hz, 4H, -*Ph*-), 2.81 (m, 2H, *dppp*), 2.78 (m, 4H, *dppp*), 2.24 (s, 12H, *Mes*), 1.93 (s, 24H, *Mes*) ppm; ^{13}C NMR (100 MHz, acetone-d_6) δ 142.9, 142.5, 141.2, 139.1, 136.65, 134.6, 132.9, 132.2, 131.3, 129.7, 129.1, 128.9, 115.1, 110.6, 26.1, 23.6, 21.2, 20.7 ppm; ^{31}P NMR (162 MHz, acetone-d_6) δ -5.26 (t, 2P, $J_{P\text{-}Pt}$ = 1088.9 Hz) ppm. Anal. Calc'd for $C_{79}H_{78}B_2P_2Pt$: C 72.65, H 6.02, found C 72.68, H 6.04.

9.2.4 Single Crystal X-Ray Diffraction Analysis

Single crystals of compound **9.1**·$4CH_2Cl_2$ were obtained from CH_2Cl_2/hexanes solution while those of **9.2**·toluene were obtained from toluene/hexanes. Data were collected on a Bruker AXS Apex II single-crystal X-ray diffractometer with graphite-monochromated Mo Kα radiation, operating at 50 kV and 30 mA at 180 K. Data were processed on a PC with the aid of the Bruker SHELXTL software package (version 6.14)[17] and corrected for absorption effects. All structures were solved by direct methods. The crystal lattice of **9.1** contains 4 CH_2Cl_2 solvent molecules per molecule of **9.1** while the lattice of **9.2** contains three toluene molecules per molecule of **9.2**. All solvent molecules were modeled and refined successfully. All non-hydrogen atoms were refined anisotropically. The positions of hydrogen atoms were

calculated, and their contributions in structural factor calculations were included. The crystal structural data of **1**·4CH_2Cl_2 and **2**·toluene have been deposited at the Cambridge Crystallographic Data Center, CCDC-797877, 797878. Crystal data for these compounds are listed in Table 9.1, and important bond lengths and angles may be found in Table 9.2.

Table 9.1: Crystallographic data for compounds 9.1 and 9.2

Compound	**9.1**	**9.2**
Formula	$C_{74}H_{84}B_2Cl_8N_2Pt$	$C_{93}H_{94}B_2P_2Pt$
FW	1501.74	1490.33
Space Group	Pnma	P2(1)/n
a, Å	23.2804(9)	24.4132(3)
b, Å	29.7380(11)	14.6769(2)
c, Å	11.1936(4)	25.1137(4)
α, °	90	90
β, °	90	109.7190(10)
γ, °	90	90
V, $Å^3$	7749.5(5)	8470.8(2)
Z	4	4
D_{calc}, g cm^{-1}	1.287	1.169
T, K	180(2)	180(2)
μ, mm^{-1}	2.126	1.736
$2\theta_{max}$, °	54.30	54.36
Reflns measured	23693	39490
Reflns used (R_{int})	8652 (0.0294)	18687 (0.0639)
Parameters	409	837
Final R Values [I > 2σ(I)]:		
R_1[a]	0.0452	0.0534
wR_2[b]	0.1208	0.1268
R values (all data):		
R_1[a]	0.0557	0.0998
wR_2[b]	0.1257	0.1495
Goodness-of-fit on F^2	1.095	0.996

[a] $R_1 = \Sigma[(|F_0| - |F_c|) / \Sigma |F_0|$

[b] $wR2 = [\Sigma w[(F_0^2-F_c^2)^2] / \Sigma[w(F_0^2)^2]]^{1/2}$

$w = 1 / [\sigma^2(F_0^2) + (0.075P)^2]$, where $P = [Max (F_0^2, 0) + 2F_c^2] / 3$

Table 9.2: Selected bond lengths (Å) and angles (°) for compounds 9.1 and 9.2.

Compound 9.1			
Pt(1)-C(1)	1.938(4)	B(1)-C(6)	1.555(6)
Pt(1)-N(1)	2.060(3)	B(1)-C(18)	1.574(6)
N(1)-C(27)	1.333(5)	B(1)-C(9)	1.583(6)
N(1)-C(31)	1.352(5)	C(1)-C(2)	1.217(5)
C(1)A-Pt(1)-C(1)	87.7(2)	C(6)-B(1)-C(18)	116.8(3)
C(1)-Pt(1)-N(1)A	96.77(14)	C(6)-B(1)-C(9)	120.6(4)
C(1)A-Pt(1)-N(1)	96.77(14)	C(18)-B(1)-C(9)	122.6(4)
N(1)A-Pt(1)-N(1)	78.72(17)	C(2)-C(1)-Pt(1)	178.6(4)
Compound 9.2			
Pt(1)-C(28)	2.009(6)	P(1)-C(27)	1.825(6)
Pt(1)-P(1)	2.2898(14)	P(1)-C(1)	1.825(6)
C(1)-C(6)	1.384(7)	C(33)-B(1)	1.560(9)
C(1)-C(2)	1.382(8)	C(36)-B(1)	1.591(9)
P(1)-C(7)	1.823(6)	C(45)-B(1)	1.584(9)
C(28)-Pt(1)-C(54)	86.2(2)	C(33)-B(1)-C(45)	120.9(5)
C(54)-Pt(1)-P(2)	87.81(16)	C(33)-B(1)-C(36)	116.7(5)
C(28)-Pt(1)-P(1)	91.09(15)	C(45)-B(1)-C(36)	122.4(6)
P(2)-Pt(1)-P(1)	94.87(5)	C(29)-C(28)-Pt(1)	176.0(5)

9.2.5 Solid State NMR

Solid-state NMR spectra were acquired using a Varian Infinity Plus console and a 9.4 T Oxford magnet at resonance frequencies of 399.7 MHz for ^{1}H, 128.3 MHz for ^{11}B, 100.5 MHz for ^{13}C, and 85 MHz for ^{195}Pt. Samples studied include neat **9.1** (solid, amorphous samples without adsorption of VOCs), as well as samples of **9.1** exposed to CH_2Cl_2, benzene, and hexane vapours in a sealed chamber for a minimum of 8 hours. The samples were packed in 4 mm o.d. zirconia rotors sealed with air-tight Teflon caps. All solid-state NMR experiments were conducted using a Varian/Chemagnetics 4mm HX MAS probe. Bloch-decay magic-angle spinning (MAS) experiments were used for ^{1}H spectra, and were referenced to the signal from solid adamantane under MAS at $\delta_{iso}(^{1}H)$ = 1.85 ppm. 90°-τ_1-180°-τ_2-acq echo experiments using 1.5 μs selective 90° pulse lengths (3.0 μs refocusing pulses) were used to acquire ^{11}B spectra of samples under stationary and MAS conditions, using high-power CW ^{1}H decoupling ($\nu_2 \approx 50$ kHz); using liquid $F_3B{\bullet}O(C_2H_5)_2$ as reference at $\delta_{iso}(^{11}B)$ = 0 ppm. ^{13}C NMR spectra were acquired using ^{1}H-^{13}C variable-amplitude cross polarisation (VACP) MAS experiments,[18, 19, 20] with high-power ($\nu_2 \approx 50$ kHz) two-pulse phase-modulated (TPPM) ^{1}H decoupling;[21] spectra were referenced to solid adamantane under MAS at $\delta_{iso}(^{13}C)$ = 38.56 ppm.[22] ^{195}Pt NMR spectra of the sample of **1**•$4CH_2Cl_2$ were acquired using the WURST-CPMG protocol;[23,24,25] three sub-spectra were collected 150 kHz apart, using a 10 kHz spikelet spacing and 10 μs WURST pulses swept from +500 to -500 kHz and using a maximum rf power corresponding to a nutation rate of ca. 75 kHz. For neat **9.1**, C_6H_6@**9.1** and hexanes@**9.1**, ^{1}H-^{195}Pt CP/CPMG experiments[26,27] were used instead of the direct WURST-CPMG method; twelve sub-spectra were collected 40 kHz apart, using a 10 kHz spikelet spacing and 6.0 μs ^{195}Pt 180° pulses. All ^{195}Pt spectra were referenced using the signal from a 1 M aqueous solution of Na_2PtCl_6 at $\delta_{iso}(^{195}Pt)$ = 0 ppm.[28,29] Simulated spectra were generated with WSOLIDS,[30] for static spectra, or SIMPSON,[31] for MAS spectra.

9.3 Results and Discussion

9.3.1 Syntheses

Compounds **9.1** and **9.2** can be readily synthesized by a Cu(I)-catalyzed transmetallation reaction using two equivalents of *p*-(dimesitylboryl)phenylacetylene with the appropriate platinum(II) dichloride. (Figure 9.2) Compound **9.3** can be prepared analogously, using previously reported procedures.[16] These complexes can then be purified by column chromatography and isolated in high yield. Compound **9.1** is a very robust molecule with excellent stability under ambient conditions in both solution and the solid state, while compound **9.2** decomposes slowly under air. Both compounds have been fully characterized by NMR, elemental analyses and single-crystal X-ray diffraction.

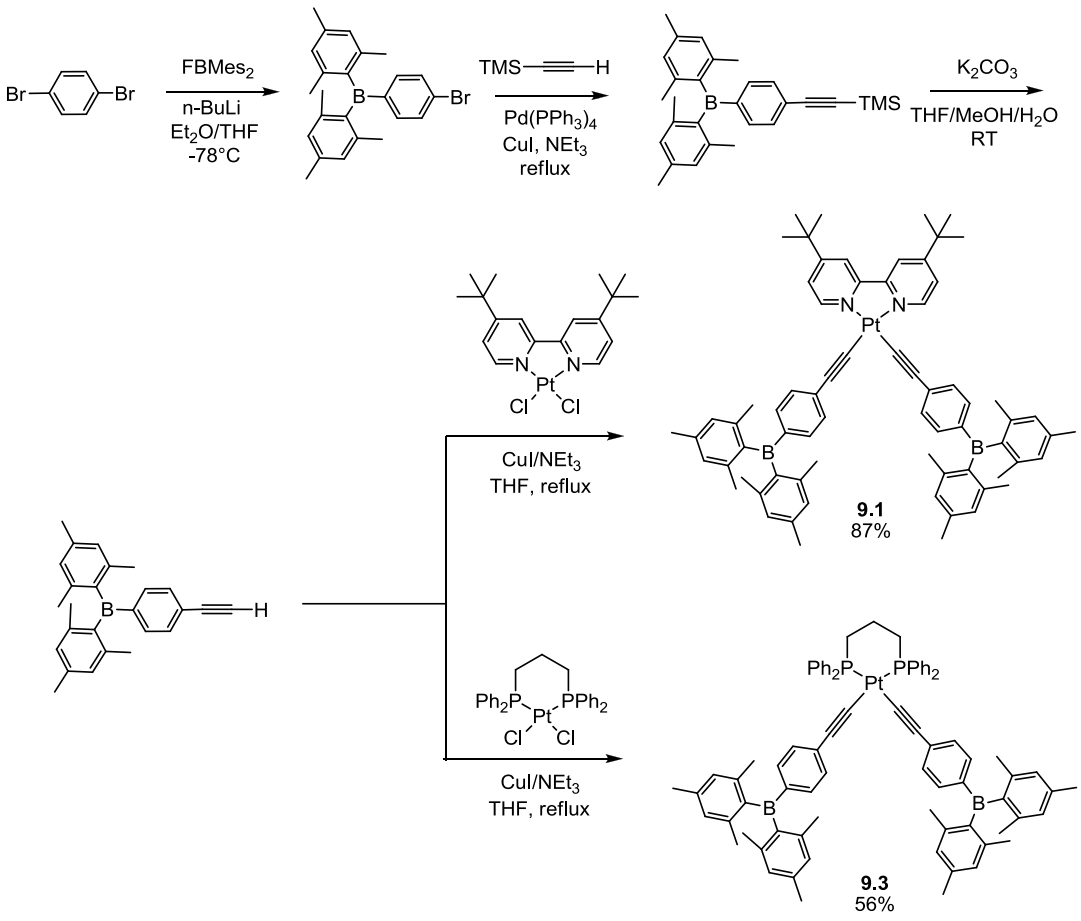

Figure 9.2: Synthesis of Pt(II) acetylides.

9.3.2 Crystal Structures

Single crystals of **9.1**•4CH_2Cl_2 and **9.2**•toluene for X-ray diffraction analyses were obtained by slow evaporation from CH_2Cl_2/hexanes and toluene/hexanes, respectively, and the structures are shown in Figure 9.3. The Pt-C bonds in **9.1**•4CH_2Cl_2 are significantly shorter than those in **9.2** due to the greater *trans*-effect of the phosphine chelate. Both compounds form crystal lattices with large voids, as evidenced by the large amount of solvent incorporated into both structures: four CH_2Cl_2 molecules per molecule of **9.1** and three toluene molecules per molecule of **9.2**. While many of the previously reported Pt(bipy) acetylide derivatives form either extended pseudolinear or dimeric antiparallel stacked structures in the solid state, with either short Pt···Pt distances (< 5 Å) or bipyridyl π–π stacking (< 4 Å), neither arrangement is observed for **9.1**•4CH_2Cl_2. Instead, the Pt(II) square planes of these molecules are oriented at approximately 75° with respect to each other, with the shortest intermolecular Pt···Pt distance being greater than 12 Å and the shortest π–π distances being ~5.7 Å (Figure 9.4). Similarly, in the crystal lattice of **9.2**•toluene (Figure 9.5), these planes are arranged nearly perpendicular to one another, and the shortest Pt···Pt distance is ~7.5 Å.

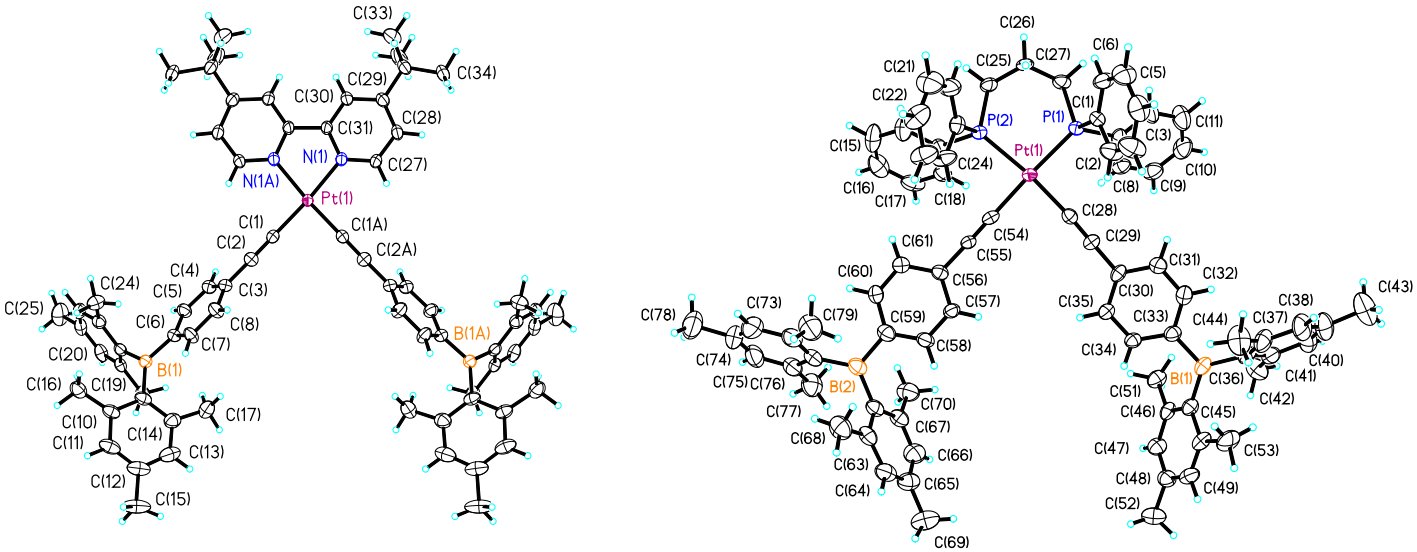

Figure 9.3: Crystal structures of 9.1 (left) and 9.2 (right).

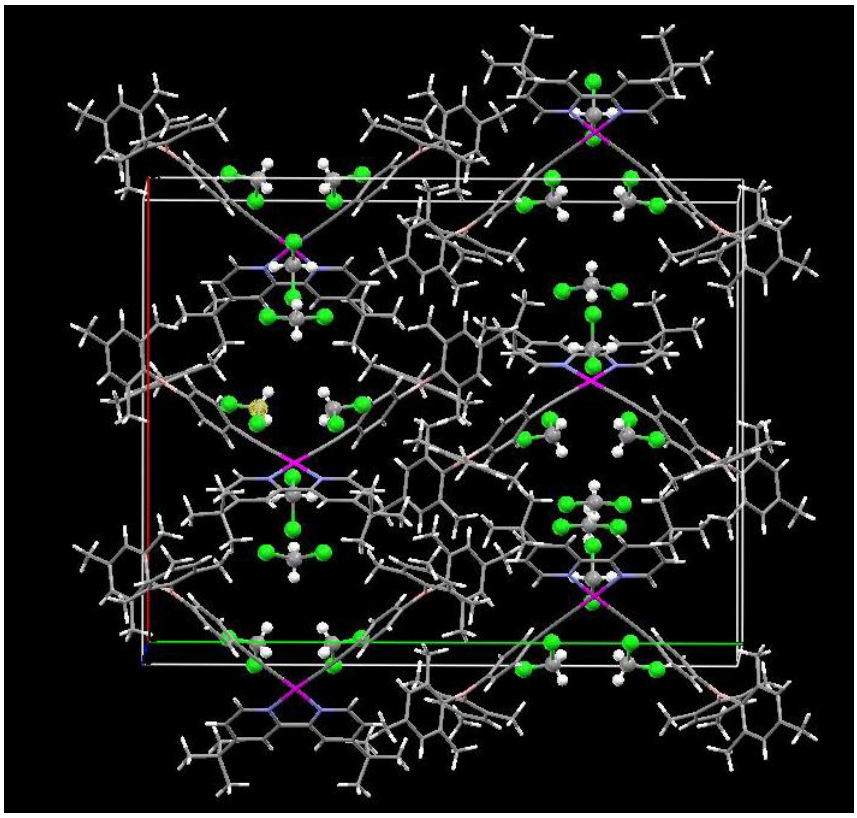

Figure 9.4: Unit cell packing diagram of **9.1**•4CH_2Cl_2 showing the locations of CH_2Cl_2 solvent molecules.

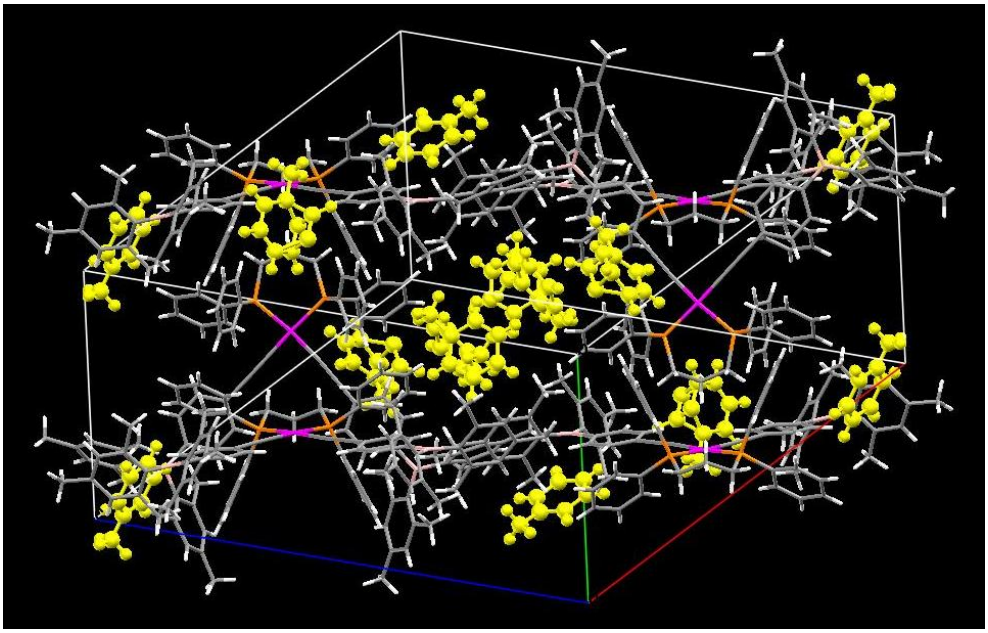

Figure 9.5: Unit cell packing diagram of **9.2**•toluene. Toluene solvent molecules are shown in yellow, with some molecules disordered.

9.3.3 Electronic and Photophysical Properties

Compound **9.1** is brightly phosphorescent in the solid state and solution (Φ = 0.73 in CH_2Cl_2). The absorption spectrum of **9.1** shows a low energy band at 407 nm in CH_2Cl_2, accompanied by a much more intense absorption at 357 nm. These transitions can be unambiguously assigned as a metal-to-ligand charge transfer (MLCT) to the bipyridine group, and a ligand-centered (LC) transition on the boron ligand, respectively. This is supported by the absorption spectra of control compounds **9.2** and **9.3**, which possess only the LC state and the MLCT state, respectively. (Figure 9.6) Cyclic voltammetry experiments further establish that the LUMO of **9.1** is centered on the bipyridine chelate, as the first reduction peak of this compound is very similar to that of **9.3**. In contrast, compound **9.2** undergoes reduction at a much more negative potential typical of triarylboranes (Table 9.3). DFT calculations further establish that the HOMOs for **9.1**-**9.3** are dominated by the acetylene π and Pt *d* orbitals, while the LUMO is located on the bipyridine chelate in **9.1** and **9.3** and the boron ligands in **9.2**, with the orbitals from the boron ligands comprising the LUMO+3 and LUMO+4 in **9.1** (see appendix, section 9.6). Therefore, compound **9.1** can be characterized as having two main electronic excited states: the lower (MLCT) state centered on the bipyridine chelate, and a higher energy (LC) state arising from the boron ligands.

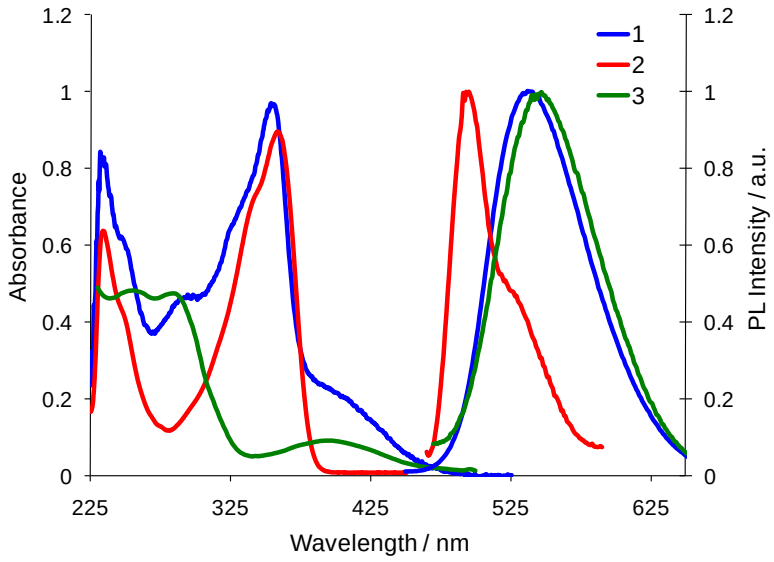

Figure 9.6: Absorption and normalized emission spectra of **9.1**-**9.3** at 10^{-5} M in CH_2Cl_2 at 298 K.

Table 9.3: Photophysical properties of 9.1-9.3

Compound	Absorption, λ_{max} ε (10^4 cm^{-1} M^{-1})[a]	λ_{max} (nm) CH_2Cl_2[a] / solid	Φ_P[b]	$E_{1/2}^{red}$ (V)[c]
9.1	248 (6.10), 357 (9.55), 407 (2.00)	541/559	0.73	-1.78
9.2	236 (6.22), 360 (8.87)	496/496	0.002	-2.26
9.3	256 (4.81), 286 (4.73), 386 (0.89)	548/535	0.51	-1.80

[a] Measured in CH_2Cl_2 at $1x10^{-5}$ M, [b] In CH_2Cl_2 solution: relative to $Ir(ppy)_3$ (Φ = 0.97 in 2-MeTHF),[10] ±10%. [c] In DMF relative to $FeCp_2^{0/+}$.

In CH_2Cl_2, compound **9.1** displays a bright and featureless yellow phosphorescence peak at 541 nm, which is similar to that of **9.3** and attributable to MLCT phosphorescence. In contrast, compound **9.2** displays a weak phosphorescence band with well resolved vibrational features at 498 nm, due to emission from the LC state on the triarylboron acetylide ligands (Figure 9.6). The absorption and emission spectra of compound **9.1** both show negative solvatochromism typical of the polar ground state in Pt(II) complexes, though the blue shift in the absorption spectrum is much greater for the low energy MLCT band (50 nm) than the intense LC band (10 nm). Similarly, the emission spectrum shows a 25 nm blue shift from hexanes to CH_2Cl_2. In contrast, the emission spectrum of **9.2** shows only a small blue shift with increasing solvent polarity (9 nm from hexane to CH_2Cl_2). In both cases, the shape of the emission band does not change significantly with solvent. Hence, we can conclude that the origin of the electronic transitions in solution remain MLCT for **9.1** and LC for **9.2** for all of the solvents we investigated; however, a remarkably different phenomenon was observed in the solid state.

9.3.4 Vapochromism

In the solid state, compound **9.1** shows reversible vapochromism on exposure to organic vapours. Both compounds **9.1** and **9.2** are luminescent in the solid state under UV irradiation, with emission energies similar to those in CH_2Cl_2 solution (Table 9.3). When solid or neat films of **9.1** are exposed to VOCs, however, the absorption and emission colors of the sample are observed to shift according to the nature of

the VOC, producing a response in a matter of seconds (Figure 9.7). These luminescent changes are reversible either by applying a vacuum or by dissolution and recasting of the film, and are persistent in the presence of the detected VOC. The original colour of the sample can also be restored on extended standing under air or mild heating to remove solvent vapour.

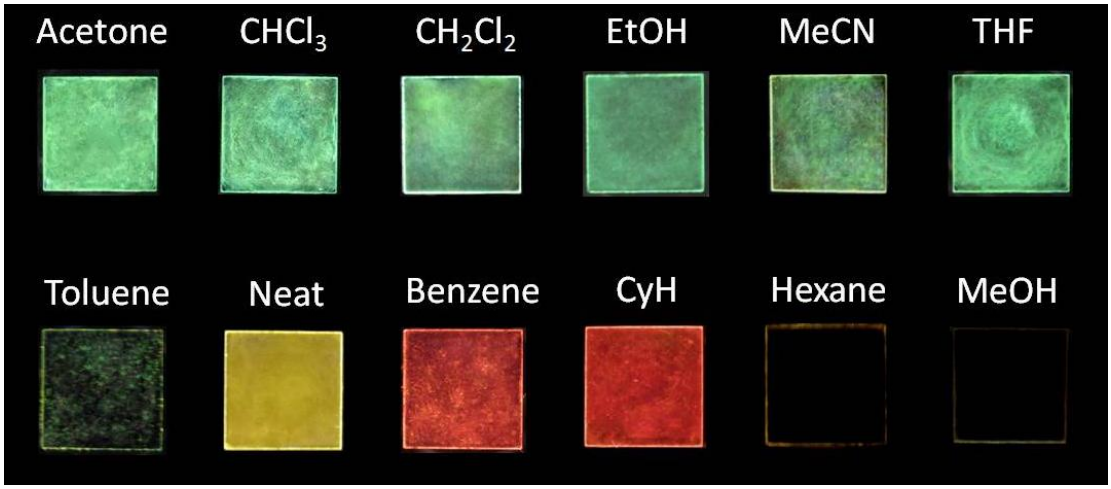

Figure 9.7: The response of solid films of **9.1** under UV irradiation to various organic vapours.

Many polar solvents, such as CH_2Cl_2, $CHCl_3$, CH_3CN, acetone, THF, and EtOH induce an emission colour shift from yellow (λ_{max} = 559 nm) to green (λ_{max} = 490-500 nm). This is highly unusual, as application of a variety of very different solvent molecules induces the same response. (Figure 9.8) In contrast, application of benzene, cyclohexane, or 1,4-dioxane (not shown) vapours switches the emission colour to red, with the appearance of a new broad emission peak at λ_{max} = 580 – 620 nm. (Figure 9.9) As dioxane contains oxygen donor atoms yet has a similar dielectric constant to benzene, the observation of a red shift suggests that solvent polarity is the key factor in determining the emission shift. Interestingly, exposure to linear hydrocarbons or MeOH quenches the emission of the sample entirely. Toluene was also observed to produce green emission, though the vapours were found to readily wet powdered films of **9.1**, making solid-state studies difficult. It should be noted however that a similar green emission peak

was present in the predominantly red emission spectra of benzene or cyclohexane-treated films of **9.1**. When **9.1** is placed in the presence of multiple solvents simultaneously, the effect of polar solvents such as CH_2Cl_2 that turn the sample green appears to be favoured.

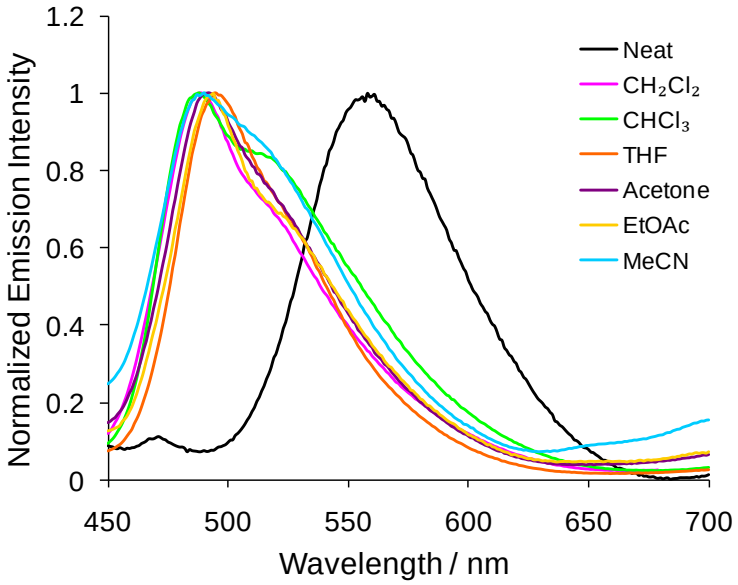

Figure 9.8: Normalized emission spectra for neat films of compound **9.1** before and after exposure to several organic vapours (λ_{ex} = 365 nm).

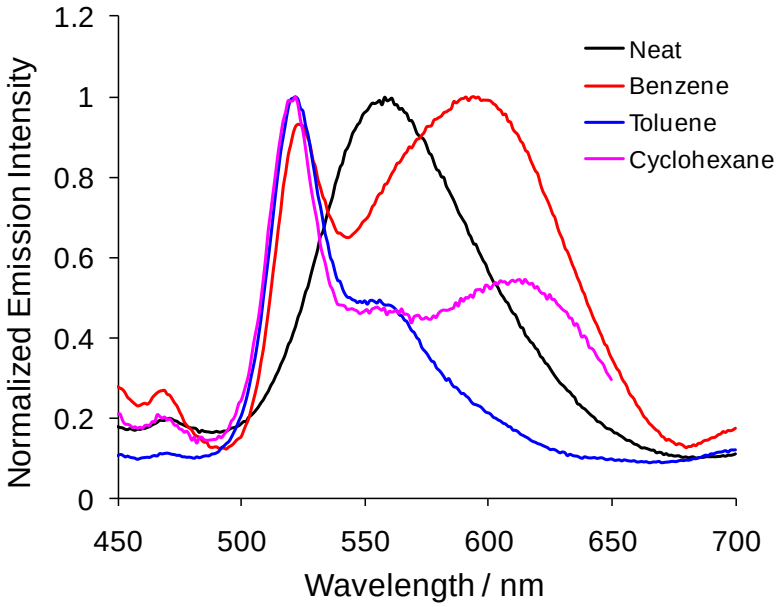

Figure 9.9: Normalized emission spectra for neat films of compound 9.1 before and after exposure to benzene, toluene and cyclohexane. (λ_{ex} = 365 nm).

This switch to green on exposure to polar solvent vapours may be explained as a solvent-induced inversion of the lowest energy excited state, from an MLCT transition to a LC transition. On exposure to vapours such as CH_2Cl_2, the emission energy and band shape of **9.1** shifts, closely resembling that of **9.2**, which emits from a ^{3}LC state with or without VOCs. This suggests that the emission from neat compound **9.2** and compound **9.1** after exposure to polar solvents have a common origin. This can be attributed primarily to a change in the MLCT level of **9.1**, as evidenced by solid-state absorption spectra of powdered films taken before and after exposure to VOCs. The absorption spectrum of a neat film of **9.1** closely resembles that observed in solution, but once VOCs such as CH_2Cl_2 are added, the MLCT band shifts to higher energy until obscured by the intense LC band.

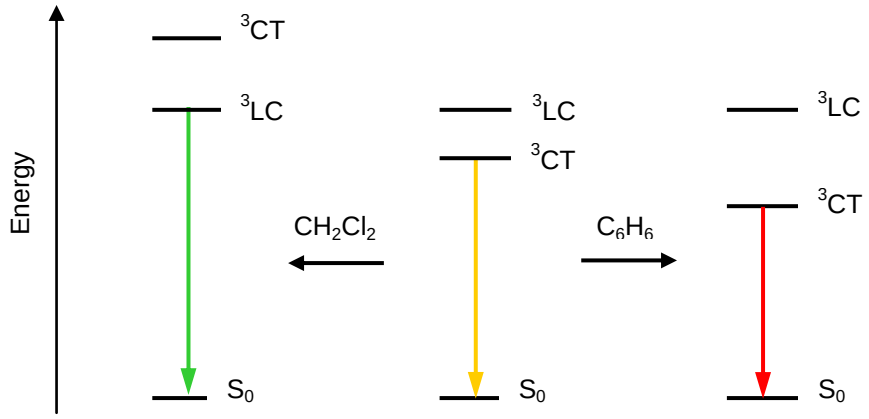

Figure 9.10: The impact of excited state level modulation on the emission colours of **9.1**, using CH_2Cl_2 and benzene as representative examples.

Inversion of CT and LC excited state energy levels due to solvent polarity has recently been demonstrated in solution-based systems by Castellano and coworkers for diacetylide Pt(II) bipyridine complexes with energetically proximate ^{3}CT and ^{3}LC states.[32] They have shown that the energy of the ^{3}CT state can be modulated by solvent polarity, leaving the ^{3}LC energy relatively unaffected. Pt(II) complexes are well known to display negative solvatochromism due to large ground state dipole moments, giving charge-transfer excited states that increase in energy with solvent polarity.[1,2] By varying the polarity of the

solvent, it is thus possible to alter the energy gap between the ^{3}CT and ^{3}LC states by modulation of the ^{3}CT energy level, thereby altering the degree of mixing between the two excited states. In this way, the lowest energy excited state from which the complex emits can be 'inverted,' from ^{3}CT in nonpolar media to ^{3}LC in polar media. However, the same "excited state inversion" phenomenon has not been observed in the solid state previously. Our observations indicate that the vapochromic response of **9.1** to polar VOCs such as CH_2Cl_2 is due to such excited state inversion, and represents the first observation of this phenomenon in solid-state systems. Conversely, nonpolar solvents such as benzene and cyclohexane appear to reduce the ^{3}CT energy, shifting the emission colour to red. Highly nonpolar solvents such as linear hydrocarbons reduce this energy further still, giving a ^{3}CT state so low in energy that vibronic quenching becomes dominant, rendering the sample non-emissive. (Figure 9.10)

Interestingly, a similar response is observed for MeOH vapour, though fluorescence quenching by methanol in various systems has been described previously.[33] In the case of **9.1**, the quenching of luminescence by methanol in the solid state may be due to the introduction of many closely spaced energy levels, which readily facilitate vibronic relaxation. Nonetheless, the fact that a similar excited state inversion was not observed for compound **9.1** in solution remains peculiar. It is likely that the localized dipole-dipole interactions between a molecule of **9.1** and guest solvent molecules occupying a specific region of free volume in the solid state differ substantially from the interactions between **9.1** and the continuously changing dipoles of the bulk solution.

9.3.5 X-ray Powder Diffraction Studies

In most previously reported Pt(II)-based vapochromic systems, the change in luminescence energy is a direct result of differences in the degree of intermolecular stacking involving the Pt(II) centers or, more rarely, π-π interactions.[1,2] However, the crystal structure of **9.1**•4CH_2Cl_2 contains no close contacts

between the square-planar Pt(II) units (all Pt-Pt distances > 12 Å). Furthermore, molecular modeling using two molecules of **9.1** (from the **9.1**•4CH_2Cl_2 crystal structure) suggests that the steric bulk of the *t*-butyl and dimesitylboron groups is inconsistent with close intermolecular contacts between the Pt atoms or the bipyridine rings, particularly as **9.1** has little conformational flexibility. To further investigate the origin of vapochromism in **9.1**, we examined this system using multinuclear solid-state NMR spectroscopy (SSNMR), and powder X-ray diffraction (PXRD). Neat **9.1** as well as samples of **9.1** exposed to the vapours of CH_2Cl_2, C_6H_6 and hexanes (termed solvent@**1** below) were studied as representative of systems featuring the yellow, green, red and quenched luminescent states, respectively.

PXRD patterns collected from neat **9.1** and from each VOC treatment are shown in Figure 9.11. It is immediately apparent that the structure of CH_2Cl_2@**9.1** matches that determined in the above single-crystal diffraction study of **9.1**•4CH_2Cl_2, and we will therefore identify this material as **9.1**•4CH_2Cl_2 below. Apart from the lower resolution, the diffraction patterns of neat **9.1**, C_6H_6@**9.1** and hexanes@**9.1** are very similar to that of **9.1**•4CH_2Cl_2, indicating that the structures of all four materials must be similar. The broadened diffraction peaks in these latter three materials are indicative of reduced long-range ordering, as compared to **9.1**•4CH_2Cl_2. This reduction in long range ordering may explain our inability to obtain X-ray quality single crystals from other solvents despite repeated attempts. It is possible that the combination of low conformational flexibility and the complicated molecular shape of **9.1** prevents stacking without void spaces, unless secondary molecules of suitable size and properties are present; these void spaces would of course provide a mechanism for reducing long-range order. The most important conclusion that can be drawn from this data is that there is only a minimal structural reorganization accompanying the vapochromism of **9.1**. Changes in metallophilic contacts can therefore be ruled out as the source of vapochromic behaviour in this system, as the crystal structure of **9.1**•4CH_2Cl_2 would require a significant reorganization to bring the Pt(II) moieties together; furthermore, this conclusion is entirely consistent with the SSNMR data presented below.

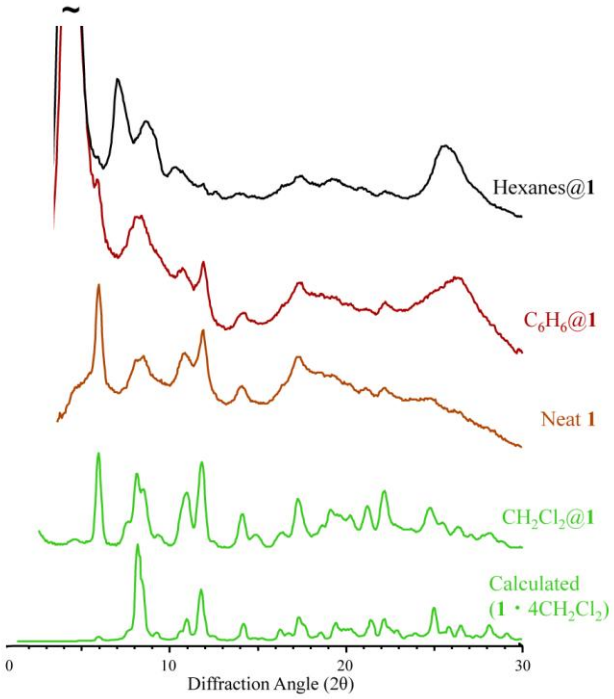

Figure 9.11: X-ray powder diffraction patterns measured after exposing **9.1** to selected solvent vapours.

9.3.6 Solid State NMR Experiments

SSNMR seems an obvious choice to characterize vapochromic systems, but to our knowledge has only been applied in two studies: the tetracyanoplatinum and tetracyanopalladium double salts of platinum tetra-arylisonitriles, with limited data.[1j,1k] The results presented below demonstrate the utility of multinuclear SSNMR for investigating vapochromic materials. First, ^{1}H and ^{13}C NMR spectra are used to demonstrate that the solvent molecules are incorporated in each material. Next, changes in the host molecules of **9.1** upon absorption of each vapour are studied directly via the use of ^{195}Pt and ^{11}B NMR.

SSNMR of Guest Solvent Molecules. Displayed in Figure 9.12 are ^{1}H and ^{13}C MAS SSNMR spectra of the four preparations of **9.1**. The changes in ^{13}C spectral resolution with sample preparation mimic those of the PXRD patterns, and are consistent with a higher degree of crystallinity in **9.1**•4CH_2Cl_2 than in the other forms. Aside from resolution changes, the vapour absorption causes only minor changes in the

isotropic chemical shifts of the host material **9.1**, consistent with the behaviour displayed in ^{13}C MAS NMR spectra of the vapochromic double salts of [Pt(arylisocyanide)$_4$][Pd(CN)$_4$] and [Pt(arylisocyanide)$_4$][Pt(CN)$_4$].[1j,1k] Both ^{1}H and ^{13}C isotropic chemical shifts are similar to those reported above from the solution NMR measurements of **9.1**. NMR peaks from the absorbed VOCs are readily observed in both ^{1}H and ^{13}C spectra. Because the intensity of the ^{1}H solvent peaks are of the same order as those from **9.1**, these spectra demonstrate conclusively that the vapochromic behaviour of **9.1** is accompanied by absorption of the VOCs into the matrix, as opposed to their simply acting as agents of structural change. Interestingly, the distinct changes observed in the ^{13}C spectrum after exposure to CH_2Cl_2 show that the sample is completely converted to the solvate form (**1**•4CH_2Cl_2) in this case.

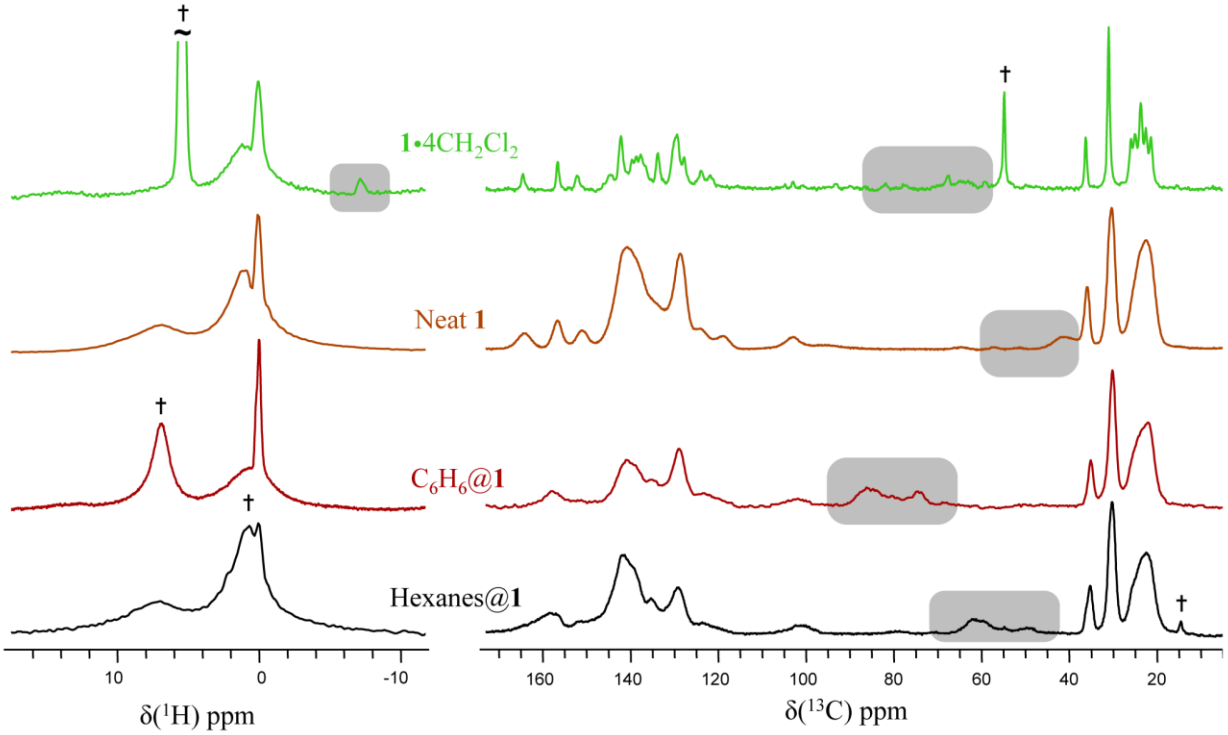

Figure 9.12: ^{1}H and ^{13}C solid-state MAS NMR spectra of samples of **9.1** exposed to selected VOCs. Spinning sidebands are marked with grey boxes, and NMR peaks from the incorporated solvents are each marked with a †. The spectra were acquired at MAS rates of 7.5 kHz for **9.1**•4CH_2Cl_2, 10 kHz for neat **9.1**, 5.5 kHz for C_6H_6@**9.1**, and 11 kHz (^{1}H spectrum)/ 8 kHz (^{13}C spectrum) for hexanes@**9.1**.

SSNMR of the Host Material. Because the Pt atom is central to the phosphorescent emission of **9.1**, the effects of VOC absorption were also studied using ^{195}Pt SSNMR. Before discussing the experimental

results, a brief description is given of the relationship between optically excited transitions and the nuclear magnetic shielding, NMS, measured using NMR. This relationship also extends to the chemical shift (CS), as this is simply the difference in NMS from a reference compound.[29,34] The NMS of a nucleus is due to a small local magnetic field induced by the large external magnetic field, as described by Ramsey.[35-37] External-field perturbed MOs, which are similar to the zero-field MOs except that they contain some admixture of virtual (unoccupied) orbitals, are the source of the response magnetic field. The amount that a particular virtual orbital mixes into a particular occupied orbital, and therefore the NMS contribution from that occupied/virtual MO pair, is inversely dependent on the energy gap between the two MOs. In addition, each MO pair's influence on the magnetic shielding depends on their degree of localization near the nucleus of interest, as well as on their shapes, determined by their constituent atomic orbitals.[37-39] The NMS is therefore dependent on a large array of occupied-virtual MO energy spacings in the valence level, while optical spectroscopy probes some of these same energy spacings one at a time. Since the colour changes observed in **9.1** must arise from solvent-induced energy shifts in the real and/or virtual MO involved in a particular optical absorption, the Pt CS tensor should change if the MO that shifts is localized near the Pt atom.

The ^{195}Pt SSNMR spectra of neat **9.1** and each vapour-treated sample are displayed in Figure 9.13. Under the conditions used (stationary samples, high-power ^{1}H decoupling), the powder pattern depends only on the platinum CS tensors, which are given in Table 9.4. Isotropic platinum chemical shifts are known to span a range of ca. 15000 ppm, and the present results are at the lower end of the +5000 to -5000 ppm range typical for Pt(II) compounds.[40,41] The CS tensors observed for neat **9.1**, **9.1**•4CH_2Cl_2, C_6H_6@**9.1**, and hexanes@**9.1** are characterized by large spans (Ω > 4000 ppm), as is typical for square-planar Pt(II) compounds; for example, Ω = 3472 ppm in (cod)PtI_2,[42] and the largest span published to date is for K_2PtCl_4, where Ω = 10500 ppm.[41,43-45] The most notable feature apparent in the data of Figure 9.13 and Table 9.4 is that the ^{195}Pt CS tensor of neat **9.1** is not measurably different than those of the three solvent-

exposed forms. From this evidence, we conclude that the vapochromic behaviour of **9.1** does not involve changes in the MOs localized on Pt. Clearly, there can be no Pt-Pt stacking in any of the preparations of **9.1**, because the metal-metal interactions would lead to Pt-localized MOs significantly different from those in **9.1**•$4CH_2Cl_2$. The solid-state NMR data therefore indicate, in agreement with the PXRD measurements and molecular modelling, that changes in Pt-Pt interactions are not responsible for the vapochromic behaviour of **9.1**.

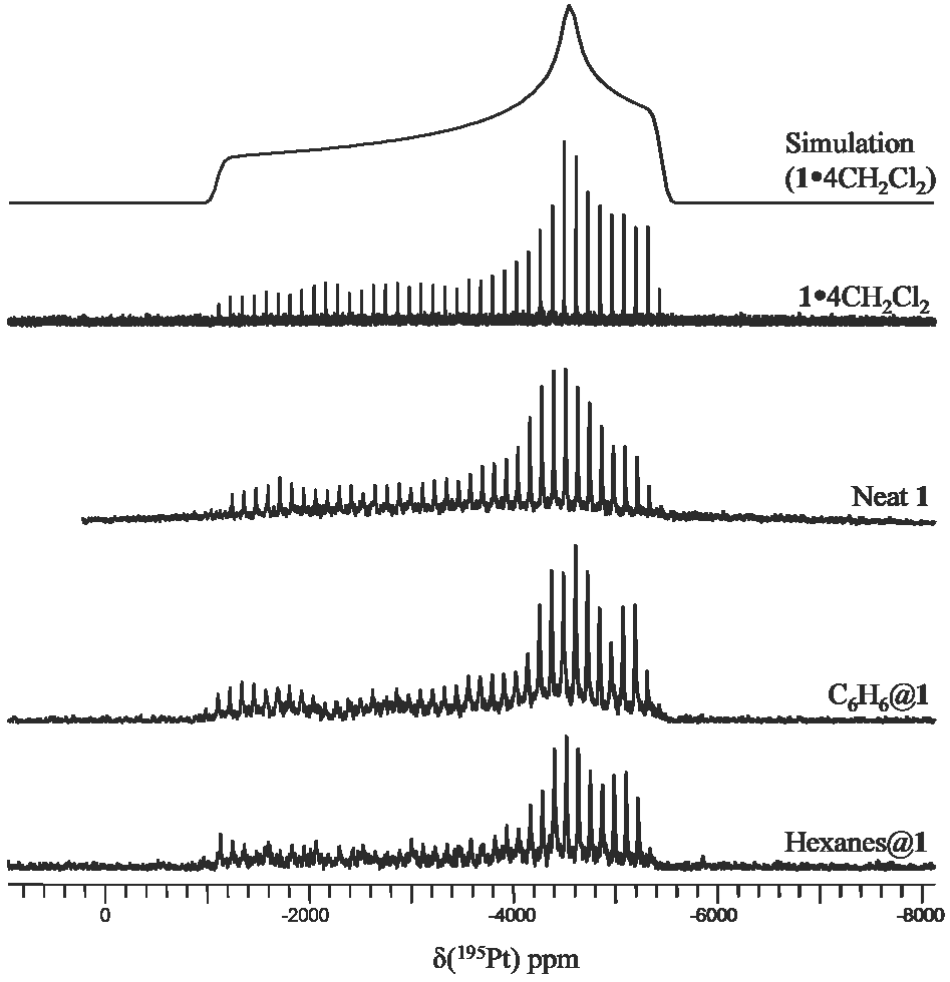

Figure 9.13: ^{195}Pt static SSNMR spectra of samples of **9.1** exposed to vapours of selected VOCs.

Table 9.4: ^{195}Pt chemical shift tensors measured from samples of 9.1 exposed to the vapours of selected VOCs.

Material	δ_{11}	δ_{22}	δ_{33}	δ_{iso}	Ω	κ
1•4CH_2Cl_2	-1100(100)	-4550(50)	-5450(100)	-3700(100)	4350(200)	-0.59(3)
Neat **1**	-1150(100)	-4450(200)	-5300(200)	-3600(200)	4150(300)	-0.59(10)
C_6H_6@**1**	-1000(100)	-4600(200)	-5350(200)	-3650(200)	4350(300)	-0.66(10)
Hexanes@**1**	-1000(100)	-4550(200)	-5350(200)	-3600(200)	4350(300)	-0.63(10)

Values for the CS tensor elements are derived using lineshape simulations, and are given here using the convention $\delta_{11} \geq \delta_{22} \geq \delta_{33}$. An alternate representation of the CS tensor is also included for convenience: the isotropic shift, $\delta_{iso} = 1/3(\delta_{11} + \delta_{22} + \delta_{33})$, the span, $\Omega = \delta_{11} - \delta_{33}$, and the skew, $\kappa = 3(\delta_{22} - \delta_{iso})/\Omega$ ($-1 \leq \kappa \leq 1$).[46] Spectral simulations are consistent with the experimental lineshapes within the ranges given in brackets for the principal components.

To further rule out chromophore-chromophore contacts as the cause of the unique vapochromic effect observed, ^{11}B SSNMR spectra of the stationary and MAS samples of **9.1**•4CH_2Cl_2 and C_6H_6@**9.1** were acquired. Because the boron atom is a distinct moiety central to the LC transition, looking for changes in the CS and EFG tensors would be another way to examine possible chromophore-chromophore interactions in the solid state induced by solvent uptake into the void space of **9.1**. The ^{11}B NMR spectra of **1**•4CH_2Cl_2 and C_6H_6@**1** are completely indistinguishable, demonstrating that the boron environment is unaltered by the absorption of these VOCs. While the boron atom in **9.1** is known to be accessible by small anions such as fluoride and cyanide, the steric crowding at this site ensures that there is no close contact with the much larger VOC molecules.

9.4 Conclusions

In summary, the first example of a triarylboron-functionalized Pt(II) acetylide compound that displays distinct luminescent responses to a variety of VOCs in the solid state has been presented. ^{1}H

and ^{13}C SSNMR spectroscopy was used to directly observe adsorption of solvent into **9.1**, and ^{195}Pt SSNMR results discount Pt-Pt metallophilic interactions as responsible for the response to VOCs. Based on optical and NMR spectroscopic data, we conclude that: (1) the vapochromic response of compound **9.1** toward polar solvents such as CH_2Cl_2 is caused by inversion of the lowest energy excited state from ^{3}MLCT to ^{3}LC in the solid state due to an increase in the MLCT level; (2) a decrease in the ^{3}MLCT level is responsible for the shift in emission color to red on exposure to benzene/cyclohexanes; and (3) the quenching response obtained by treatment of **9.1** with linear hydrocarbons or MeOH is likely due to the introduction of many closely spaced energy levels, which readily facilitate vibronic relaxation. As ^{11}B and ^{195}Pt NMR spectra show no changes on exposure to VOCs, we postulate that interactions between adsorbed solvent molecules and the bipyridine chelate are likely responsible for changes in the MLCT level, though it remains unclear why a similar effect is not observed in solution. This study demonstrates that metal-metal or π-π stacking interactions between molecules of the sensor are not necessary for a vapochromic response, and that interactions between the sensor and VOC analyte can indeed be sufficient.

9.5 Notes and References

The work described in this chapter has been published as:

- Z. M. Hudson, C. Sun, K. J. Harris, B. E. G. Lucier, R. W. Schurko, S. Wang, *Inorg. Chem.* **2011**, *50*, 3447

References

(1) a) M. Kato, A. Omura, A. Toshikawa, S. Kishi, Y. Sugimoto, *Angew. Chem.* **2002**, *114*, 3315. b) W. Lu, M. C. W. Chan, N. Zhu, C.-M. Che, Z. He, K.-Y. Wong, *Chem. Eur. J.* **2003**, *9*, 6155. c) J. Ni, L.-Y. Zhang, H.-M. Wen, Z.-N. Chen, *Chem. Commun*., **2009**, 3801. d) J. Ni, Y.-H. Wu, X. Zhang, B. Li, L.-Y. Zhang, Z.-N. Chen, *Inorg. Chem.* **2009**, *48*, 10202. e) M. Kato, S. Kishi, Y. Wakamatsu, Y. Sugi, Y. Osamura, T. Koshiyama, M. Hasegawa, *Chem. Lett.* **2005**, *34*, 1368. f) C. E. Buss, C. E. Anderson, M. K. Pomije, C. M. Lutz, D. Britton, K. R. Mann, *J. Am. Chem. Soc.* **1998**, *120*, 7783. g) C. E. Buss, K. R. Mann, *J. Am. Chem. Soc.* **2002**, *124*, 1031. h) Y. Kunugi, L. L. Miller, K. R. Mann, M. K. Pomije, *Chem. Mater*. **1998,** *10*, 1487. i) C. A. Daws, C. L. Exstrom, J. R. Sowa Jr., K. R. Mann, *Chem. Mater.* **1997,** *9*, 363. j) C. R. Exstrom, J. R. Sowa Jr. C. A. Daws, D. Janzen, K. R. Mann, G. A. Moore, F. F. Stewart, *Chem. Mater.*, **1995**, *7* , 15. k) P. K. Isbester, A. Zalusky, D. H. Lewis, M. C. Douskey, M. J. Pomije, K. R. Mann, E. Munson, *J. Catal. Today*, **1999**, *49*, 363.

(2) a) P. Du, J. Schneider, W. W. Brennessel, R. Eisenberg, *Inorg. Chem.* **2008**, *47*, 69. b) T. J. Wadas, Q.-M. Wang, Y. Kim, C. Flaschenreim, T. N. Blanton, R. Eisenberg, *J. Am. Chem. Soc.* **2004**, *126*, 16841. c) L. J. Grove, A. G. Oliver, J. A. Krause, W. B. Connick, *Inorg. Chem.* **2008**, *47*, 1408. d) L. J. Grove, J. M. Rennekamp, H. Jude, W. B. Connick, *J. Am. Chem. Soc.* **2004**, *126*, 1594. e) W. Lu, M. C. W. Chan, K.-K. Cheung, C.-M. Che, *Organometallics* **2001,** *20*, 2477. f) J. S. Field, C. D. Grimmer, O. Q. Munro, B. P. Waldron, *Dalton Trans.*, **2010**, *39*, 1558. g) M. Albrecht, G. van Koten, *Adv. Mater.* 1999**, 11**, 171 and references therein. h) K. Matsumoto, K. Sakai, *Adv. Inorg. Chem.* **1999**, *49*, 375. i) S. Kitagawa, K. Uemura, *Chem. Soc. Rev.* **2005**, *34*, 109.

(3) a) M. J. Katz, T. Ramnial, H. Z. Yu, D. B. Leznoff, *J. Am. Chem. Soc.*, **2008**, *130*, 10662. b) J. Lefebvre, R. J. Batchelor, D. B. Leznoff, *J. Am. Chem. Soc.*, **2004**, *126*, 16117. c) A. Luquin, C. Elosúa, E. Vergara, J. Estella, E. Cerrada, C. Bariáin, I. R. Matías, J. Garrido M. Laguna, *Gold Bull.* **2007**, *40*, 225. d) C. Bariáin, I. R. Matías, I. Romeo, J. Garrido, M. Laguna, *Sensor. Actuator.*, **2001**, B76, 25. e) A. L. Balch, *Struct. Bond.* **2007**, *123*, 1, Springer-Verlag, Berlin. f) M. A. Rawashdeh-Omary, M. Omary, J. P. Fackler Jr., R. Galassi, B. R. Pietroni, A. Brurini, *J. Am. Chem. Soc.* **2001**, *123*, 9689. g) V. W. W. Yam, E. C.-C. Cheng, *Chem. Soc. Rev.* **2008**, *37*, 1806.

(4) J. Pang, E. J.-P. Marcotte, C. Seward, R. S. Brown, S. Wang, *Angew. Chem., Int. Ed.*, **2001**, *40*, 4042.

(5) a) Z. M. Hudson, S. Wang, *Acc. Chem. Res.*, **2009**, *42*, 1584. b) D. Tanaka, T. Takeda, T. Chiba, S. Watanabe J. Kido, *Chem. Lett.* **2007**, *36*, 262. c) F. Jäkle, *Chem. Rev.* **2010,** *110*, 3985. d) F. Jäkle, *Coord. Chem. Rev.* **2006**, *250*, 1107. e) C. D. Entwistle, T. B. Marder, *Angew. Chem. Int. Ed.* **2002**, *41*, 2927. f) C. D. Entwistle, T. B. Marder, *Chem. Mater.* **2004**, *16*, 4574. g) S.-T. Lam, N. Zhu, V. W. W. Yam, *Inorg. Chem.* **2009**, *48*, 9664.

(6) a) T. Noda, Y. Shirota, *J. Am. Chem. Soc.* **1998**, *120*, 9714. b) T. Noda, H. Ogawa, Y. Shirota, *Adv. Mater.* **1999**, *11*, 283. c) Y. Shirota, M. Kinoshita, T. Noda, K. Okumoto, T. Ohara, *J. Am. Chem. Soc.* **2000**, *122*, 1102. d) Y. Shirota, *J. Mater. Chem.* **2005**, *15*, 75. e) H. Doi, M. Kinoshita, K. Okumoto, Y. Shirota, *Chem. Mater.* **2003**, *15*, 1080. f) W.-L. Jia, D. R. Bai, T. M. McCormick, Q.-D. Liu, M. Motala, R. Wang, C. Seward, Y. Tao, S. Wang, *Chem. Eur. J.* **2004,** *10*, 994. g) W.-L. Jia, M. J. Moran, Y.-Y. Yuan, Z.-H. Lu, S. Wang, *J. Mater. Chem.* **2005**, *15*, 3326. h) W.-L. Jia, X.-D. Feng, D. R. Bai, Z.-H. Lu, S. Wang, G. Vamvounis, *Chem. Mater.*, **2005**, *17*, 164. i) F.-H. Li, W.-L. Jia, S. Wang, Y.-Q. Zhao, Z.-H. Lu, *J. Appl. Phys.*, **2008**, *103*, 034509.

(7) a) J. C. Collings, S. Y. Poon, C. L. Droumaguet, M. Charlot, C. Katan, L. O. Pålsson, A. Beeby, J. A. Mosely, H. M. Kaiser, D. Kaufmann, W.-Y. Wong, M. Blanchard-Desce, T. B. Marder, *Chem. Eur. J.* **2009**, *15*, 198. b) Z. Yuan, N. J. Taylor, R. Ramachandran, T. B. Marder, *Appl. Organomet.*

Chem. **1996**, *10*, 305. c) Z. Yuan, C. D. Entwistle, J. C. Collings, D. Albesa-Jové, A. S. Batsanov, J. A. K. Howard, H. M. Kaiser, D. E. Kaufmann, S.-Y. Poon, W.-Y. Wong, C. Jardin, S. Fathallah, A. Boucekkine, J. F. Halet, N. J. Taylor, T. B. Marder, *Chem. Eur. J.* **2006**, *12*, 2758.

(8) a) C. R. Wade, A. E. J. Broomsgrove, S. Aldridge, F. P. Gabbaï, *Chem. Rev.* **2010,** *110*, 3958, and references therein. b) T. W. Hudnall, C.-W. Chiu, F. P. Gabbaï, *Acc. Chem. Res.* **2009**, *42*, 388.

(9) a) G. J. Zhou, C. L. Ho, W.-Y. Wong, Q. Wang, D.-G. Ma, L.-X. Wang, Z.-Y. Lin, T. B. Marder, A. Beeby, *Adv. Funct. Mater.*, **2008**, 18, 499. b) Z. M. Hudson, C. Sun, M. G. Helander, H. Amarne, Z.-H. Lu, S. Wang, *Adv. Funct. Mater.*, **2010**, *20*, 3426.

(10) T. Sajoto, P. I. Djurovich, A. B. Tamayo, J. Oxgaard, W. A. Goddard, M. E. Thompson, *J. Am. Chem. Soc.,* **2009**, *131*, 9813.

(11) N. M. O'Boyle, A. L. Tenderholt, K. M. Langner, *J. Comp. Chem*., **2008**, *29*, 839.

(12) M. J. Frisch *et al*, Gaussian 03, Revision C.02, Gaussian, Inc., Wallingford, CT, 2004.

(13) Z. An, S. A. Odom, R. F. Kelley, C. Huang, X. Zhang, S. Barlow, L. A. Padilha, J. Fu, S. Webster, D. J. Hagan, E. W. Van Stryland, M. R. Wasielewski, S. R. Marder, *J. Phys. Chem. A*. **2009**, *113*, 5585.

(14) S. Huertas, M. Hissler, J. E. McGarrah, R. J. Lachicotte, R. Eisenberg, *Inorg. Chem.* **2001**, *40*, 1183.

(15) G. Annibale, M. Bortoluzzi, G. Marangoni, B. Pitteri, *Transition. Met. Chem*. **2005**, 30, 748.

(16) M. Hissler, W. B. Connick, D. K. Geiger, J. E. McGarrah, D. Lipa, R. J. Lachicotte, R. Eisenberg, *Inorg. Chem.* **2000**, *39*, 447.

(17) SHELXTL Version 6.14, Bruker AXS, 2000-2003.

(18) A. Pines, J. S. Waugh, M. G. Gibby, *J. Chem. Phys.* **1972,** *56*, 1776.

(19) A. Pines, M. G. Gibby, J. S. Waugh, *J. Chem. Phys.* **1973,** *59*, 569.

(20) O. B. Peersen, X. L. Wu, I. Kustanovich, S. O. Smith, *J. Magn. Reson. Ser. A* **1993,** *104*, 334.

(21) A. E. Bennett, C. M. Rienstra, M. Auger, K. V. Lakshmi, R. G. Griffin, *J. Chem. Phys.* **1995,** *103*, 6951.

(22) W. L. Earl, D. L. Vanderhart, *J. Magn. Reson.* **1982,** *48*, 35.

(23) R. Bhattacharyya, L. Frydman, *J. Chem. Phys.* **2007,** *127*, 8.

(24) L. A. O'Dell, R. W. Schurko, *Chem. Phys. Lett.* **2008,** *464*, 97.

(25) L. A. O'Dell, A. J. Rossini, R. W. Schurko, *Chem. Phys. Lett.* **2009,** *468*, 330.

(26) I. Hung, A. J. Rossini, R. W. Schurko, *J. Phys. Chem. A* **2004,** *108*, 7112.

(27) R. Siegel, T. T. Nakashima, R. E. Wasylishen, *J. Phys. Chem. B* **2004,** *108*, 2218.

(28) R. K. Harris, P. Reams, K. J. Packer, *J. Chem. Soc. Dalton Trans.* **1986**, *5*, 1015.

(29) R. K. Harris, E. D. Becker, S. M. C. De Menezes, R. Goodfellow, P. Granger, *Pure Appl. Chem.* **2001**, *73*, 1795.

(30) K. Eichele, R. E. Wasylishen, *WSOLIDS*, 2.0.18; University of Alberta: Edmonton, 2000.

(31) M. Bak, J. T. Rasmussen, N. C. Nielsen, *J. Magn. Reson.* **2000,** *147*, 296.

(32) a) S. Goeb, A. A. Rachford, F. N. Castellano, *Chem. Commun.*, **2008,** 814. b) I. E. Pomestchenko, F. N. Castellano, *J. Phys. Chem. A* **2004,** *108,* 3485. c) C. She, A. A. Rachford, X. Wang, S. Goeb, A. O. El-Ballouli, F. N. Castellano, J. T. Hupp, *Phys. Chem. Chem. Phys.* **2009**, *11*, 8586.

(33) I. Gryczynski, J. R. Lakowicz, *Photochem. Photobiol.*, **1995**, *62*, 426.

(34) R. K. Harris, E. D. Becker, S. M. C. De Menezes, P. Granger, R. E. Hoffman, K. W. Zilm, *Pure Appl. Chem.* **2008,** *80*, 59.

(35) N. F. Ramsey, *Phys. Rev.* **1950,** *78*, 699.

(36) C. J. Jameson in *Multinuclear NMR*, 1st ed.; Mason, J., Ed. Plenum Press: New York, U.S.A., 1987.

(37) J. Autschbach, T. Ziegler in *Encyclopedia of Nuclear Magnetic Resonance*, D. M. Grant, R. K. Harris, Eds. John Wiley and Sons: Chichester U.K., 2002; Vol. 9, pp 306-323.

(38) C. D. Cornwell, *J. Chem. Phys.* **1966,** *44*, 874.

(39) J. B. Grutzner, in *Recent Advances in Organic NMR Spectroscopy*, J. B. Lambert, R. Rittner, Eds. Norell Press: Landisville, U.S.A., 1987; pp 17-42.

(40) R. J. Goodfellow in *Multinuclear NMR*, 1st ed.; J. Mason, Ed. Plenum Press: New York, 1987; p 3.

(41) T. M. Duncan, *A Compilation of Chemical Shift Anisotropies*. Farragut Press: Chicago, 1990.

(42) M.-H. Thibault, B. E. G. Lucier, R. W. Schurko, F.-G. Fontaine, *Dalton Trans.* **2009**, 7701.

(43) H. J. Keller, H. H. Rupp, *Z. Naturforsch. Part A* **1970**, *A 25*, 312.

(44) H. J. Keller, H. H. Rupp, *Z. Naturforsch. Part A* **1971**, *A 26*, 785.

(45) S. W. Sparks, P. D. Ellis, *J. Am. Chem. Soc.* **1986**, *108*, 3215.

(46) J. Mason, *Solid State Nucl. Magn. Reson.* **1993**, *2*, 285.

9.6 Appendix: DFT Calculations

9.6.1 MO Diagrams for 9.1:

-5.66 eV

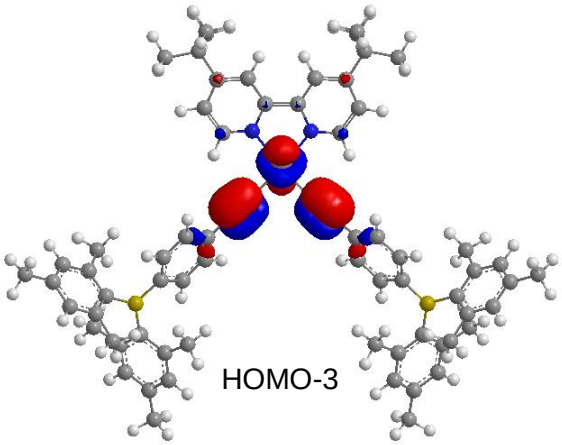

-5.64 eV

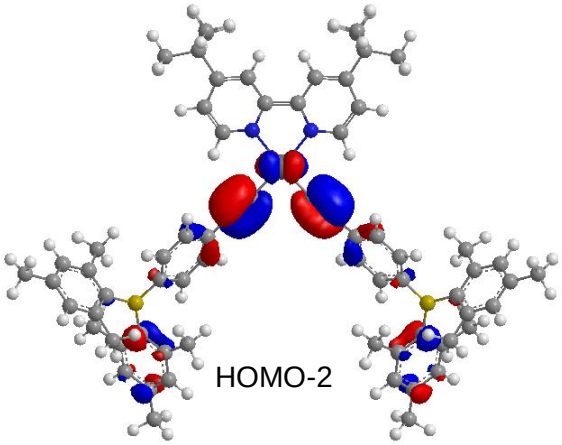

-5.12 eV

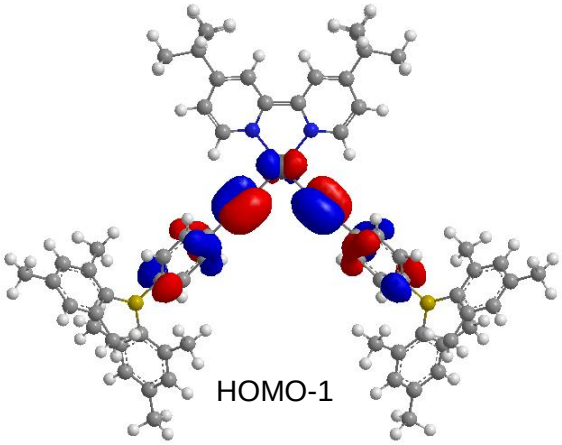

-5.08 eV

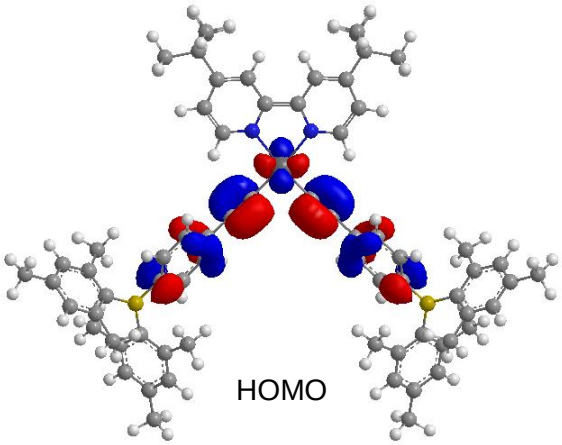

-2.56 eV

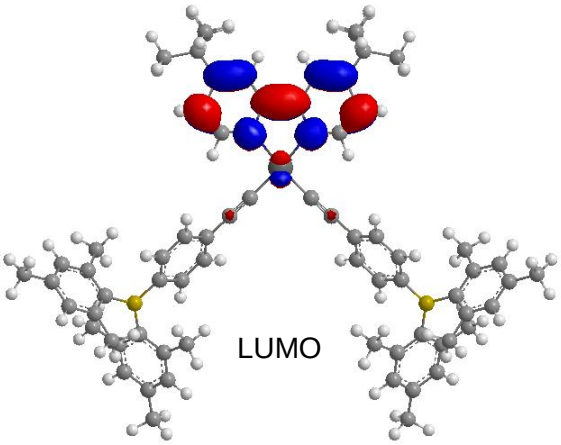

-1.72 eV

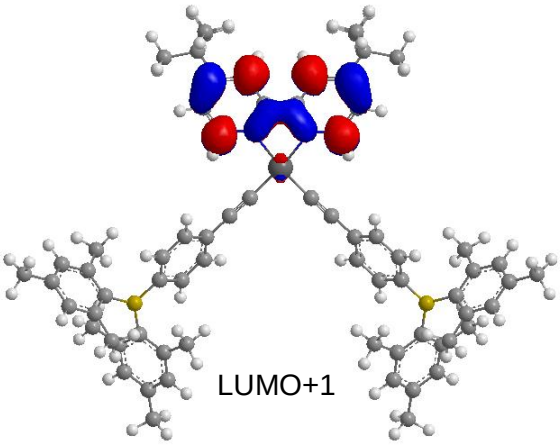

-1.50 eV

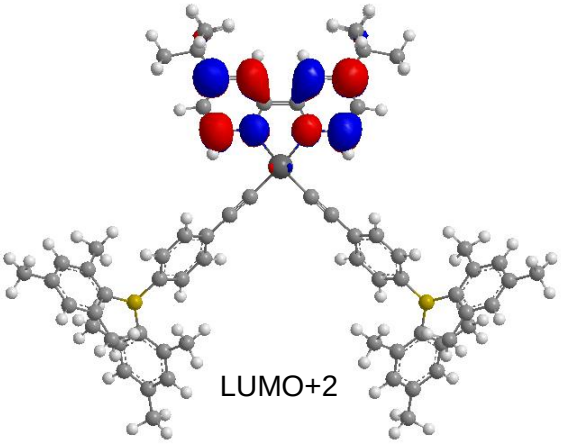

-1.34 eV

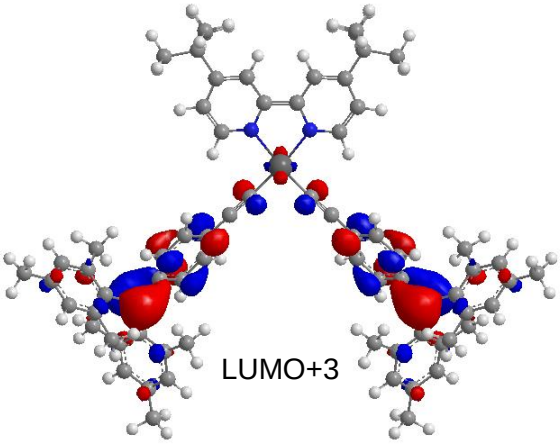

-1.32 eV

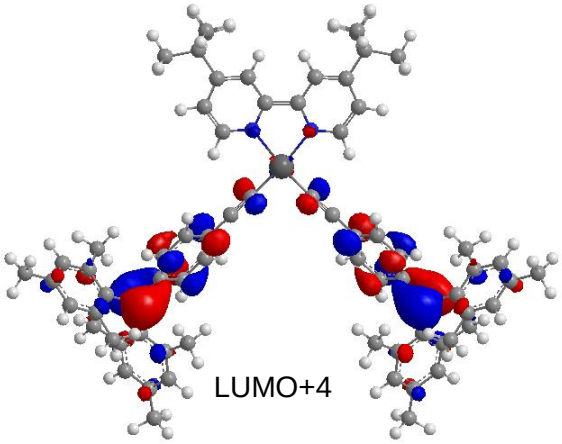

9.6.2 MO Diagrams for 9.2:

-5.36 eV

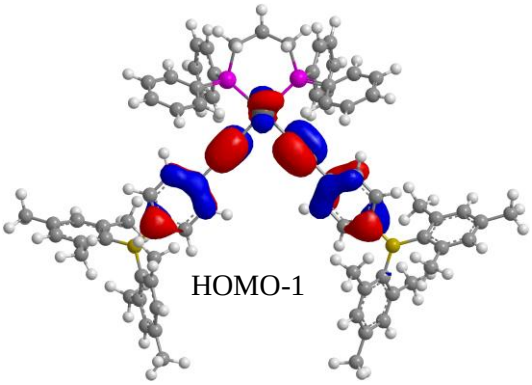

HOMO-1

-5.16 eV

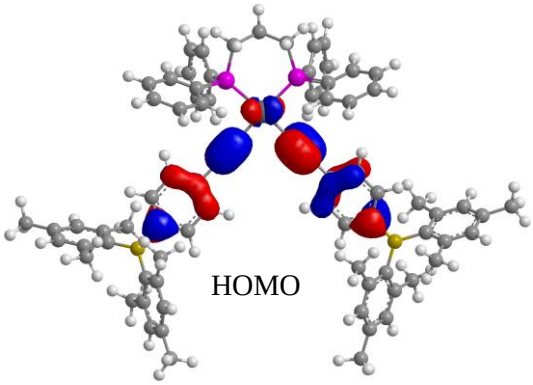

HOMO

-1.40 eV

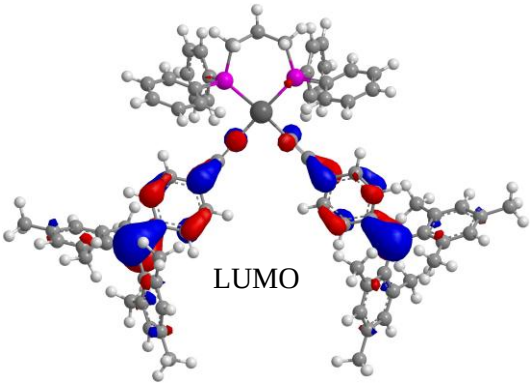

LUMO

-1.19 eV

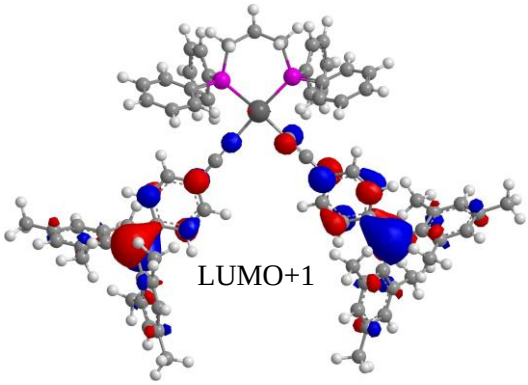

LUMO+1

Chapter 10

Summary and Outlook

In this work we have prepared a broad array of novel organoboron-and organoplatinum-containing π-conjugated materials whose properties have been investigated for optoelectronic applications. We have described the first example of a dual-emissive triarylboron compound, capable of both fluorescent and phosphorescent emission at ambient temperature. Furthermore, by controlling experimental parameters such as fluoride concentration, oxygen level, and detector delay time, this material was observably luminescent in any of six emission states. We have also examined a nonconjugated donor-acceptor organoboron compound containing both Lewis basic and Lewis acidic sites, found to be reversibly switchable between three fluorescent states on addition of acid or fluoride. Finally, we have investigated the photophysical properties of platinum(II)-acetylacetonate complexes with nonconjugated triarylboron-containing antenna chromophores. These studies demonstrate the versatility of multi-chromophore materials containing a triarylboron group, which can both promote efficient luminescence and act as a convenient receptor for fast and reversible multi-colour switching.

We have also demonstrated the substantial utility of triarylboron-containing materials in OLEDs. Through our studies of triarylboron-functionalized complexes of platinum(II), we have shown that the boron group can significantly enhance both metal-to-ligand charge-transfer and phosphorescent quantum yields. Furthermore, the presence of the bulky, electron-accepting dimesitylboron group was found to improve both the film-forming properties of Pt(II) complexes and their electron-transporting capabilities. As a result, we have successfully fabricated highly efficient green and orange electroluminescent devices incorporating our materials as phosphorescent emitters. Furthermore, after optimization of the device structures we have achieved the first example of a platinum-based OLED with an external quantum efficiency above 20%.

Though the performance of these devices was impressive, their commercial viability remained limited due to the lack of a low-cost method for their preparation. Literature methods required multiple steps, high temperatures, excess ligand and long reaction times, and resulted in only low yields of the desired product. We thus developed an efficient and high-yield one-pot synthesis of cyclometalated platinum(II) *β*-diketonates, requiring only stoichiometric amounts of ligand and three hours' reaction time at ambient temperature. This method showed broad substrate scope across a wide range of *N^C*-chelate ligands, and was successfully extended to *P^C* chelate phosphines and *C^C* chelate carbene complexes as well.

The use of carbenes in Pt(II) complexes containing triarylboron presented a unique opportunity as well. Though we had achieved high efficiency phosphorescence in a series of *N^C*-chelate complexes with good colour tunability from green to red, efficient blue phosphors based on this design remained elusive. However, by adapting our newfound synthetic methods we were able to prepare the first examples of triarylboron-functionalized metal-carbene complexes, achieving efficient blue-green and sky-blue phosphorescence by careful ligand design. Furthermore, preliminary electroluminescent devices based on these emitters showed efficiencies among the highest demonstrated to date for carbene-based OLEDs.

We also sought to address a problem more central to OLED technology, namely that the complex multilayer structures typically used to fabricate OLEDs were innately costly and time-consuming to manufacture. We thus developed a pair of *N*-heterocyclic carbazole-based host materials with both hole- and electron-transporting functionality, eliminating the need for discrete charge-transport layers. Furthermore, these materials were prepared by a simple synthetic route in only two steps. Using these compounds as ETL, HTL and host with $Ir(ppy)_2(acac)$ as emitter, we successfully fabricated the most efficient single-layer OLEDs reported in literature.

Finally, our research on triarylboron-containing platinum alkyne complexes led to the serendipitous discovery of the first vapochromic triarylboron compound. This material showed bright yellow luminescence as a neat solid, and rapidly experienced a variety of emission colour changes in response to various organic vapours. The nature of this vapochromic behaviour was investigated in detail by optical and multinuclear solid-state NMR spectroscopy, and it was found that the origin of vapochromism in this material differed from all previously known examples.

Though this work represents significant progress in the understanding of boron-containing metal complexes, many opportunities remain for further research. While triarylboron-containing complexes of Pt(II) and Ir(III) now appear in numerous studies, there are many other transition metals, such as Fe, Cu, Zn, Ru, Re, and Hg for which only a handful of such reports exist. Furthermore, triarylboranes containing many other transition metals as well as lanthanides and actinides have yet to appear in literature. This presents a wealth of opportunities for research that is sure to uncover new photophysical properties and chemical phenomena.

This thesis has also greatly expanded the body of work on nonconjugated donor-acceptor triarylboranes, and many opportunities still exist in this area. Specifically, expansion of this research to include donor groups such as phosphines, sulphides and carbenes may lead to new discoveries in optoelectronics and small-molecule activation. Enhancing the Lewis acidity of the boron site may lead to new properties and reactivities as well.

Though presented only in a single chapter here, our work represents the first example of a single-layer OLED with efficiencies comparable to state-of-the-art electroluminescent devices. Few reports appear in literature of such single-layer structures, with the vast majority of studies making use of complex multilayer architectures. As OLEDs become more prevalent in commercial lighting and displays, the

advantage afforded by cost-effective OLED production will become increasingly important. For this reason, it is expected that research on single-layer OLEDs will continue, and will seek to improve the efficiency and lifetime of these devices as well as expand their use to a wider array of visible colours.

While we have greatly improved upon existing methods for the preparation of cyclometalated platinum(II) β-diketonates, many classes of common phosphorescent materials still lack a mild and efficient synthetic route. Most notably, cyclometalated complexes of Ir(III) remain the most widely used phosphors in OLEDs, yet often require long reaction times at high temperatures to prepare. We predict that the knowledge gained from our studies on Pt(II) can be applied to improving the syntheses of many other classes of organometallic compounds as well.

Finally, we have made significant advances in the use of triarylboron-containing complexes as phosphorescent dopants for OLEDs. Future work in this area may focus on the use of boron-based phosphorescent dopants incorporating metals other than Pt(II), and the development of dopants with high colour purity for full-colour displays and solid-state lighting. In particular, continuing efforts to prepare deep-blue phosphors based on triarylboron may prove to be an exciting challenge.